1 OF 2

PB84
153253

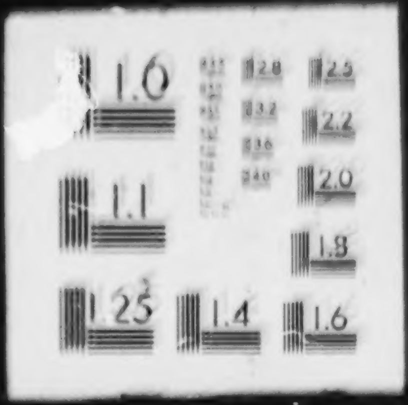
1.0
2.8
2.5
3.2
2.2
3.6
4.0
2.0
1.1
1.8
1.25
1.4
1.6

PB84-153253

Burner Criteria for NOx Control. Volume 2 Heavy-Oil and Coal-Fired Furnaces and the Evaluation of Radiative Heat Transfer Models

International Flame Research Foundation
Ijmuiden (Netherlands)

Prepared for

Industrial Environmental Research Lab.
Research Triangle Park, NC

Feb 84

U.S. Department of Commerce
National Technical Information Service
NTIS

PB84-153253

EPA-600/7-84-015a
February 1984

BURNER CRITERIA FOR NO_X CONTROL
Volume II.
Heavy-oil and Coal-fired Furnaces and The Evaluation of Radiative Heat Transfer Models

By

M. P. Heap, T. W. Lowes,
R. Walmsley, H. Bartelds
and P. LeVaguerese

International Flame Research Foundation
Ijmuiden, Holland

Contract No. 68-02-0202

EPA Project Officer: G. Blair Martin

Industrial Environmental Research Laboratory
Office of Environmental Engineering and Technology
Research Triangle Park, NC 27711

Prepared for

U. S. ENVIRONMENTAL PROTECTION AGENCY
Office of Research and Development
Washington, DC 20460

REPRODUCED BY
NATIONAL TECHNICAL
INFORMATION SERVICE
U.S. DEPARTMENT OF COMMERCE
SPRINGFIELD, VA. 22161

TECHNICAL REPORT DATA

(Please read Instructions on the reverse before completing)

1. REPORT NO. EPA-600/7-84-015a	2.	3. RECIPIENT'S ACCESSION NO. PB84 153253
4. TITLE AND SUBTITLE Burner Criteria for NOx Control; Volume II. Heavy-oil- and Coal-fired Furnaces and the Evaluation of Radiative Heat Transfer Models		5. REPORT DATE February 1984 6. PERFORMING ORGANIZATION CODE
7. AUTHOR(S) M. Heap, T. Lowes, R. Walmsley, H. Bartelds, and P. LeVaguerese		8. PERFORMING ORGANIZATION REPORT NO.
9. PERFORMING ORGANIZATION NAME AND ADDRESS International Flame Research Foundation Research Station (IVO) c/o KHNS Ijmuiden, Holland		10. PROGRAM ELEMENT NO. 11. CONTRACT/GRANT NO. 68-02-0202
12. SPONSORING AGENCY NAME AND ADDRESS EPA, Office of Research and Development Industrial Environmental Research Laboratory Research Triangle Park, NC 27711		13. TYPE OF REPORT AND PERIOD COVERED Phase II Final; 7/74-7/75 14. SPONSORING AGENCY CODE EPA/600/13

15. SUPPLEMENTARY NOTES IERL-RTP project officer is G. Blair Martin, Mail Drop 62-B, 919/541-7504. Volume I is EPA-600/2-76-061a.

16. ABSTRACT The report describes Phase II of a research program, the overall objective of which was to specify burner design criteria for minimum pollutant emissions from both pulverized coal and residual fuel-oil-fired combustors. Phase II included both furnace investigations and the evaluation of radiative heat transfer models which could later be applied to the development of an analytical tool capable of predicting combustor performance; the models helped generalize the results obtained in the furnace experiments. The furnace investigation had three major objectives: providing further information on NOx formation in pulverized coal flames; extending the furnace investigations to include fuel oils; and identifying methods of satisfying combustor process requirements while minimizing NOx emissions through burner design. Results show the emission characteristics of a subscale practical burner, and the development of a tertiary air injection system to minimize NOx formation by using outboard staged air ports. Emissions from heavy fuel oil were found to be most dependent on the method of atomization; in general, the lowest emissions were produced from the narrowest spray angles. The report describes the development of several radiative heat transfer models and compares their predictive capabilities with both experimental results and hypothetical test cases.

17. KEY WORDS AND DOCUMENT ANALYSIS

a. DESCRIPTORS		b. IDENTIFIERS/OPEN ENDED TERMS	c. COSATI Field/Group	
Pollution	Fuel Oil	Pollution Control	13B	
Nitrogen Oxides	Residual Oils	Stationary Sources	07B	
Burners	Natural Gas	Radiative Heat Transfer	13A	
Design	Heat Transfer		14G	20M
Combustion	Mathematical Models		21B	12A
Coal			21D	

18. DISTRIBUTION STATEMENT Release to Public	19. SECURITY CLASS *(This Report)* Unclassified	21. NO. OF PAGES 185
	20. SECURITY CLASS *(This page)* Unclassified	22. PRICE

NOTICE

This document has been reviewed in accordance with U.S. Environmental Protection Agency policy and approved for publication. Mention of trade names or commercial products does not constitute endorsement or recommendation for use.

ABSTRACT

This report describes the second phase of a research program, the overall objective of which was the specification of burner design criteria for minimum pollutant emissions from both pulverized-coal- and residual-fuel-oil-fired combustors. This phase of the program included both furnace investigations and the evaluation of radiative heat transfer models which could later be applied to the development of an analytical tool capable of predicting combustor performance; thus helping to generalize the results obtained in the furnace experiments.

The furnace investigation had three major objectives:

1. The provision of further information on NO_x formation in pulverized coal flames.
2. Extend the furnace investigations to include fuel oils.
3. Investigate methods of satisfying combustor process requirements while minimizing NO_x emissions through burner design.

Results are presented which show the emission characteristics of a subscale practical burner, and the development of a tertiary air injection system to minimize NO_x formation via the use of outboard staged air ports. Emissions from dual-fuel systems were investigated by firing both natural gas and coal simultaneously. Emissions from heavy fuel oil were found to be the most dependent upon the method of atomization and, in general, the lowest emissions were produced from the narrowest spray angles.

The report describes the development of several radiative heat transfer models and their predictive capabilities are compared with both experimental results and hypothetical test cases. Three model types are described: two-flux models, four-flux models, and a continuous intensity distribution model (CID). The latter model appears to have an accuracy approaching that of a zone model, although both complexity and computing times are increased.

TABLE OF CONTENTS

Page No.

1.0 SUMMARY 1-1

1.1 Program Overview 1-1
1.2 Furnace Investigations 1-3
1.3 Radiative Heat Transfer Models 1-8

2.0 FURNACE INVESTIGATIONS TO IDENTIFY BURNER DESIGN PARAMETERS CONTROLLING NO_x FORMATION IN NITROGEN-CONTAINING FUELS 2-1

2.1 Introduction 2-1
2.2 Experimental Conditions 2-8
2.3 Results of the Furnace Investigations 2-18
2.4 Thermal Effects and Nitric Oxide Formation in Diffusion Flames 2-70
2.5 Conclusions and Implications for Further Investigations 2-81

3.0 THE DEVELOPMENT OF MODELS TO CALCULATE RADIANT HEAT TRANSFER IN FURNACES 3-1

3.1 Introduction 3-1
3.2 Methods Available for the Evaluation of Radiant Exchange 3-6
3.3 The Development of Two and Four-Flux Models of Radiant Exchange 3-13
3.4 The Development of a Radiative Heat Transfer Model Utilizing a Continuous Intensity Distribution with Six Parameters 3-43
3.5 The Representation of the Radiative Properties of Furnace Gases 3-54
3.6 Conclusions and Summary 3-71

4.0 REFERENCES AND NOMENCLATURE 4-1

LIST OF FIGURES

Page No.

2.1 Emission Characteristics of Pulverized Coal Flames Produced with Radial Fuel Injection 2-3

2.2 Emission Characteristics of Pulverized Coal Flames Produced with Axial Fuel Injection 2-4

2.3 Reproducibility of Emission Levels with Natural Gas Firing 2-7

2.4 Reproducibility of Emission Levels with Pulverized Coal Firing 2-9

2.5 Details of the Triple Concentric Burner Showing Two Tertiary Duct Diameters 2-12

2.6 Sketch Showing the Construction of the Subscale Practical Burner 2-13

2.7 Details of Fuel Oil Injectors 2-14

2.8 Coal Spreader Injector 2-16

2.9 The Effect of Excess Air on NO Emission Subscale Practical Burner 2-20

2.10 The Effect of Excess Air on NO Emission Subscale Practical Burner 2-21

2.11 The Effect of Excess Air on NO Emission Subscale Practical Burner 2-22

2.12 The Effect of Coal Spreader Position on NO Emission 2-23

2.13 The Effect of Primary Air Supply 2-23

2.14 Effect of Fuel Injector Type with Subscale Practical Burner 2-25

2.15 The Effect of Swirl on the Emission Characteristics of Pulverized Fuel Flames Produced with a Coal Spreader 2-26

2.16 Tertiary Systems 2-28

2.17 Emission Characteristics of Triple Concentric Systems 2-30

2.18 Emission Characteristics of Triple Concentric Systems 2-31

2.19 Emission Characteristics of Triple Concentric Systems 2-32

2.20 Emission Characteristics of Triple Concentric Systems 2-33

2.21 Emission Characteristics of Triple Concentric Systems 2-34

2.22 The Influence of Fuel Injector Type and Staging 2-36

Page No.

2.23 Emission Characteristics of Triple Concentric Burners 2-37

2.24 The Effect of Staging Upon Flame Characteristics Produced with a Subscale Practical Burner 2-38

2.25 The Effect of Dual Fuel Firing on NO Formation 2-42

2.26 The Effect of Dual Fuel Firing on NO Formation 2-43

2.27 The Effect of Dual Fuel Firing on NO Formation 2-44

2.28 The Effect of Dual Fuel Firing on NO Formation 2-45

2.29 The Effect of Dual Fuel Firing on NO Formation 2-46

2.30 Comparison of NO Formation when Air is Excluded from the Primary Stream 2-48

2.31 The Effect of Coal Gas Ratio on NO Emission with Dual Fuel Firing 2-49

2.32 The Effect of Coal Gas Ratio on NO Emissions with Dual Fuel Firing 2-50

2.33 The Effect of Coal Gas Ratio on NO Emissions with Dual Fuel Firing 2-51

2.34 The Effect of Coal Gas Ratio on NO Emissions with Dual Fuel Firing 2-52

2.35 The Influence of Pressure Jet Spray Angle 2-56

2.36 The Influence of Pressure Jet Spray Angle 2-57

2.37 The Influence of Pressure Jet Spray Angle 2-58

2.38 The Influence of Pressure Jet Spray Angle 2-59

2.39 The Influence of Steam Atomized Injector Spray Angle and Air Preheat 2-61

2.40 The Influence of Atomizer Type on NO Formation in Fuel Oil Flames 2-62

2.41 The Influence of Swirl Vanes Attached to the Nozzle 2-63

2.42 The Influence of Swirl Vanes Attached to the Nozzle 2-64

Page No.

2.43 The Influence of Swirl Vanes Attached to the Nozzle 2-65
2.44 The Influence of Swirl Vanes Attached to the Nozzle 2-66
2.45 Change in Emissions Due to Movement of the Nozzle Toward the Burner Throat 2-68
2.46 The Influence of Divergent Angle of the Burner Exit 2-69
2.47 The Influence of Secondary Velocity 2-71
2.48 The Influence of Secondary Velocity 2-72
2.49 The Effect of Preheat on the Emission Characteristics of a Subscale Practical Burner 2-73
2.50 The Effect of Load on the Emission Characteristics of a Subscale Practical Burner 2-74
2.51 Natural Gas 5% Excess Air - The Effect of Furnace Temperature on NO Formation 2-77
2.52 No. 6 Fuel Oil, 5% Excess Air - The Effect of Furnace Temperature on NO Formation 2-77
2.53 Pulverized Coal 15% Excess Air - The Effect of Furnace Temperature on NO Formation 2-78
2.54 The Influence of Air Preheat Level 2-79
2.55 The Influence of Air Preheat Level 2-80
3.1 Radiant Energy Balance in a Specified Direction 3-4
3.2 Intensity Distributions for Two-Flux Methods 3-8
3.3 Heat Transfer Between Parallel Black Plates Separated by a Gray Radiating Gas 3-10
3.4 Distribution of Emissive Power in a Heat Generating and Radiating Gray Gas Between Parallel Black Plates 3-11
3.5 Coordinate Systems Defining Position and Direction of Intensity 3-16

Page No.

3.6 Intensity Distribution for Two-Flux Models in Axisymmetric Systems 3-18

3.7 Intensity Distributions Between Parallel Cylinders 3-19

3.8 Intensity Distribution for Four-Flux Model in Axisymmetric Systems 3-22

3.9 Intensity Distribution for Six-Flux Model in Cartesian Coordinates 3-25

3.10 Predictions of Incident Radiant Wall Heat Flux Distributions Using the Zone Method with Different Attenuation Coefficient Formulations 3-28

3.11 Predictions of Incident Radiant Wall Heat Flux Distributions Using the Four-Flux Model with Different Attenuation Coefficient Formulations 3-29

3.12 Comparison of Predictions by Zone Method and Four-Flux Model with Experimental Results 3-31

3.13 Comparison of Zone Method and Flux Models 3-33

3.14 Comparison of Zone Method and Flux Models 3-35

3.15 Comparison of Zone Method and Four-Flux Model 3-36

3.16 Comparison of Zone Method and Four-Flux Model 3-37

3.17 Comparison of Radiative Heat Flux Predictions by the Two-Flux Schuster-Schwarzschild Model, the Four-Flux Model and the Zone Method 3-38

3.18 Prediction of Incident and Net Radiation Flux at Sidewall for Different Attenuation Coefficients Using the Zone Method 3-39

3.19 Comparison of Radiative Heat Flux Predictions by the Two-Flux Schuster-Schwarzchild Model, the Four-Flux Model and the Zone Method 3-41

3.20 Prediction of Incident and Net Radiation Flux at Sidewall for Different Attenuation Coefficients Using the Zone Method 3-42

Page No.

3.21 Intensity Distributions in a Cross Section of a Cylindrical Furnace 3-44

3.22 Intensity Distributions on a Longitudinal Section of A Cylindrical Furnace 3-45

3.23 Intensity Distributions in a Longitudinal Section of a Cylindrical Furnace 3-46

3.24 Intensity Distribution for CID-6 Model 3-49

3.25 Comparison of Predictions by the CID-5 Model with Experimental Results 3-50

3.26 Comparison of Two-Flux Model, Four-Flux Model and CID-5 Model Predictions with a Zone Method Prediction 3-51

3.27 Comparison of Four-Flux Model and CID-5 Model Predictions with a Zone Method Prediction 3-52

3.28 Comparison of Four-Flux Model and CID-5 Model Predictions with a Zone Method Prediction 3-53

3.29 Prediction of Narrow Angle Traverses Through a Natural Gas Flame Using Different Gray Gas Attenuation Coefficients 3-62

3.30 Predictions of Narrow Angle Traverses Through a Natural Gas Flame Using Different Gray Gas Attenuation Coefficients 3-63

3.31 Prediction of Narrow Angle Traverses Using a 1 Clear/ 2 Gray Gas Attenuation Formulation 3-66

3.32 Prediction of Narrow Angle Traverses Using a 1 Clear/ 2 Gray Gas Attenuation Formulation 3-67

LIST OF TABLES

		Page No.
2-1	Nominal Composition of Slochteren Natural Gas	2-10
2-2	Properties of No. 6 Fuel Oil	2-10
2-3	Properties of High Volatile Coal	2-10
2-4	Details of Dual Fuel Injector Systems	2-17
2-5	Input Conditions for Investigations Involving the Subscale Practical Burner	2-19
2-6	Emission Levels for Subscale Burner Investigations	2-19
2-7	Input Conditions for Tertiary Air Injection Systems	2-29
2-8	Input Conditions for Dual Fuel Investigations	2-40
2-9	Summary of Flue Gas NO Concentrations for the Dual Fuel Investigations	2-41
3-1	Definition of Factors "a" and "b" in Generalized Two-Flux Equations	3-9
3-2	Constants for the Clear/2 Gray Formulation	3-65
3-3	Constants Used in the Four-Gray Gas Formulation	3-70

1.0 SUMMARY

1.1 Program Overview

This report describes the second phase of a research program whose overall objective is the specification of burner design criteria for minimum pollutant emissions from both pulverized coal and residual fuel oil-fired combustors. The first phase of the program was concerned with the definition of the effect of various burner design parameters upon the formation of nitrogen oxides (NO_x) in both pulverized coal and natural gas flames. Both input/output investigations and detailed flame mapping were carried out in an attempt to establish those flow and mixing patterns which yielded the most promise for controlling NO_x emissions by burner redesign.

The major accomplishment of this first series of furnace investigations was the demonstration that under subscale conditions NO_x emissions from pulverized coal flames could be varied by a factor of four. This variation was achieved mainly by the selection of three burner design parameters:

- the method of fuel injection. Any tendency to rapidly mix the coal with all the combustion air resulted in higher emissions. The lowest emissions were achieved with a high velocity axial fuel injector which maintained a coherent fuel jet of high coal density;
- optimum level of swirl to provide a stable ignition source at the fuel injector without mixing the fuel too rapidly with the secondary air. Swirl refers to the fact that the secondary air stream has both a tangential and axial velocity component;
- the degree of primary air. Primary air refers to that air which is mixed with the pulverized coal prior to delivery into the furnace. NO_x emissions were lowest when the minimum amount of primary air was used consistent with maintaining slow mixing of the fuel jet with the secondary air.

Although burner conditions had been identified which gave low NO_x emissions, it was readily recognized that such a burner design would be unsuitable for use in existing wall-fired utility boilers.

The second series of furnace trials were planned to achieve three major goals:

- to provide further information on the formation of NO_x in pulverized coal flames to aid in interpretation of the results;
- to extend the investigation to include residual fuel oil firing in order to define those parameters which give minimum emissions; and
- to investigate methods of satisfying process requirements and produce minimum emissions. This involves the definition of the combustion requirements of practical systems as well as an attempt to reduce emissions via burner design.

In addition to the furnace investigations, a parallel effort was to be conducted throughout the entire program to aid in the development of an analytical tool which would allow the extrapolation of the experimental results to furnaces and conditions outside those actually investigated.

Recognizing the futility of attempting to develop a completely predictive model for nitric oxide formation for the types of flames investigated in the experimental sections of the program, it was decided to initiate a program of model development which would provide the components of a modular model. This empirical model would consist of three separate components:

1. Subscale physical modeling to allow flow field and mixing patterns to be assessed which would be part of the final phase of the program.
2. A heat transfer model, which when combined with the heat release profiles calculated from the above, would enable the temperature field to be calculated which is described in this report.
3. A multiple reactor model which would combine information generated by the first two components, a suitable kinetic mechanism and a

minimum number of adjustable empirical constants to predict pollutant formation which could be constructed when an adequate kinetic mechanism was available.

The intended use for this model would be to predict trends associated with such parameters as injector type, extremes of swirl level, fuel type, etc. It was argued that even though it would not be possible to combine the physical and heat transfer models with a suitable reactor model in this program, the satisfactory separate operation of either component would represent a significant contribution. In the second phase of the research program several radiant heat transfer models were developed and evaluated.

1.2 Furnace Investigations

The furnace investigations covered a wide range of topics, some of them exploratory or diagnostic as well as those concerned with an assessment of burner parameters capable of providing combustion conditions suitable for practical situations, and yet with minimum pollutant emission characteristics. The experimental investigations were carried out in a partially-cooled refractory tunnel furnace with three fuels: natural gas, a residual fuel oil of 0.24 percent nitrogen, and a bituminous coal of 1.05 percent nitrogen content. The trials were conducted over a six-week period during which time emphasis was placed upon five separate areas:

- the determination of the emission characteristics of a subscale practical burner to enable comparisons to be made with the moving block swirl burner used exclusively during the first phase of the program;
- the development of a burner with a tertiary air supply to produce low NO_x flames which satisfy practical requirements;
- an investigation of the emission characteristics of flames produced with the simultaneous firing of pulverized coal and natural gas;
- to establish the influence of various burner design parameters of pollutant emission from residual oil flames; and
- a comparative study of the influence of air preheat on NO_x formation from natural gas, residual fuel oil and pulverized coal.

The most significant results are summarized in the following.

- Emission Characteristics of a Subscale Practical Burner

Results were obtained in the IJmuiden tunnel furnace which were similar to those reported by Armento.(7) NO_x emissions increased with increasing excess air although the precise influence of preheat, excess air and firing rate were not duplicated. Very high NO levels (in excess of 1700 ppm) were recorded at high firing rates and 450°C preheat with an almost uncooled furnace. These high emissions are probably due to an increasing contribution of thermal NO and to more complete loss of nitrogen from the coal char because of the higher temperatures.

Shown below is an example of how the emissions from the subscale burner could be modified by changing the method of fuel injection and the amount of air supplied with the coal in the primary stream. Reducing the tendency of the coal jet to spread and mix rapidly with the combustion air reduces emissions by more than 28 percent for a given set of input conditions.

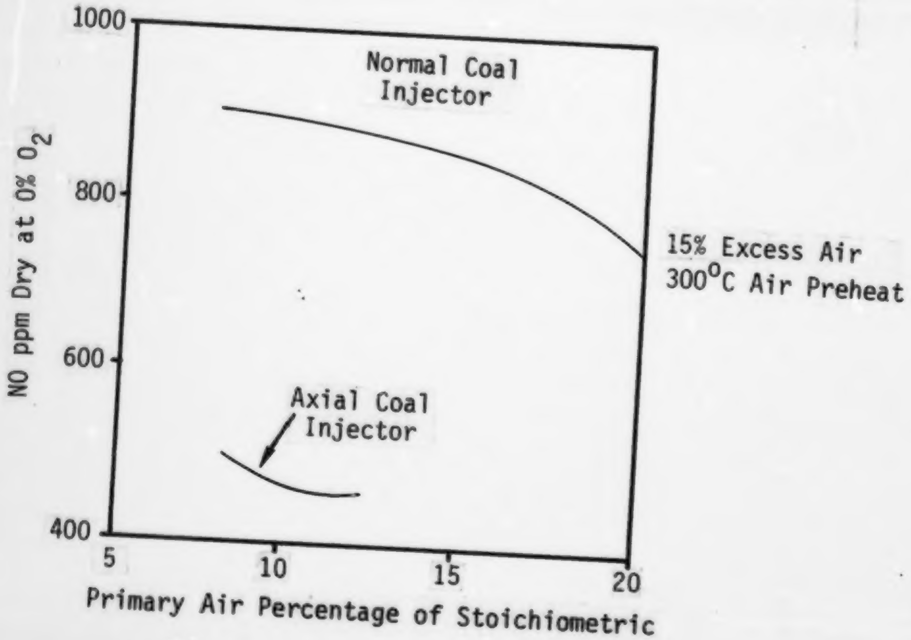

Emission Levels from a Subscale Practical Burner Can be Reduced by Modifying the Method of Fuel Injection

- Tertiary Air Injection to Reduce NO_x Formation

The total combustion air supply was divided into three streams to delay the mixing of the fuel with all the air by injecting one of these streams (tertiary air) from the periphery of the burner. In the most successful application of the technique 40% reductions in emissions from the subscale practical burner were achieved with 20% of the stoichiometric air requirement supplied in the tertiary stream. Incorrect designs caused 300% increases in emission from natural gas-fired tertiary air systems.

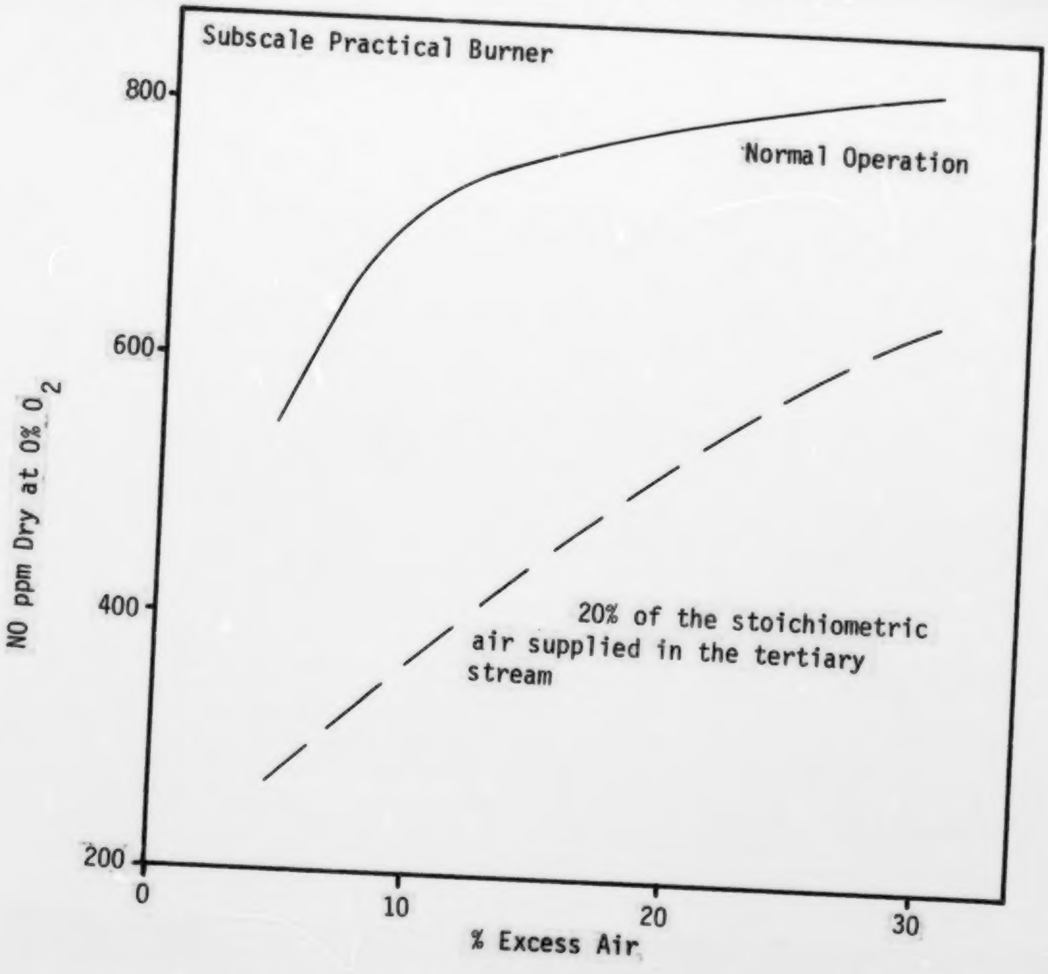

The Use of Tertiary Air Injection Can Reduce NO_x Emissions from Coal-Fired Burners by a Substantial Amount

- Emission Characteristics of Dual Fuel Systems

NO_x emissions resulting from the simultaneous firing of gaseous and solid fuels are not additive. The emission characteristics of dual fuel firing are dependent upon burner parameters such as fuel injector type. The results presented below are for a fixed total heat input and show the emissions from simultaneous coal-plus-gas firing as a ratio of emissions with coal alone as a function of the fractional heat input due to coal. The fractional conversion of fuel nitrogen to NO increases with decreasing nitrogen content. Mixing gas and coal reduces the overall nitrogen content of the combined fuel which could partially explain the increased emission due to combined firing. The rate of volatile fuel nitrogen evolution is dependent upon particle heating rate, and therefore, gas temperature which will vary in the early stages of the flame as a result of mixed fuel firing. The heating rate may also affect char nitrogen content and the lower emissions from combined firing shown below may be the result of reduced char nitrogen conversion.

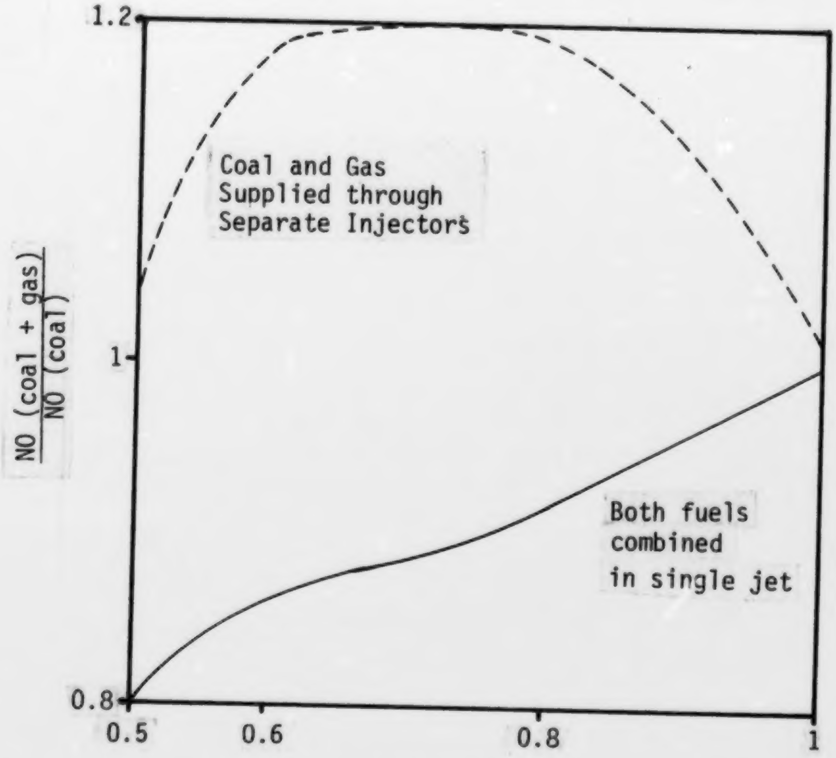

Effect of Mixed Fuel Firing on NO_x Emissions

- Emission Characteristics of Fuel Oil Flames

The emission characteristics of fuel oil containing significant quantities of bound nitrogen appear to follow similar trends to those observed with coal. Lower NO emissions were generally obtained if the fuel spray was narrow. The lowest emissions of approximately 100 ppm were obtained with axial fuel oil injection produced with an air blast atomizer. Further work is required under cold wall conditions to ensure that low NO conditions do not produce excessive amounts of particulate matter. The influence of thermal effects (air preheat and furnace heat extraction rate) should be investigated more fully. As shown below the influence of air preheat was found to vary with the fuel atomizer design.

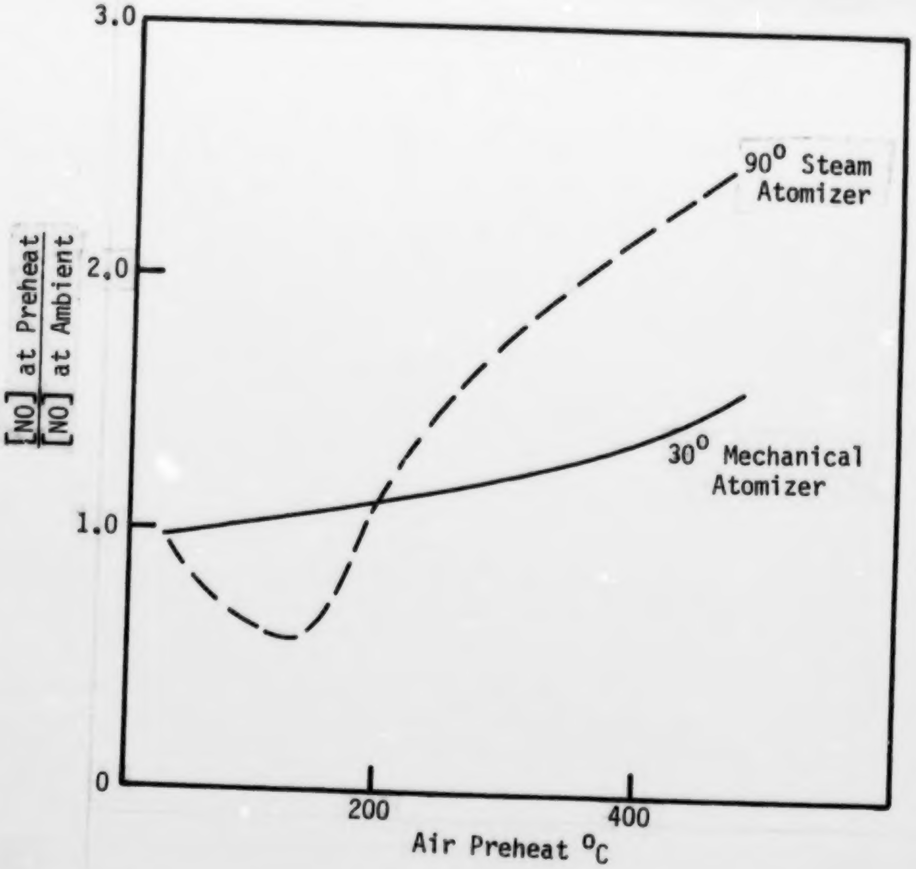

The Effect of Air Preheat on NO_x Emission from Residual Fuel Oil Can be Dependent Upon Atomizer Design Parameters

1.3 Radiative Heat Transfer Models

The ability to calculate radiative exchange within combustion systems is a necessary component of a predictive procedure capable of calculating combustor performance. The various methods of evaluating radiant heat exchange in enclosures have been reviewed from several aspects:

- their accuracy;
- their computational convenience;
- their suitability for coupling with elliptic field equations describing flow, mixing and heat release;
- their suitability for combining with the results of physical models to provide a short-term solution.

Effort was concentrated upon the development of flux models because of their suitability for integration with flow field models.

Although the Zone Method of analysis provides the most accurate method for the evaluation of radiant heat exchange under certain well-defined conditions it was deemed less appropriate for the needs of the total program. Its accuracy is reduced considerably if reasonable restrictions are placed on computer storage and run time where steep temperature and concentration gradients occur and there are wide variations in attentuation coefficients throughout the furnace volume. In general, flux models are less accurate than the Zone Method because of approximations involved in the description of intensity distribution at point. For those instances requiring greater accuracy continuous intensity distribution (CID) models have been developed whose accuracy is comparable to the accuracy of the Zone Method, but which require reduced computer requirements. They also have the added advantage that they can be combined easily with prediction procedures for other transfer processes.

The report describes the development of several radiative heat transfer models and their predictive capabilities have been compared with both experimental results and hypothetical test case results. Comparison with experimental furnace results does not necessarily provide the best method of evaluating radiative heat transfer models since discrepancies between measurement and prediction can be attributed to either: 1) errors in the calculation of radiative exchange; or 2) errors in the representation of the emission/absorption/scattering characteristics of the bounding walls and the furnace gases (which may include solid particles such as soot, ash, etc.). The following models have been developed and their characteristics evaluated:

- 2-flux models based upon the Spherical Harmonics and the Discrete Coordinate Method. Both of these are capable of predicting radiative heat transfer to furnace side walls with errors of less than 9 percent in the absence of steep axial gas and wall temperature gradients. Larger errors occur if steep gradients do exist as no account is taken of exchange perpendicular to the main 2-flux coordinate direction.

- 4-flux models based upon the Discrete Coordinate Method which gives predictions with errors of less than 10 percent in most instances even though steep axial wall and temperature gradients do occur. If the end wall is much cooler than the adjacent gas zone higher errors can occur close to this cold wall. Only slight errors are introduced into the prediction of total heat transferred because overpredictions in certain areas are balanced by underprediction in other areas.

- A CID model which represents the intensity distribution around a point as a continuous function (the discrete coordinate method assumes the intensity is constant over a certain solid angle introducing discontinuities). The CID model appears to have an accuracy approaching that of a Zone Model.

Inaccuracies in the prediction of radiative heat transfer in furnaces may be associated with the representation of the emission/absorption properties of furnace gases. Unidirectional intensity measurements are compared with predictions involving the representation of the real combustion gases as a gray gas, the sum of four gray gases or the sum of one clear and two gray gases.

Although it cannot be claimed the one gray gas assumption is accurate, it appears that for the circumstances tested it is equally as effective as either of the other approaches if steep concentration and temperature gradients do not exist. If gradients do exist, deviations between measured and predicted intensities can increase up to 40 percent. These errors are attributed to the representation of the radiative properties of the gases rather than to that of the wall. An extensive assessment of these errors has not been possible because of a lack of information on the spectral distribution of attenuation coefficients under furnace conditions.

2.0 FURNACE INVESTIGATIONS TO IDENTIFY BURNER DESIGN PARAMETERS CONTROLLING NO_x FORMATION IN NITROGEN-CONTAINING FUELS

2.1 Introduction

In an earlier furnace investigation the influence of several burner parameters on the emission of nitrogen oxides (NO_x) from natural gas and pulverized coal flames had been established(1). The burner parameters investigated include:

- the method of fuel injection;
- the position of the fuel injector relative to the burner exit;
- the geometry of the burner exit;
- the burner throat cross-sectional area;
- the degree of swirl applied to the secondary air; and
- the fraction of the total air supplied with the coal at fixed excess air levels.

The three parameters found to have a major influence on NO_x formations were the method of fuel injection, the degree of swirl, and the amount of primary air supplied with the coal.

The emission characteristics of two high volatile coals were investigated and it was found that NO_x levels varied by over 400 percent for fixed preheat and excess air levels. With the higher nitrogen coal, maximum emissions were found to be higher than those measured with the lower nitrogen coal, although the increase was not directly proportional to the increased nitrogen content. However, minimum emissions from both coals were similar. It was readily apparent from these studies that burner conditions giving rise to rapid coal/air mixing also produced high NO_x emissions. Conversely, those burner conditions which delayed coal/air mixing tended to give the lowest emissions. Unfortunately, the delayed mixing also produced long flames which could not be considered suitable for utility boiler applications since flame impingement upon the opposing wall would probably occur.

In order to explain the observations, two basic assumptions were made:

- Fuel NO accounted for the major portion of the total emission.
- Volatile fuel nitrogen fractions were mainly responsible for fuel NO formation.

Support for the former assumption was later provided by Pershing et al(2) who burned pulverized coal with both air and argon/oxygen mixtures. Pershing reports that for a single coal flame 80 percent of the total NO_x emission can be attributed to fuel nitrogen oxidation. The latter assumption was based on the fact that significant quantities of nitric oxide were produced very early in the combustion process, and the conditions under which a large proportion of the char burns out are mainly dependent upon input conditions and not upon burner variables. The studies of Fenimore(3), De Soete(4), Bartok et al(5) and Sarofim(6) indicated that under laboratory conditions fuel NO formation can be minimized if reaction takes place under fuel-rich conditions. Consequently, it appears that the design of low NO_x emitting combustion systems for pulverized coal and heavy fuel oil must delay the mixing of all the combustion air with the fuel for as long as possible consistent with the attainment of complete combustion.

These general conclusions are illustrated by the results presented in Figures 2.1 and 2.2. Figure 2.1 shows the emission characteristics of a radial fuel injector. The coal and primary air are injected at right angles to the secondary air stream from the burner throat, thus providing rapid coal/air mixing. The emission characteristics for two fuels of different nitrogen contents are almost insensitive to the amount of primary air, and the level of secondary air swirl. These are the burner conditions which give short, stable, intense flames; unfortunately, they also correspond to the conditions which maximize NO production. Alternatively, the results presented in Figure 2.2 illustrate those burner conditions which restrict NO formation. The coal is maintained as a coherent jet on the flame axis and is injected with the minimum primary air and at the maximum velocity. The ignition front which surrounds the coal jet provides the "diffusion flame" type environment for reaction of the fuel nitrogen intermediates.

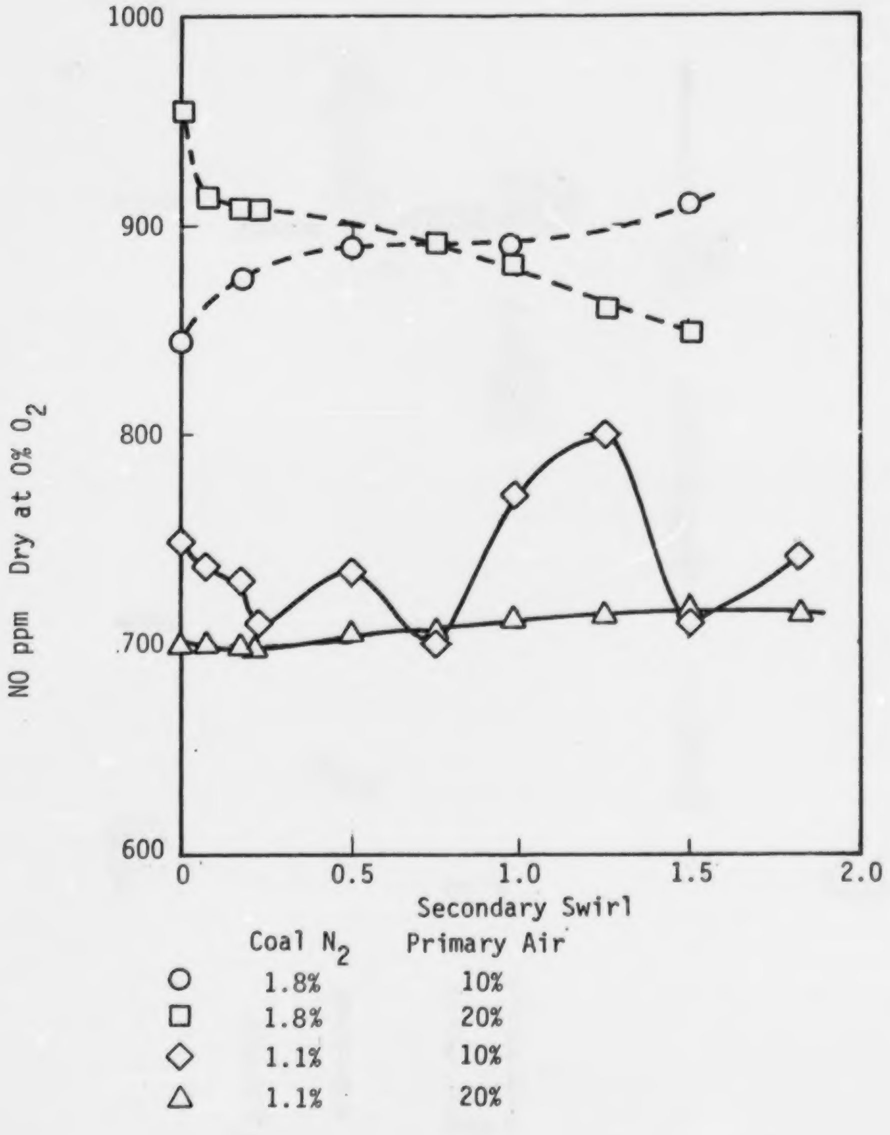

Figure 2.1. Emission Characteristics of Pulverized Coal Flames Produced with Radial Fuel Injection (5% Excess Air, 300°C Preheat)

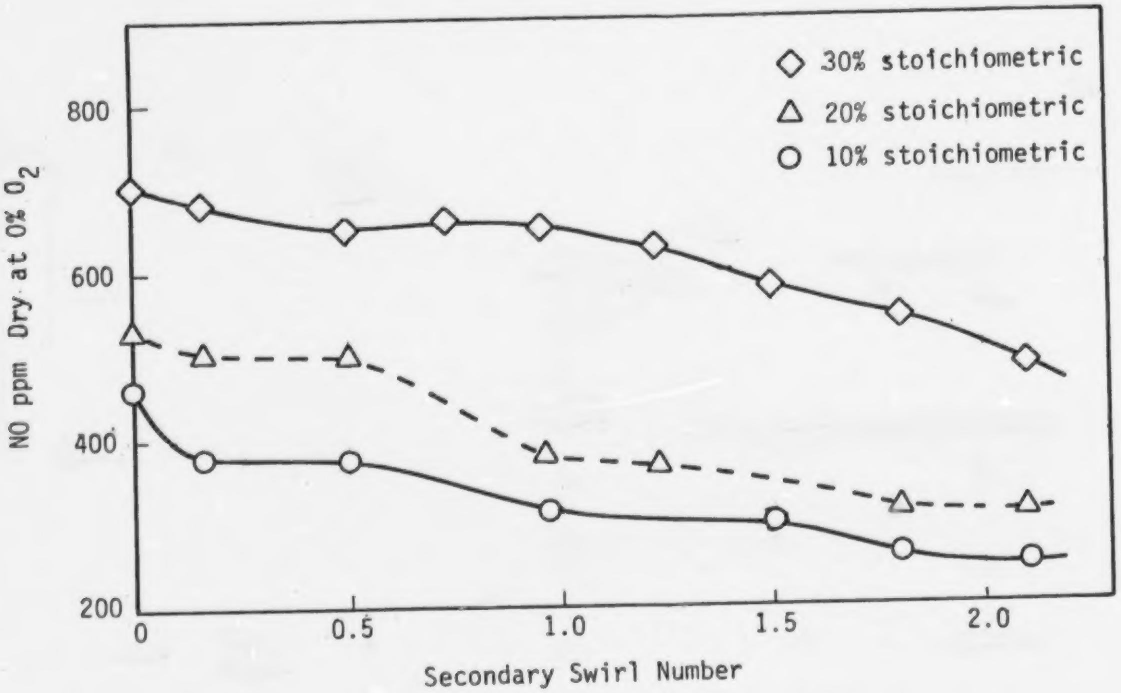

Figure 2.2. Emission Characteristics of Pulverized Coal Flames Produced with Axial Fuel Injection (300°C Preheat, 5 Percent Excess Air and 1.1 Percent Nitrogen Coal)

Based upon the results of the first series of investigations a second series of furnace investigations was planned with the following objectives:

- To Determine the Influence of Burner Design Parameters on NO_x Formation in Fuel Oil Flames

  In simplistic terms, fuel oil can be considered as an intermediate case between natural gas and pulverized coal with respect to nitrogen content and preparation to burn time. From experience gained in earlier investigations, it could be expected that the following factors would influence NO formation in fuel oil flames:

  - the mode of atomization;
  - the path of fuel oil droplets in relation to the recirculation zone;
  - the composition of the atomizer fluid; and
  - the rate of entrainment of external recirculation.

  Consequently, a series of investigations were planned with the intention of varying the design characteristics of the fuel/air injection process which would influence the above factors.

- To Establish the Characteristics of a Subscale Practical Burner

  The earlier investigations were carried out using a versatile test burner which was capable of simulating a wide variety of fuel/air mixing patterns. By comparing the emission characteristics of this test burner with those of a subscale practical burner being used by Armento and Sage(7) it was hoped to provide a basis for comparison between two investigations concerned with the emission of NO_x from pulverized coal flames. A further objective was to investigate those modifications which would allow NO_x emissions to be reduced from a practical system.

- To Quantify the Influence of Air Preheat on Pollutant Emission for Different Burner Parameters

  The influence of air preheat on pollutant formation in turbulent diffusion flames had been investigated by several workers(7,8,9). The object of these investigations was to establish the influence of both burner parameters and air preheat upon NO formation since the effect of preheat may be influenced by the rate of fuel/air mixing. It was argued that the rate of devolatization would increase with increasing air preheat levels providing the opportunity for more of the volatile nitrogen compounds to react under fuel-rich conditions.

- To Identify NO_x Control Options Which Do Not Compromise System Efficiency

Burner modifications which control NO_x emissions and yet do not satisfy system requirements are unacceptable. A triple concentric burner system was designed with the intention of satisfying the dual criteria of low pollutant emission and acceptable combustion characteristics. In this burner the total air supply was divided into three streams in an attempt to produce short intense flames with rapid burnout and yet achieve low NO_x emissions because of the generation of fuel-rich mixtures in the early stages of heat release.

- To Determine the Influence of Dual-Fuel Firing on NO_x Emissions

One of the general conclusions drawn from the earlier investigations was that the oxygen content of the primary stream had a strong influence on nitric oxide production. Consequently, it was planned to use fuel gas as the transport medium to test the hypothesis that the lowest NO levels would be obtained when the volatile fractions were denied the presence of oxygen as they were released from the coal particles. A full series of investigations were planned to establish the effect of several methods of firing gaseous and solid fuels simultaneously.

One of the major factors concerning the credibility of furnace investigations is the reproducibility of the experimental results. It can be seen from the results presented in Figure 2.3 that emission levels measured with natural gas were reproducible. The coals used in both investigations were purchased from the same mine; however, the

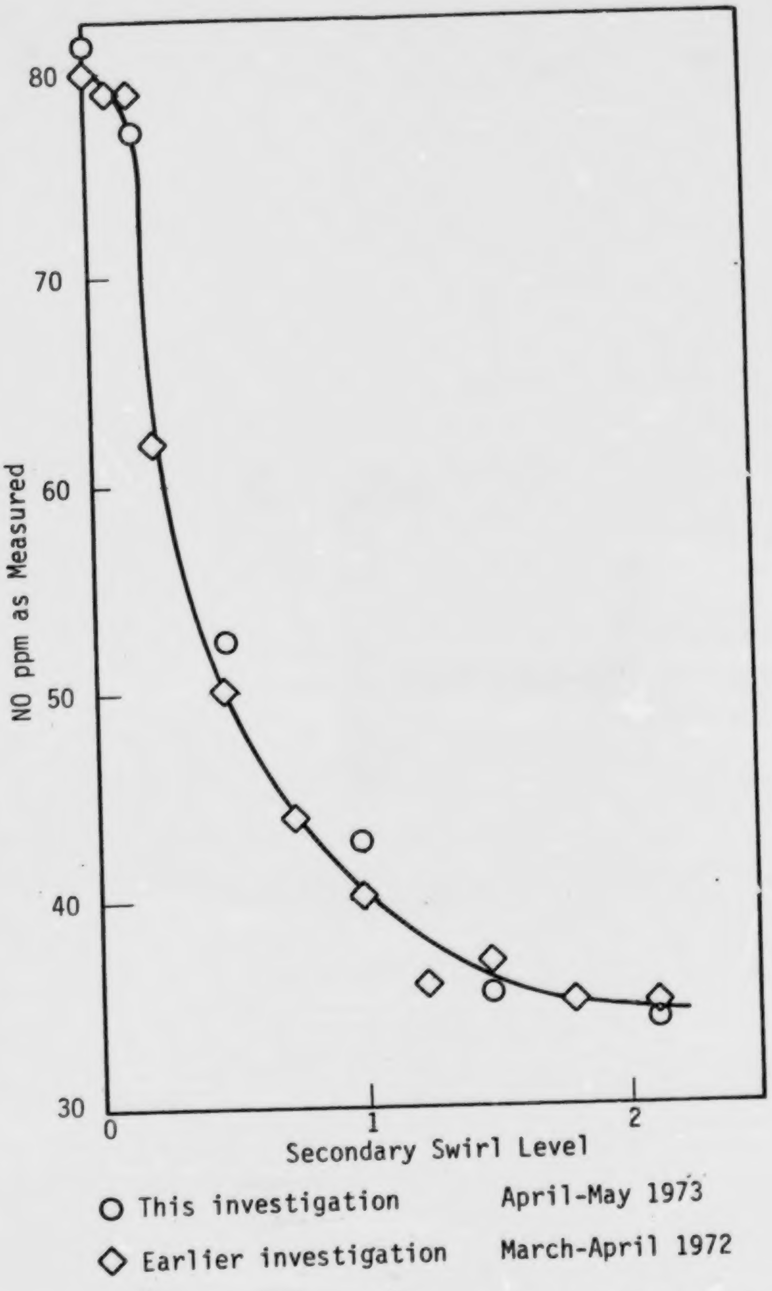

Figure 2.3. Reproducibility of Emission Levels with Natural Gas Firing (5% Excess Air, Ambient Air and a Divergent Fuel Injector)

precise experimental conditions were not duplicated. The results presented in Figure 2.4 clearly indicate that the results of both investigations are comparable.

F 2.4

2.2 Experimental Conditions

Furnace

The investigations were carried out in the IJmuiden No. 1 furnace, a complete description of which has been presented earlier(1). The furnace is a horizontal, refractory tunnel of approximately square cross section, with internal dimensions 2m x 2m x 6.25m. In these investigations only the minimum cooling load was employed in order to prevent excessive refractory temperatures.

furnace

Fuels

Details of the fuels used during the investigations are given in Tables 2-1, -2 and -3 for Slochteren natural gas, No. 6 fuel oil and the high volatile coal. The coal was purchased from the same mine as that used during the earlier investigations.

Tables 1, 2, 3

Burners

Three basic burner systems were used during these investigations:

- the double concentric swirl burner used in the earlier tests;
- a triple concentric burner; and
- a subscale practical burner.

Details of the double concentric burner designed by Leuckel(8) have been presented in an earlier report. The burner readily allows the influence of a large number of burner parameters on the formation of nitric oxide to be investigated with the expenditure of the minimum amount of experimental time. This burner also provided the primary and secondary sections of a triple concentric burner system. Several tertiary injection systems were designed, based upon two tertiary duct diameters of 340 and 402 mm. The tertiary air could be injected either with or without swirl

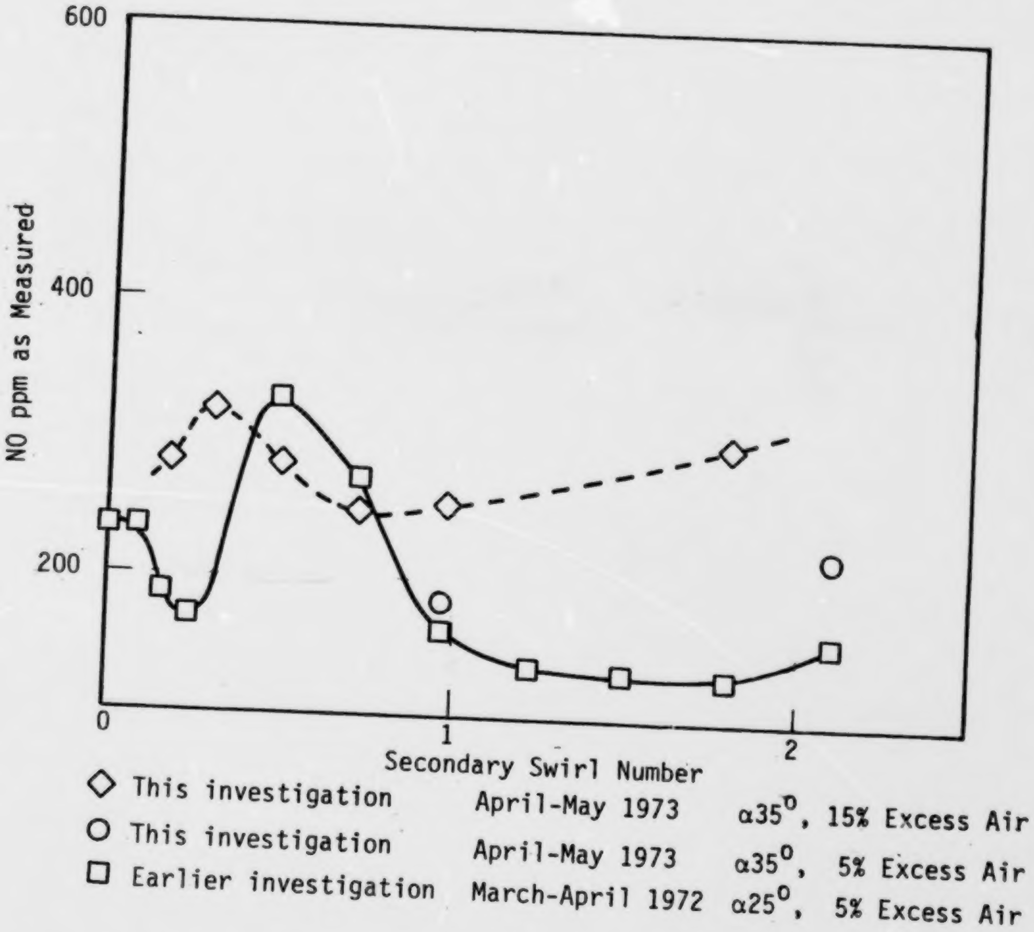

Figure 2.4. Reproducibility of Emission Levels with Pulverized Coal Firing (300° Preheat Axial Fuel Injection 10% Primary Air)

Table 2-1. Nominal Composition of Slochteren Natural Gas

Component	Percentage by Volume
CH_4	81.3
C_2H_6	2.9
C_3H_8	0.4
C_4H_{10}	0.1
C_nH_m	0.1
CO_2	0.8
N_2	14.4

Table 2-2. Properties of No. 6 Fuel Oil

Carbon content	86.05%
Hydrogen content	11.54%
Sulfur content	0.57%
Nitrogen content	0.24%
Density	870 kg/Nm^3
Viscosity	800 sec R.1 @ 50°C
L.C.V.	9800 Kcal/kg

Table 2-3. Properties of High Volatile Coal

Volatile content	32.68%
Ash content	6.20%
Carbon content	78.48%
Hydrogen content	4.77%
Nitrogen content	1.05%
Sulfur content	0.75%
L.C.V.	7480 Kcal/kg dry

imparted by three interchangeable sets of fixed vanes with angles of 30°, 45° and 60°. A schematic of the assembled triple concentric system is presented in Figure 2.5 illustrating the various possibilities.

Figure 2.6 presents details of the subscale practical burner. This basic design was also used by Armento and Sage(7). The secondary air was swirled by six fixed curved swirl vanes. Two refractory exits were constructed with 35° and 45° divergent exits.

Fuel Injection Systems

All three of the burner systems described above were constructed so as to accept a primary fuel gun of 60.4 mms outside diameter. The moving block swirl burner would also accept a fuel gun of 115 mms outside diameter suitable for pulverized coal and coal/gas firing. With the exception of the coal spreader injector (described below), the fuel injectors used for natural gas and pulverized coal had been used previously and were described in Volume I.

Three types of fuel oil atomizers were used during the furnace investigations:

- Pressure jet atomizers - (Figure 2.7a) the mechanical atomizers were designed to operate at 20 atmospheres. Spray angles of 30°, 50°, 70° and 90° were available.
- Air atomized - the single hole air atomized injector is detailed in Figure 2.7b. This atomizer was used, not because it was considered typical of industrial practice, but because it provided a situation in which the nitrogen-containing fuel could be maintained as a single jet on the flame axis. If the results obtained with pulverized coal could be considered as an indicator, then this type of injector should give low NO_x emissions although the flame characteristics of this low emission oil flame would be as unsuitable for utility boilers as the comparable coal flame. This injector was originally designed by Leuckel(8).

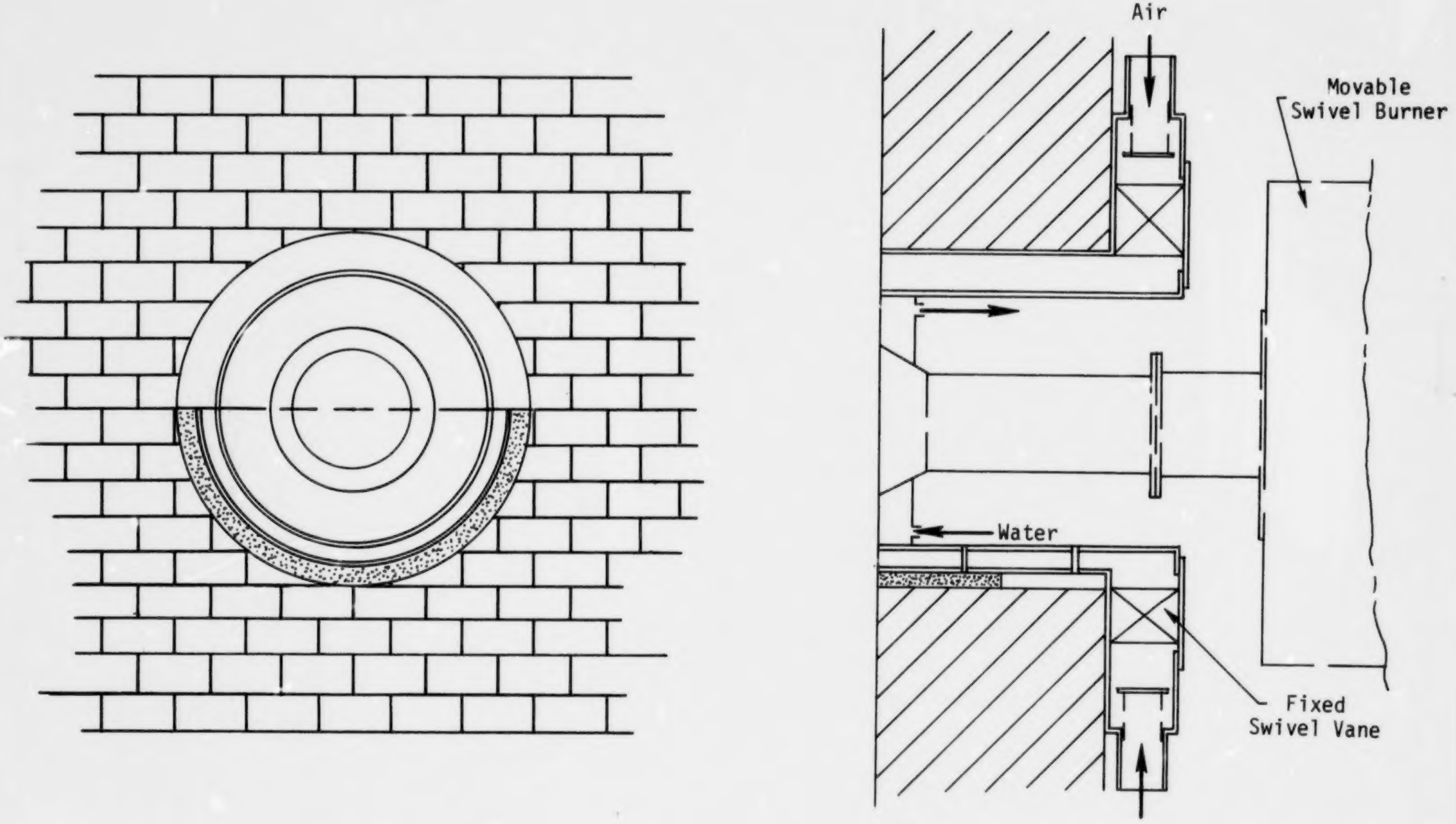
Air
Movable
Swivel Burner
Water
Fixed
Swivel Vane

Figure 2.5. Details of the Triple Concentric Burner Showing Two Tertiary Duct Diameters

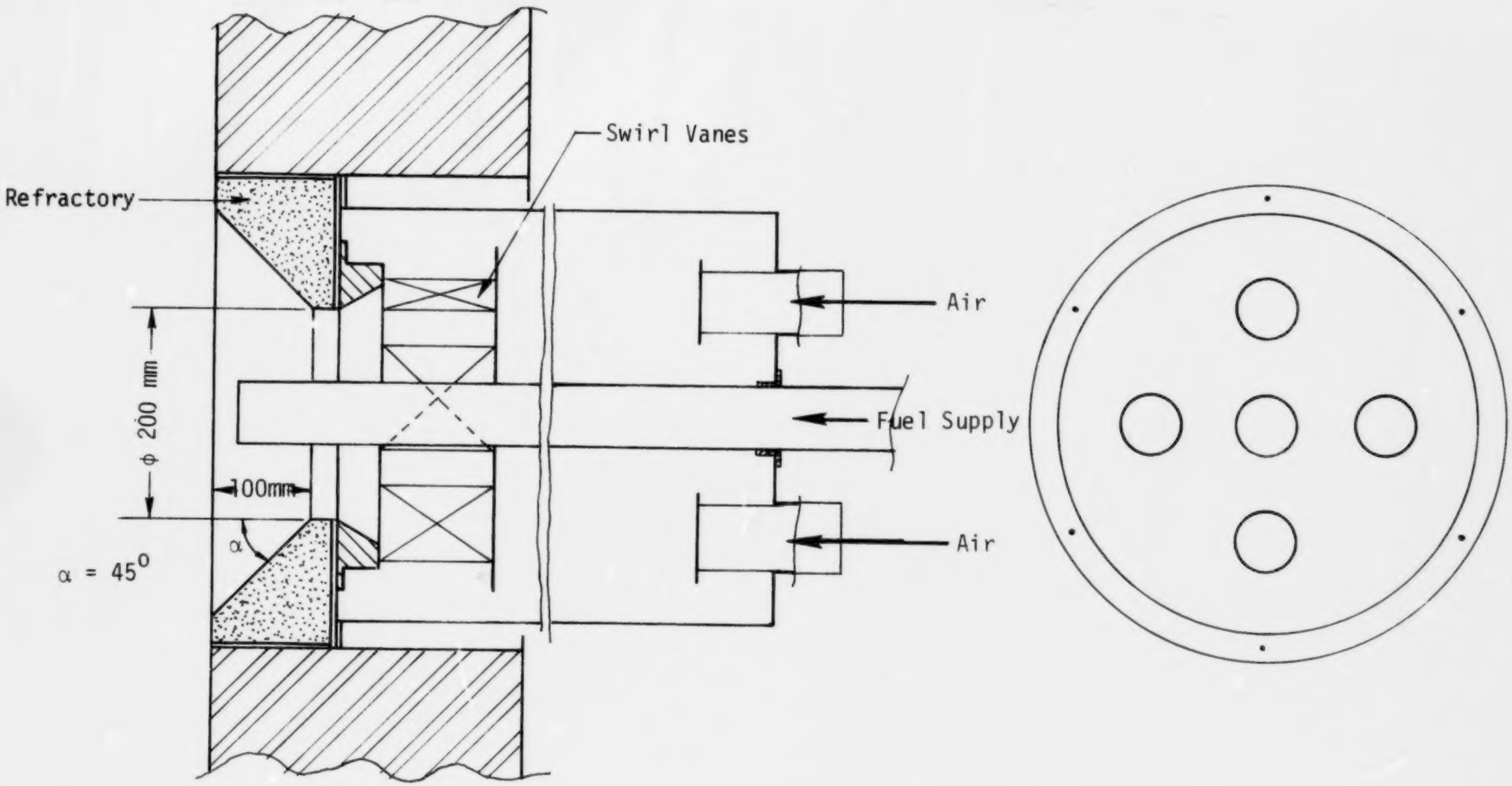
Swirl Vanes
Refractory
Air
Fuel Supply
Air
φ 200 mm
100mm
α
α = 45°

Figure 2.6. Sketch Showing the Construction of the Subscale Practical Burner (after the design of Armato(7).

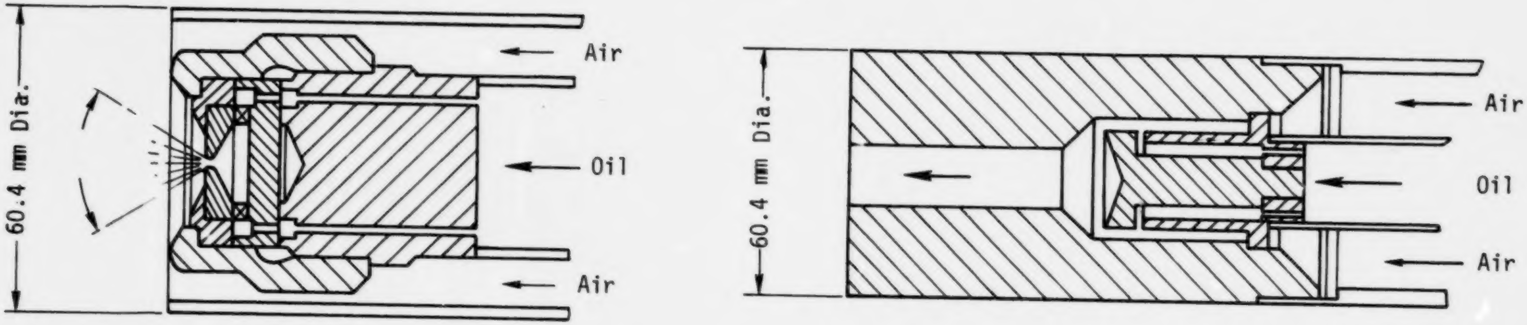
Air
Oil
Air
60.4 mm Dia.
Air
Oil
Air
60.4 mm Dia.

2.7a Pressure Jet

2.7b Single-Hole Air Atomized Injector

Figure 2.7. Details of Fuel Oil Injectors

- Steam atomized - several steam atomized Y-Jets of 70°, 80° and 90° were available. The designs for these Y-Jets were provided by Hamworthy Engineering, Ltd., of Poole England.

Figure 2.8 presents details of the coal spreader, the design of which was based upon information given by Armento and Sage(7). This is a subscale version of the type of injectors used in wall-fired utility boilers, the function of which is to provide stable early ignition with minimum flame length. F8

Two different methods were employed to simultaneously burn pulverized coal and natural gas. Both fuels were delivered through the same injector, either natural gas was added to the coal primary air mixture or natural gas was used instead of primary air as the coal transport medium. Two types of gas injectors were used:

- the gas was injected through 16 9.6 mm diameter holes from the periphery of the throat at an angle of 60° to the burner axis, and
- the gas was supplied through an annular duct surrounding the axial coal feed. The gaseous fuel was then injected through 16 separate orifices parallel to or perpendicular to the burner axis.

Four different coal injectors were used during the dual fuel investigations; three axial and one radial. Details of the fuel injection system are presented in Table 2-4. T4

Measurement Systems

The analytical and sampling techniques used in the second series of furnace investigations were those used in the first furnace trials and have been described in detail elsewhere(1).

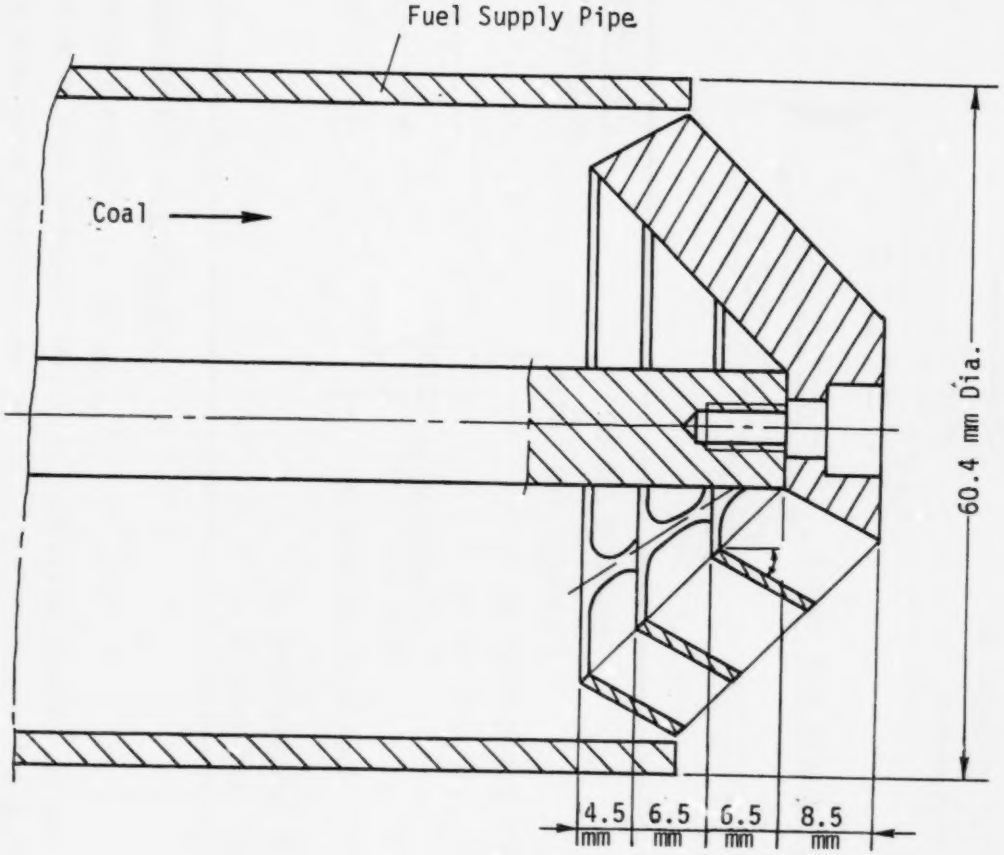
Fuel Supply Pipe
Coal
60.4 mm Dia.
4.5 mm
6.5 mm
6.5 mm
8.5 mm

Figure 2.8. Coal Spreader Injector

Table 2-4. Fuel Injector Characteristics

Peripheral Gas Injector

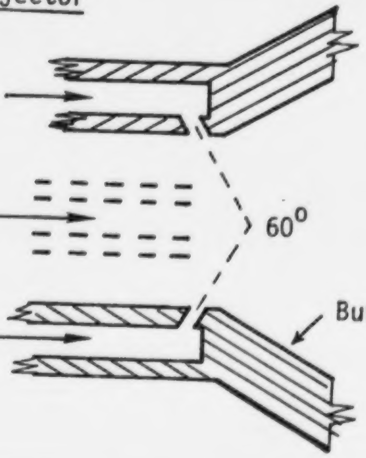
Gas
Coal
60°
Gas
Burner Exit Divergent

16 Injection Orifices
9.6 mm dia.

Axial or Radial Gas Injection

16 Gas Orifices

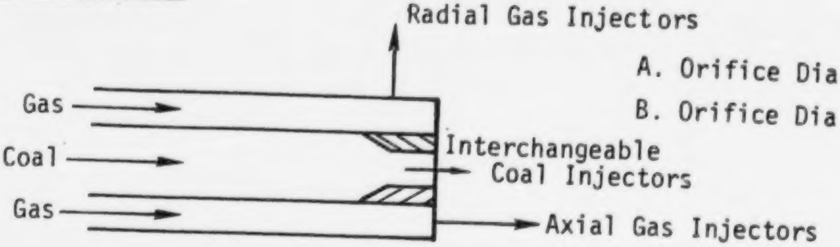
Radial Gas Injectors
Gas
Coal
Gas
Interchangeable Coal Injectors
Axial Gas Injectors

Radial Gas Injectors

A. Orifice Dia. 9.6 mm
B. Orifice Dia. 4.7 mm

Axial Gas Injectors

C. Orifice Dia. 9.6 mm
F. Orifice Dia. 3.2 mm

Interchangeable Coal Injector

Outside Diameter 60 mm

Single Hole Axial Injector	No. 1	Orifice Diameter 46 mm
Single Hole Axial Injector	No. 2	39 mm
Single Hole Axial Injector	No. 3	33 mm
Radial Hole Injector (16 Holes)	No. 36	96 mm

2.3 Results of the Furnace Investigations

2.3.1 The Emission Characteristics of a Subscale Practical Burner

The emission characteristics of a burner system similar to that used in the work of Armento and Sage(7) was investigated in the IFRF furnace to provide a basis for comparison between the two investigations. Details of the input conditions and measured emissions are presented in Tables 2-5 and 2-6. Figures 2.9, 2.10 and 2.11 present the measured NO* levels as a function of excess air at three firing rates. Preheat level was found to have very little influence on NO emissions below 300°C, but emissions increased considerably between 300°C and 450°C. Similar trends were observed with load, very little influence on emissions was observed when load was increased up to 200 kg/hr, but further load increases caused a considerable increase in the NO emissions.

T5
T6
F 9, 10,
11

NO levels greater than 1700 ppm were measured at high loads, high excess air and high preheat. These results were obtained when the furnace was almost uncooled and the wall temperatures in the vicinity of the burner were approximately 1600°C. These high emission levels could not be repeated when the wall temperature was held below 1400°C even though the burner input conditions were controlled at the same level. Under cold wall conditions emissions levels were reduced by greater than 500 ppm to about 1200 ppm.

Figures 2.12 and 2.13 show the influence of primary air percentage and position of the fuel injector on the emission characteristics of the subscale practical burner. As in the earlier investigations, movement of the coal injector forward from the throat reduced emissions of NO. The amount of NO emitted was also reduced when the proportion of primary air was increased. This observation tends to conflict with some of the earlier results and it is believed that the increase in axial momentum decreased the tendency for the coal to spread radially. Changes in both the position of the fuel injector and the proportion of primary air reduced emissions but also caused a visible increase in flame length.

F
12, 13

---

* All NO levels presented in this section refer to values corrected to 0 percent O_2 unless stated otherwise.

Table 2.5. Input Conditions for Investigations Involving the Subscale Practical Burner

Run No.	Firing Rate kg/hr	Preheat °C
195	200	300
197	200	450
199	300	450
201	150	450
204	300	300
205	150	300
206	150	150
207	200	150

Table 2.6. Emission Levels for Subscale Burner Investigations (Nominal Baseline Input 200 kg/hr)

	NO ppm				
Excess Air	5%	10%	15%	20%	30%
Run No. 195	558	724	764	789	828
197	867	1027	1142	1178	1225
199	1166	1472	1718	1809	1792
201	825	1071	1138	1254	1329
204	898	990	1150	1161	1155
205	417	572	711	809	880
206	517	628	685	736	844
207	475	609	762	833	877

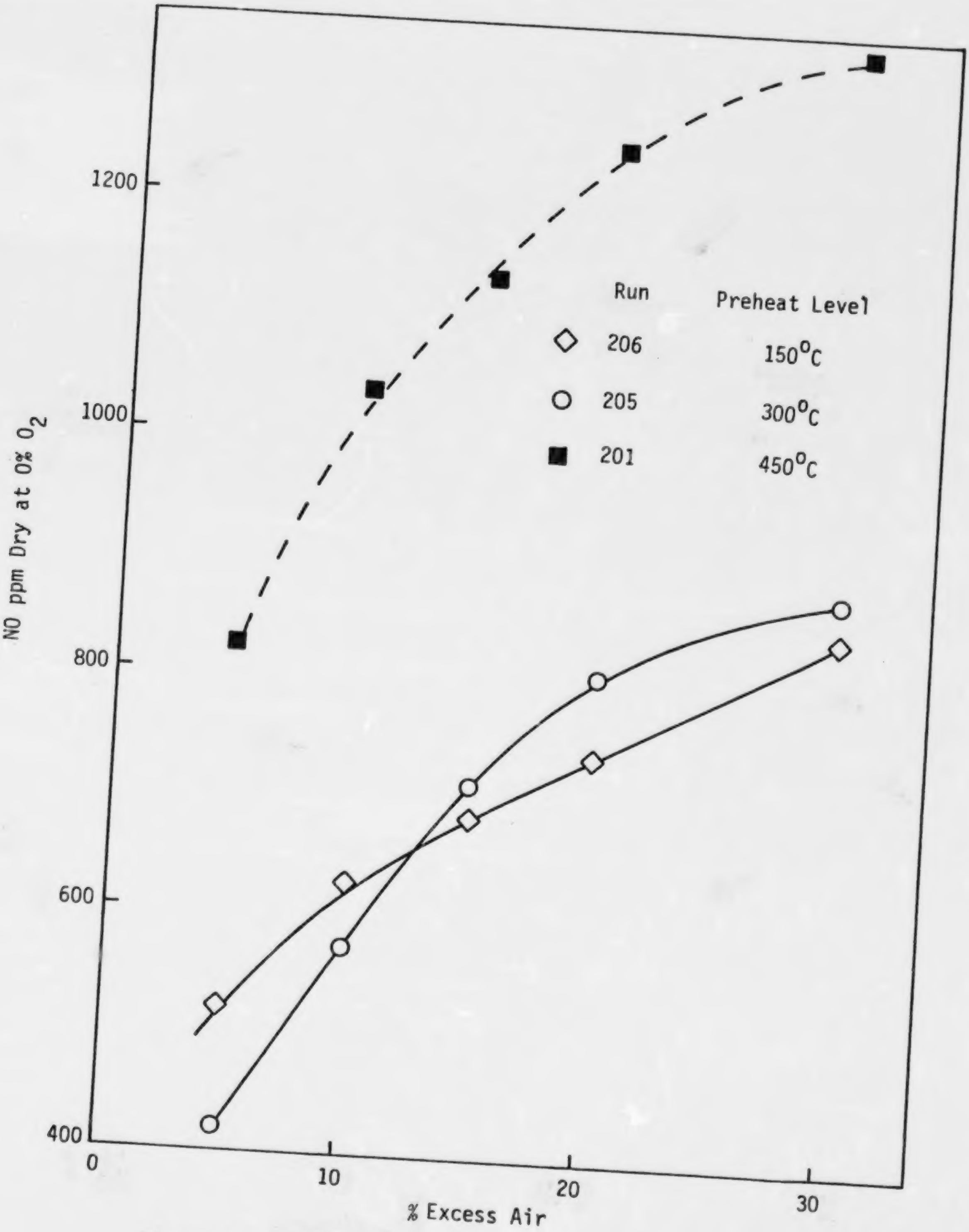

Figure 2.9. The Effect of Excess Air on NO Emission
Subscale Practical Burner (Coal Rate 150 kg/h)

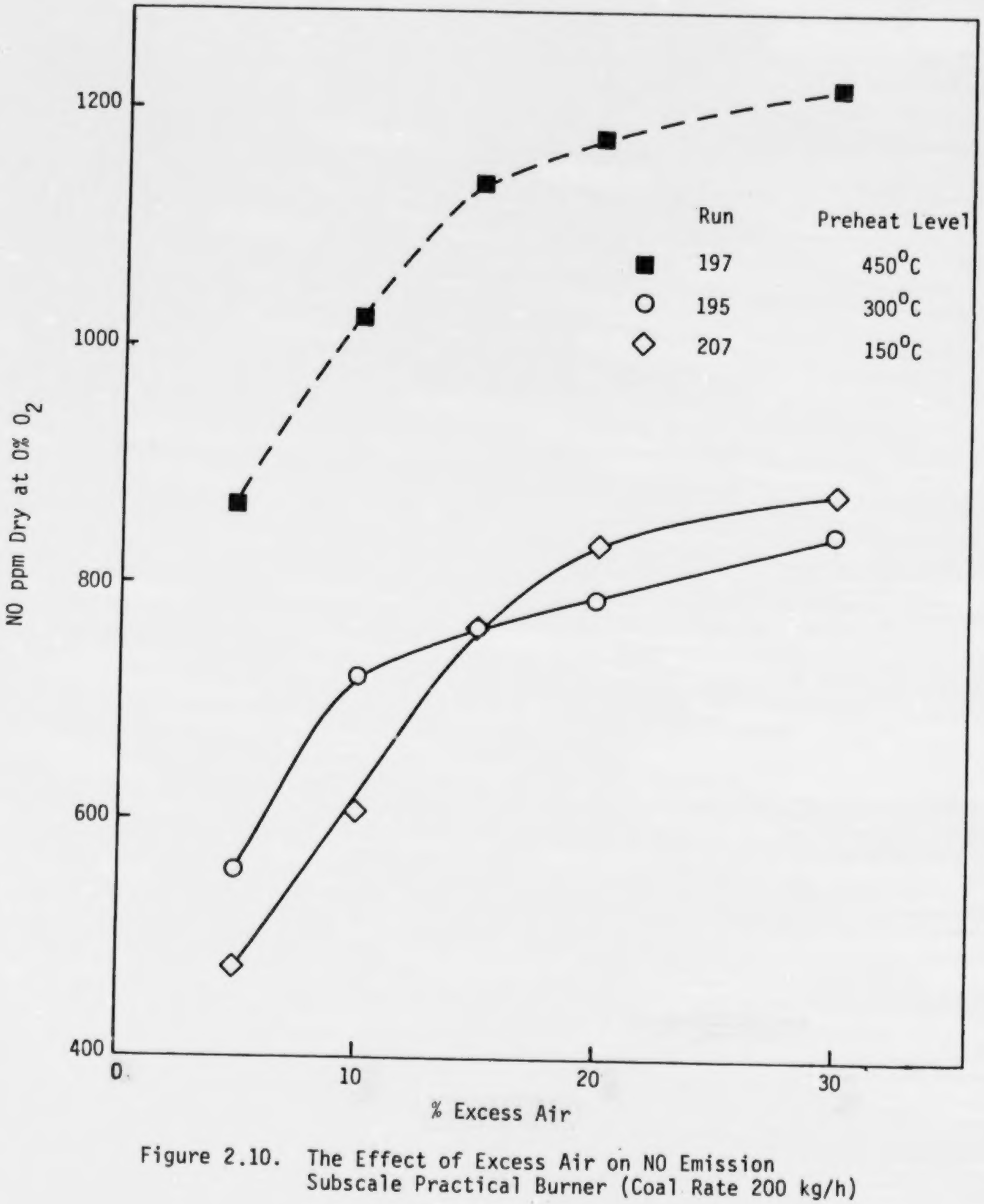

Figure 2.10. The Effect of Excess Air on NO Emission Subscale Practical Burner (Coal Rate 200 kg/h)

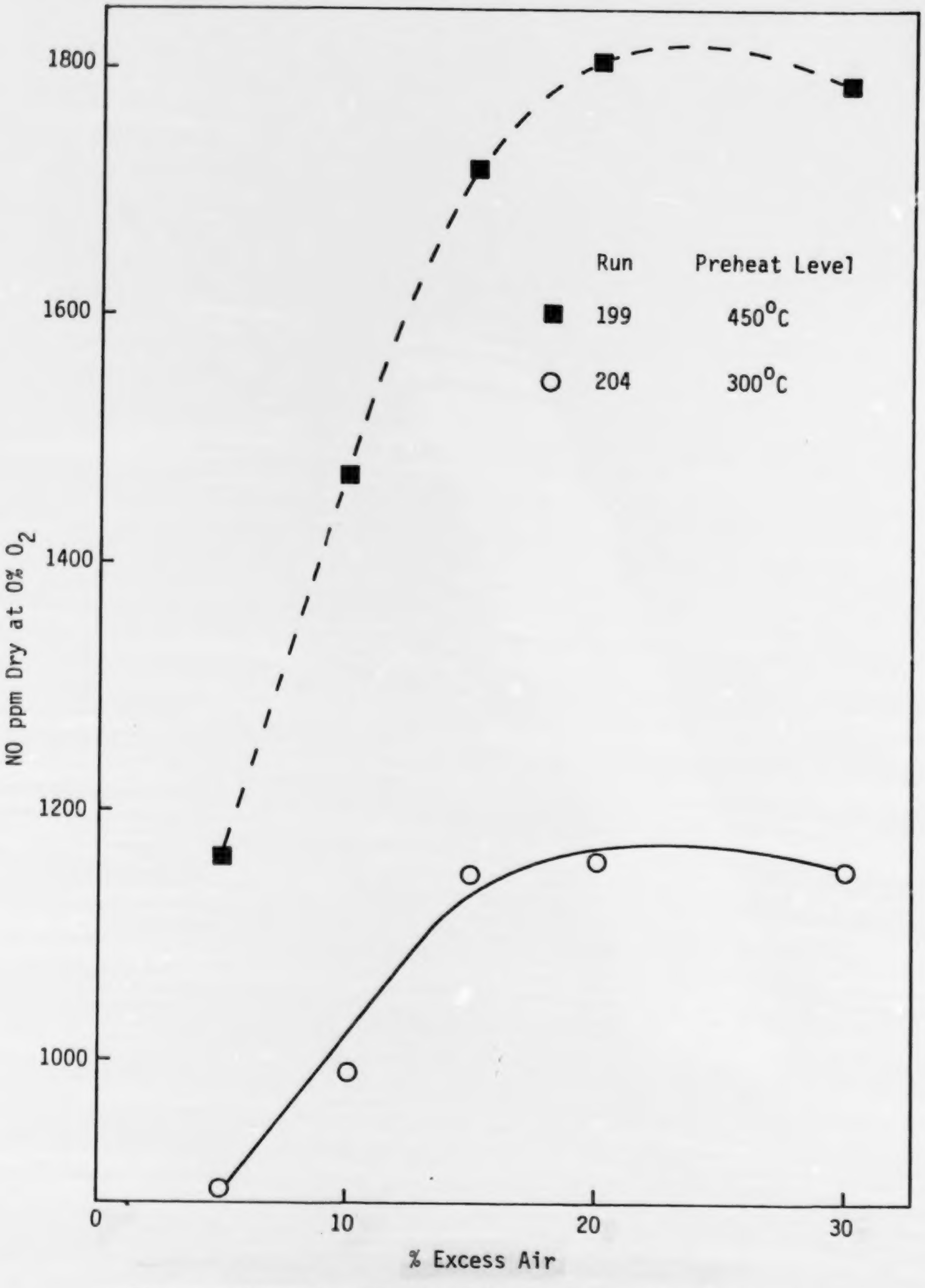

Figure 2.11. The Effect of Excess Air on NO Emission Subscale Practical Burner (Coal Rate 300 kg/h)

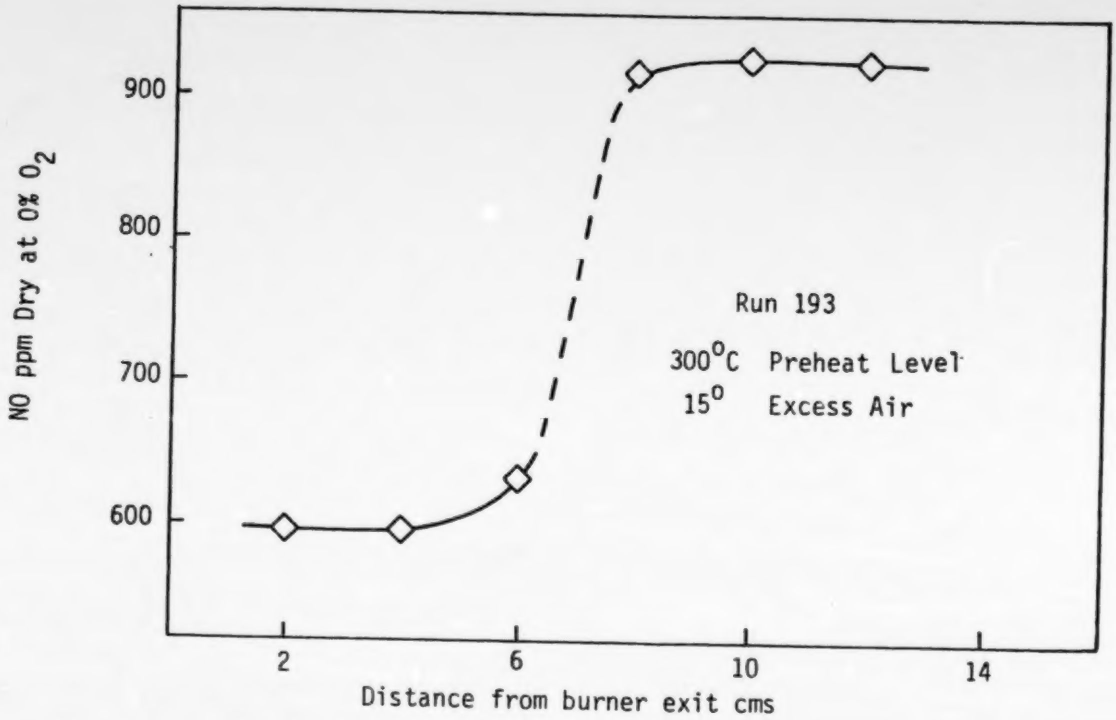

Figure 2.12. The Effect of Coal Spreader Position on NO Emission (Subscale Practical Burner Coal Input 200 kg/hr)

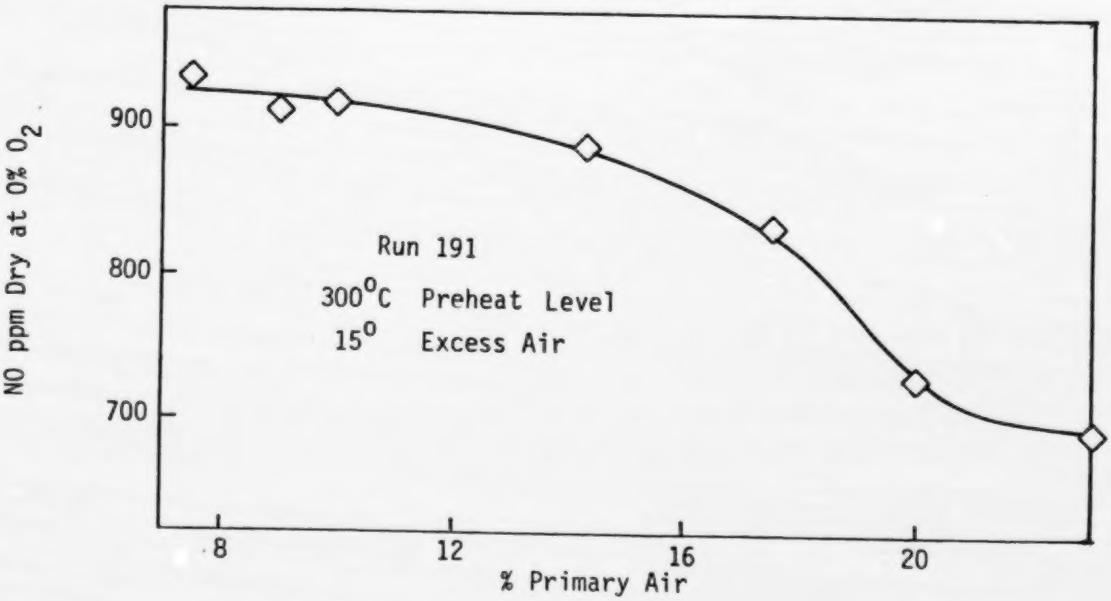

Figure 2.13. The Effect of Primary Air Supply (Coal Subscale Practical Burner)

Changing the fuel injector type also gave significant variations in the NO concentration of the combustion products (see Figure 2.14). The use of a radial coal injection nozzle increased emissions slightly, and in agreement with earlier observations, it was found that emissions were almost independent of the amount of primary air. Emissions from this fixed swirl burner could be reduced by 400 ppm if an axial coal injector was used. However, the visible flame length also increased. F14

The results presented in Figure 2.15 were obtained with the coal spreader injector and the movable block swirl burner in an attempt to learn more about the interaction of secondary swirl and fuel injection characteristics. The measurements indicate three distinctly different zones: F15

- at low swirl levels the fuel jet remains on the burner axis and the ignition front could not be established at the injector;
- at medium swirl levels the emissions are maximum, the coal jet diverges around an internal recirculation zone producing a short, high intensity flame; and
- at high swirl levels the tail of the flame appears to collapse, producing a "ball" flame, and the NO level is reduced by approximately 300 ppm. As the swirl was increased, the flame went through an unstable condition when the flame would change from the low to the high NO level intermittently. It is believed that these changes in flame characteristics could have been triggered by small variations in coal feed rate and reflect some influence of heat release on the static pressure field.

NOTE: NO_x emissions were found to be correlated best using relative swirl (R_s) where zero is axial secondary air flow and 1.0 is maximum tangential velocity.

2.3.2 Tertiary Air Injection to Control NO_x Formation

The results presented in the previous section give an indication of the emission characteristics of a subscale version of a burner used in systems of practical interest. Although the combustion environment was different from those encountered in utility boilers, the measured emission levels were typical of those reported for practical systems and are very

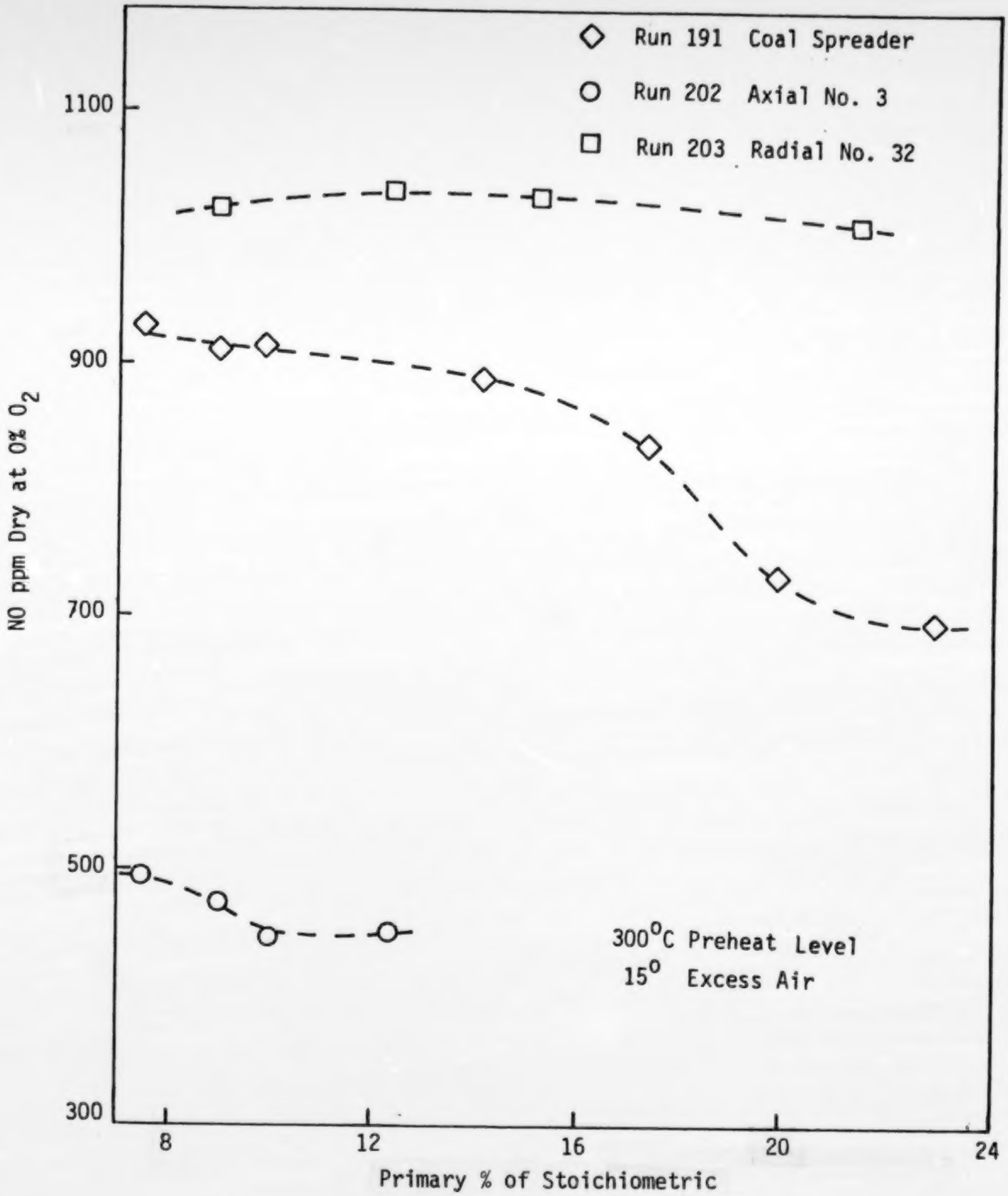

Figure 2.14. Effect of Fuel Injector Type With Subscale Practical Burner

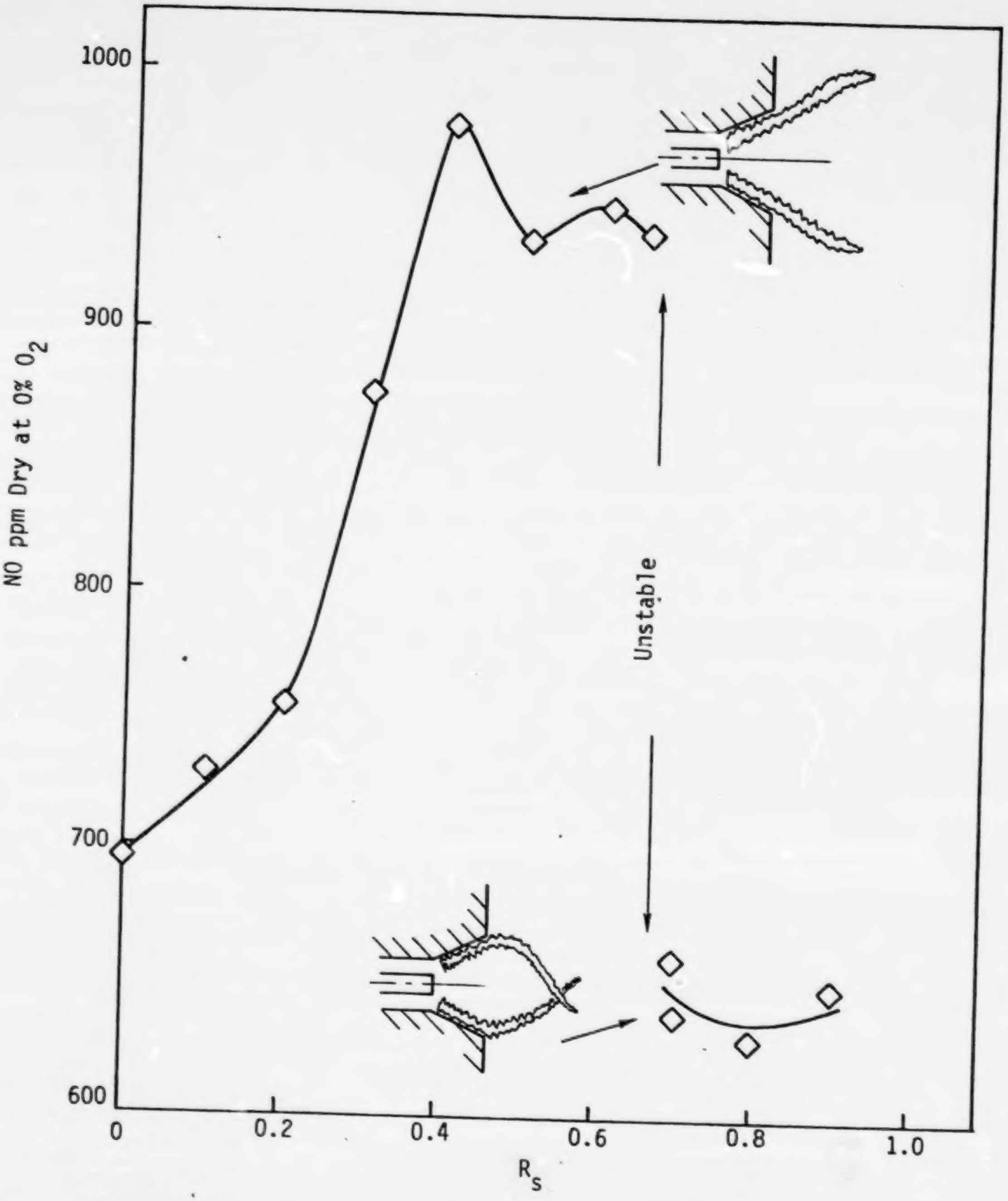

Figure 2.15. The Effect of Swirl on the Emission Characteristics of Pulverized Fuel Flames Produced with a Coal Spreader

similar to those reported by Armento(7). Attempts were made to reduce emissions by making minor changes to the burner and the air supply. The major objective of the second series of furnace investigations was to attempt to reduce NO formation by delaying fuel/air mixing and yet produce a flame of similar size and shape to that produced by operational burners. It was hoped that this could be attained by dividing the air into three streams:

- primary air supplied with the fuel;
- secondary air introduced at the burner throat in the annulus around the fuel injector; and
- tertiary air injected from the furnace wall at the periphery of the burner exit.

Sketches of the various tertiary air injection systems used throughout the investigations are presented in Figure 2.16, and Table 1.7 lists the conditions investigated. If ϕ_{ps}, the equivalence ratio of the primary/secondary stream, is less than 1, the burner was being operated in a staged condition. Prior to the furnace investigations it was intended that the influence of the design parameters of the S-type system would occupy the major effort. However, preliminary investigations rapidly indicated that as air was transferred from the secondary to the tertiary stream NO emissions increased rather than decreased. An example of these preliminary results for natural gas is presented in Figure 2.17. NO levels were more than doubled when 50 percent of the total air was supplied through the tertiary duct. These were precisely those furnace conditions which had yielded NO levels of less than 30 ppm without tertiary injection. The increase in emission was unexpected, and the exit area of the tertiary duct was reduced to increase the exit velocity. This modified version is labeled R in Figure 2.16.

F16
T7
F17

The results with the modified tertiary duct were still not encouraging although the increased emission with tertiary air injection was not as pronounced as had been experienced earlier. The results obtained with this system are presented in Figures 2.18 through 2.21. The influence of tertiary air injection was found to vary with both the type of fuel and the method of fuel injection. Minor reductions in NO emissions were observed with natural

F18
20,21

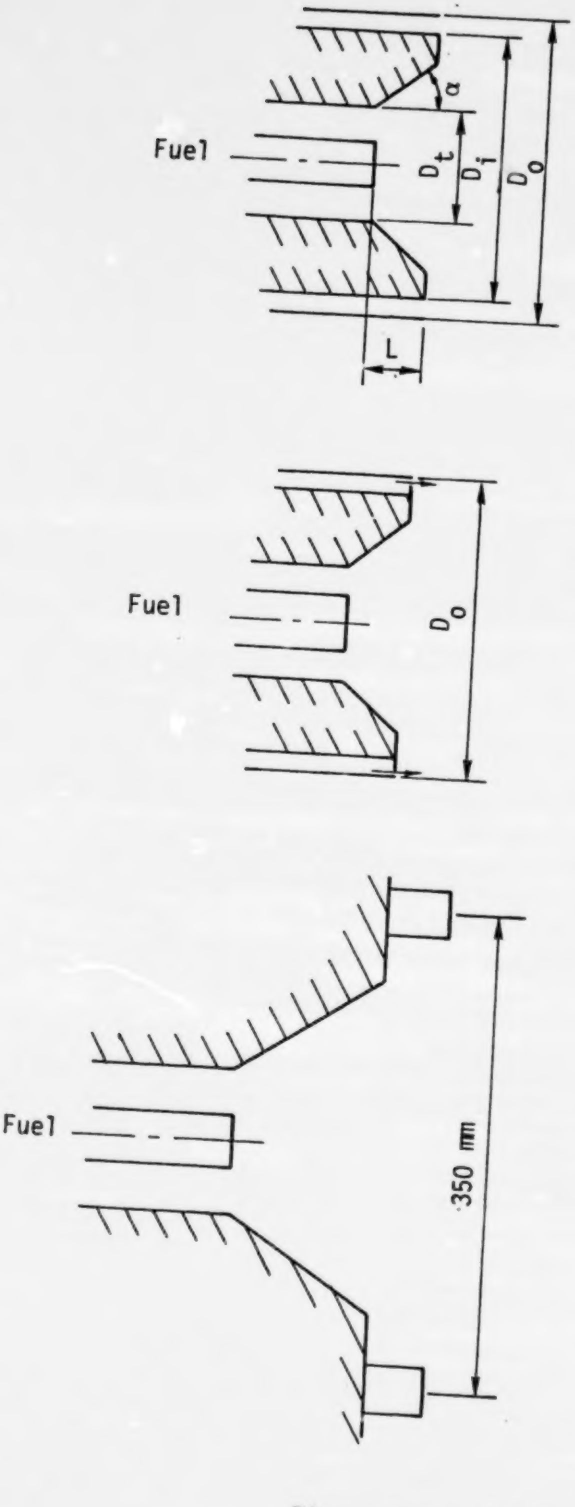
Fuel
α
D_t
D_i
D_o
L
Fuel
D_o
Fuel
350 mm

Duct S

$L/D = 1$

$D_t = 131$ mm

$D_i = 250$ mm

$D_o = 340$ mm

Duct R

(As Above)

Tertiary Air Injected Through an 8 mm Slit

$D_o = 340$ mm

Ring 1: Injection Top Bottom (2 x 14) 12 mm Holes

Ring 2: Injection Through 28 12 mm Holes Arranged Symmetrically

Figure 2.16. Tertiary Systems

Table 2.7. Input Conditions for Tertiary Air Injection Systems

(ϕ_{ps} is the Primary Zone Equivalence Ratio and ϕ_t is the Fraction of Stoichiometric Air Supplied in the Tertiary Duct)

Run	Fuel Injector Type	Tertiary Systems	ϕ_{ps}	ϕ_t	Excess Air (%)	Preheat (°C)
87	Radial no. 33 gas	S	1.05	0	5	30
88	Radial no. 33 gas	S	.925	0.125	5	30
89	Radial No. 33 gas	S	.75	0.30	5	30
90	Radial No. 33 gas	S	.50	0.55	5	30
103	Radial no. 33 gas	R	.925	0.125	5	30
104	Radial no. 33 gas	R	.75	0.30	5	30
105	Radial no. 33 gas	R	.50	0.55	5	30
106	Radial No. 33 gas	R	.35	0.70	5	30
107	Pressure jet 30° oil	R	1.05	0	5	30
108	Pressure jet 30° oil	R	.95	0.10	5	30
109	Pressure jet 30° oil	R	.75	0.30	5	30
110	Pressure jet 30° oil	R	.50	0.65	5	30
111	Radial no. 32 coal	R	1.15	0	15	300
112	Radial no. 32 coal	R	.90	0.25	15	300
113	Radial no. 32 coal	R	.75	0.40	15	300
114	Radial no. 32 coal	R	.50	0.65	15	300
118	Single hole no. 3 coal	R	1.15	0	15	300
119	Single hole no. 3 coal	R	.90	0.25	15	300
120	Single hole no. 3 coal	R	.75	0.40	15	300
121	Single hole no. 3 coal	R	.50	0.65	15	300
222	Single hole no. 2 coal	ring 1	0.95	0.2	15	300
226	Single hole no. 4 coal	ring 1	0.95	0.2	15	300
227	Radial no. 32 coal	ring 1	0.95	0.2	15	300
228	Radial A coal	ring 1	0.95	0.2	15	300
229	Coal spreader	ring 1	0.95	0.2	15	300
285	Coal spreader	ring 2	0.95	0.2	15	300
210	Coal spreader	ring 1	0.95	0.2	15	300
211	Coal spreader	ring 1	1.00	0.15	15	300

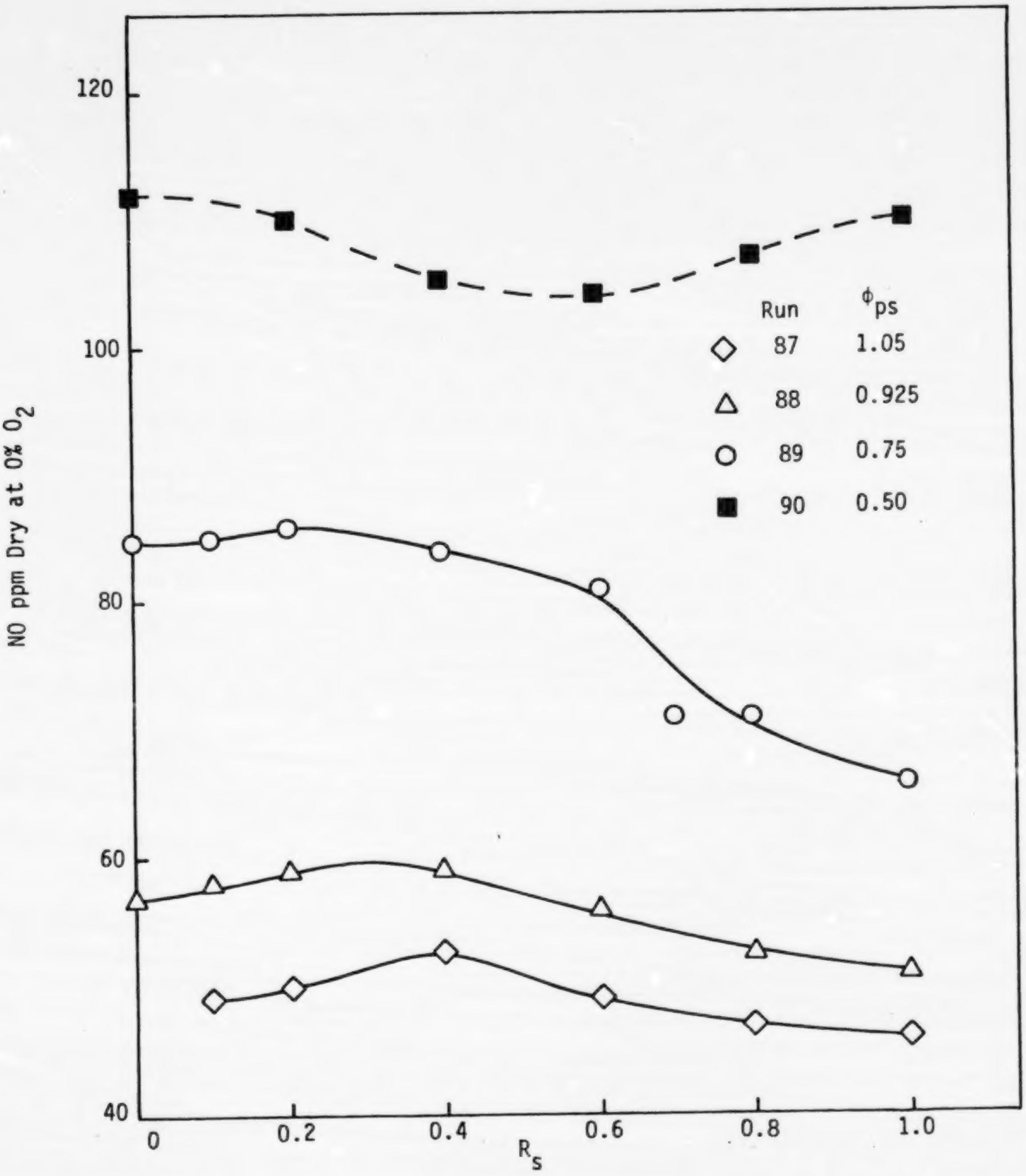

Figure 2.17. Emission Characteristics of Triple Concentric Systems (Natural Gas Fired)

(ϕ_{ps} is the fraction of stoichiometric air supplied in the primary and secondary streams)

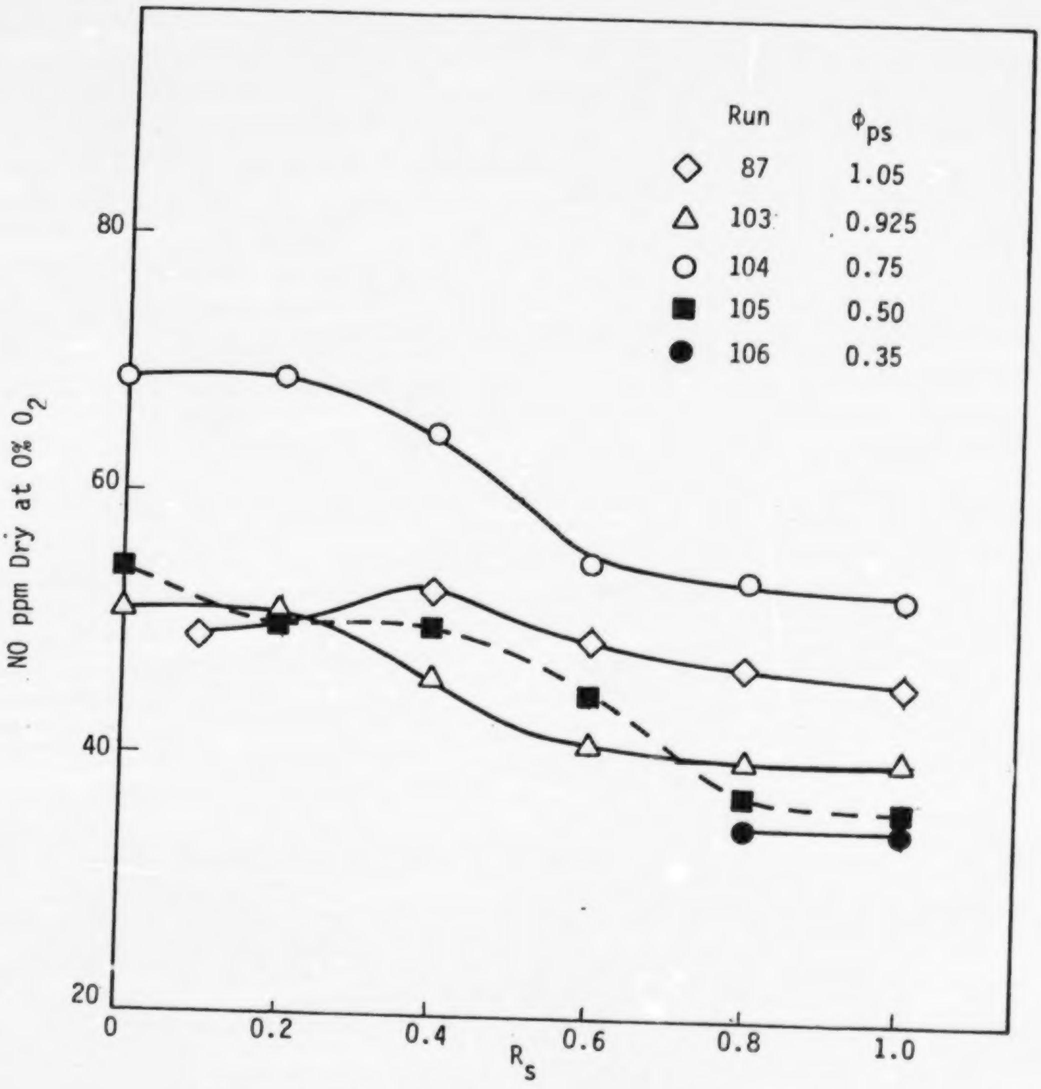

Figure 2.18. Emission Characteristics of Triple Concentric Systems (Natural Gas Fired)

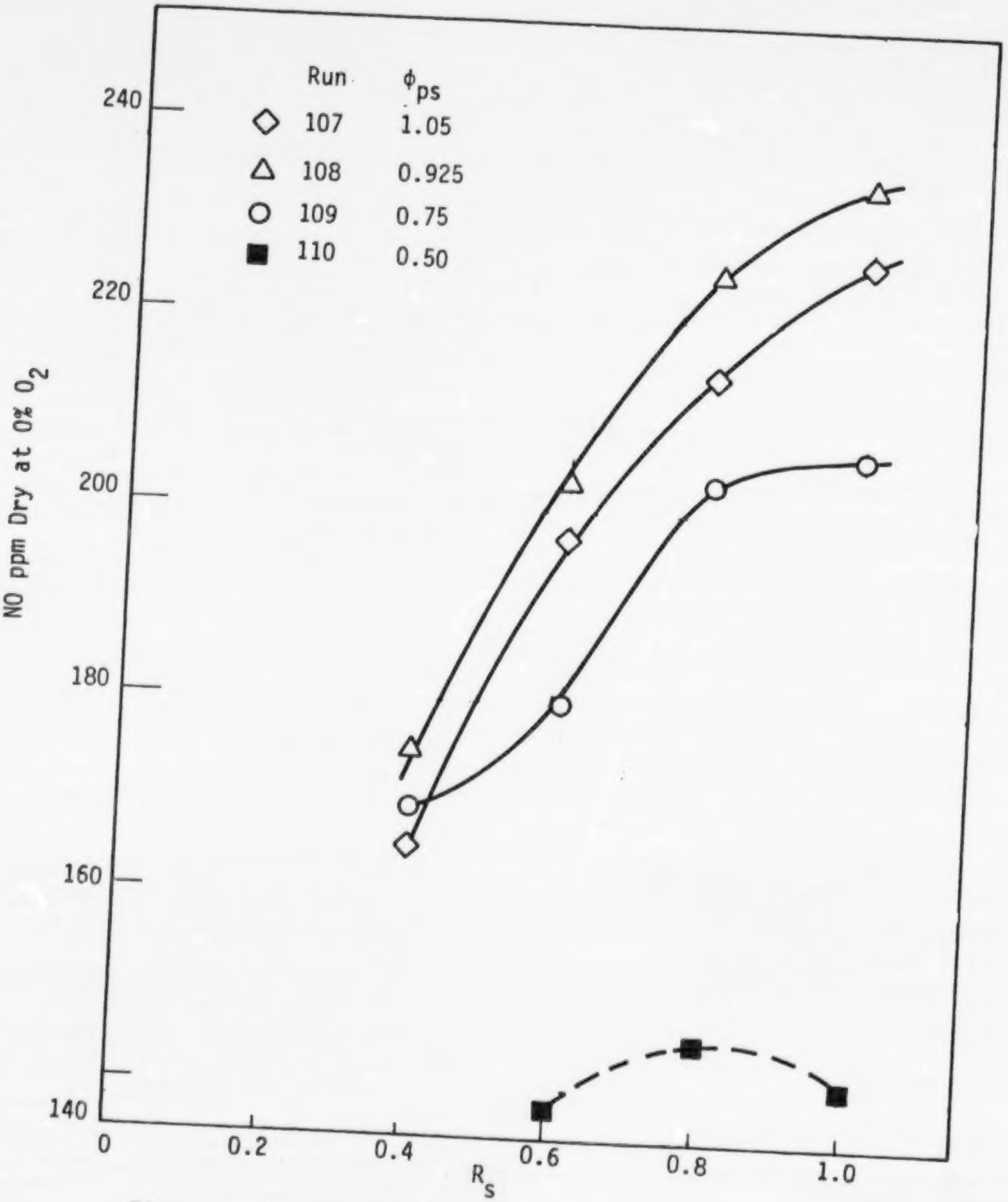

Figure 2.19. Emission Characteristics of Triple Concentric Systems (Oil Fired)

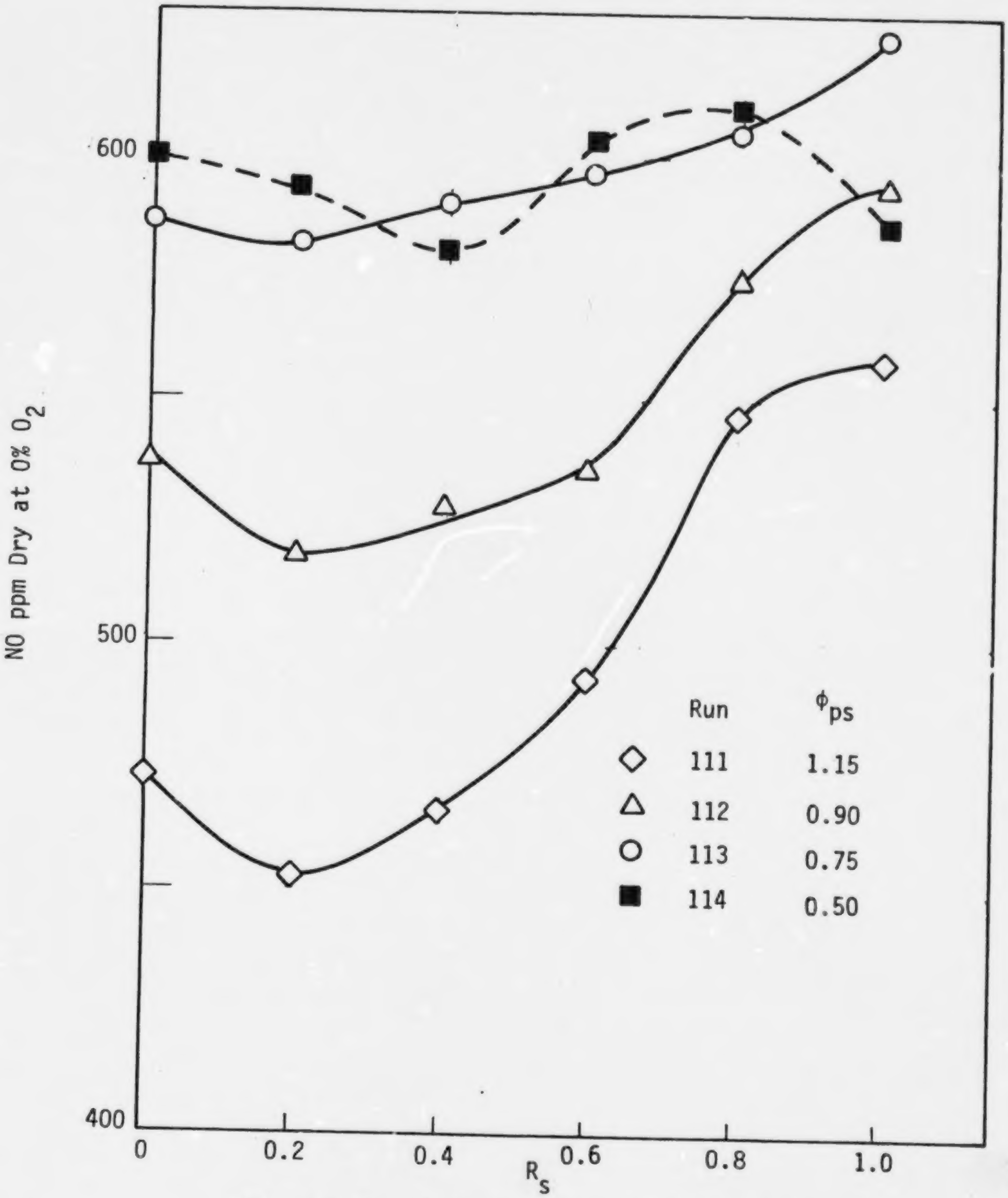

Figure 2.20. Emission Characteristics of Triple Concentric Systems (Coal Fired With Radial Fuel Injector

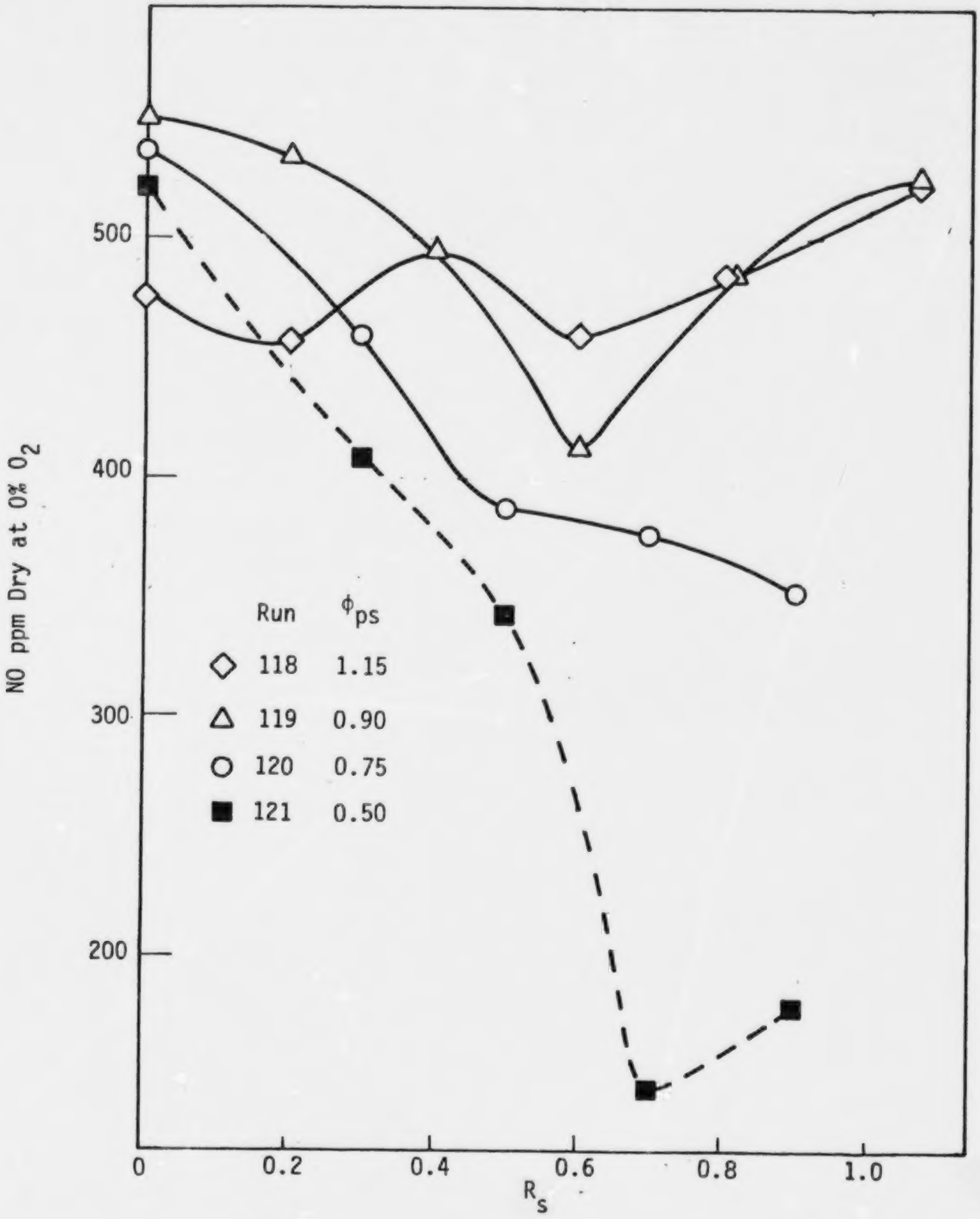

Figure 2.21. Emission Characteristics of Triple Concentric System (Coal Fired With Axial Fuel Injector)

gas while significant reductions were observed when 50 percent of the stoichiometric air requirement was supplied in the primary/secondary section of an oil flame. With radial coal injection emissions increased as the tertiary air flow increased. Reduced emission levels were only observed with coal at high tertiary air rates with axial fuel injection.

A third method of injecting tertiary air was also investigated. Two rings were constructed which could be inserted into the furnace through the measuring slots and placed around the burner exit. Air could be injected either symmetrically around the total perimeter or from two sectors above and below the burner. The tertiary air could not be supplied preheated because of the necessary rearrangements to the air delivery system. The effect of various fuel injection systems with the tertiary rings can be seen in Figure 2.22. The emission levels fall into two bands corresponding to the two different injector types. The lower emissions were produced with single hole injectors. Once more radial injectors and the coal spreader produce high emissions. Comparison of runs 229 and 285 show that with the coal spreader there were no significant effects of the asymmetric tertiary injection upon flue NO levels.

F-22

Figure 2.23 illustrates how the use of the tertiary air injection system modified the emission characteristics of the subscale practical burner. As the overall excess air was varied the tertiary airflow was maintained constant, thus the stoichiometry of the primary section varied as the overall excess air increased. At the lowest tertiary airflow and the highest excess air level emissions from the unstaged system were slightly lower than those from the staged system. This is probably because under these conditions the primary stage is not oxygen deficient. The results presented in Figure 2.23 were obtained with a system in which no optimization had been attempted and yet NO emissions were reduced by almost fifty percent. There is a natural concern that this reduction in NO emission was accompanied by a decrease in combustion efficiency or the production of unacceptable combustion characteristics. Figure 2.24 compares axial temperature, nitric oxide and carbon burnout measurements for a staged and unstaged flame. Measured temperatures are lower in the staged flame and 2m from the firing

F-23

F-24

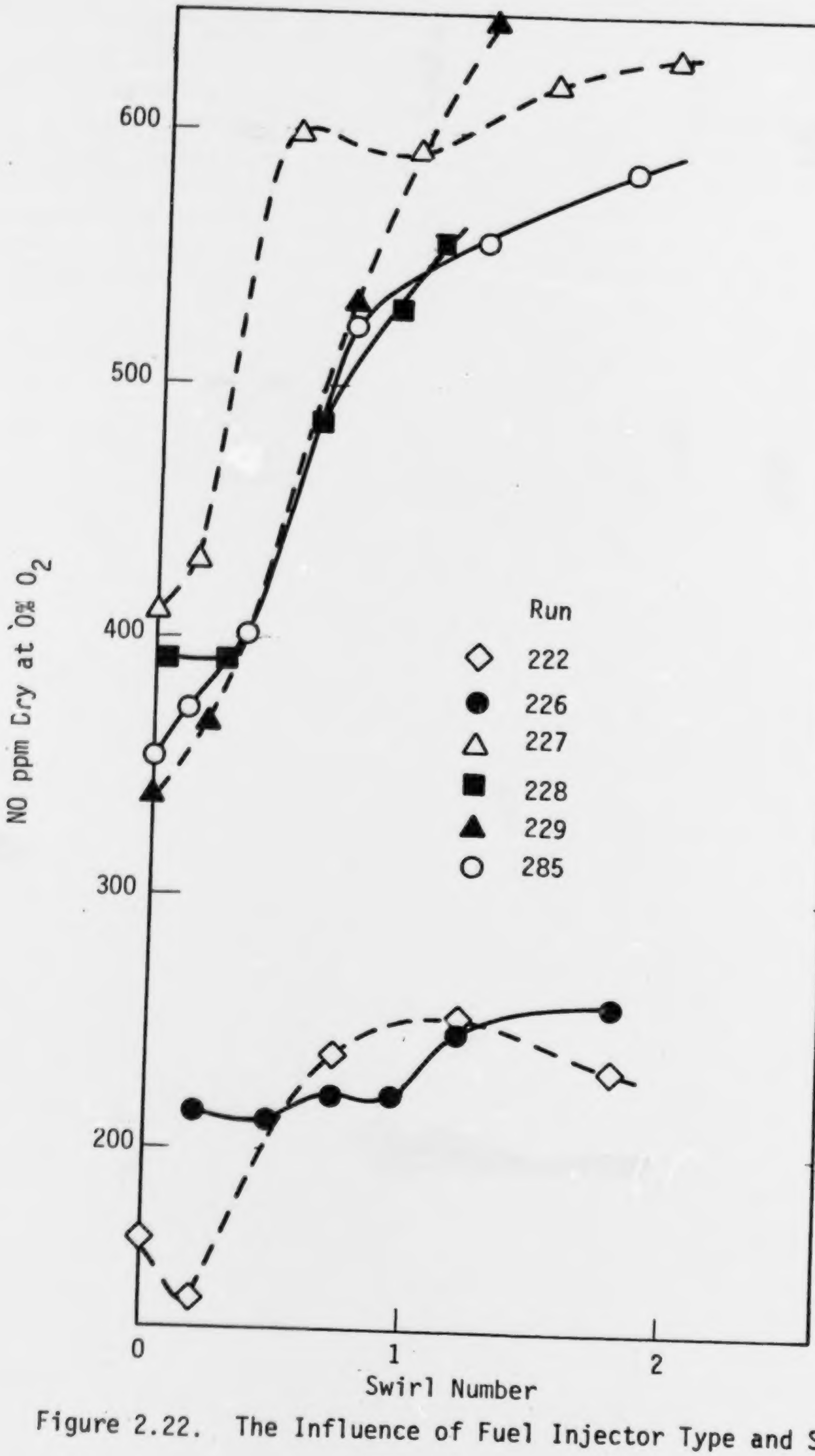

Figure 2.22. The Influence of Fuel Injector Type and Staging

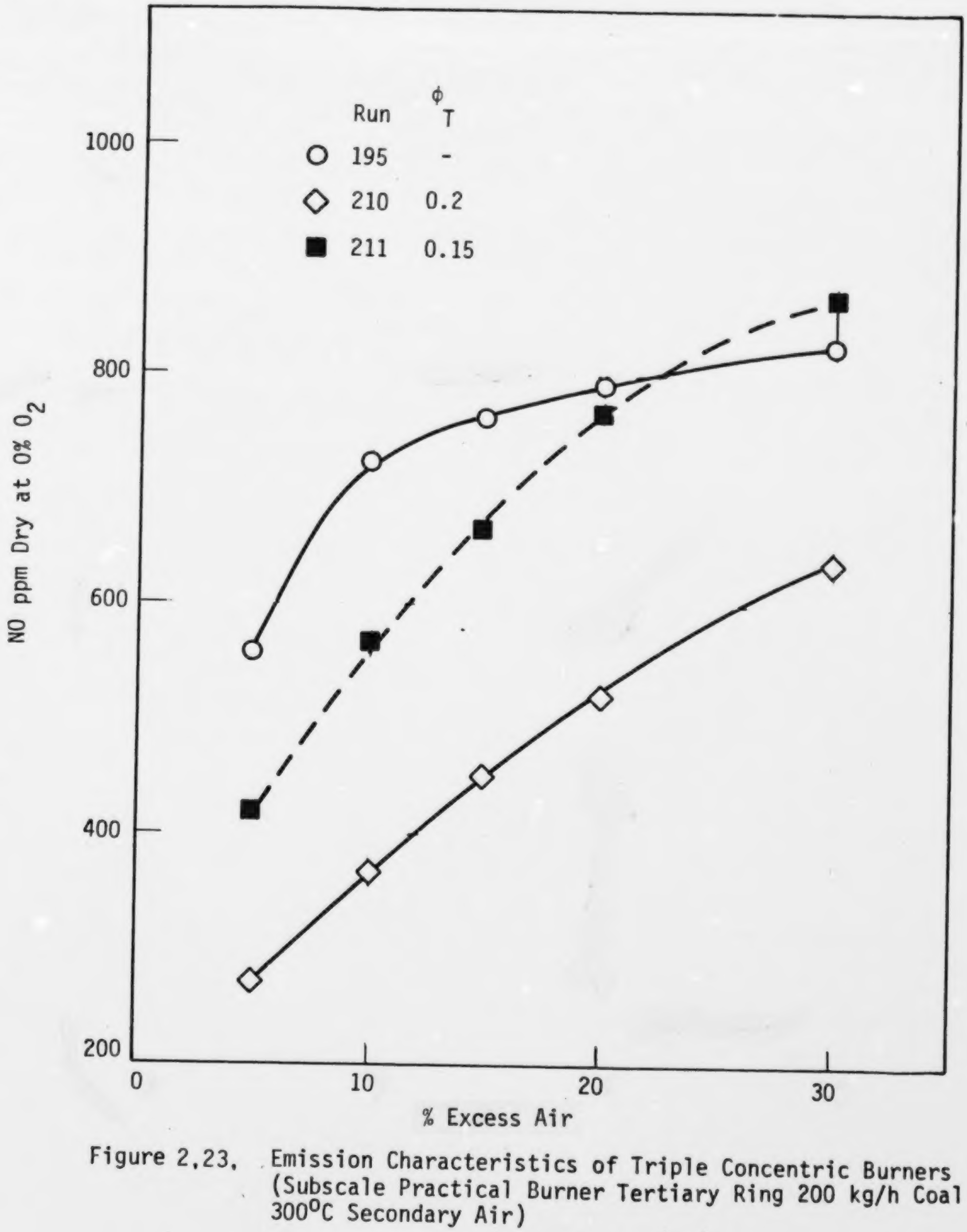

Figure 2.23. Emission Characteristics of Triple Concentric Burners (Subscale Practical Burner Tertiary Ring 200 kg/h Coal 300°C Secondary Air)

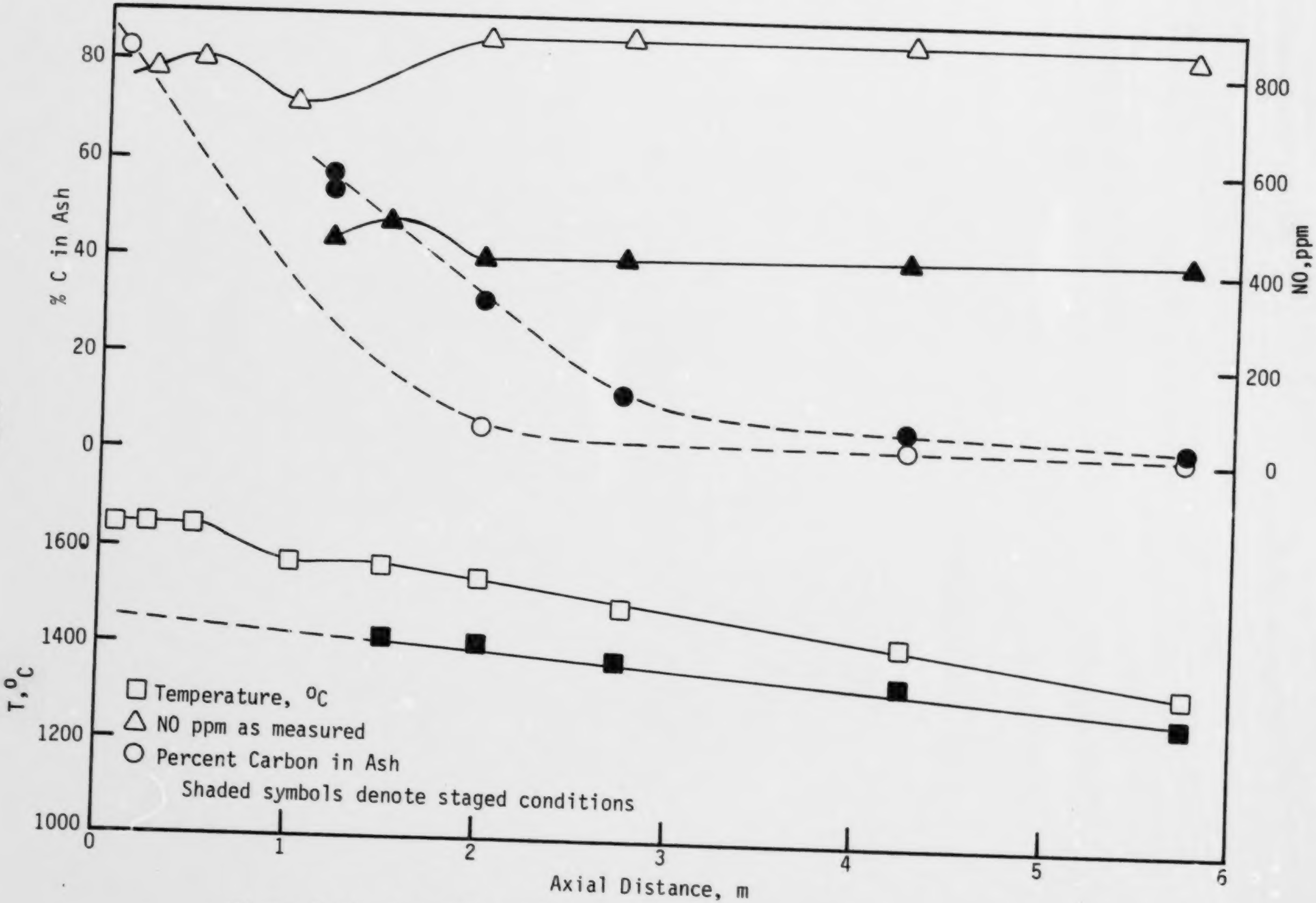

Figure 2.24. The Effect of Staging Upon Flame Characteristics Produced with a Subscale Practical Burner

wall a solid sample contained almost 30 percent carbon, whereas in the unstaged flame there was only 5 percent carbon left in the fly ash at that point. However, there was almost no difference in the carbon content of the solid sample collected four meters from the firing wall.

2.3.3 The Emission Characteristics of Dual Fuel Systems

Firing pulverized coal and natural gas simultaneously provides an approximate simulation of a low nitrogen, high volatile content fuel. Total thermal input and excess air levels were normally maintained constant at 2.6 MW throughout these tests which were carried out with the moving block swirl burner and the fuel injectors described earlier. Details of the experimental conditions and the resulting emissions are presented in Tables 2.8 and 2.9.

T8,9

- The Influence of the Method of Fuel Injection

The influence of the method of fuel injection for combined firing can be seen in Figures 2.25 through 2.29. The results presented in Figures 2.25 and 2.26 were obtained with separate fuel injection for the solid and gaseous inputs. The coal was injected on the axis at two different velocities and the gas was injected radially (injectors A and B) or axially along the periphery of the coal jet (injectors C and F). Emissions from the lower velocity coal injector were generally higher than those from the higher velocity injectors. The influence of the method of natural gas injection upon flue gas NO concentration appears to be dependent upon the axial coal injection velocity. For high coal injection velocities there does not appear to be a strong influence of the method of gas injection but at the lower velocity emissions were considerably higher with the higher velocity gas injector.

Figs 25, 26
27, 28, 29

The results presented in Figure 2.27 were obtained with the peripheral gas injector. It can be seen that the emissions measured with the radial injector were not the highest, nor were the lowest NO emissions obtained with the highest coal injection velocity which is contrary to experience with single fuel firing.

Table 2-8. Input Conditions for Dual-Fuel Investigations

Run No.	Fuel Ratio		Injector Type		Throat Diameter cm	% Primary Air	Remarks
	Coal	Gas	Coal	Gas			
122	.5	.5	2	A	17.6	10	
123	.5	.5	2	B	17.6	10	
124	.5	.5	2	C	17.6	10	
127	.5	.5	2	F	17.6	10	
128	1.0	-	2	-	17.6	10	Outer gun in position: 1.3 MW Total heat input
129	1.0	-	32	-	17.6	10	
130	1.0	-	32	-	17.6	10	1.3 MW Total heat input
131	.50	.50	32	-	17.6	10	
132	.50	.50	2	-	17.6	10	
133	.50	.50	1	-	17.6	10	
137	.50	.50	3	-	17.6	10	
138	.62	.38	3	-	17.6	10	
139	.77	.23	3	-	17.6	10	
140	1.0	-	3	-	17.6	10	
141	.50	.50	3	B	17.6	10	
142	.62	.38	3	B	17.6	10	
143	.77	.23	3	B	17.6	10	
144	.62	.38	32	B	17.6	10	
145	.77	.23	32	B	17.6	10	
148	.50	.50	32	B	17.6	10	
149	.50	.50	1	B	17.6	10	
150	.50	.50	1	C	17.6	10	
151	.50	.50	1	F	17.6	10	
156	.50	.50	1	-	17.6	-	
157	.50	.50	2	-	17.6	-	
158	.50	.50	3	-	17.6	-	
164	.50	.50	1	peripheral	13.1	10	
165	.50	.50	2	"	13.1	10	
166	.50	.50	32	"	13.1	10	
167	.50	.50	3	"	13.1	10	
168	.50	.50	3	-	13.1	10	
169	.62	.38	3	peripheral	13.1	10	
170	.62	.38	32	"	13.1	10	
171	.77	.23	3	"	13.1	10	
172	1.0	-	3	-	13.1	10	

Table 2.9. Summary of Flue Gas NO Concentrations for the Dual Fuel Investigations

Run No.	R_s										
	0.0	0.1	0.2	0.3	0.4	0.5	0.6	0.7	0.8	0.9	1.0
122	300	304	300	307	310	323	330	329	348	346	360
123	303	288	262	278	282	302	308	314	317	312	326
124	264	263	282	307	-	334	-	360	-	389	-
127	358	352	344	262	272	310	-	340	-	366	-
128	520	466	405	349	405	332	-	343	-	380	-
129	641	646	-	711	735	798	792	842	815	-	-
130	518	-	540	-	606	-	652	-	658	-	692
131	-	485	494	575	600	-	600	599	573	555	-
132	305	-	327	-	355	-	377	-	411	433	-
133	334	-	344	-	435	-	544	-	-	-	-
137	240	-	-	291	325	334	-	367	-	408	- *
138	337	-	-	326	-	391	-	343	-	440	- *
139	292	-	-	359	-	413	-	435	-	460	-
140	449	-	-	-	477	512	507	522	521	508	505*
141	305	332	332	-	354	-	363	-	363	344	-
142	272	-	270	-	312	-	340	-	335	389	-
143	336	-	340	-	432	-	430	-	444	450	-
144	576	-	572	-	599	-	630	-	620	-	-
145	653	-	675	-	670	-	681	-	652	-	660
148	521	-	545	-	575	-	564	-	540	550	-
149	495	-	559	-	387	-	432	-	439	437	-
150	410	-	458	-	392	-	433	-	453	487	-
151	525	-	523	-	565	-	570	-	544	547	-
156	363	-	379	-	407	-	413	-	430	418	-
157	327	-	-	-	397	-	468	-	395	399	-
158	284	-	290	-	429	-	347	-	367	378	-
164	561	-	583	-	587	-	460	-	551	-	-
165	479	-	485	-	482	-	451	-	518	-	-
166	507	-	519	-	542	-	545	522	-	-	-
167	486	-	499	-	518	522	604	-	594	-	-
168	395	-	398	-	395	-	592	-	592	-	-
169	522	-	551	-	633	-	697	-	-	-	- *
170	520	-	515	529	-	528	-	-	-	-	-
171	508	-	380	414	412	447	705	683	-	-	-
172	505	-	503	-	433	-	583	-	717	738	-

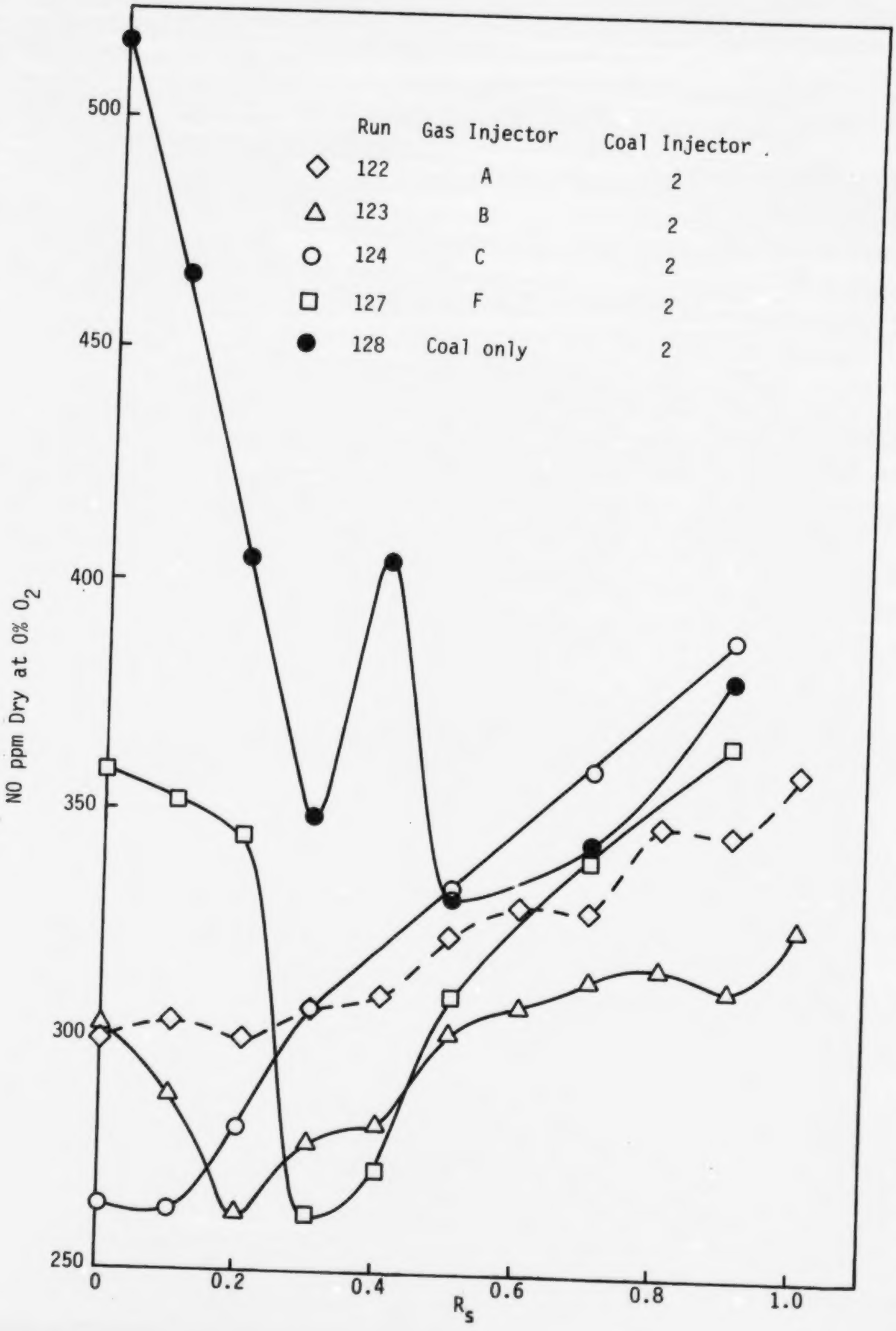

Figure 2.25. The Effect of Dual-Fuel Firing on NO Formation (Coal and Gas Injected Separately)

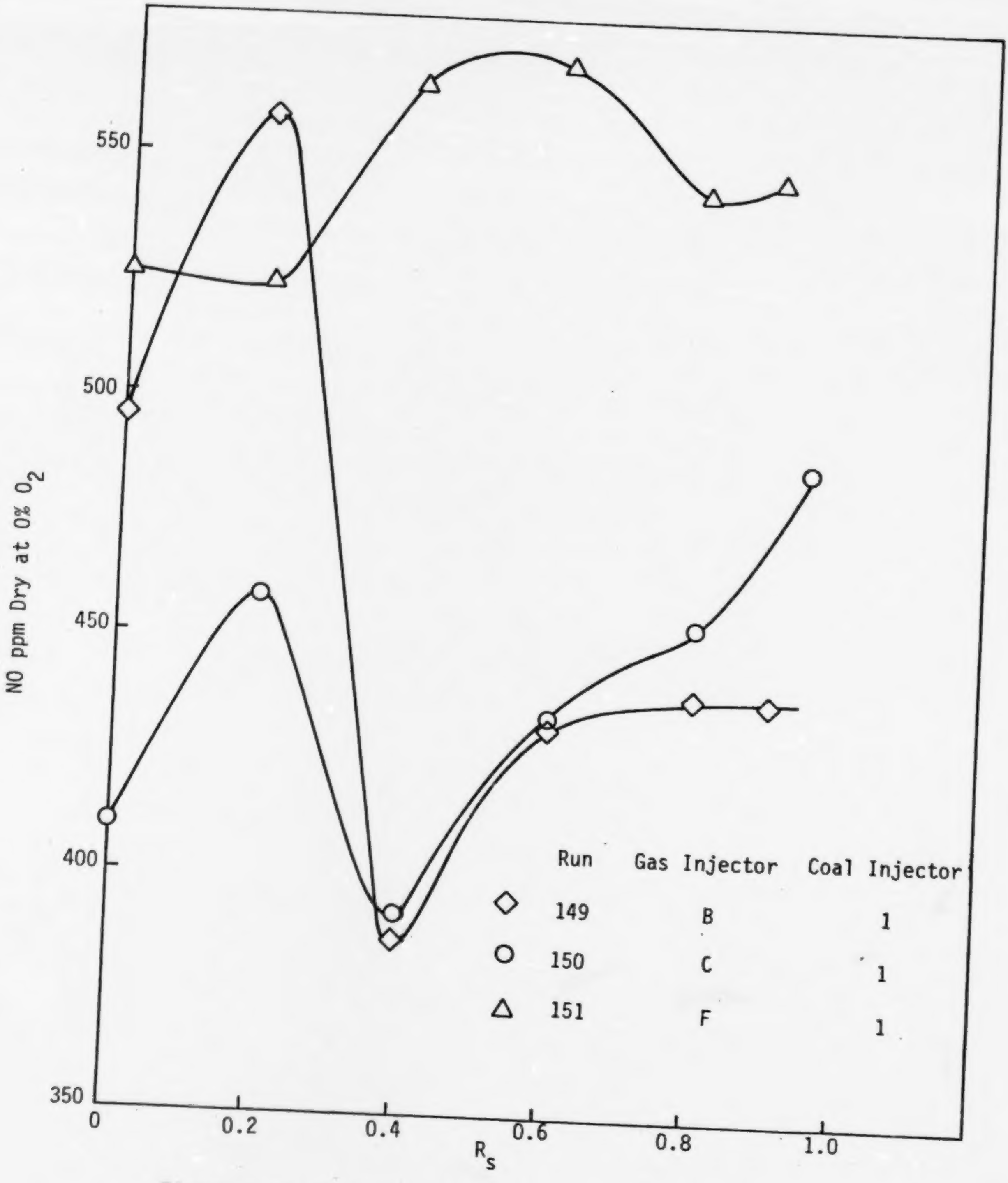

Figure 2.26. The Effect of Dual Fuel Firing on NO Formation (Coal and Gas Injected Separately)

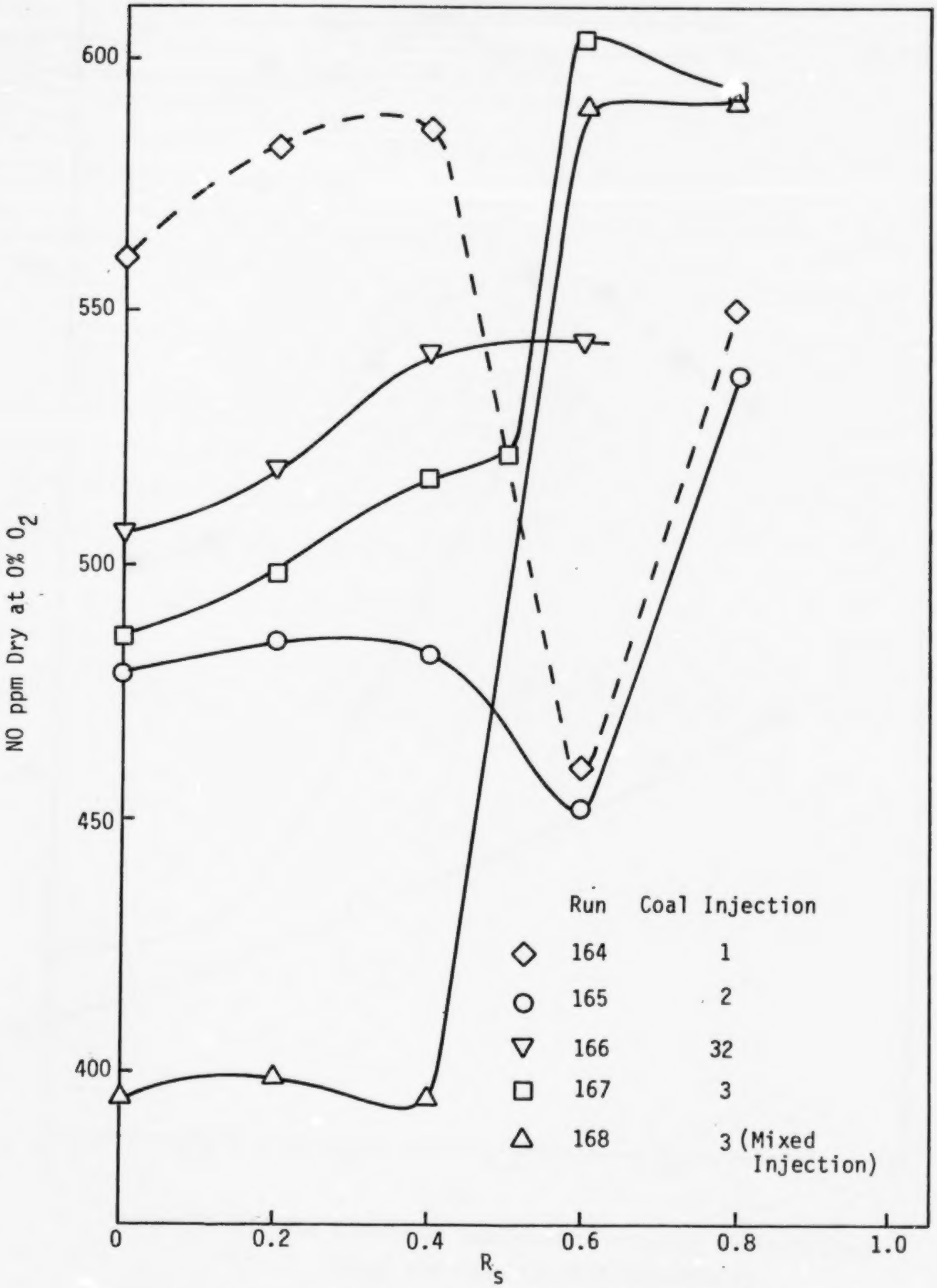

Figure 2.27. The Effect of Dual Fuel Firing on NO Formation (Coal and Gas Injected Separately)

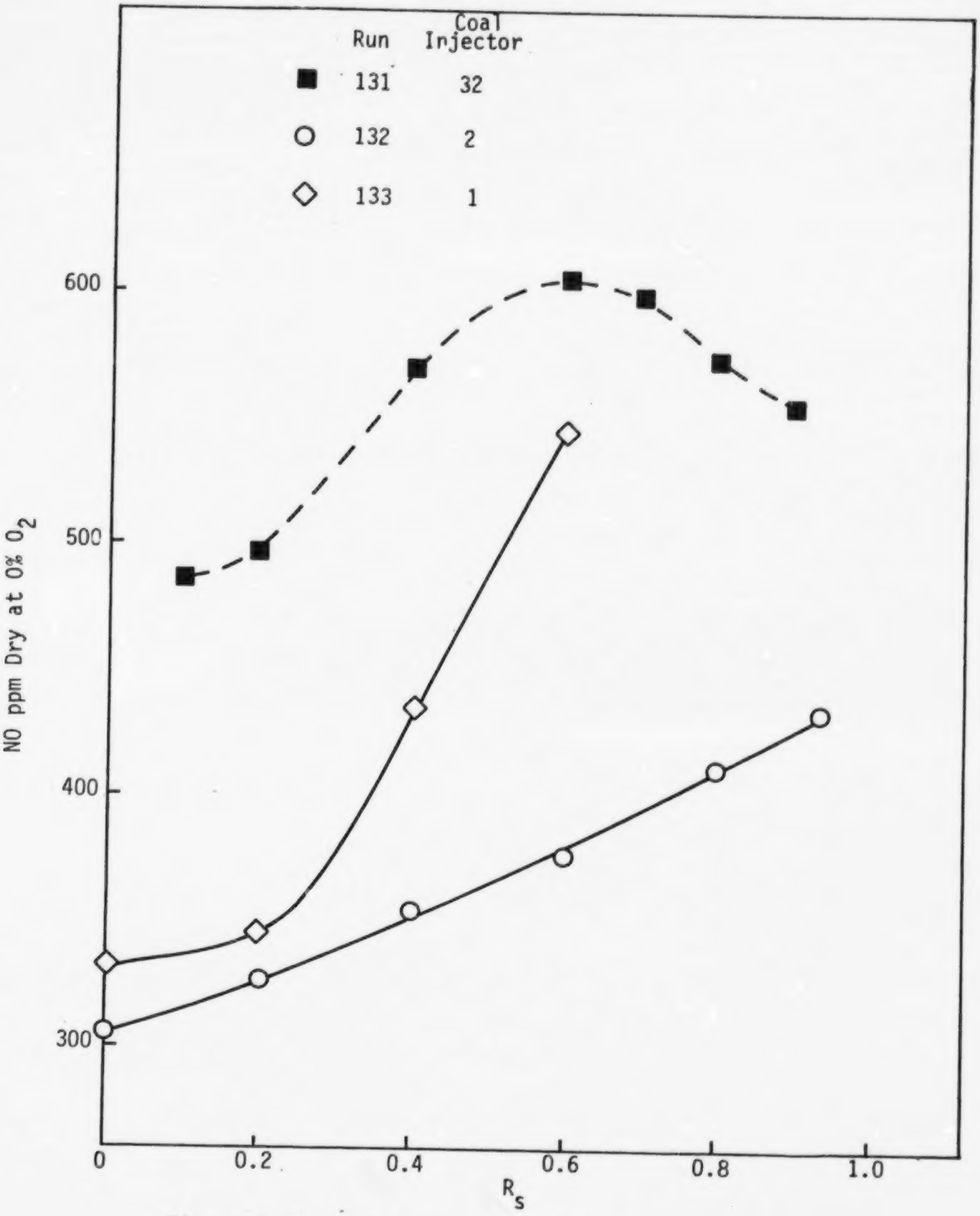

Figure 2.28. The Effect of Dual-Fuel Firing on NO Formation (Coal and Gas Injected Separately)

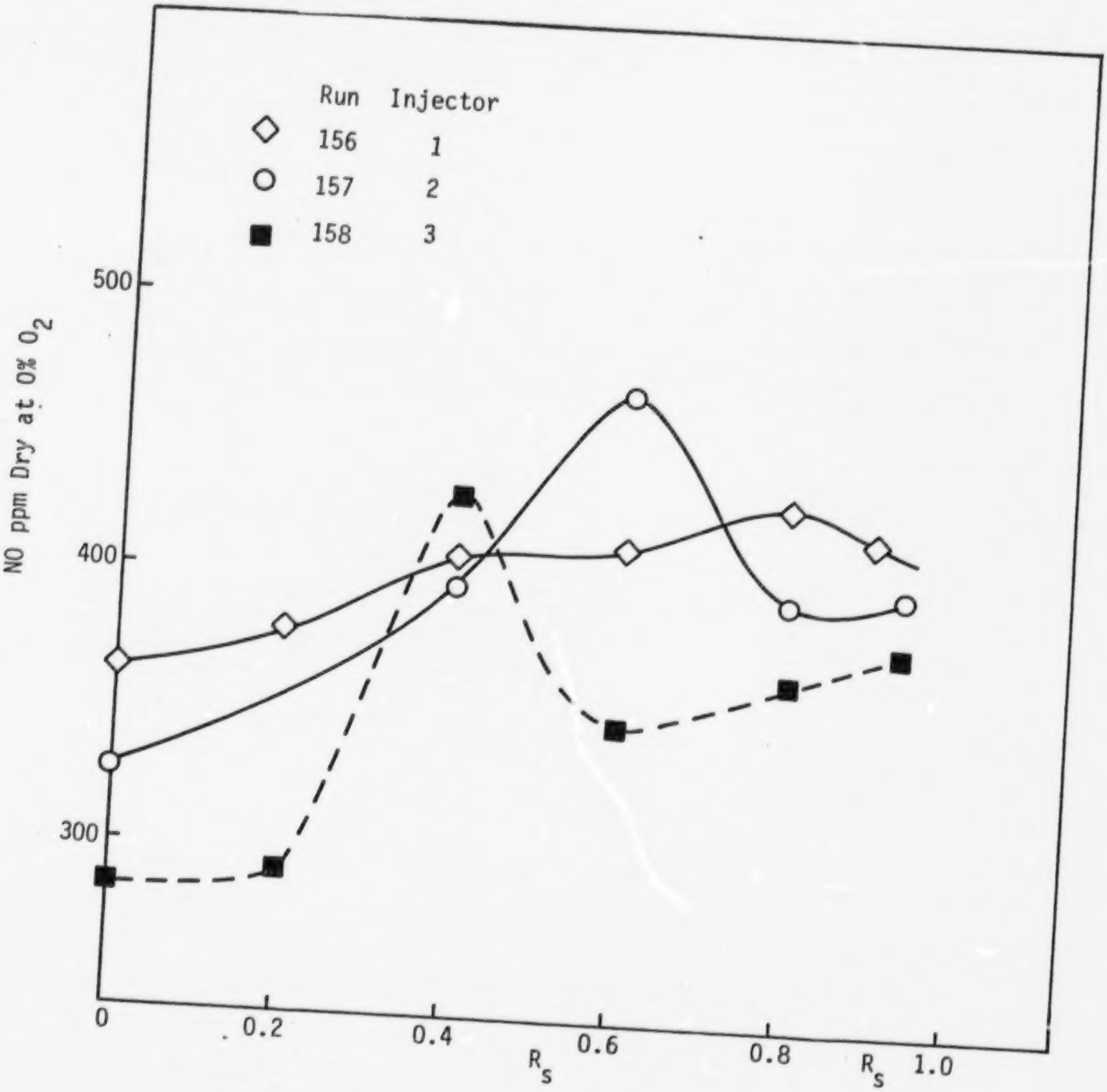

Figure 2.29. The Effect of Dual-Fuel Firing on NO Formation (Natural Gas Used as Coal Transport)

The results presented in Figure 2.28 were obtained by adding the natural gas portion of the fuel input to the primary air and coal stream and supplying the mixture through a single injector. In this instance the emissions are in quantitative agreement with the influence of fuel injection method on emissions from pulverized coal:

- emissions are a minimum with high velocity axial fuel injection, and
- emissions are maximum with radial fuel injection.

The emission characteristics of dual-fuel systems when oxygen is excluded from the coal stream are presented in Figure 2.29. Natural gas was used as the transport medium. It can be seen that emissions are almost independent of fuel injector type.

Figure 2.30 compares the emission characteristics of flames which have air mixed with the coal at the time of injection and with natural gas as the sole transport medium. Following the assumptions discussed earlier, it would be expected that NO formation would be reduced for the case of no air in the fuel stream. However, the results suggest that the process is much more complex than this. One fuel injector exhibits the expected trend at high swirl, but with the other fuel injector emissions were generally higher when air was excluded from the primary jet.

- The Effect of Coal:Gas Ratio

When both coal and natural gas were supplied through a single fuel injector it was found that NO emissions increased as the coal:gas ratio increased (see Figure 2.31). However, when the two fuels were injected separately an effect of the method of fuel injection was observed on the influence of coal:gas ratio. When both fuels are fired radially the emissions increase as the coal fraction increased, but with axial coal injection and radial gas injection there appears to be an optimum coal:gas ratio for minimum emissions (compare Figures 2.32 and 2.33). With peripheral gas injection the measured NO levels were independent of coal:gas ratio at both low and high swirl levels (see Figure 2.34).

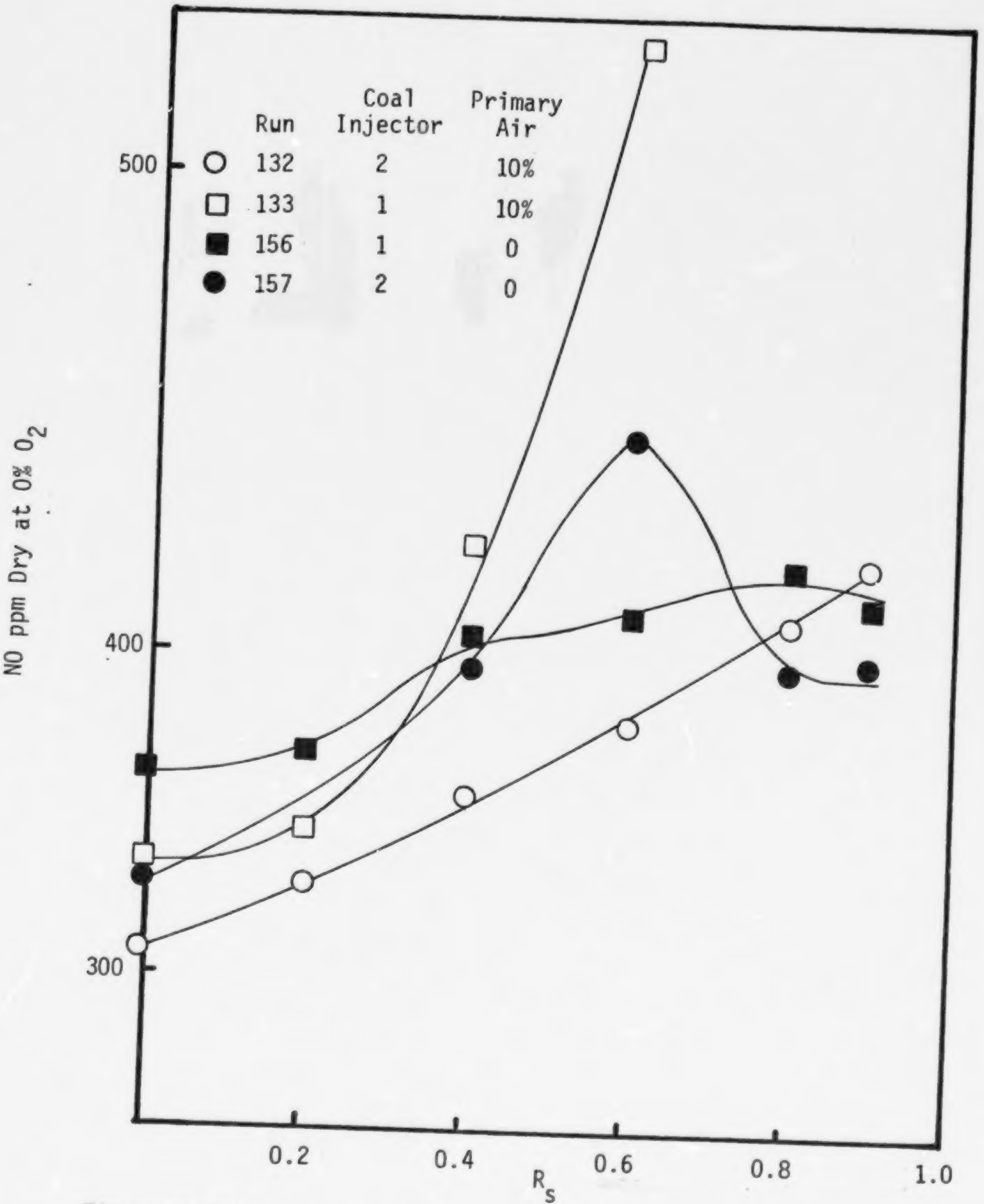

Figure 2.30. Comparison of NO Formation when Air is Excluded from the Primary Stream

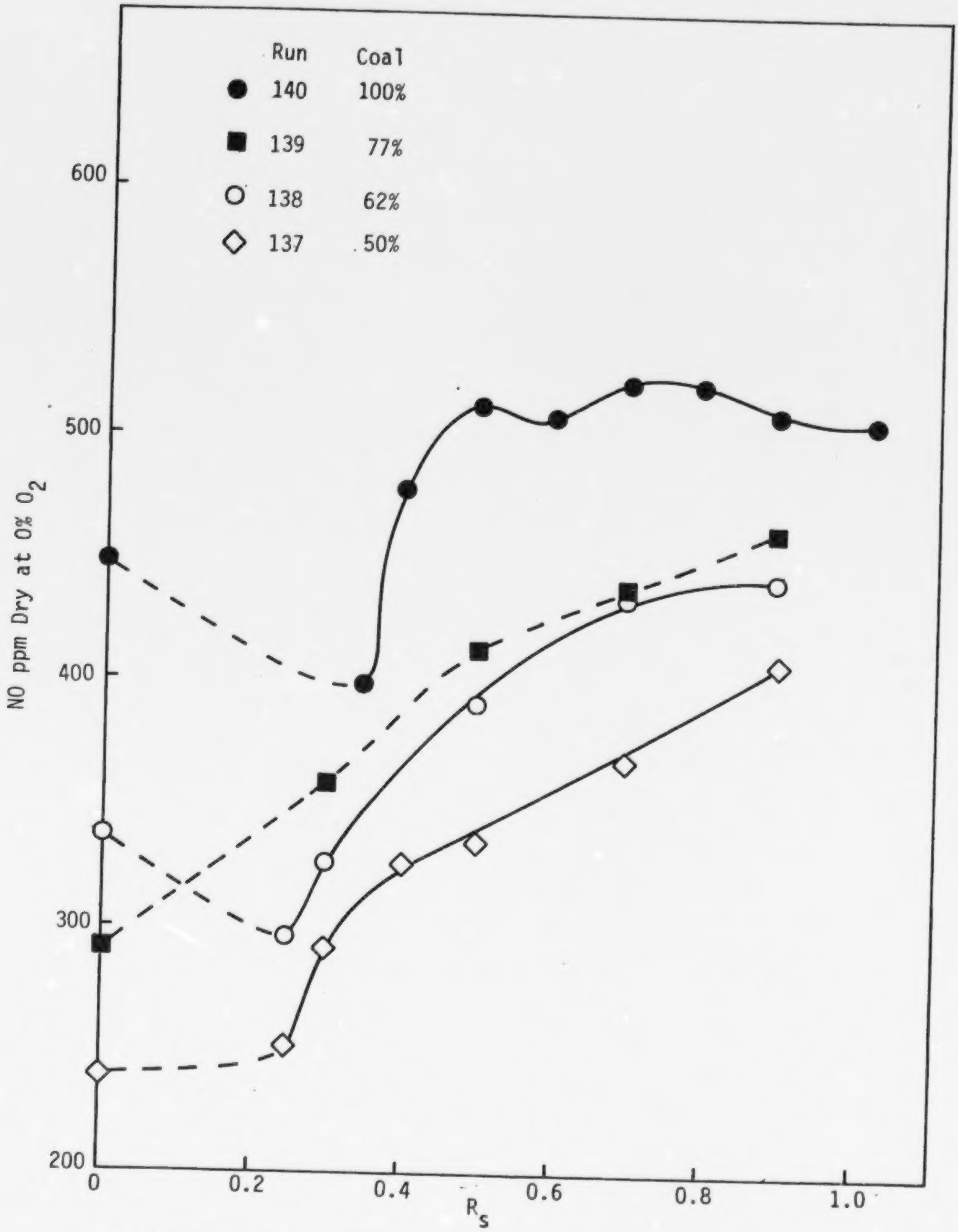

Figure 2.31. The Effect of Coal Gas Ratio on NO Emissions with Dual-Fuel Firing

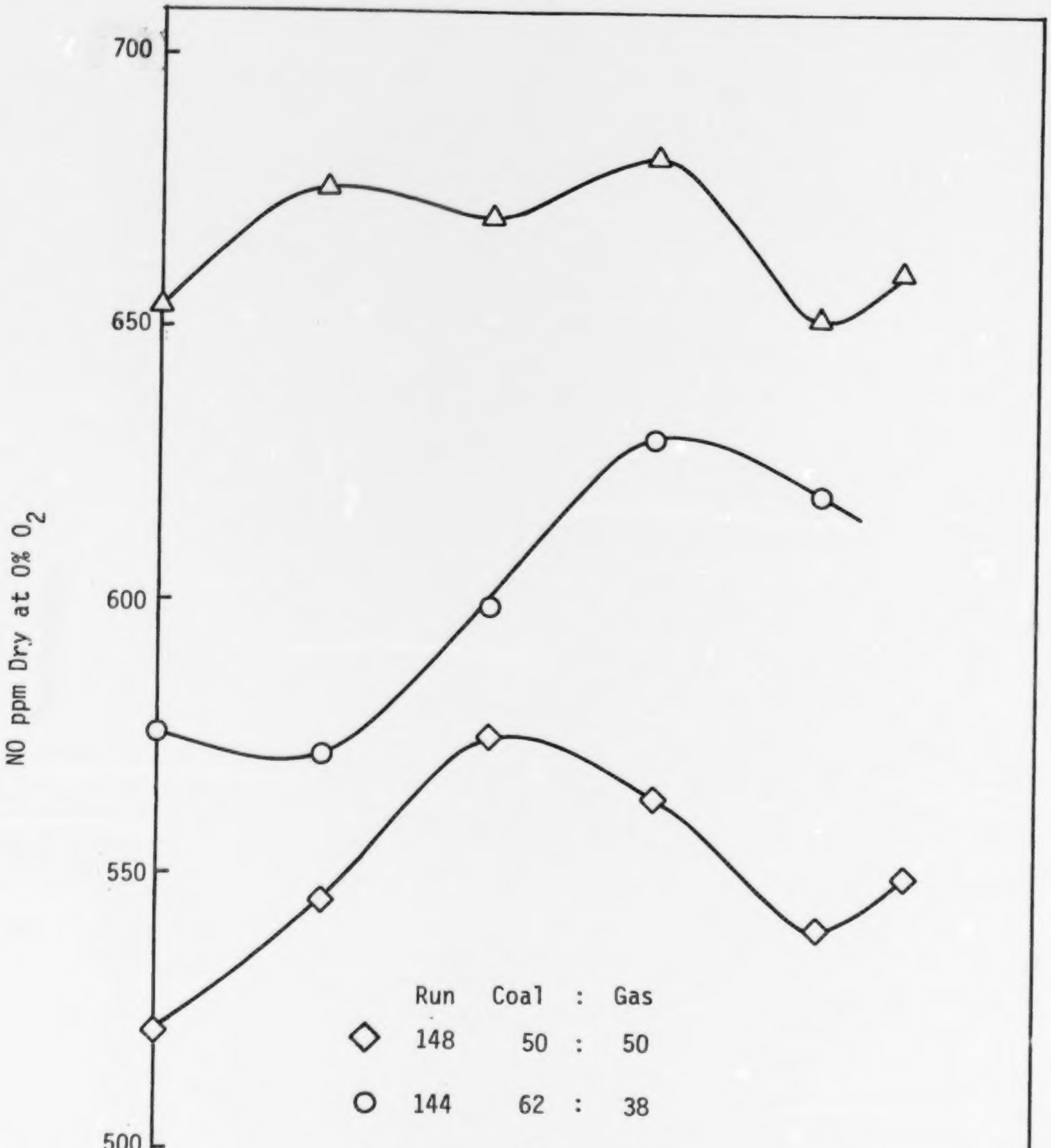

Figure 2.32. The Effect of Coal Gas Ratio on NO Emissions with Dual-Fuel Firing

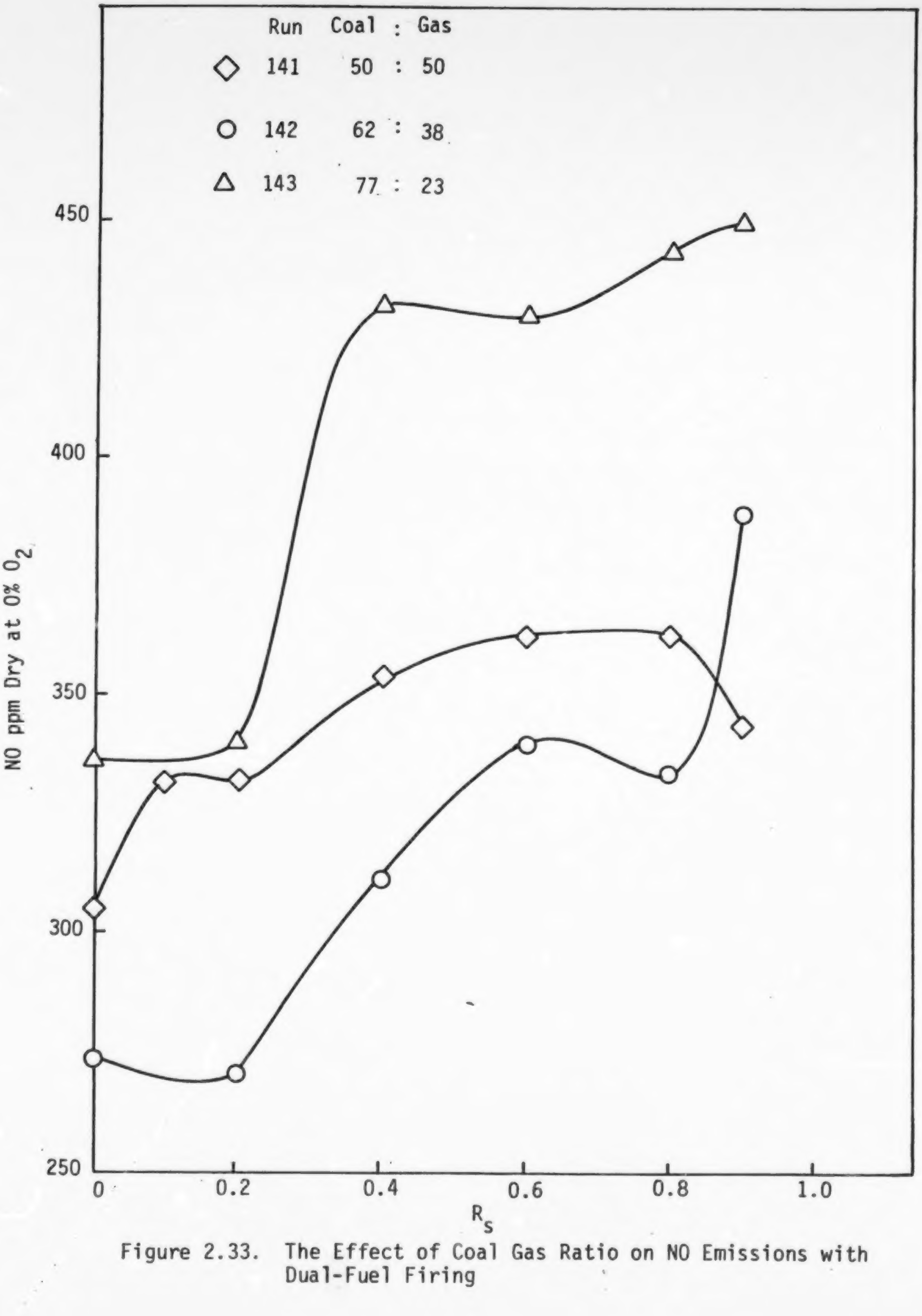

Figure 2.33. The Effect of Coal Gas Ratio on NO Emissions with Dual-Fuel Firing

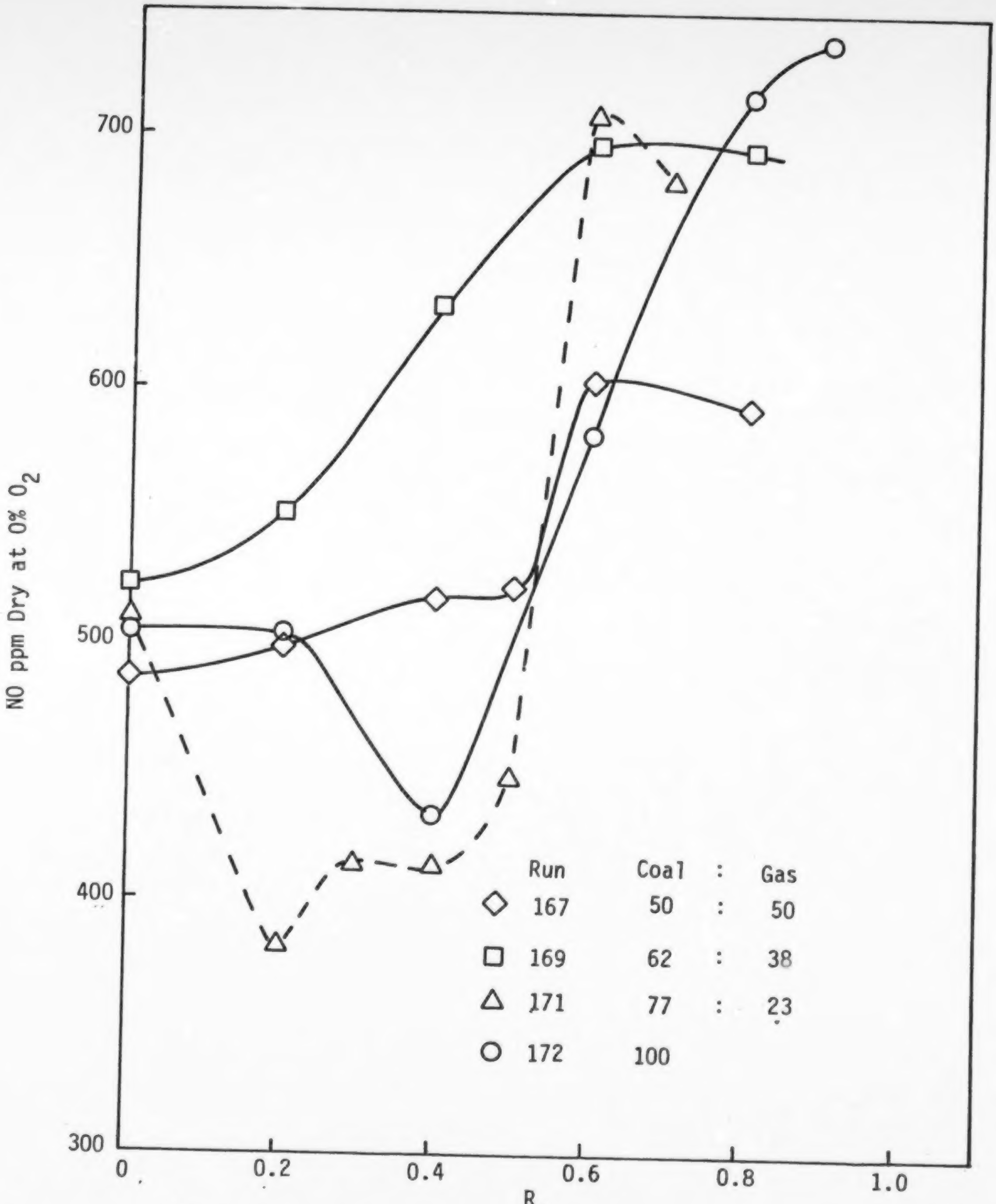

Figure 2.34. The Effect of Coal Gas Ratio on NO Emissions with Dual-Fuel Firing

2.3.4 The Influence of Burner Parameters on the Emission Characteristics of Fuel Oil Flames

In the previous set of furnace investigations it was observed that burner parameters had a considerable influence on the emission characteristics of both pulverized coal and natural gas flames. A series of parametric investigations were carried out in an attempt to identify those burner conditions giving low levels of nitric oxide emission for residual fuel oil firing. Typical results from these investigations are discussed below. In all cases the swirl level in the secondary air stream was considered as a secondary variable and the primary variables were the method of atomization, the vane angle of swirl vanes attached to the nozzle, the secondary air velocity, the position of the oil nozzle and the angle of the burner divergent. The firing rate and excess air level were maintained constant at 1.3 MW and 5 percent, respectively. Input conditions and results are tabulated in Tables 2.10 and 2.11.

- Oil Atomization and NO Emissions

The angle of the oil spray dictates the path of the oil droplets through any recirculation zone and into the air stream, and therefore, has a strong influence upon flame stability as well as dictating the flame shape. Narrow spray angles produce long narrow flames. The emission characteristics of four different pressure jet spray angles were investigated and the results are presented in Figures 2.35 through 2.38. With the nozzle in the throat, emissions are increased as the secondary swirl level increases and as the spray angle is widened. This effect was most apparent when the oil nozzle was fitted with 45° swirl vanes. Narrow spray angles will delay the fuel/air mixing process, delay heat release and these effects will reduce both fuel and thermal NO formation. Increasing the swirl level will increase the rate of mixing, thus negating the influence of the spray angle. The effect of spray angle is less pronounced when the nozzle is placed at the burner exit. The movement of the oil nozzle forward normally results in reduced emissions, both because of decreased mixing rates which also increases flame length and the increased vitiation of the combustion air with combustion products prior to combustion.

Table 2.10 Input Conditions for Investigations with Residual Fuel Oil

Run	Burner, Throat Dia. mm	Swirl Vane Angle (o)	Burner Position	Spray Angle (degree)
STEAM ATOMIZED				
12a	176	45	Throat	100
25	↓		↓	90
30				80
31				90
40	131			80
41	↓			90
PRESSURE JET				
3	176	45	Exit	90
4	↓	45	Throat	↓
7			↓	
8			Exit	
9			Throat	70
10			Exit	↓
11			Throat	50
12			Exit	↓
15		45	Exit	70
16		45	Throat	↓
17		30	Exit	
18		30	Throat	
19			↓	30
20			Exit	↓
21		45	↓	
22		45	Throat	
23		30	Exit	
24		30	Throat	
32		45	↓	50
33		45	Exit	↓
34	131		Throat	
36	↓		↓	30

Table 2.11 Flue Gas NO Concentrations (Corrected to 0% O_2) for Investigations with Residual Fuel Oil

	R_s																				
Run	0	0.5	1	1.5	2.0	2.5	3.0	3.5	4.0	4.5	5.0	5.5	6.0	6.5	7.0	7.5	8.0	8.5	9.0	9.5	10
3	155	159	169	163	152	176															
4	246		248		254		252		253				248				235			241	
7						187							215							236	
8						100		157		181		176		183		194		209		218	
9	158			190		171		187		238		253		235		251		253		294	
10					195		138	139		151		194		199				208		213	
11		152				162		173		173		188		180		217		213		222	
12	179		161		104		141		139		151		184		188		204		209		
12a	240		246		234		202			199		218		208			218			209	
15	158	179	181	192	182		162						186								
16	215		209				215		228		223		243		260		277		262		
17	151	154	152	144	130	86															
18	161		181		186		200		204		197		207		178		175		156	138	
19				108		126		139		155		155		165		183				214	
20											125			153		163				165	
21	186	190	181		139	106		148		163											
22	140				152		156					181				195		196		202	
23	190	176	182	155	135																
24	192		220		202		131		131		151						155			155	
25	241		223		282		221		219		214		207		210		202			214	
30	196		171		202		150		161		173		172		177				176		
32	178		178		174		181		169		193		223				167			164	
33	179	180	181	170	131	101	150		160												
34	168		165		163		161		219		234		246		255		255		253		
36	147		148		153		181				208		247		240						
40	278		263		243		245		251				242							266	
41	270		255		241		236		256		257				265				267		
52	109				107			128			143			152			181			189	
63	182				176				176				208				234			243	
173	243		252		238		217		142		168		163		171		181		188		197
174	153		149		154		163		152		141		155		174		196		202		210
175	215		202		182		187		171		150		160		167		169		170		177

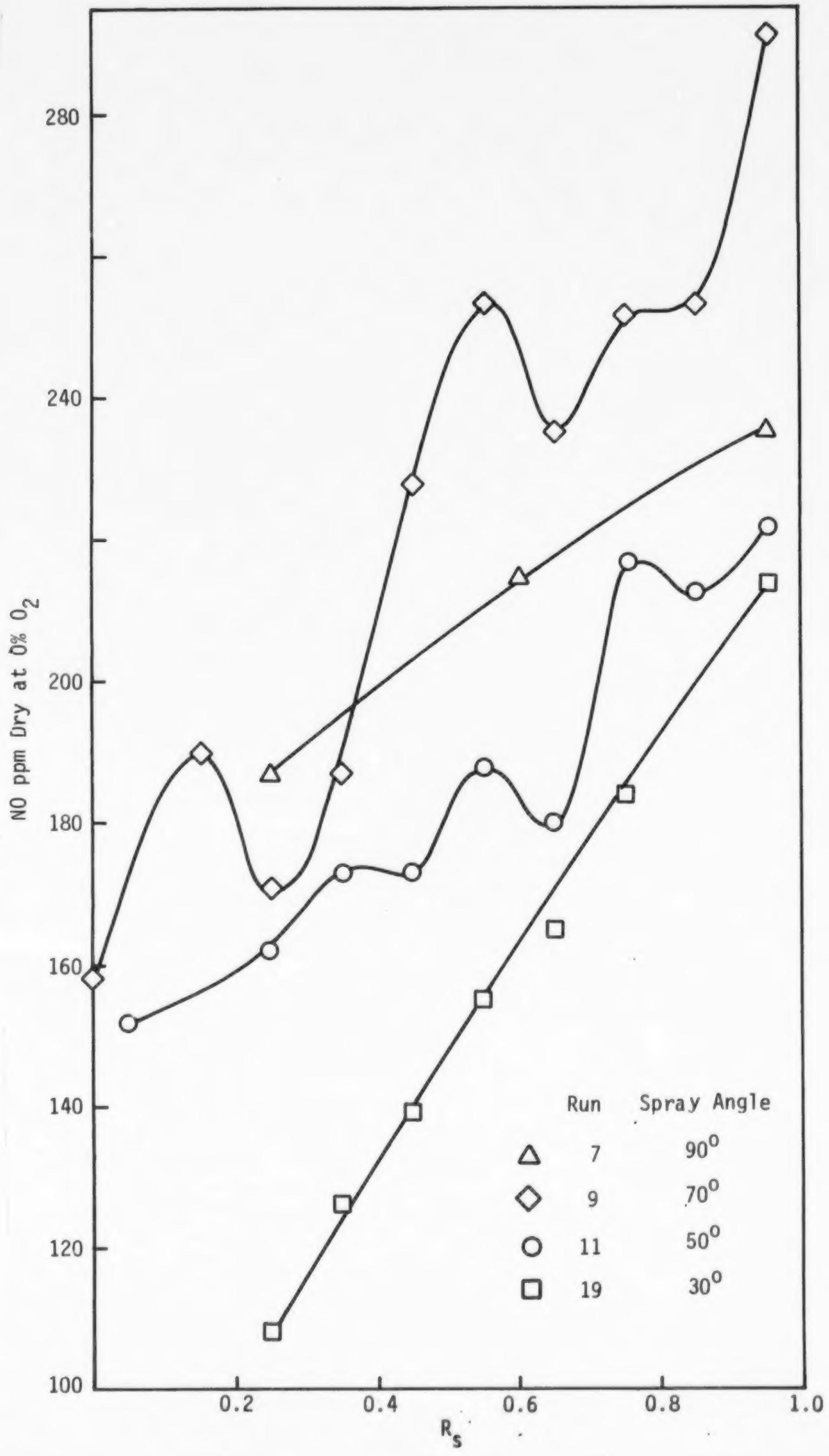

Figure 2.35. The Influence of Pressure Jet Spray Angle (Nozzle at the Throat)

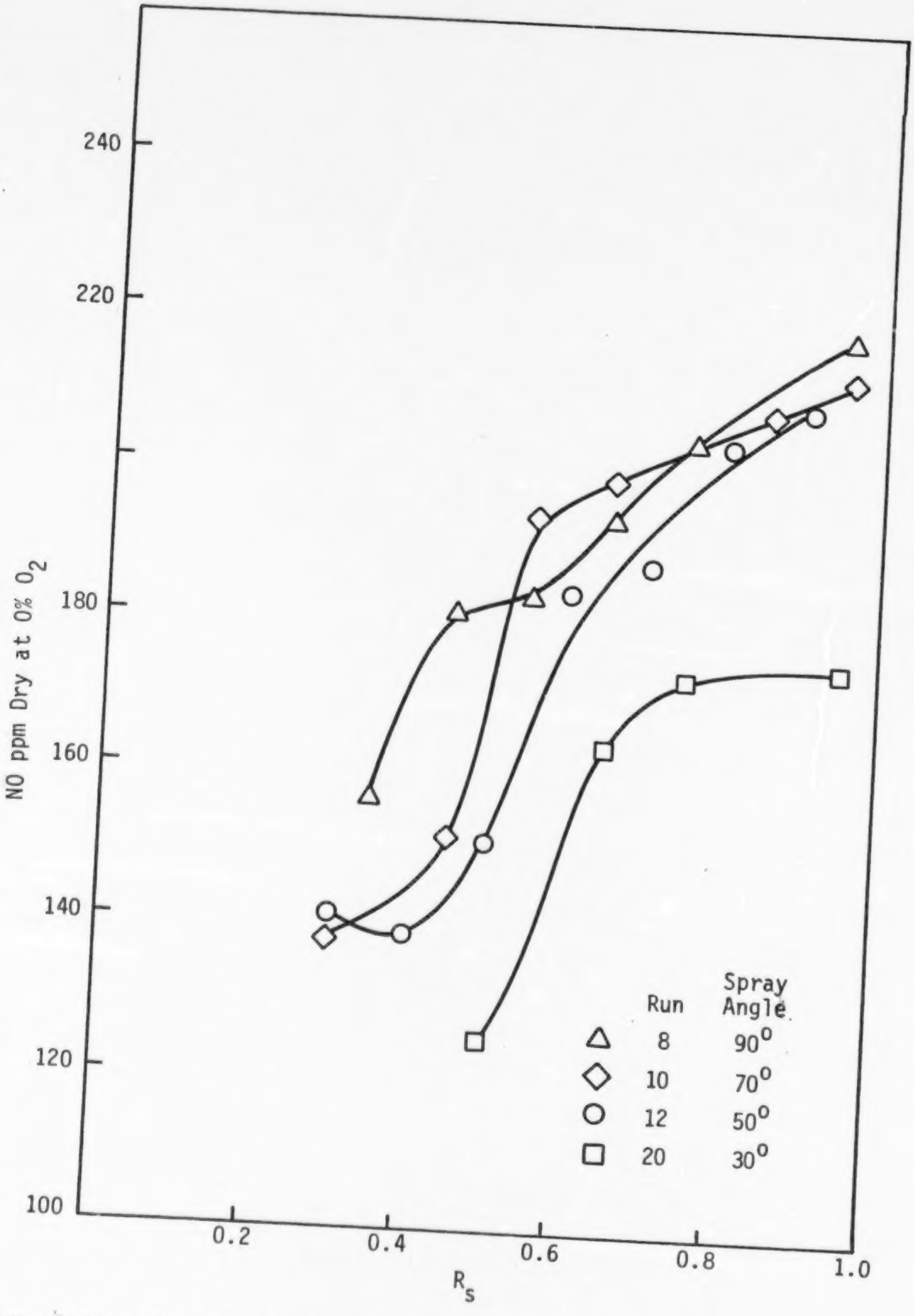

Figure 2.36. The Influence of Pressure Jet Spray Angle (Nozzle at the Exit)

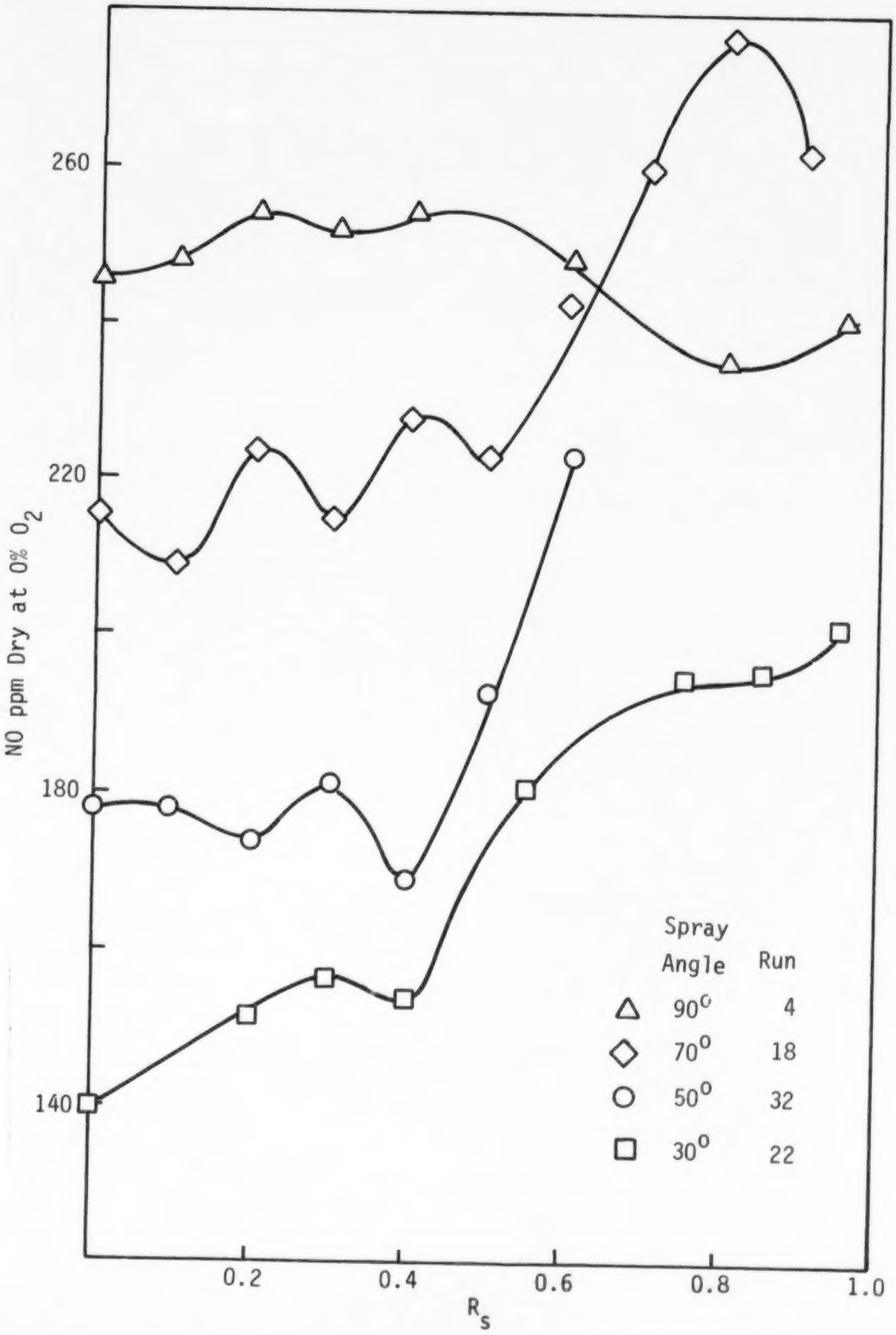

Figure 2.37. The Influence of Pressure Jet Spray Angle (Nozzle at the Throat with 45° Swirl Vane)

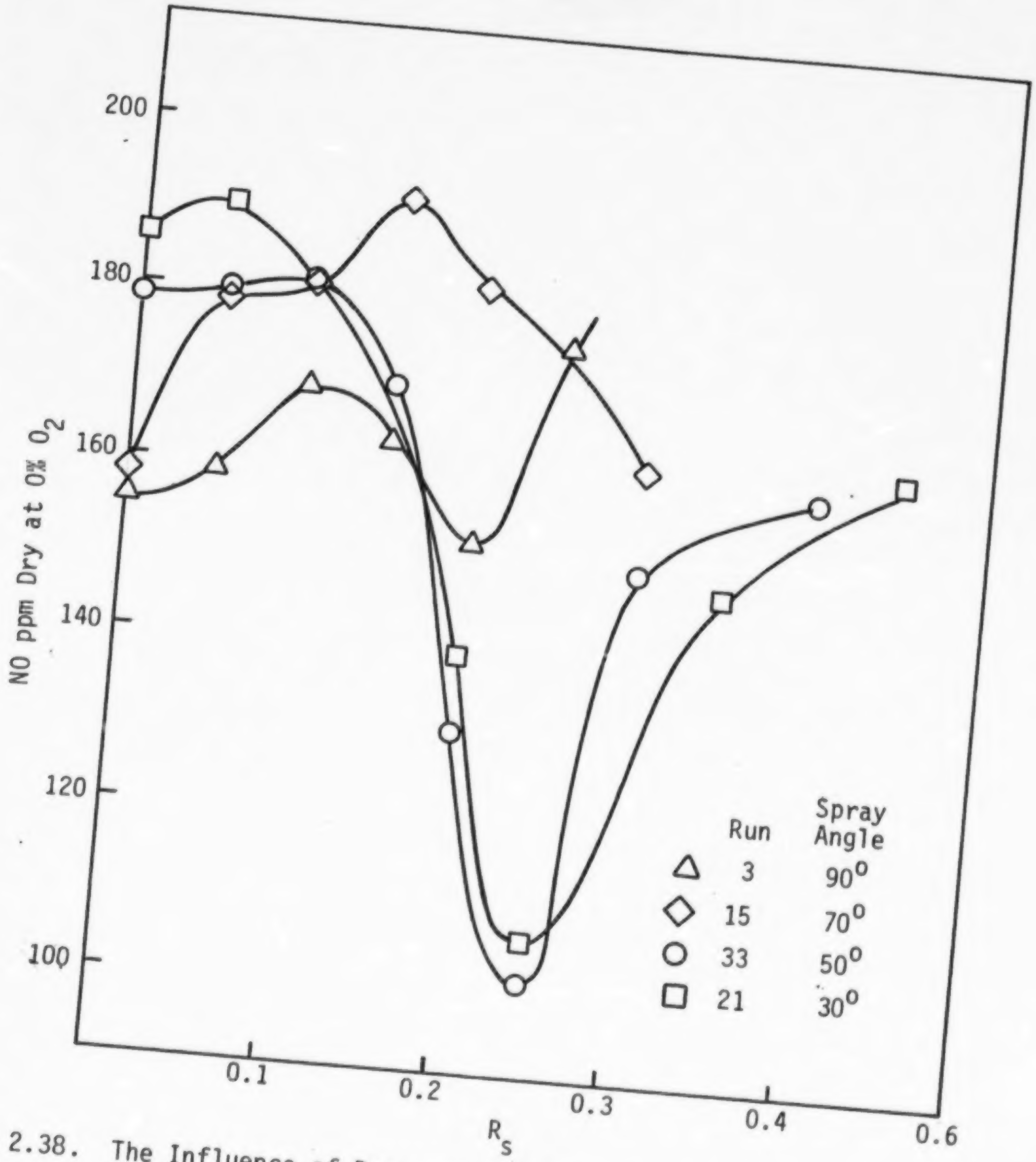

Figure 2.38. The Influence of Pressure Jet Spray Angle (Nozzle at the Exit with 45° Swirl Vanes)

With steam atomized oil injectors the effect of spray angle is less pronounced. With ambient temperature air emissions from 90° and 100° spray angles were found to be similar, although a considerable reduction was observed for an 80° nozzle. When the second air was preheated to 150°C emissions were generally reduced below the no preheat level (see Figure 2.39). The decrease in NO with a small increase in preheat (ambient to 150°C) shown by the results presented in Figure 2.39 is a surprising observation. Increasing enthalpy would normally cause an increase in flame temperature which would increase thermal NO production. One explanation for the observations is that this increase in thermal NO is more than offset by a decrease in fuel NO production attributable to a change in the fuel/air mixing rates or a change in heat release caused by the increase in preheat level. At high swirl levels emissions are not strongly dependent upon spray angle, but at low swirl levels a 90° spray gave the lowest emission.

F39

Figure 2.40 compares the emission levels obtained for the three different types of oil injector. The single-hole air-atomized injector generally gave lower emissions than either the steam or pressure atomized injectors. This observation follows the general argument presented earlier to explain the low NO levels obtained with a high velocity, single-hole coal injector. The delayed fuel/air mixing reduces fuel NO formation and also reduces peak flame temperatures.

F40

- Swirl Vanes

Swirl vanes fitted to the oil nozzle act as self-cleaning bluff bodies and promote flame stabilization at low swirl levels. The size and intensity of the recirculation zone formed on the axis with the swirl vanes attached will depend upon both the vane angle and the swirl level of the secondary air. Thus, it is reasonable to expect that these parameters will also influence NO formation. The extent of this influence for two pressure jets (30° and 70° spray angles) with the nozzle and vanes placed either at the burner throat or the burner exit can be seen in Figures 2.41 through 2.44. All four parameters influence the exhaust emission level. Maximum concentrations were observed with the wider

F41,42
✓43,44

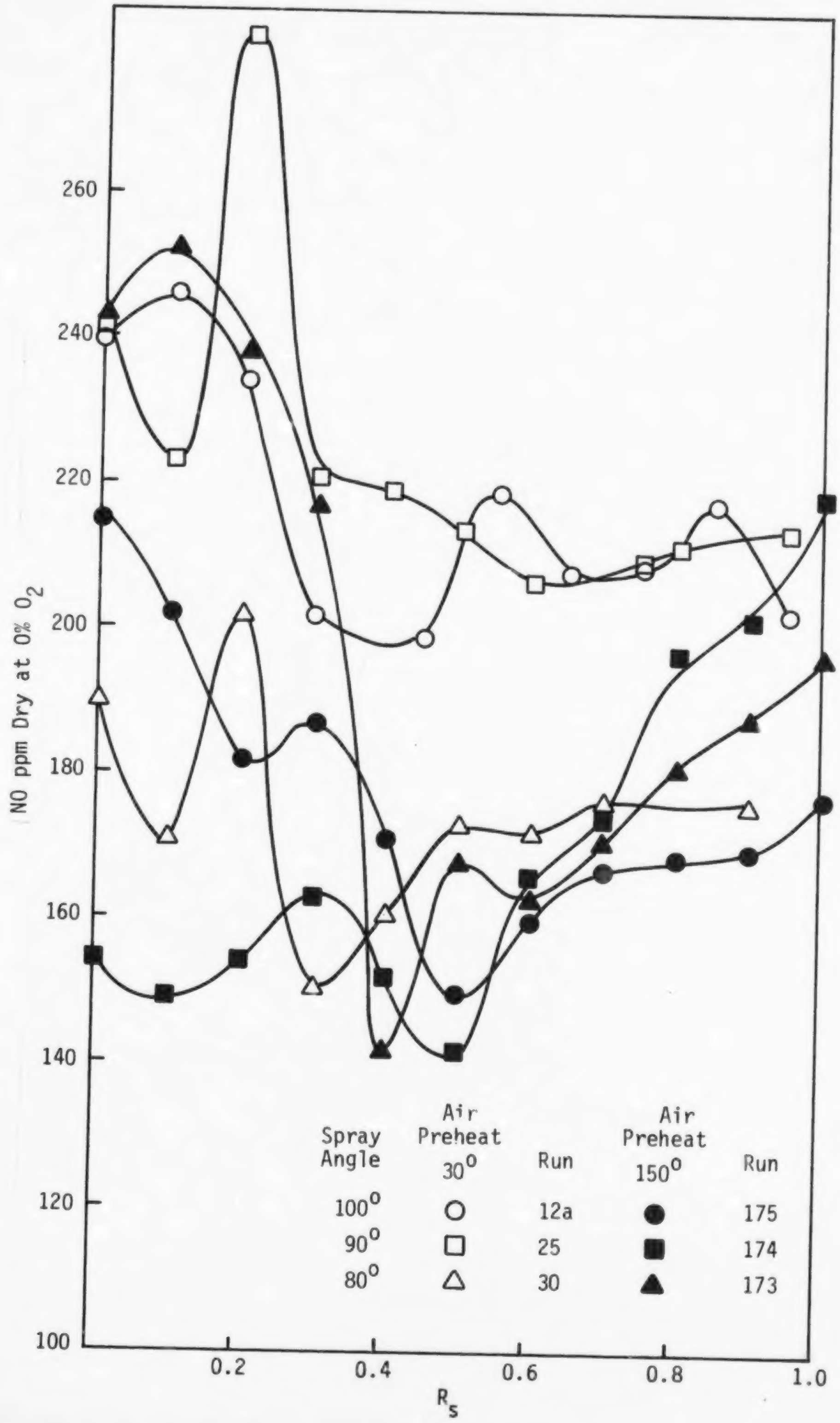

Figure 2.39. The Influence of Steam Atomizer Injector Spray Angle and Air Preheat (Nozzle in the Throat)

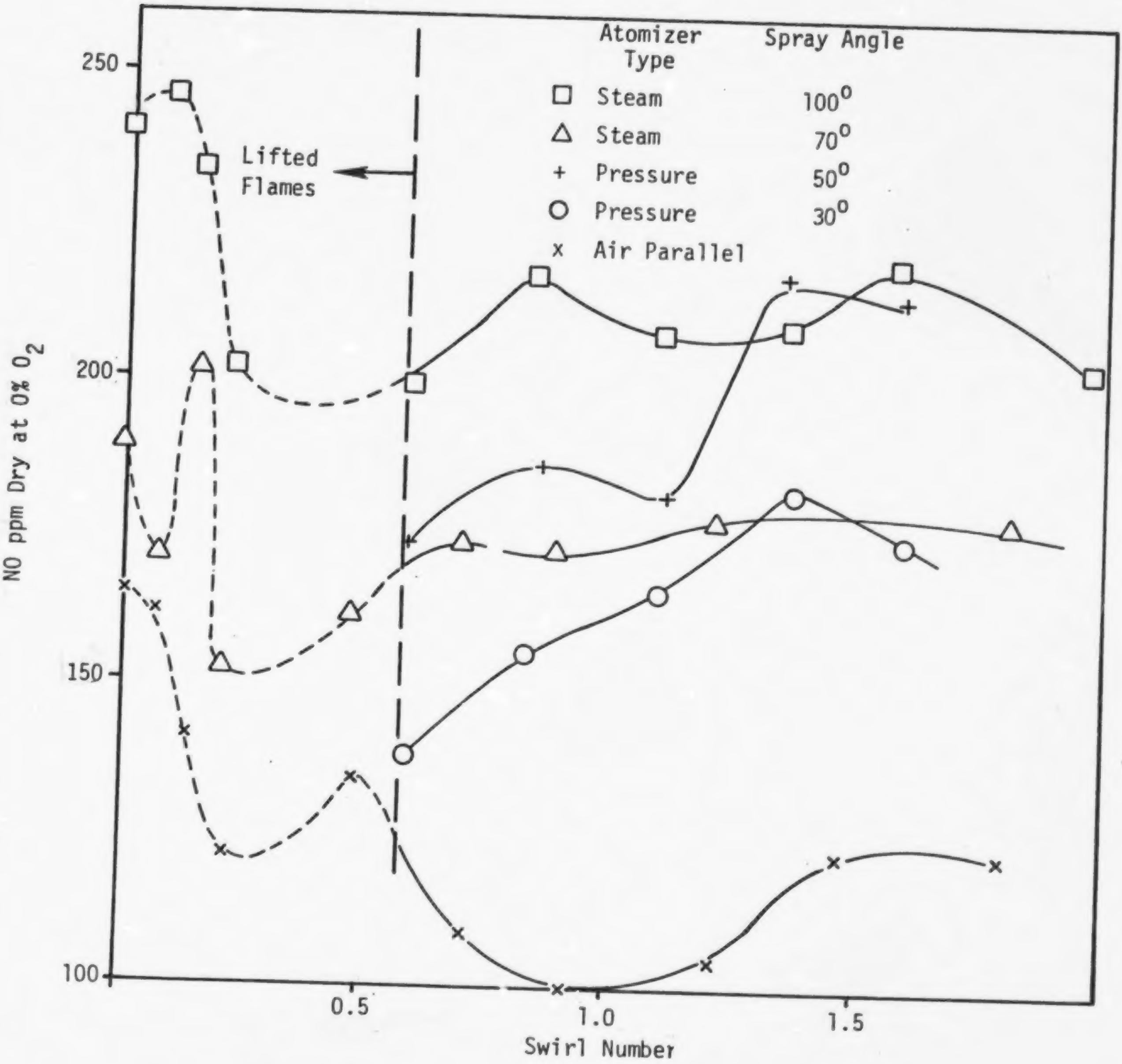

Figure 2.40. The Influence of Atomizer Type on NO Formation in Fuel Oil Flames

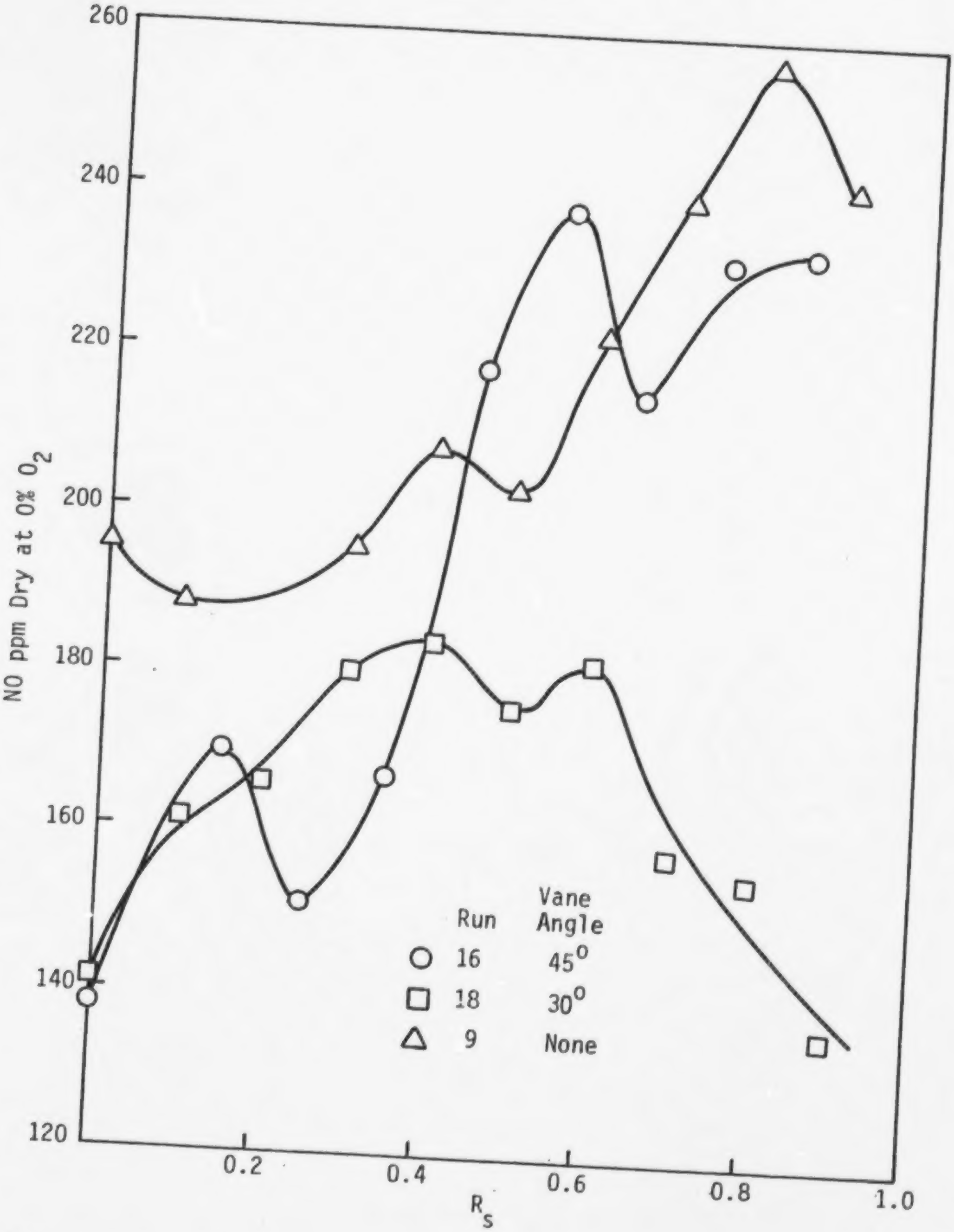

Figure 2.41. The Influence of Swirl Vanes Attached to the Nozzle (70° Pressure Jet in the Throat)

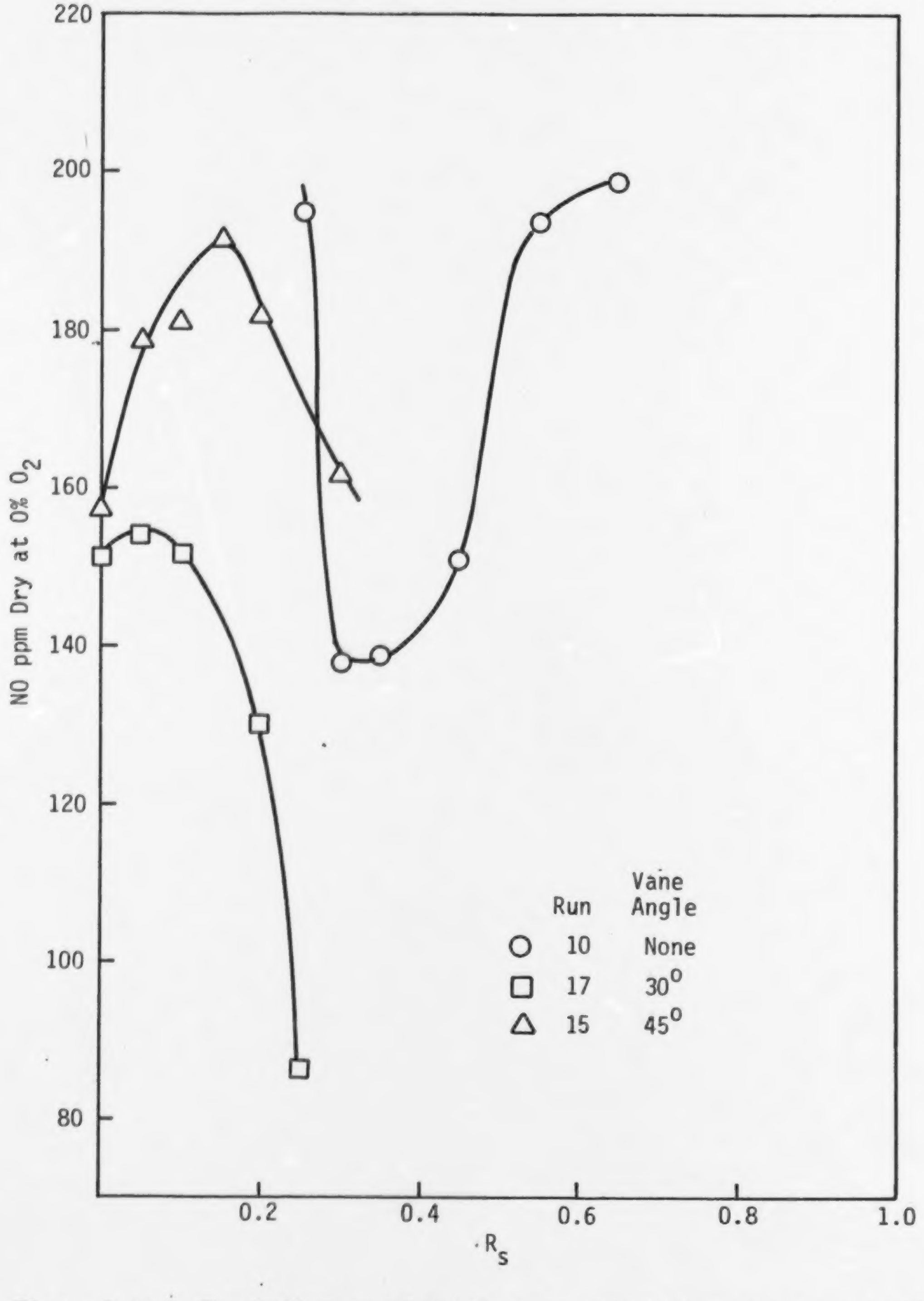

Figure 2.42. The Influence of Swirl Vanes Attached to the Nozzle (70° Pressure Jet at the Exit)

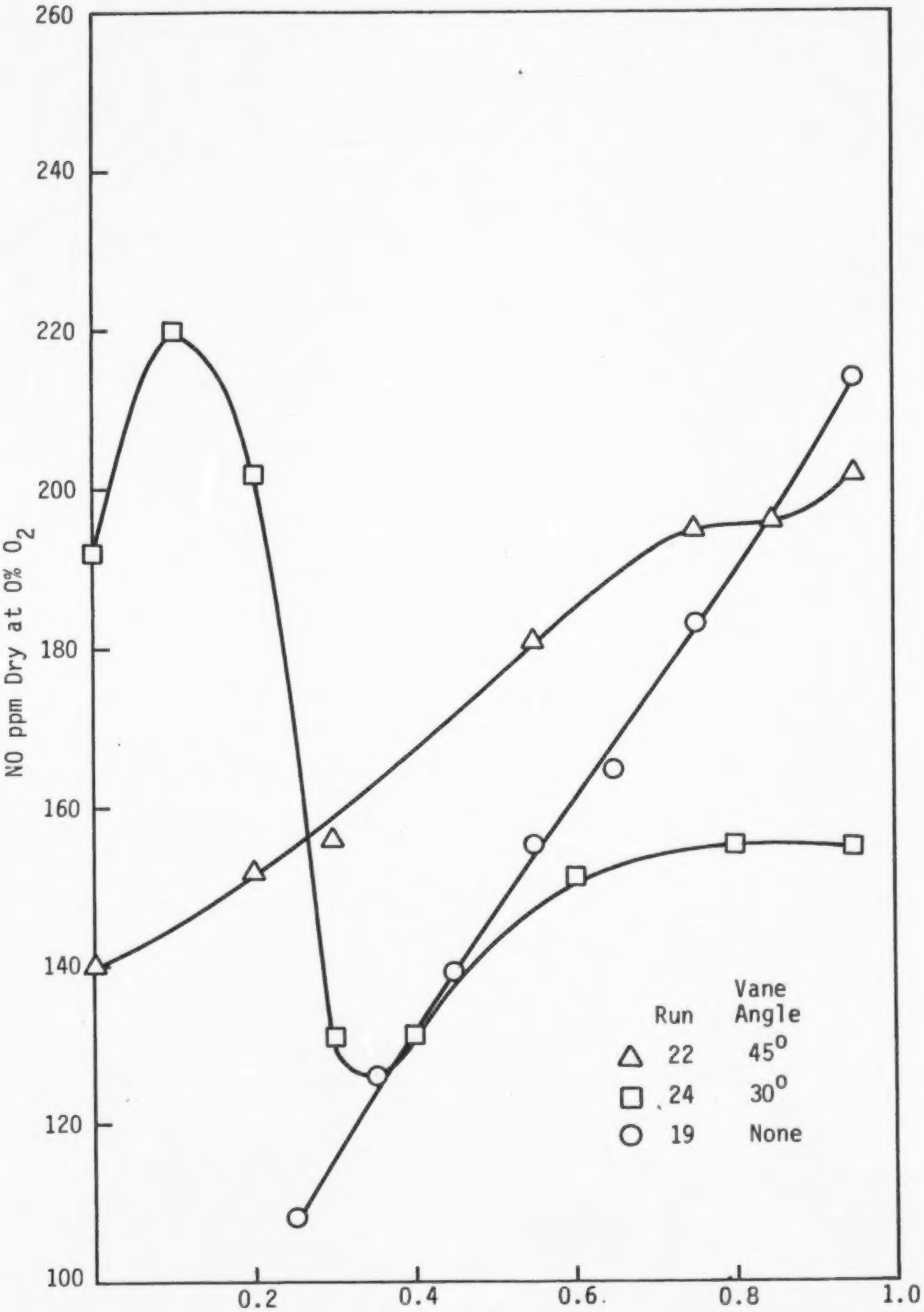

Figure 2.43. The Influence of Swirl Vanes Attached to the Nozzle (30° Pressure Jet in the Throat)

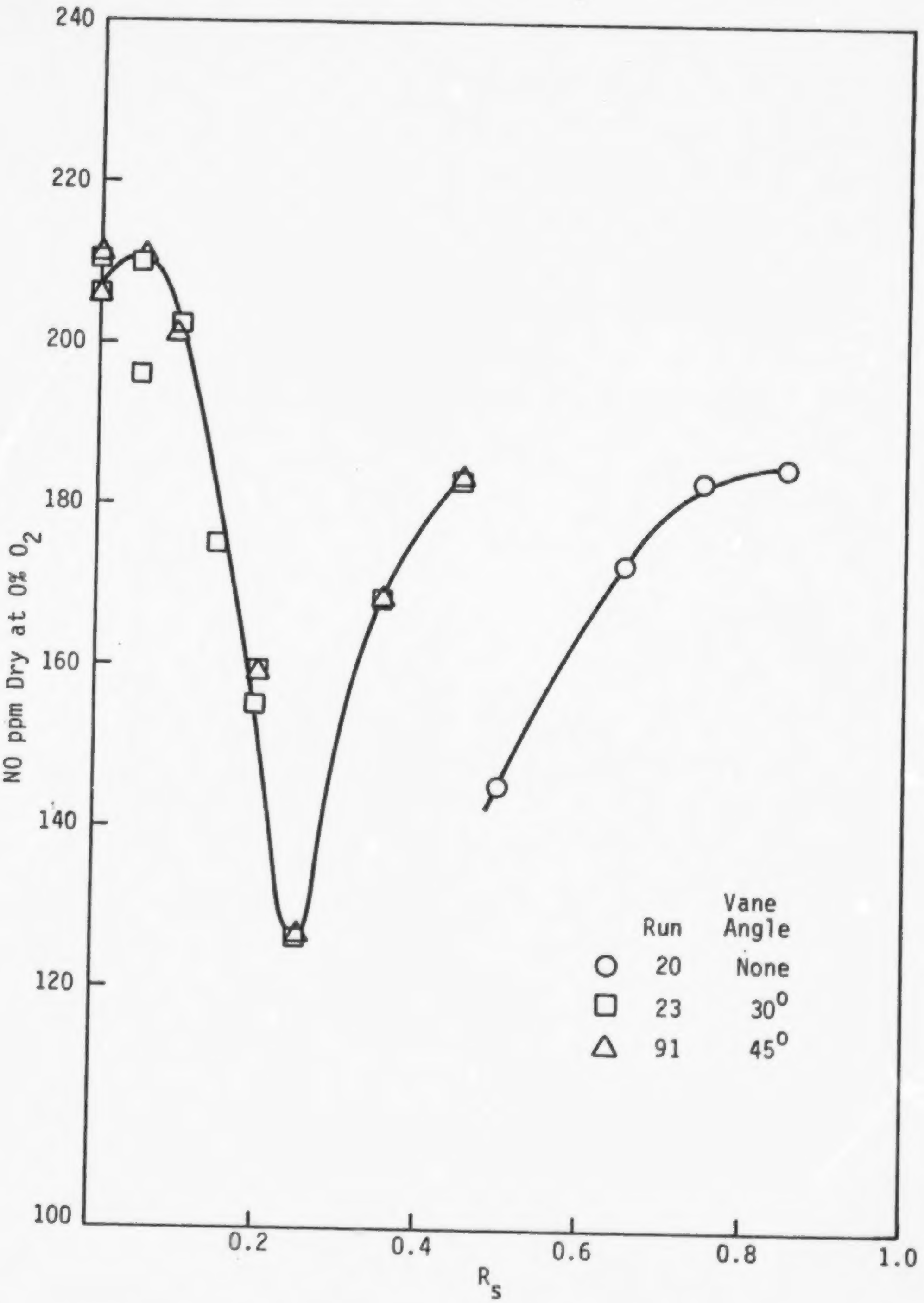

Figure 2.44. The Influence of Swirl Vanes Attached to the Nozzle (30° Pressure Jet at the Exit)

spray angle with the nozzle in the throat. Minimum emission levels obtained with the two angles were similar when the nozzle was placed at the burner exit. Minimum emissions at zero secondary swirl were found with the 30° spray and 45° swirl vanes.

- Position of the Fuel Injector

Results presented earlier indicated that the position of the fuel injector, whether in the throat or at the exit, had an influence upon the emission of nitric oxide. Emissions were generally lower with the nozzle at the exit. Figure 2.45 compares the emission characteristics of flames produced with a single 80° steam atomized injector with three different swirl vanes attached to the nozzle, with the nozzle placed at different positions relative to the burner exit. This position was determined by the point at which a stable flame could be maintained at the nozzle. With zero secondary swirl the flame front was established some distance from the nozzle. As the nozzle was pulled towards the burner throat the flame would jump back to the nozzle at some point. The necessary movement to achieve this effect differed for all three vane swirlers. As shown in Figure 2.45, this movement produced a 50 ppm reduction in exhaust emissions for the 30° and 45° vanes, producing stable flames with low burner pressure drops.

- Divergent Angle

The ability to vary the divergent angle of the burner exit is restricted by the possibility of oil spray impingement on the water-cooled burner causing coke buildup. Figure 2.46 illustrates the reduced emissions obtained by narrowing the exit angle with a pressure jet atomizer.

- Secondary Air Velocity

In a small laboratory scale furnace Pershing(9) found that increasing the velocity of the second air stream from 100 to 200 ft/sec reduced nitric oxide emissions both from No. 2 fuel oil and No. 2 fuel oil doped to give a nitrogen content equivalent to 0.3 percent. This is contrary

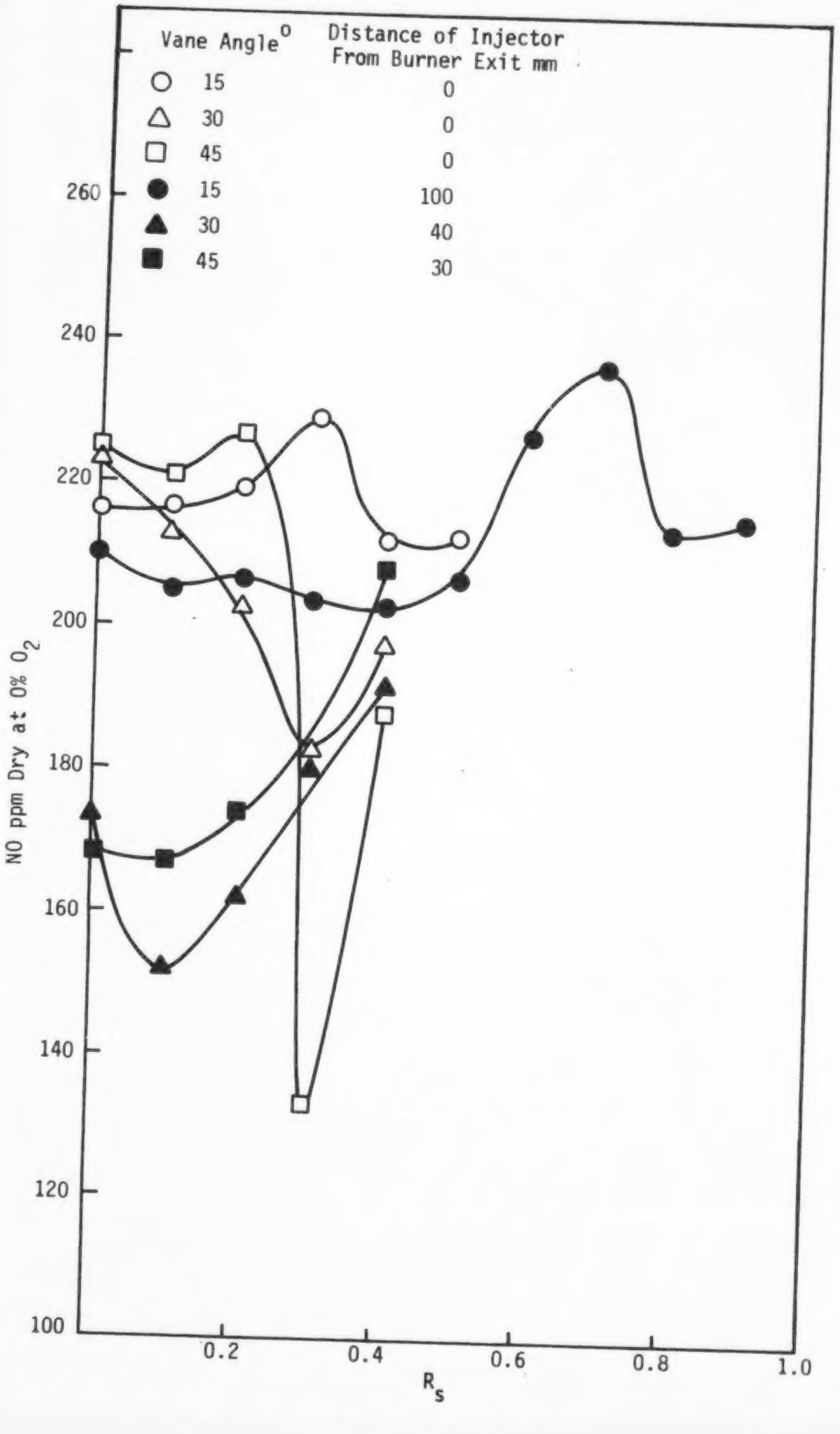

Figure 2.45. Change in Emissions Due to Movement of the Nozzle Toward the Burner Throat

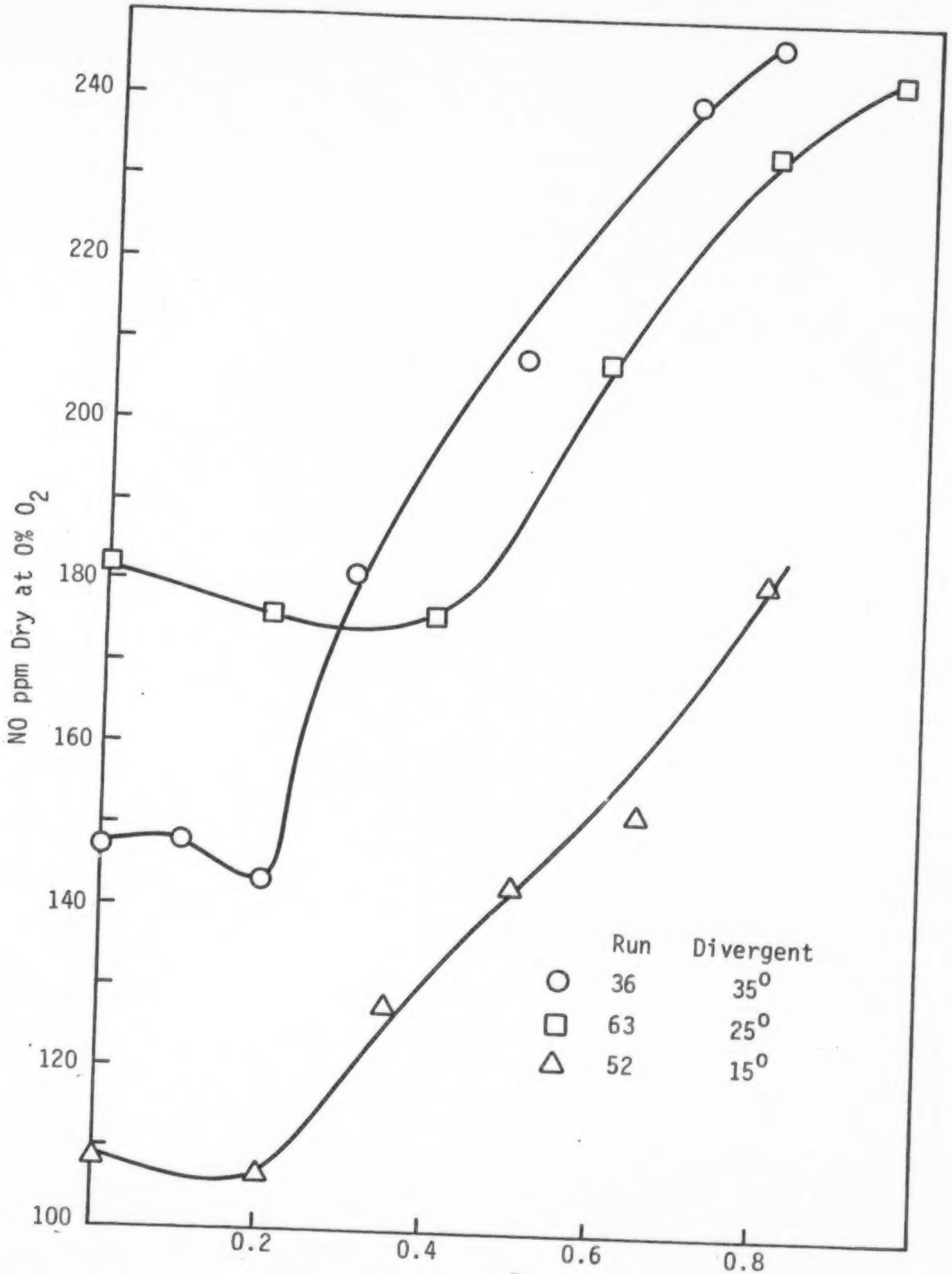

Figure 2.46. The Influence of Divergent Angle of the Burner Exit (30^0 Pressure Jet in the Throat)

F 47, 48

to the results presented in Figures 2.47 and 2.48. For both pressure jets and steam atomized injectors, emissions increased as the throat area was reduced, which caused an increase in the throat velocity.

The results discussed above were obtained to provide preliminary information on the influence of emission characteristics on heavy fuel oil flames. Although all the parameters investigated had some influence, virtually all emissions fell in a band between 100 and 300 ppm. One obvious limitation of this preliminary series of experiments was the lack of some method of assessing particulate emissions. Since the furnace was operated with a minimum cooling load, smoke emissions were not a problem. The results do indicate that lower emission from oil flames could be obtained by modifying the burner; however, in all cases this would produce a larger and/or narrower flame.

2.4 Thermal Effects and Nitric Oxide Formation in Turbulent Diffusion Flames

Two of the most interesting observations made during the furnace investigations involved the influence of air preheat level:

- High NO levels were recorded from pulverized coal flames under high load and high preheat conditions.
- Emissions from fuel oil flames were lower with an air preheat of 150°C than when the oil was burned with no air preheat, but with the same burner conditions.

In the refractory tunnel furnace used in these investigations the actual flame temperature is strongly dependent upon the bulk gas temperature which, in turn, is dependent upon the thermal input and the furnace cooling load. The investigations with the subscale practical burner were conducted in an almost uncooled furnace and involved variations in both load and air preheat level.

F 49, 50

Figures 2.49 and 2.50 are cross plots of data presented in an earlier section showing the influence of preheat and fuel firing rate on NO emissions from pulverized coal flames. NO formation appears to be independent of preheat level at low firing rates below 300°C for all excess air levels. This

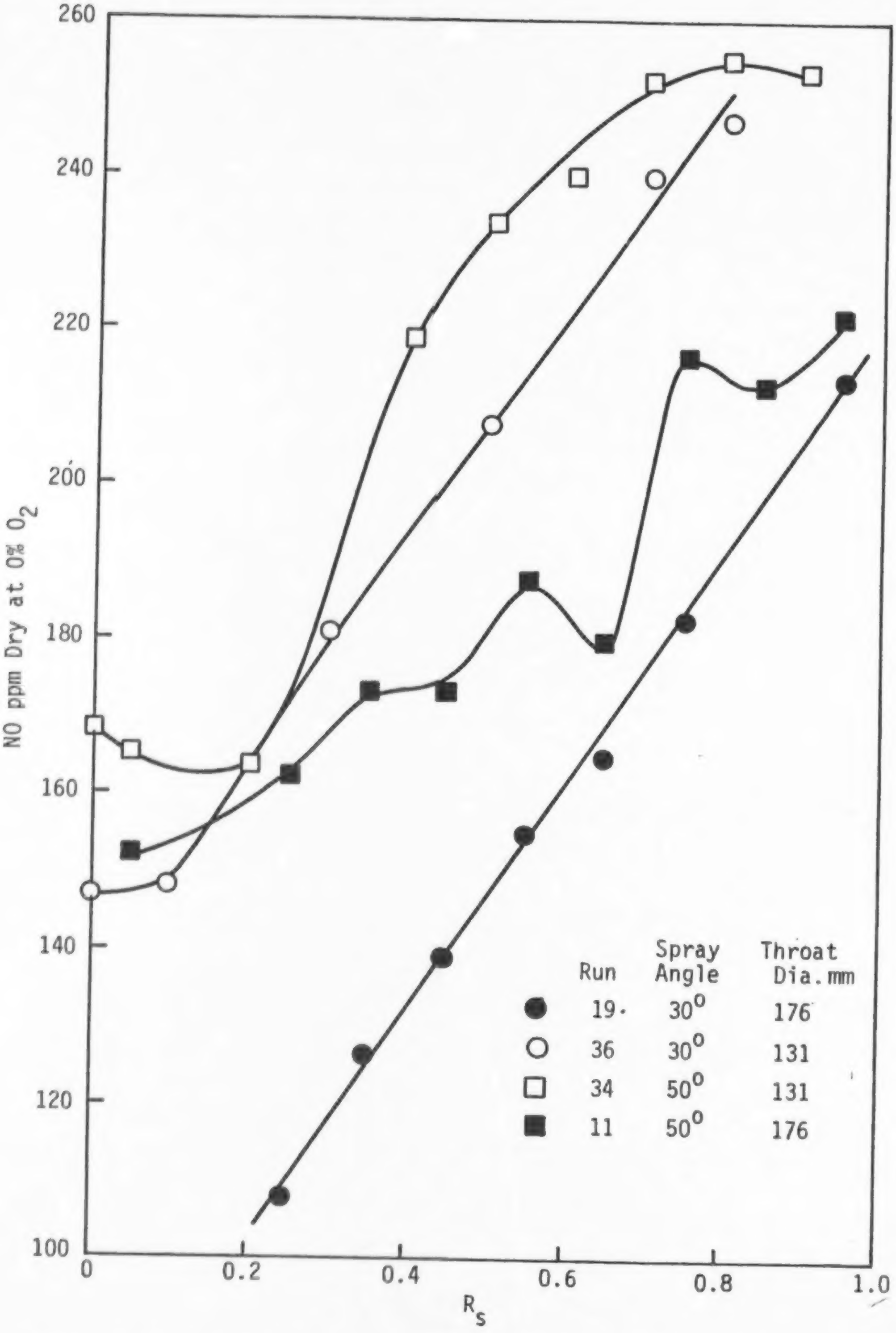

Figure 2.47. The Influence of Secondary Velocity (Pressure Jet in the Throat)

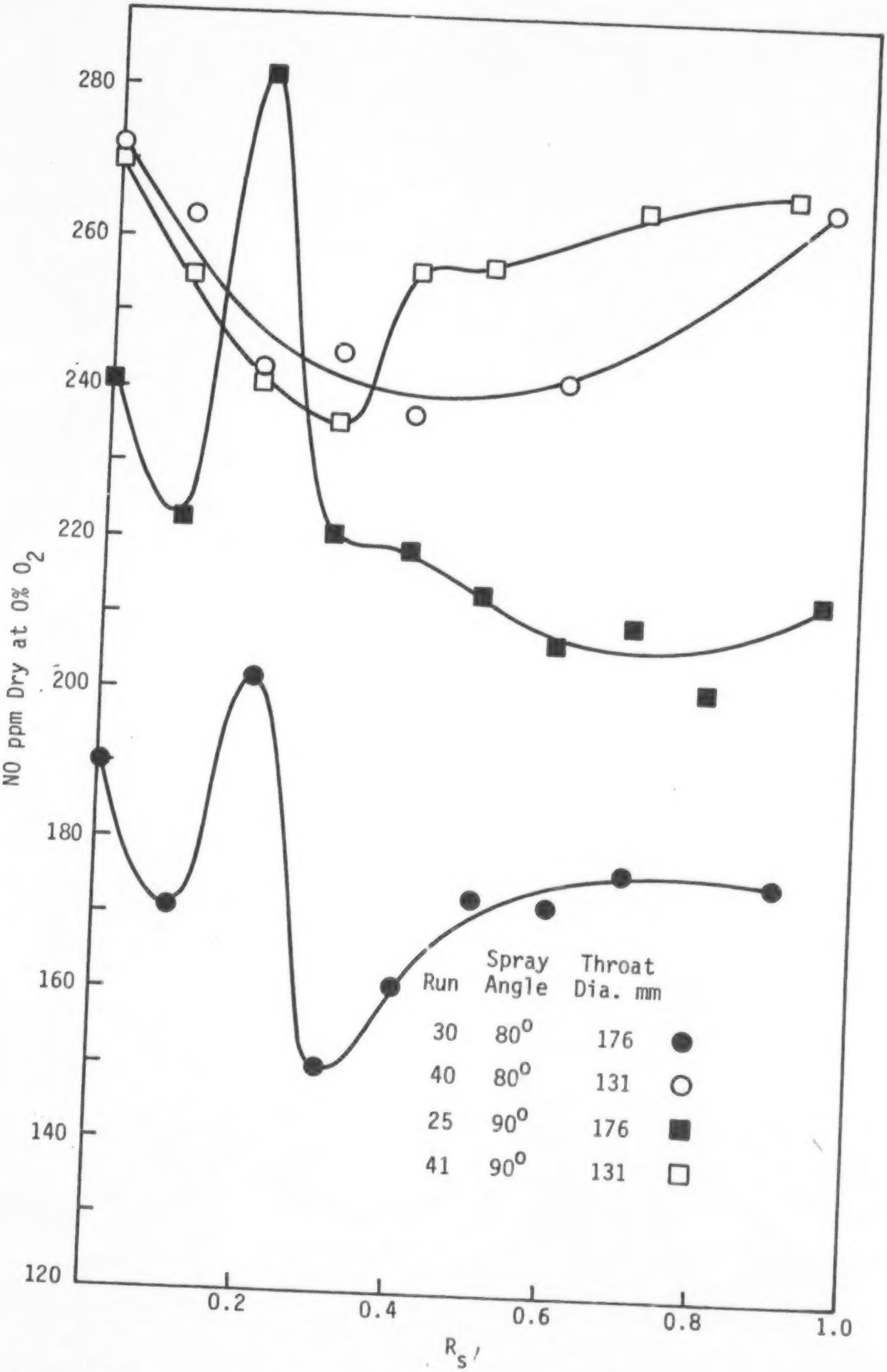

Figure 2.48. The Influence of Secondary Velocity (Steam Atomized in the Throat)

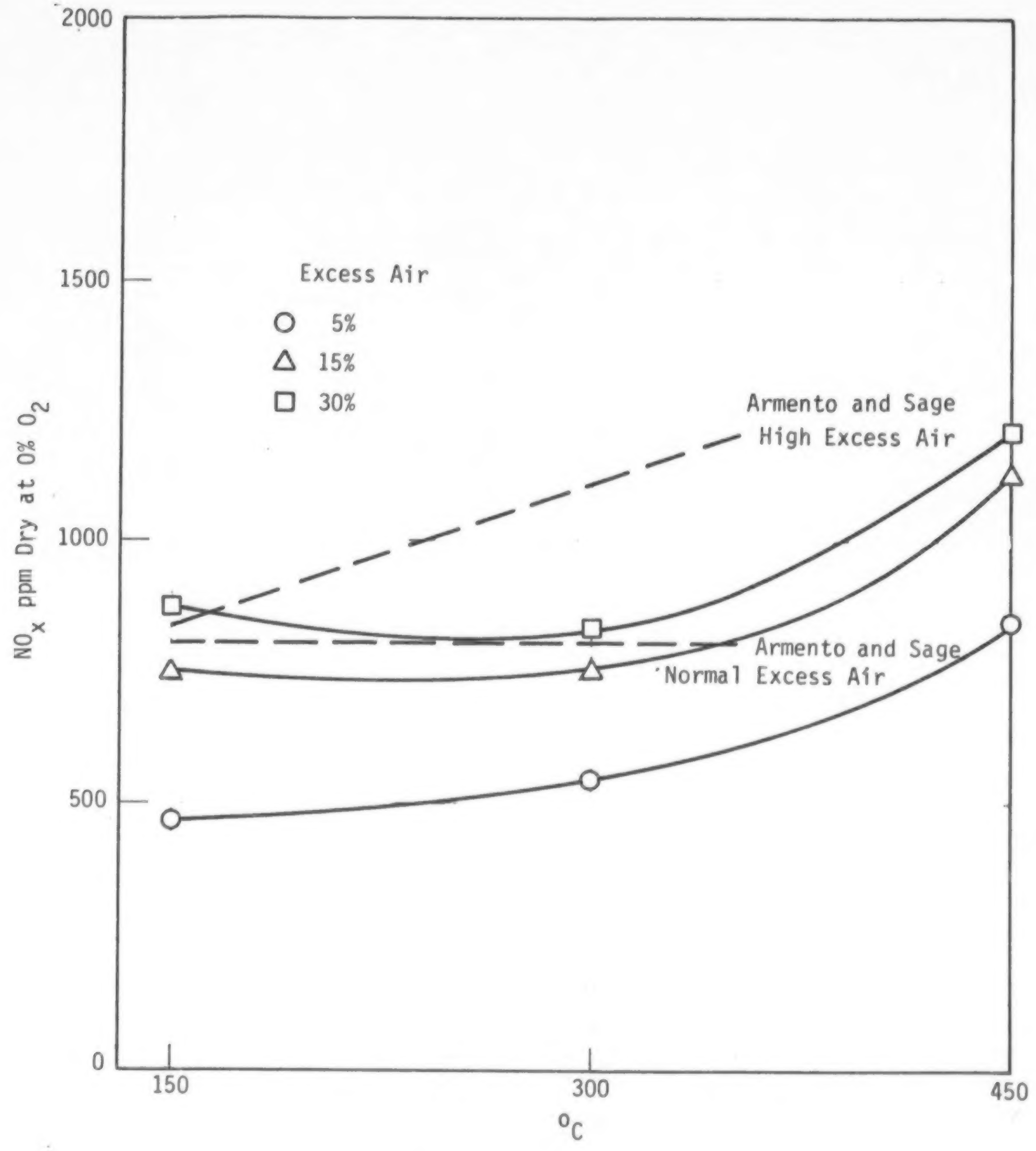

Figure 2.49. The Effect of Preheat on the Emission Characteristics of a Subscale Practical Burner (Firing Rate 200 kg/hr Coal)

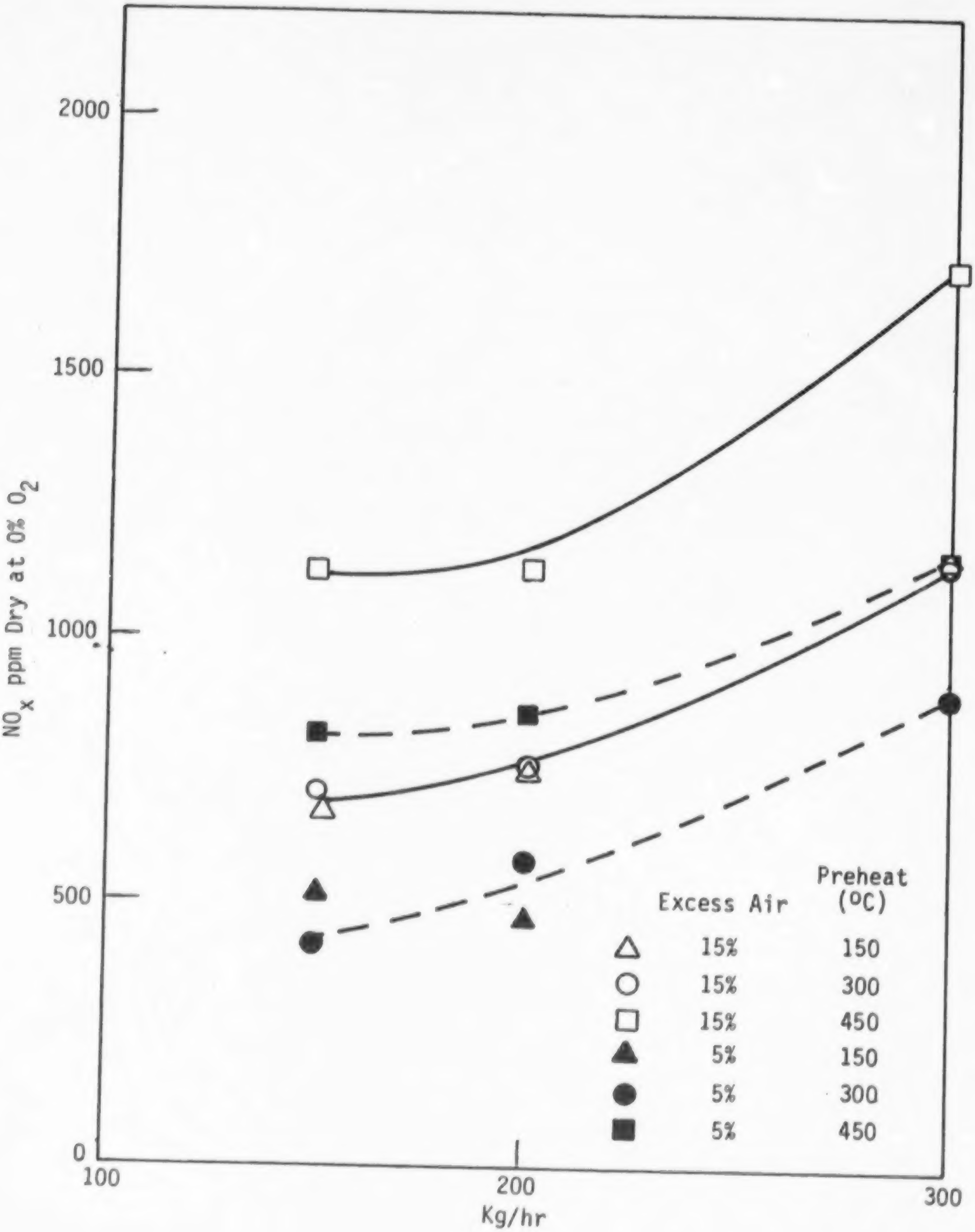

Figure 2.50. The Effect of Load on the Emission Characteristics of a Subscale Practical Burner

contradicts work reported by Pershing(2) and Armento(7). Pershing found that for pulverized coal flames NO emissions increased by about 30 percent when the preheat level was raised from 140°C to 260°C, although the results do show some effect of swirl level. The Armento and Sage results are plotted on Figure 2.46 for Ohio coal. NO emissions are independent of preheat at normal excess air levels, but the effect of preheat increases as the excess air level increases. The maximum preheat level used by Armento was about 320°C and in this temperature range there is some degree of agreement between the results obtained in both investigations. The major discrepancy between the two investigations concerns high excess air firing. In Armento's tests high excess air refers to levels greater than 25 percent, and normal is nominally 15 percent excess air, but covers data with excess air levels between 7 and 25 percent.

The burners and the firing rate used by Armento were virtually the same as those used in the present investigation and yet the results were dissimilar. The major differences between the two investigations were the following:

- Fuel type. Armento used an Ohio coal with 1.07 percent nitrogen and 30 percent volatile content.
- Furnace cooling load. The furnace used by Armento was cylindrical and had a cooled refractory wall.
- Volumetric heat release rate. The volumetric heat release rate in the IJmuiden furnace was six times less than that in the B&W furnace. Armento reports that increasing the "quench" rate an unspecified amount by removing some of the refractory furnace liner reduced the emission level by 20 percent.

These results suggest that the "temperature environment" of the flame (i.e., wall temperature, bulk gas temperature) will influence the formation of nitric oxide in pulverized coal flames. In an attempt to ascertain the extent of this influence, emission levels were measured during the transient conditions obtained as the furnace was heated by flames with constant input conditions.

F 51, 52, 53

The results presented in Figures 2.51, 2.52 and 2.53 show flue gas NO concentrations, furnace wall temperatures and combustion product temperature as a function of time from ignition as the furnace temperature was used during the heating cycle. The wall temperature was measured by a thermocouple embedded in the refractory and the gas temperature was measured by a suction pyrometer positioned 2.75m from the firing wall. It can be seen that the NO emission increased with time, both for the natural gas and the pf flame. However, the emission from the oil flame was almost constant during the heating period.

Natural gas does not contain fuel nitrogen; the total emission is due to thermal NO formation. As it has already been established that an increase in bulk furnace temperature produces an increased emission(1), the results presented in Figure 2.48 were not unexpected. Therefore, it is reasonable to expect that an increase in bulk gas temperature will also increase thermal NO formation in both coal and oil flames. The work of Pershing et al(2) suggests that under preheated conditions approximately 50 percent of the total emission from fuel oil flames is thermal NO. Therefore, it is surprising that the increase in bulk gas temperature as the furnace wall temperature increases does not cause an increase in NO emissions from fuel oil flames although it does from coal flames. No complete explanation is available for the results shown in Figures 2.52, 2.53 and 2.54.

F 54

The emissions from pf flames should be almost independent of bulk temperature since the rate of fuel NO formation is not strongly dependent upon temperature and a large proportion of the total emission can be attributed to fuel NO. Thus the influence of bulk gas temperature probably reflects an influence of coal heating rate on volatile fuel nitrogen compound formation.

F 55

The effect of air preheat on NO formation in fuel oil flames appears to be dependent on the method of oil atomization and the swirl level of the combustion air (see Figure 2.54 and 2.55). With a 90° spray angle steam atomized jet NO emissions first decrease and then increase as the temperature of the combustion air is raised from ambient to 450°C. Emissions at 150°C were lower than those measured at ambient combustion air temperatures. At low swirl levels emissions appear to be strongly dependent upon air preheat

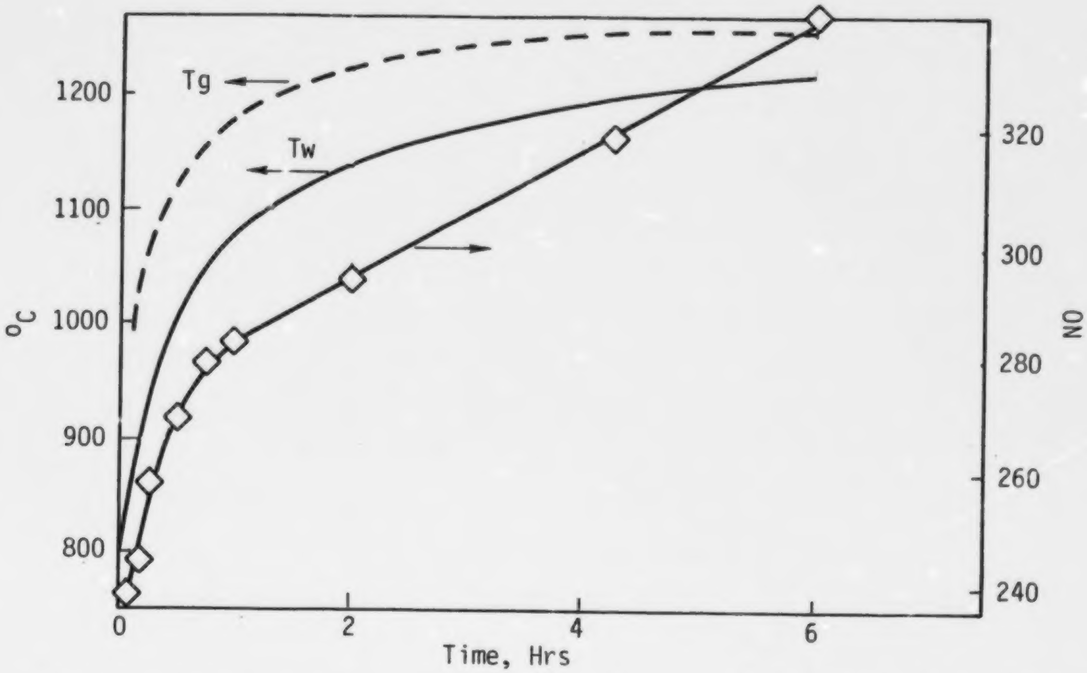

Figure 2.51. Natural Gas 5% Excess Air - The Effect of Furnace Temperature on NO Formation

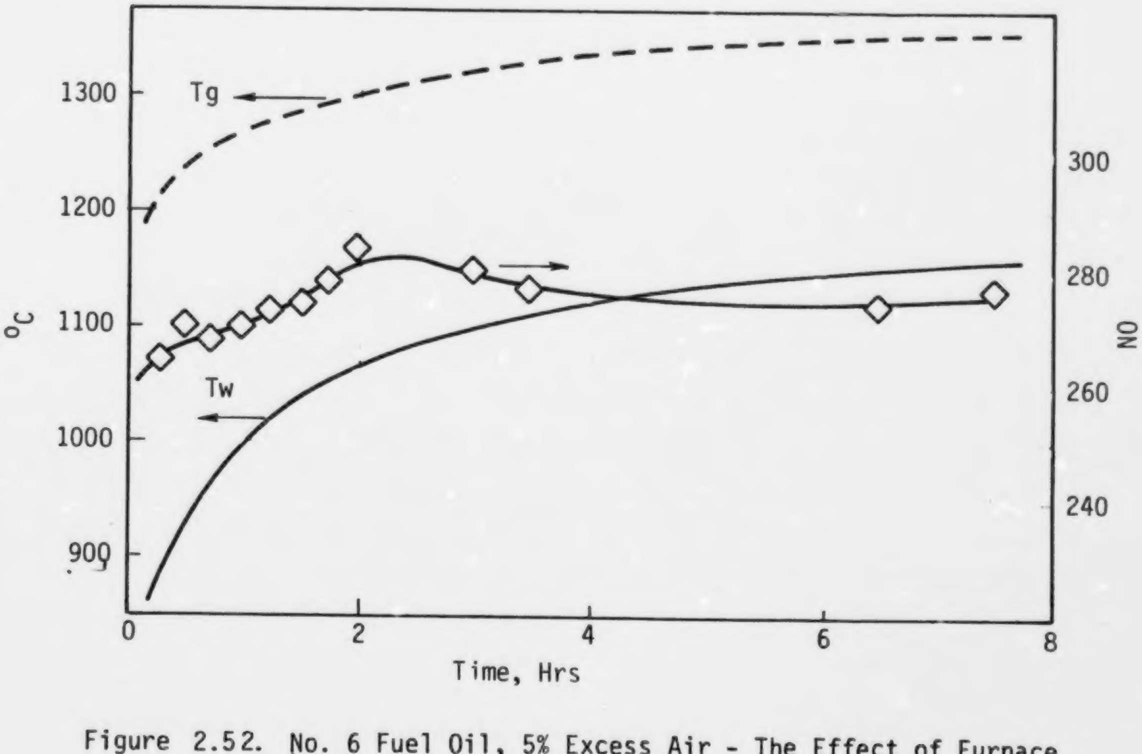

Figure 2.52. No. 6 Fuel Oil, 5% Excess Air - The Effect of Furnace Temperature on NO Formation

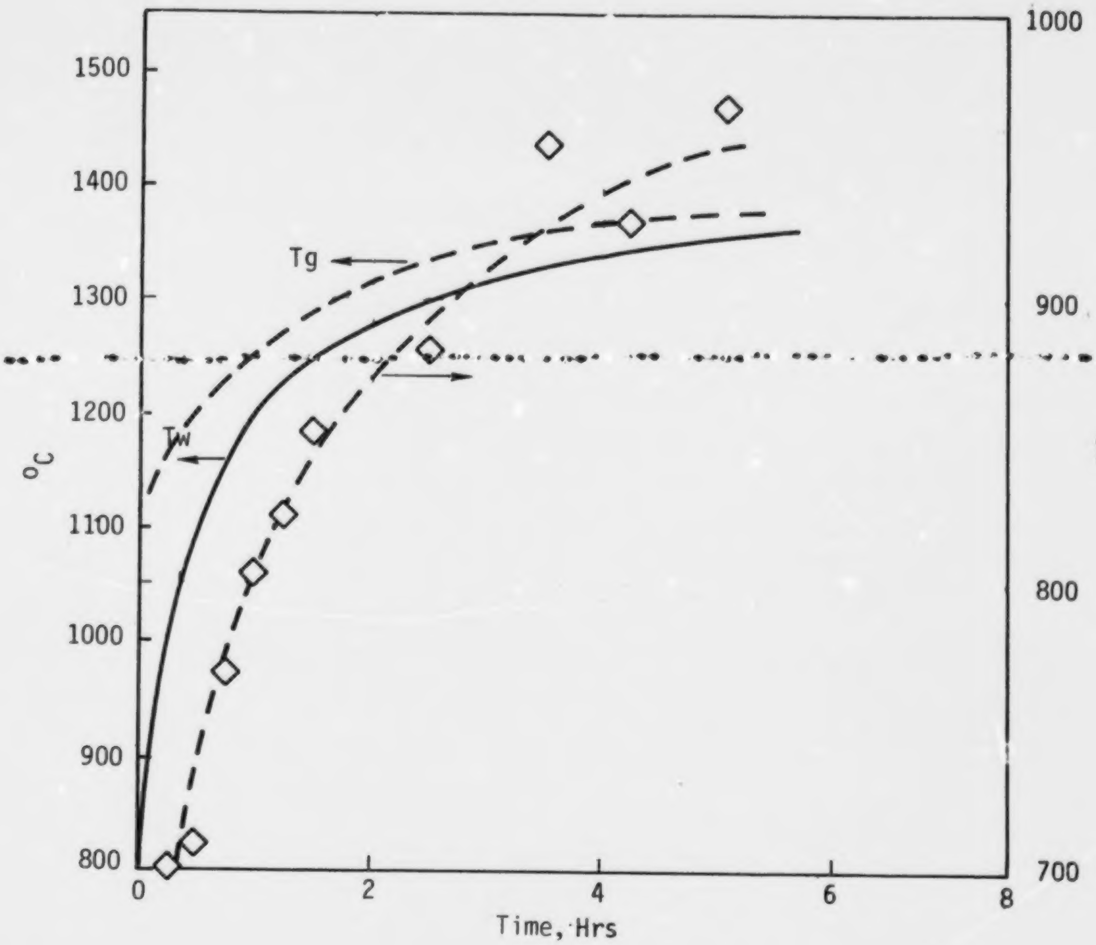

Figure 2.53. Pulverized Coal 15% Excess Air - The Effect of Furnace Temperature on NO Formation

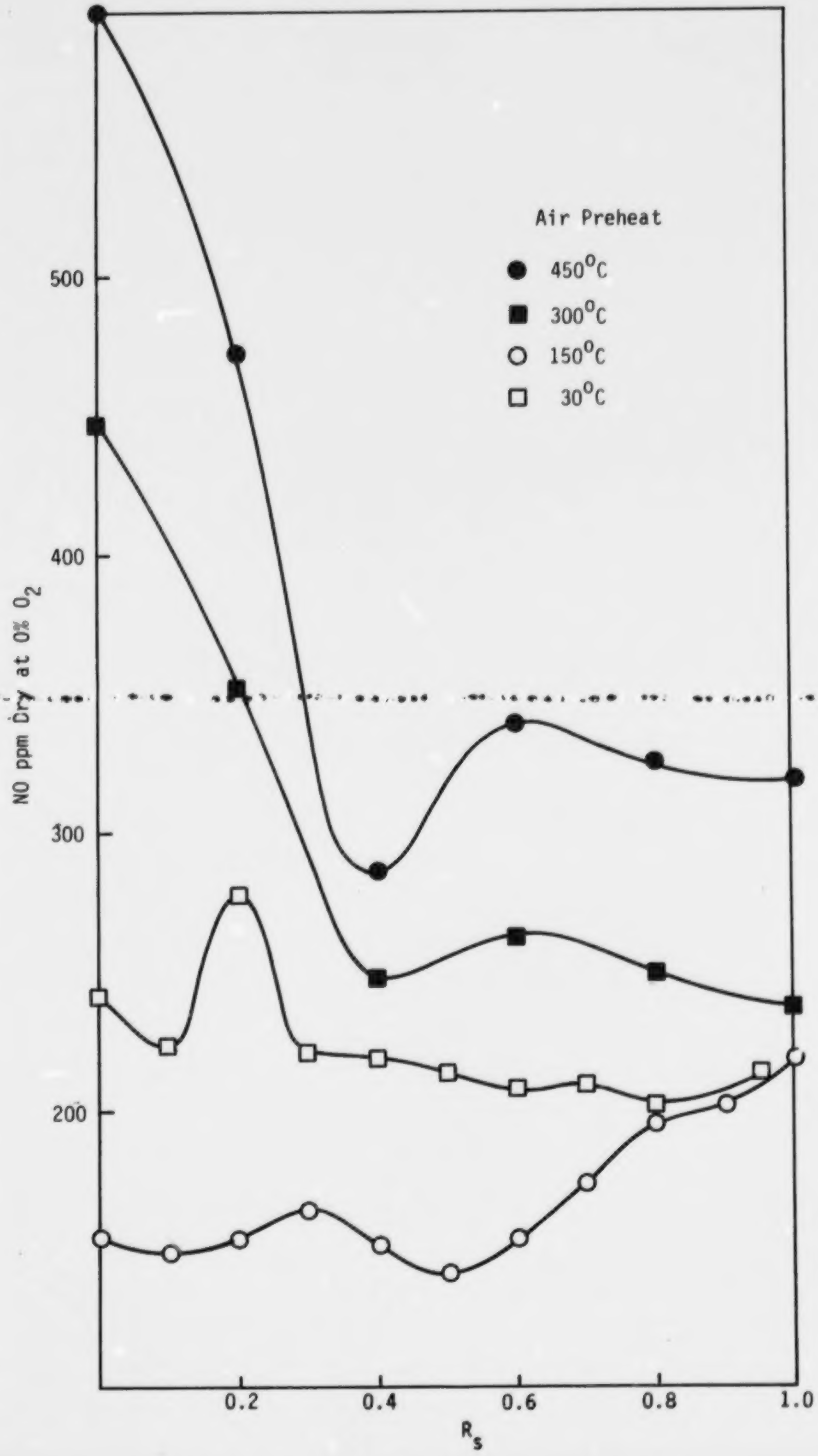

Figure 2.54. The Influence of Air Preheat Level (on 90° Steam Atomizer)

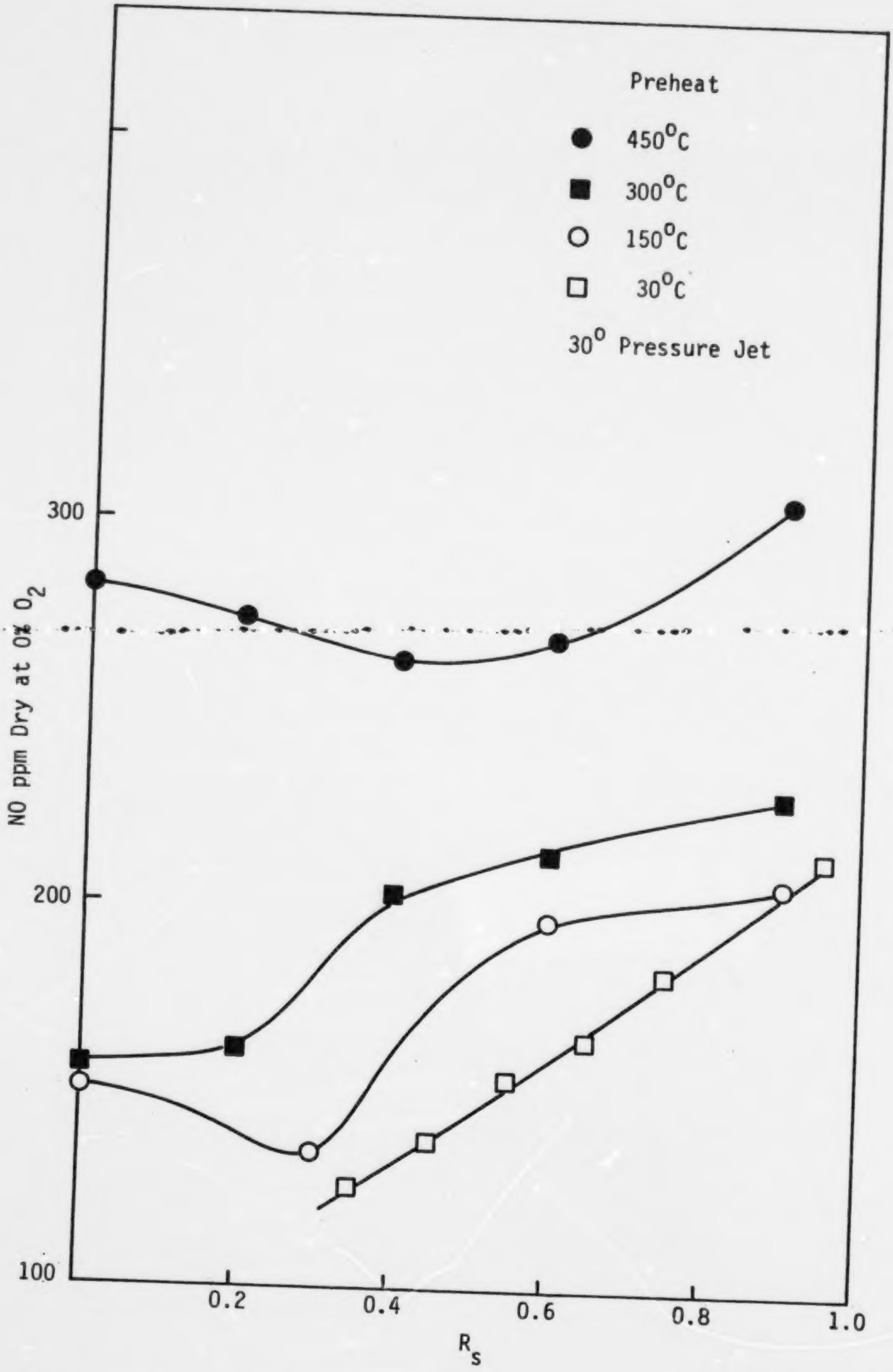

Figure 2.55. The Influence of Air Preheat Level (30° Pressure Jet)

and there appears to be a big increase in emissions as the preheat level is increased from 300 to 450°C. This also applies to the pressure jet results (Figure 2.55); however, with this atomizer, emissions increase continually as the preheat level is increased from ambient to 450°C.

All of these results suggest that care must be exercised if any empirical correlations are proposed based upon a theoretical flame temperature calculated for a given fuel and excess air level. The temperature of importance is the actual temperature of the heat release zone which is dependent upon parameters other than the fuel/air ratio and the properties of the fuel and air because the reactants also contain combusted products. Consequently, the temperature of the flame will vary both temporally and spatially because of the turbulent nature of the flow. Other parameters which affect the temperatures of the flame include furnace wall temperature, heat and heat release rate. Although the conversion of simple nitrogen compounds to NO in premixed flames may be insensitive to temperature, the formation of fuel NO in turbulent diffusion flames may be strongly dependent upon temperature. Fuel heating rate is known to influence the rate of volatile evolution from coal particles. The composition of the products of inert pyrolysis of model nitrogen-containing compounds show a dependence of temperature(10). The increased emissions at high preheat levels may also be due to the strong temperature sensitivity of thermal NO formation. At low firing rates and preheat levels all the NO emission from coal flames could be attributed to fuel NO, and the increased emissions at 450°C preheat may be due to thermal NO formation.

2.5 Conclusions and Implications for Further Investigations

The second series of furnace investigations confirmed the general conclusions which were reached after the initial furnace test series. The formation of both thermal and fuel NO in turbulent diffusion flames is strongly dependent upon mixing rate of fuel, air and recirculating combustion products and that these mixing rates can be controlled to minimize NO emissions by optimizing burner design parameters. For nitrogen-containing fuels it appears that the major burner design objective is the limitation of oxygen availability in the early stages of heat release and which will therefore reduce the fraction of fuel nitrogen converted to NO. Two methods have proved successful in accomplishing this objective with both coal and residual fuel oil:

- The Method of Fuel Injection

  With both fuels those injectors which divert the fuel toward the burner axis produce lower NO emissions than those fuel injectors which spread the fuel over a wide angle and thus more of the fuel mixes rapidly with the air. The series of investigations with fuel oil indicated that narrow spray angles produced lower NO emissions but that they also tended to produce longer flames than wide angled sprays.

- Air Distribution

  Delayed fuel/air mixing was accomplished by varying both the tangential momentum of the combustion air stream at the burner and by dividing the total combustion air into two separate streams and injecting one stream from the periphery of the burner exit.

It appears that the latter method of delaying fuel oil mixings and thus reducing NO formation shows considerable promise for the future because there appears to be reduced tendency to increase flame length as the NO emission is lowered. Initially tests with tertiary air systems increased rather than decreased NO emissions indicating that this method of NO control is open to abuse. However, the results of the investigations with the tertiary air injection and the subscale practical burner were most encouraging and indicated that further work is necessary to evaluate the potential for this approach.

Further investigations involving tertiary air injection should attempt to optimize the injection system to try to determine the optimum point for staged air addition. However every effort should be made to use the burner for the staging device and to maintain a compact design to facilitate implementation of the concept in practical boilers.

In the two furnace investigations reported to date the air preheat level was maintained constant at approximately 300°C. Future tests must involve the investigation of thermal effects with nitrogen-containing fuels. The experiments in which measurements of NO emissions were made as the furnace warmed up strongly suggest that a more controlled series of experiments should be conducted to assess the effect of heat extraction rate on NO formation. Since the experiments in the IFRF tunnel furnace involve single flames which can "see" furnace walls on all sides, a single flame in a hot wall furnace can be likened to the center flames of a multiburner wall-fired boiler. Also a single flame in a more highly cooled furnace could be considered to be more representative of the burners on the edge of the matrix. Other thermal effects to be included in the experiment should be an attempt to determine if there is an optimum air preheat level for the performance of the staged burner.

All the investigations reported earlier with fuel oil firing were conducted in a relatively hot environment which maximized the burnout of particulate. More tests are necessary to ensure that these conditions which minimize NO formation do not unduly increase particulate emissions. Thus future tests should be conducted at various furnace heat extraction rates. The conflicting influence of air preheat level should also be investigated.

One objective of the investigations involving the dual fuel firing and the use of natural gas as a coal transport medium was to exclude oxygen from the coal jet thus preventing oxidation of the volatile nitrogen compounds as they were evolved from the coal. As this did not have any significant influence on the formation of nitrogen oxides it must be concluded that:

a) the emission is dominated by the NO produced from nitrogen remaining in the char and thus the use of natural gas as the transport medium will have little effect on the oxygen availability in the char burnout region;

b) the volatile nitrogen compounds are not released from the coal immediately. If there was a time delay before the nitrogen compounds were evolved then mixing between the primary and secondary stream could have occurred and oxygen might still be available to allow oxidation volatile nitrogen compounds;

c) the use of natural gas as a transport medium will vary the environment surrounding the coal particles. It has been shown that when a gaseous fuel is mixed with a low volatile coal carbon burnout time is increased(11) rather than decreased. This was attributed to a reduction in carbon oxidation rate because of oxygen starvation. This effect could also influence particle temperatures and reduce the rate of volatile evolution thus affecting fuel NO formation.

3.0 THE DEVELOPMENT OF MODELS TO CALCULATE RADIANT HEAT TRANSFER IN FURNACES

3.1 Introduction

The preceding section has demonstrated the importance of both mass transfer rates and thermal effects upon the formation of NO in coal, oil and gas flames. These thermal effects not only relate to the furnace input conditions (air preheat) but also to the furnace environment (bulk gas temperature, wall temperature). Radiant transfer plays an important role in the establishment of the thermal environment and the ability to predict radiant heat transfer in combustors would aid in the design of advanced environmentally acceptable combustion systems burning coal or coal-derived fuels. The overall problem of predicting radiative exchange within any enclosure can be subdivided into three separate categories.

1. Evaluation of the radiant exchange between all points in the enclosure when the temperature, absorption, emission, scattering, absorptivity, emissivity and reflectivity of the participating surfaces and the species within the enclosure are known. This can be considered as a mathematical problem involving the solution of complex integro-differential equations.
2. Evaluation of the radiative properties of all surfaces and species which is a physical problem.
3. Evaluation of the temperature and concentration of all emitting species which in the case of a furnace, requires knowledge of mass transfer, heat release rates, the sources and sinks of radiative gases and solids and of convective heat transfer.

The development of an analytical tool to evaluate radiant exchange can be decoupled from the development of the methods used to predict species concentrations and heat release profiles within the enclosure. However, the requirements of these methods must be borne in mind during the development of the model to evaluate radiant exchange since the two must be combined at some point.

The ultimate goal of this general class of work is the prediction of combustor performance based upon design details without recourse to empiricism or the need for physical measurements. This goal is far outside our present day capability for all but the most simple systems (two-dimensional gas fired); consequently, some intermediate condition must be sought which will aid in the attainment of the ultimate goal. This section of the report describes the development and evaluation of several radiation models which could be utilized both in the final fully-predictive analytical tool or in some intermediate semiempirical model which would be developed for a specific application, and it is recognized that this tool would aid in the iterative procedure of R&D and would not be a complete design tool. The development of the radiation model was based upon the major premise that it would ultimately be part of a more complete predictive capability including elliptic field equations which would describe the flow and mixing patterns in a furnace and which, when coupled with the appropriate chemistry, would also calculate heat release profiles and pollutant concentrations. However, in the short-term it should be suitable for use with a more empirical approach.

The empirical approach considered during the development of the radiation model would consist of three general steps:

1. A nonreacting physical model of the combustor which would model the flow and mixing thus allowing heat release profiles to be calculated assuming a mixed burned hypothesis.
2. Evaluation of the heat flux to the furnace wall and the gas temperature profiles by combining the information gained in 1 with a radiation exchange model.
3. The calculation of pollutant formation by using temperature and mixing fields in an empirical model which would include adjustable constants which could be fitted to experimental information.

The following sections describe the development and evaluation of radiation models as well as a discussion of the representation of the radiative properties of furnace gases and does not consider the other components of the empirical models.

The basis for the solution of all radiation problems is the equation of radiant energy transfer derived by formulating a balance on the monochromatic radiant energy taken along a pencil of rays enclosed within an elemental solid angle passing in a specified direction through a small volume element in an emitting/absorbing/scattering medium. Consider the small volume element shown in Figure 3.1, the radiant energy transfer equation can be expressed by (12)*

$$\underset{(1)}{(\hat{n}.\nabla)\, I_\lambda} = \underset{(2)}{-\,(K_{\lambda a} + K_{\lambda s})\, I_\lambda}$$

$$+ \underset{(3)}{K_{\lambda a}\, I_{b\lambda}} + \underset{(4)}{K_{\lambda s} \frac{1}{4\pi} \int_{4\pi} I_\lambda\, (\omega)\, d\omega} \qquad (1)$$

where

term (1) represents the gradient of intensity in the specified direction;

term (2) represents the reduction in intensity due to absorption within the volume and due to scattering out of the specified direction;

term (3) represents the increase in intensity due to emission from the control volume; and

term (4) represents the increase in intensity due to scattering of incident radiation into the specified direction.

When scattering is zero or largely forward directed, equation 1 simplifies to

$$(\hat{n}.\nabla)\, I = -\, K_a I + K_e\, I_b \qquad (2)$$

---

* For complete definition of all terms see Nomenclature, p. 4-4.

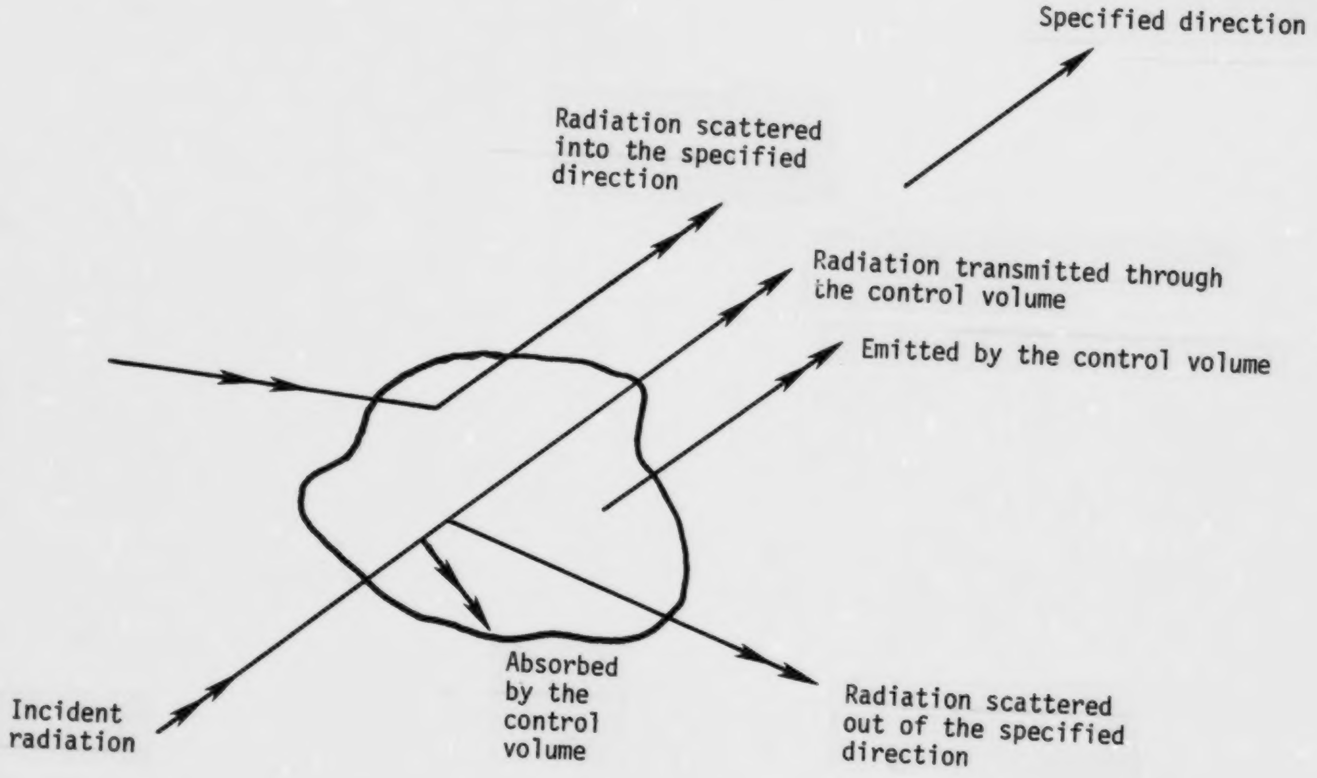
Specified direction
Radiation scattered into the specified direction
Radiation transmitted through the control volume
Emitted by the control volume
Incident radiation
Absorbed by the control volume
Radiation scattered out of the specified direction

Figure 3.1. Radiant Energy Balance in a Specified Direction

where K_e the Planck mean absorption coefficient, describes emission

$$K_e = \frac{\int_o^\infty K_{\lambda a} \, E_{b\lambda} \, d\lambda}{E_b} \tag{3}$$

and K_a describes absorption

$$K_a = \frac{\int_o^\infty K_{a} \int_\Omega I_\lambda \, d\omega \, d\lambda}{\int_\Omega I \, d\omega} \tag{4}$$

K_a is an absorption coefficient which is dependent upon I_λ and is, therefore, a function of the conditions throughout the medium and at its bounding surfaces. If it is assumed that $K = K_{\lambda a} = K_a = K_e$ = constant along a step of Δx then equation 2 can be integrated along the beam I giving:

$$I_{x+\Delta x} = I_x e^{-K\Delta x} + (1 - e^{-K\Delta x}) \frac{\sigma T_g^4}{\pi} \tag{5}$$

This relationship is valid for a gray medium (i.e., a medium in which the absorption coefficient is independent of wavelength) when scattering is neglected.

Combustion chambers contain gas mixtures which absorb and emit in certain wavebands and suspended particulate matter (soot, pulverized coal and fly ash) which behave as a continuium although not necessarily gray, over the wavelength of interest. If it could be assumed that emission and absorption of radiation by furnace gases were independent of wavelength it would greatly simplify calculations of radiative exchange within combustion chambers. As this is not the case, the representation of the radiative properties of furnace gases becomes an important factor in the calculation of radiant heat transfer in furnaces and it will be discussed in more detail in Section 3.5.

3.2 Methods Available for the Evaluation of Radiant Exchange

Several different techniques have been developed to solve the radiant energy transfer equations for real systems; these include:

- Monte Carlo methods (13,14)
- the Zone method (15,16)
- the Electrical Analogue method (17); and
- Flux methods (12,18,19,20,21,22)

All of these methods are fundamentally based and in their limit return to the exact solution.

Monte Carlo sampling techniques have been used to provide a statistical approach to the radiative exchange process. Thus, in Monte Carlo methods the probable paths of small bundles of energy is computed rather than solving simultaneously for the entire behavior of all the energy involved in the process. The method involves the generation of random numbers, and errors will occur if satisfactory tests are not applied to ensure randomness. Howell (13) does not recommend the use of the Monte Carlo method if other techniques are available to solve a particular problem.

In the Zone method the radiating system is divided into a number of surface and volume zones and exchange between each zone pair is calculated. The Zone method has been applied to furnaces where it has had reasonable success in predicting heat flux to various heat sinks (23,24,25). However, more serious errors have been found in the temperature profiles calculated for the furnace gases. These errors have been attributed to incorrect allowance for emission and absorption, and the coarse zone sizing. In principle, the method is not limited to coarse zoning, however, in practice the zone size is restricted by computation time.

Oppenheim (17) developed the Electrical Analogue method which replaces the radiative quantities (e.g., emission, heat fluxes) in a combustion chamber of electrical quantities (e.g., potentials, currents) in an electric network. Stott and Garrod (23) have reported the results of calculations based upon this technique.

This report concentrates upon the development of flux methods since they can be combined more easily with other models which are able to predict flow and mixing patterns in a furnace enclosure. The exact integro-differential equation of radiative heat transfer is replaced by approximate differential equations which can be easily solved by standard finite difference techniques(12,24).

In flux methods the problem of radiative exchange is solved by considering that the solid angle of 4π steradians surrounding a point is divided into a number of solid angles in which the intensity of radiation is assumed to be a specific function. In this way the complex integro-differential equation resulting from the integration of equation (1) over all solid angles can be reduced to a set of partial differential equations. Two general methods (12) have been used to obtain the set of partial differential equations:

- the Discrete Coordinate Method; and
- the Spherical Harmonics Method.

Flux methods are normally described by the number N of solid angle subdivisions and the developed equations are usually referred to as an N-flux method.

3.2.1 Two-Flux Methods

Two-flux methods were originally developed for astrophysical problems where radiative transfer is predominantly in one direction. Viskanta (12) has reviewed the various two-flux approximations which are:

- the Schuster-Schwarzschild (18,19);
- the Schuster-Hamaker (20); and
- the Milne-Eddington (21,22)

and the assumed intensity distributions are presented in Figure 3.2. The Schuster-Hamaker method differs from the Schuster-Schwarzschild method by a factor of 1/2 which represents the mean obliquity. The Schuster-Schwarzschild and Milne-Eddington methods are similar in their two-flux

3-7

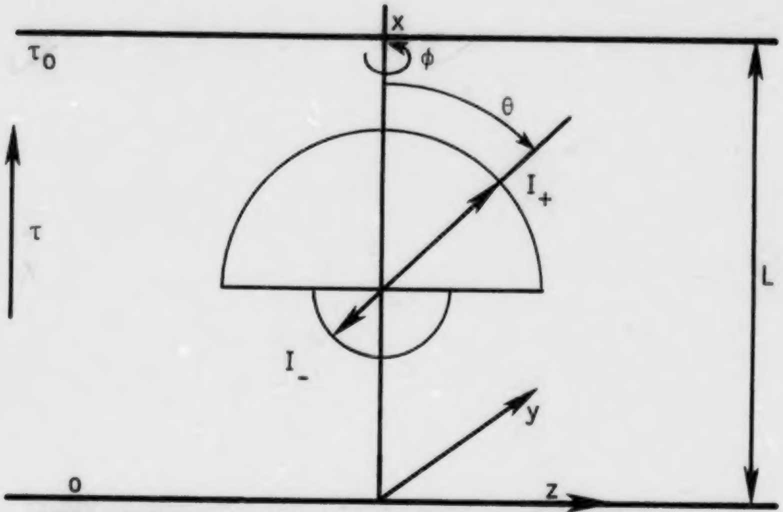
x
τ_0
ϕ
θ
I_+
τ
L
I_-
y
o
z

Milne-Eddington approximation of intensity
Schuster-Schwarzschild approximation of intensity

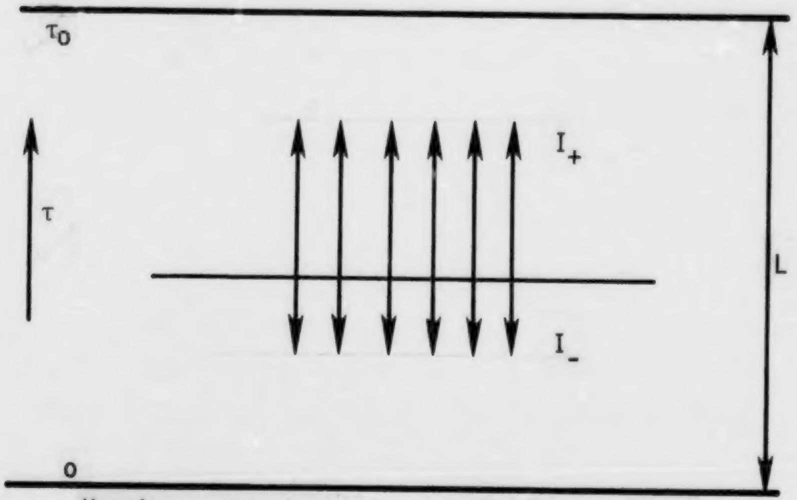
τ_0
I_+
τ
L
I_-
o

Hamaker approximation of intensity assuming parallel beams

Figure 3.2. Intensity Distributions for Two-Flux Methods

forms, but are different in origin as they are derived from the Discrete Coordinate and Spherical Harmonics approximations, respectively.

Siddall (25) derived a set of general equations which can be applied to the three two-flux methods by adjustment of two factors "a" and "b" which are defined in Table 3-1.

$$\frac{dq^+}{d\tau} = 2a\ E_b - (a+b)q^+ - (a-b)q^- \tag{6}$$

$$\frac{-dq^-}{d\tau} = 2a\ E_b - (a-b)q^+ - (a+b)q^- \tag{7}$$

Table 3-1. Definition of Factors "a" and "b" in Generalized Two-Flux Equations (after Siddal(25))

Factor	Two-Flux Formulation		
	Milne-Eddington	Schuster-Schwarzschild	Schuster-Hamaker
a	$1 - W_o$	$1 - W_o$	$1/2 - W_o/2$
b	3/4	1	$1/2 + W_{o/2}$

W_o is the fraction of extinction due to scatter, $K_s/(K_a+K_s)$ and equals zero when scatter is neglected.

Using equations 6 and 7, Siddal compared the different approximations with the exact solution for the case of an emitting/absorbing gray gas between infinite parallel plates. The approximate solutions diverge significantly from the exact solution when the discrepancy between the real intensity distribution and the assumed distributions becomes excessive (see Figures 3.3 and 3.4). Siddall concluded that the Schuster-Schwarzschild and the Milne-Eddington approximations gave better agreement with the exact solution than the Schuster-Hamaker approximation. However, neither were as accurate as a coarse zone method (see Figure 3.4).

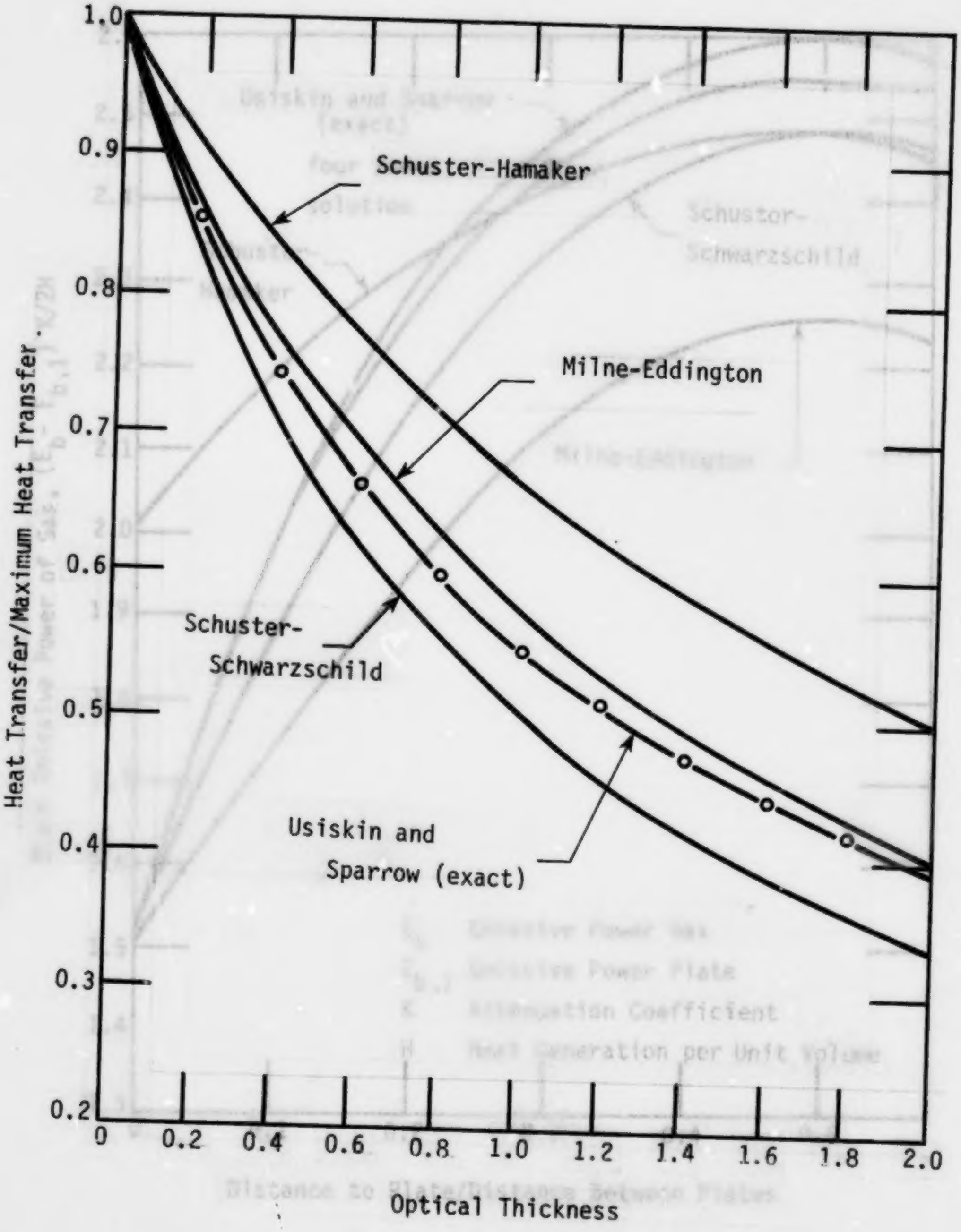

Figure 3.3. Heat Transfer Between Parallel Black Plates Separated by a Gray Radiating Gas (After Sidall (28))

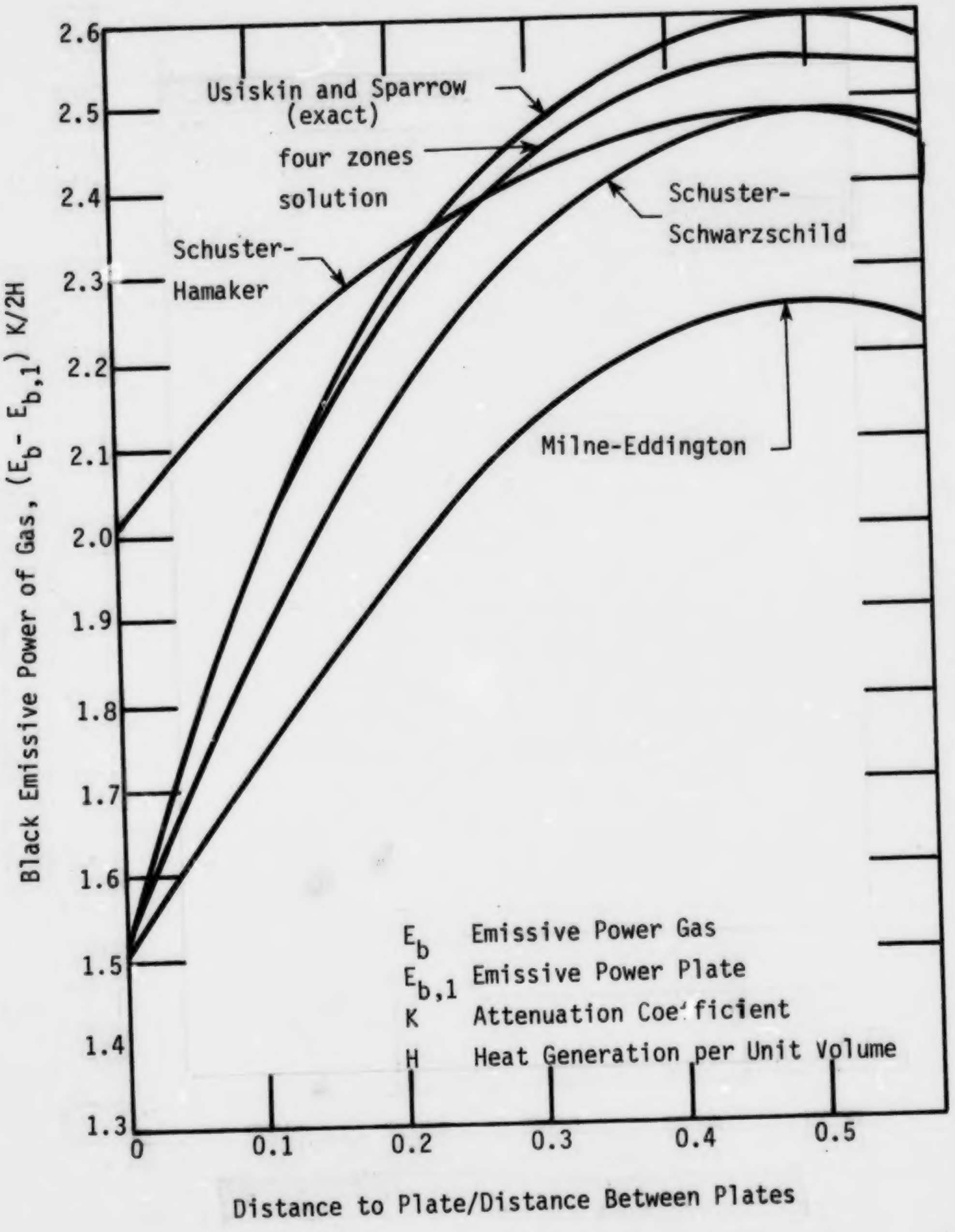

Figure 3.4. Distribution of Emissive Power in a Heat Generating and Radiating Gray Gas Between Parallel Black Plates at Equal Temperature (After Sidall(28))

Gosman and Lockwood (26) developed an extended two-flux method for axisymmetric systems based upon the Schuster-Hamaker approximation which was in essence a two-flux solution for both the radial and axial directions. Due to problems associated with the evaluation of an appropriate absorption coefficient these workers include a "flux model absorption coefficient" and a real gas absorption coefficient. Consideration of their basic equations shows that:

- when the flux model coefficient equals the real absorption coefficient, the model gives the Schuster-Hamaker approximation;
- when the flux model coefficient equals twice the real absorption coefficient the model yields the Schuster-Schwarzschild approximation.

The above is consistent with the earlier discussion concerning the obliquity factor and as the Schuster-Schwarzschild method is generally more accurate, the use of a flux model coefficient equal to twice the real gas absorption coefficient can be justified.

3.2.2 Multi-Flux Solutions

Siddall (25) suggested that the predictive capabilities of flux methods could be improved by increasing the number of subdivisions around the solid angle of 4π steradians. Thus the assumed intensity distribution will more readily approximate to the real distribution than is possible in the two-flux cases illustrated in Figure 3-2. In the limit at $N \rightarrow \infty$ both the Discrete Coordinate and the Spherical Harmonics methods tend towards the exact solution. As the number of partial differential equations increases linearly with the number of solid angle subdivisions, a computational limit is imposed on the number of flux directions. Consequently, further development must be concentrated on the approximation which can give acceptable predictions for a minimum number of subdivisions without introducing mathematical problems.

3.3 The Development of Two and Four-Flux Models of Radiant Exchange

After reviewing the available information it was decided to concentrate upon the development of flux models to describe radiant transfer. This decision was based upon a desire to couple the radiation model with some other predictive tool, either purely mathematical or a combined empirical physical model, which would be capable of describing mass transfer and heat release. It was decided that initially flux models should be developed based upon the Discrete Coordinate method in polar coordinates using the clear/gray gas approximation.

Equation 1 provides the basis of all flux models

$$(\hat{n}.\nabla)\, I_{\lambda} = -(K_{\lambda a} + K_{\lambda s}) I_{\lambda} + K_{\lambda a} I_{b\lambda} + K_{\lambda s} \frac{1}{4\pi} \int_{4\pi} I_{\lambda}(\omega)\, d\omega \qquad (1)$$

but it is only valid for monochromatic radiation.

If sufficient spectral information is known, equation 1 can be expressed in waveband form. However, because of the success of Johnson et al(27) and the lack of such information it was decided to use the clear/gray approximation to account for the nongrayness of the radiating medium. Thus equation 1 can be expressed in the following form.

$$\begin{aligned}(\hat{n}.\nabla) &= \sum_{n=1}^{n=m} (\hat{n}.\nabla)\, I_n \\ &= \sum_{n=1}^{n=m} -K_{gs,n}\, I_n + a_{gs,n}\, K_{gs,n} \frac{\sigma T_{gs}^{\,4}}{\pi} \qquad (8)\end{aligned}$$

where $K_{gs,n}$ and $a_{gs,n}$ are derived from a statistical fit of total emissivity partial pressure pathlength curves for the radiating species under consideration over the expected temperature range.

The assigned intensity distribution around a point is a basic assumption in all flux models. This assumption is necessary in order to replace the basic integro-differential equation by a set of partial differential equations. The assumed distribution is dependent upon the number of fluxes being considered. In order to derive flux model equations for axisymmetric systems it is necessary to integrate equation 1 over all solid angles and over the entire spectrum giving

$$\int_{\lambda=0}^{\infty}\int_{\omega=0}^{4\pi}(n.\nabla)I_\lambda d\omega d\lambda = -\int_{\lambda=0}^{\infty}\int_{\omega=0}^{4\pi}(K_{\lambda a}+K_{\lambda s})\,I_\lambda d\omega d\lambda$$

$$+\int_{\lambda=0}^{\infty}\int_{\omega=0}^{4\pi}K_{\lambda a}I_{b\lambda}d\omega d\lambda$$

$$+\int_{\lambda=0}^{\infty}\int_{\omega=0}^{4\pi}K_{\lambda s}\,\frac{1}{4\pi}\int_{\omega=0}^{4\pi}I_\lambda(\omega)d\omega d\omega d\lambda \qquad (9)$$

Equation 9 describes radiative heat transfer with the equation of transfer integrated over all solid angles and all wavelengths. By reversing the sequence of integration it can be seen that it does not matter whether a formulation about the emission/absorption/scattering behavior of the participating media is introduced first followed by the integration over all solid angles or the integration over all solid angles is carried out first followed by a formulation of the radiative behavior of the media.

With this in mind one can conclude that flux-model equations derived for one gray gas can be extended to non-gray gas situations, also neglecting scatter during the derivation of the flux-model equations does not limit the approach to nonscattering systems. Extension to scattering systems is possible if scatter appears to be important in the system being considered.

Neglecting scatter and assuming a gray gas equation 9 becomes

$$\int_{0}^{4\pi}(\hat{n}.\nabla)I d\omega = \int_{0}^{4\pi}\left(-K_{gs}I + a_{gs}K_{gs}\frac{\sigma T_{gs}^{4}}{\pi}\right)d\omega \qquad (10)$$

$(\hat{n}.\nabla)I$ can be expanded giving equation (11) in cylindrical polar coordinates

$$(\hat{n}.\nabla)I = n_r \left(\frac{\partial I}{\partial r}\right)_{\theta,z} + \frac{n_\theta}{r}\left(\frac{\partial I}{\partial \theta}\right)_{r,z} + n_z \left(\frac{\partial I}{\partial z}\right)_{r,\theta} \tag{11}$$

and the vector $\hat{n}$ is equal to

$$\hat{n} = (n_r, n_\theta, n_z) = (\cos\phi, \sin\phi\cos\gamma, \sin\phi\sin\gamma) \tag{12}$$

r,z and θ are the coordinates in the cylindrical-polar system, ϕ and γ are the coordinates in the spherical system. Both these coordinate systems are necessary to define the position and direction of the intensity at point P, and are shown in Figure 3.5.

The second term at the right-hand side of equation 11 can be expanded. The derivative of intensity in θ-direction equals zero for constant ϕ and γ in axisymmetric situations. Due to the rotation of the coordinate system with increasing ϕ other components of this derivative are not necessarily zero. These components, in which a term with a ϕ-derivative and a term with a γ-derivative have been substituted into equation 11 giving

$$(\hat{n}.\nabla)I = \cos\phi \left(\frac{\partial I}{\partial r}\right)_{\theta,z} - \frac{1}{r}\sin\phi\cos^2\gamma\left(\frac{\partial I}{\partial \phi}\right)_{\gamma,r,z}$$
$$+ \frac{1}{r}\cos\phi\sin\gamma\cos\gamma\left(\frac{\partial I}{\partial \gamma}\right)_{\phi,r,z} + \sin\phi\sin\gamma\left(\frac{\partial I}{\partial z}\right)_{r,\theta} \tag{13}$$

Equation 10 can then be written in the form

$$\int_0^{4\pi} (\hat{n}.\nabla)I d\omega = \int_0^{2\pi}\int_0^{\pi} \cos\phi \left(\frac{\partial I}{\partial r}\right)_{\theta,z} \sin\phi \, d\phi d\gamma$$
$$- \frac{1}{r}\int_0^{2\pi}\int_0^{\pi} \sin^2\phi\cos^2\gamma\left(\frac{\partial I}{\partial \phi}\right)_{\gamma,r,z} d\phi d\gamma$$

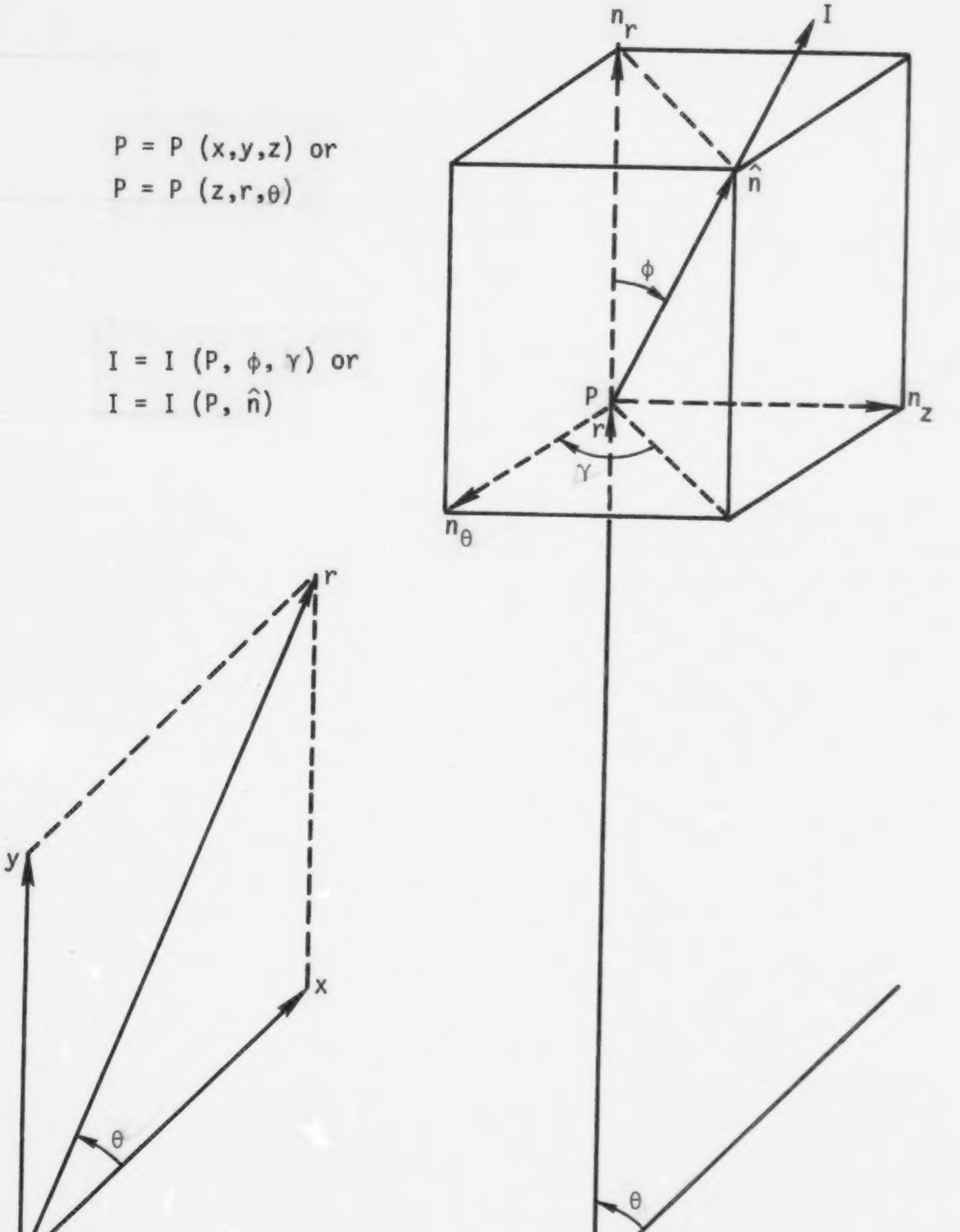
P = P (x,y,z) or
P = P (z,r,θ)
I = I (P, φ, γ) or
I = I (P, n̂)
n_r
I
n̂
φ
P
n_z
r
γ
n_θ
r
y
x
θ
o
θ
z

Figure 3.5. Coordinate Systems Defining Position and Direction of Intensity

$$+ \frac{1}{r} \int_0^{2\pi} \int_0^{\pi} \cos\phi \sin\phi \sin\gamma \cos\gamma \left(\frac{\partial I}{\partial \gamma}\right)_{\phi,r,z} d\phi d\gamma$$

$$+ \int_0^{2\pi} \int_0^{\pi} \sin^2\phi \sin\gamma \left(\frac{\partial I}{\partial z}\right)_{r,\theta} d\phi d\gamma$$

$$= \int_0^{2\pi} \int_0^{\pi} \left(K_{gs} I + a_{gs} K_{gs} \frac{\sigma T_{gs}^4}{\pi}\right) \sin\phi \, d\phi d\gamma \qquad (14)$$

Equation 14 is still general, but in order to distinguish between various models it is now necessary to make an assumption about the distribution of intensity. Since equation 14 was derived for a gray gas, if it were to be used with more than one gray gas, then they must be summed to produce the total equation.

3.3.1 Two-Flux Models in Axisymmetric Systems

The most simple method of calculating heat flux to furnace sidewalls utilizes a two-flux model. The assumed intensity distribution is illustrated in Figure 3.6. Two different ordinary differential equations are obtained by integrating over the upper and lower hemispheres which introduces the problem of the discontinuity at $\phi = \pi/2$. When the discontinuity is divided between the two hemispheres, equation 14 gives

F3.6

$$\frac{d}{dr} \pi I_r + \frac{\pi}{2} \left(\frac{I_r - J_r}{r}\right) = -2K\pi I_r + 2aK\sigma T^4 \qquad (15)$$

$$- \frac{d}{dr} \pi J_r + \frac{\pi}{2} \left(\frac{I_r - J_r}{r}\right) = -2K\pi J_r + 2aK\sigma T^4 \qquad (16)$$

However, if the discontinuity is assumed to be in the upper hemisphere as illustrated in Figure 3.7, the equations become

F3.7

$$\frac{d}{dr} \pi I_r + \pi\left(\frac{I_r - J_r}{r}\right) = - 2K\pi I_r + 2aK\sigma T^4 \qquad (17)$$

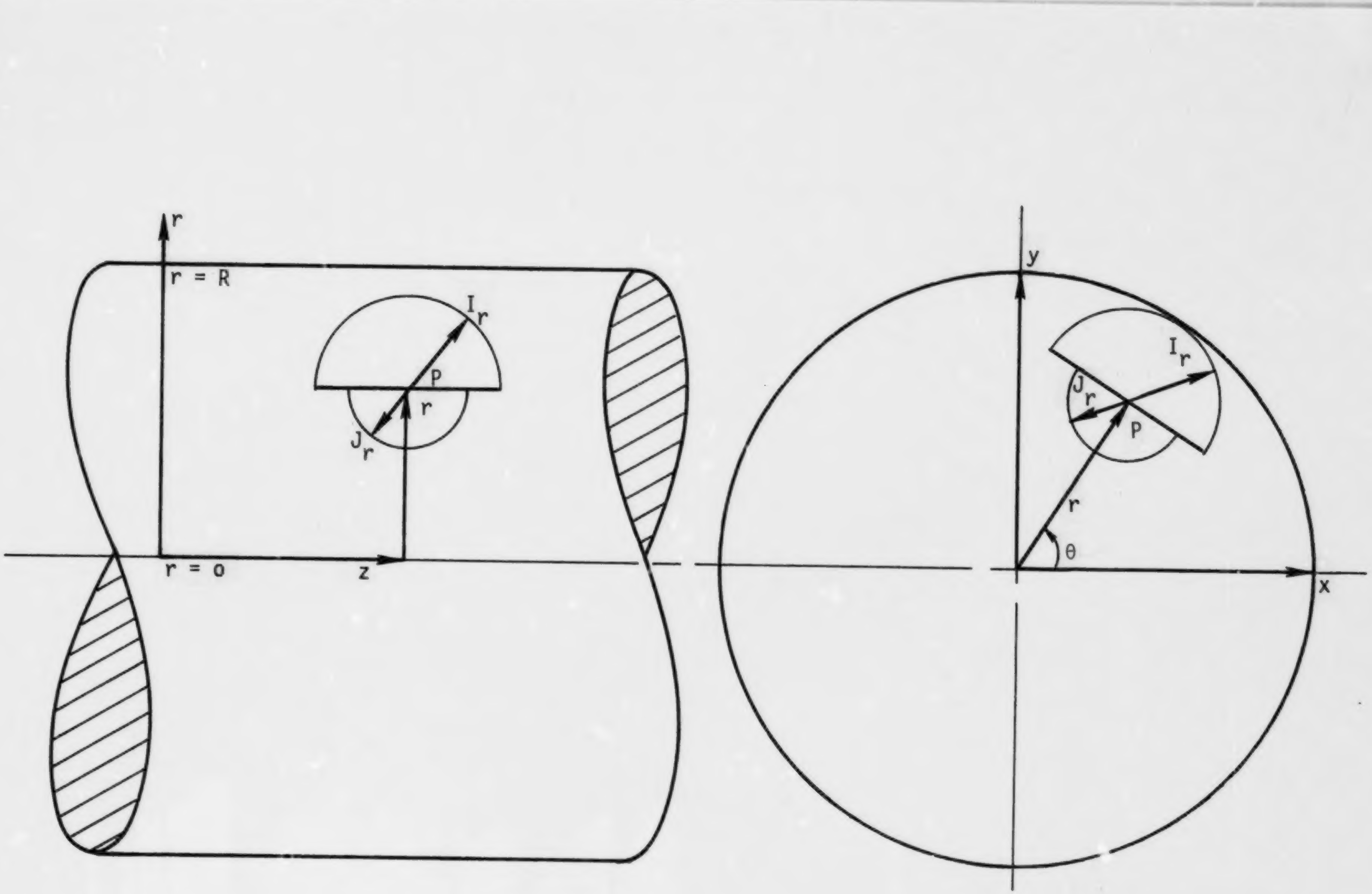
r
r = R
I_r
P
r
J_r
r = o
z
y
I_r
J_r
P
r
θ
x

Figure 3.6. Intensity Distribution for Two-Flux Models in Axisymmetric Systems

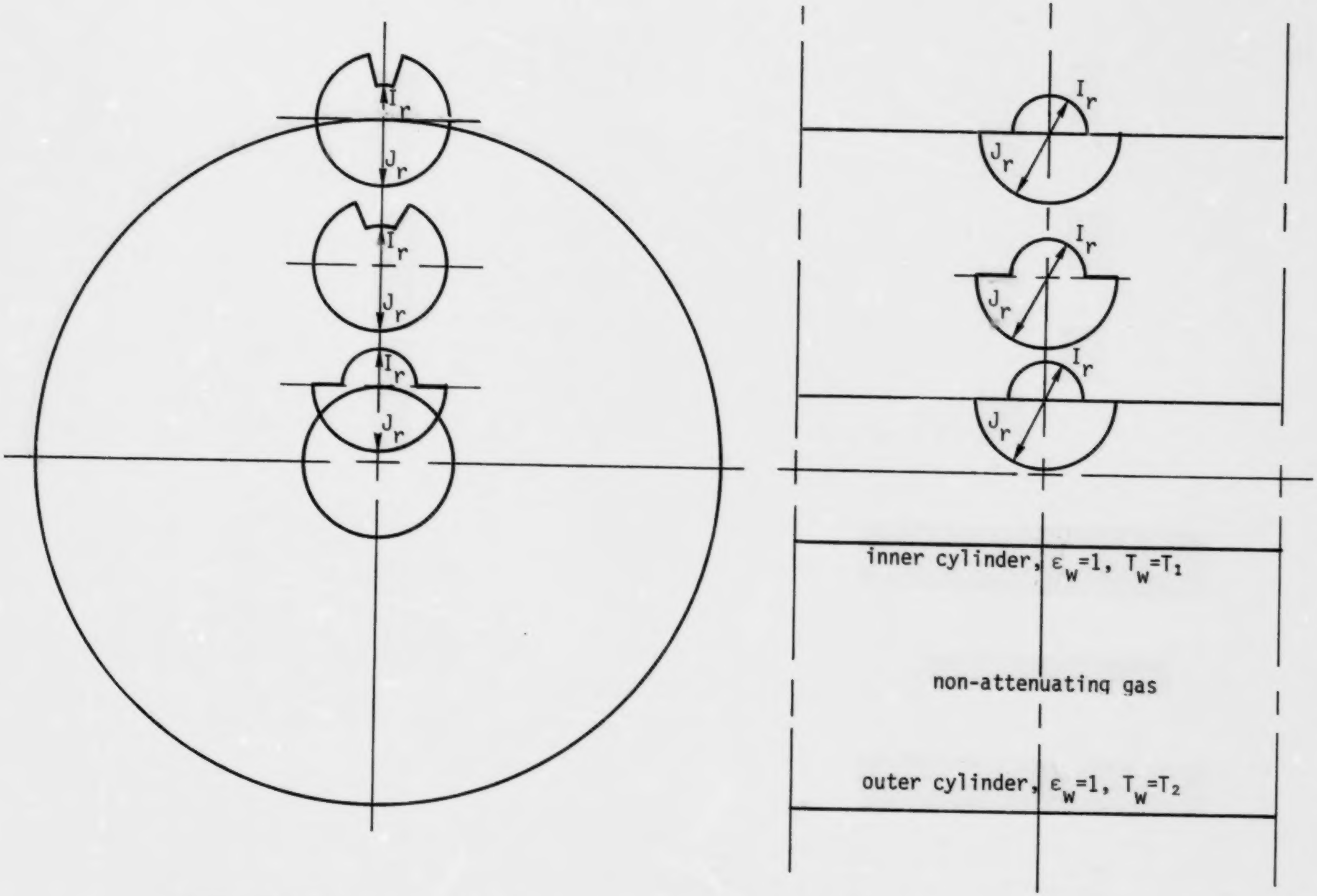
I_r
J_r
I_r
J_r
I_r
J_r
I_r
J_r
I_r
J_r
I_r
J_r
inner cylinder, $\varepsilon_w=1$, $T_w=T_1$
non-attenuating gas
outer cylinder, $\varepsilon_w=1$, $T_w=T_2$

Figure 3.7. Intensity Distributions Between Parallel Cylinders

$$- \frac{d}{dr} \pi J_r = -2K\pi J_r + 2aK\sigma T^4 \tag{18}$$

The model requires two necessary assumptions which involve personal judgement

- the assumed distribution of intensity; and
- $\partial I/\partial\phi$ and $\partial I/\partial\lambda$ which leads to the radius terms of the form

$$\pi\left(\frac{I_r - J_r}{r}\right).$$

From equations 15 and 16 the net flux q_r is given by

$$q_r = \pi \ (I_r - J_r) \tag{19}$$

and the boundary conditions at the furnace axis and wall are given by equations 20 and 21 respectively

$$q_r = 0 \tag{20}$$

$$\pi J_r = \varepsilon_w \sigma T_w{}^4 + (1 - \varepsilon_w)\pi I_r \tag{21}$$

The equations are solved in the form $\pi(I_r-J_r)$ and $\pi(I_r+J_r)$. In this form the ordinary differential equations can be replaced by a set of finite difference equations, which deliver a series of 3 x 3 matrices, where $\pi(I_t-J_r)$ and $\pi(I_r+J_r)$ are linked only to the immediate neighbors in the finite difference grid.

3.3.2 A Four-Flux Discrete Coordinate Model for Axisymmetric Systems

The advantages of a four-flux model over a two-flux model are:

1. It has the ability to calculate net axial fluxes which may be important in some instances.
2. It allows the intensity distribution around a point to be described more accurately.

The assumption concerning the intensity distribution for the four-flux model is illustrated in Figure 3.8. The radiation intensity is assumed constant over a certain solid angle, thus

F3.8

$I = I_z$ in +z -direction over π steradians

$I = I_r$ in +r -direction over π steradians

$I = J_z$ in -z -direction over π steradians

$I = J_r$ in -r -direction over π steradians

The integration of equation 14 is now executed separately over π steradians in each coordinate direction with the following integration limits

$+z : 0 \leq \gamma < \pi;\ \text{arcot}(\sin\gamma) \leq \phi < \text{arcot}(-\sin\gamma)$

$+r : 0 \leq \gamma < 2\pi;\ 0 \leq \phi < \text{arcot}(\sin\gamma)$

$-z : \pi \leq \gamma < 2\pi;\ \text{arcot}(-\sin\gamma) \leq \phi < \text{arcot}(\sin\gamma)$

$-r : 0 \leq \gamma < 2\pi;\ \text{arcot}(\sin\gamma) \leq \phi < \pi$

The discontinuity is again divided between two touching solid angles giving the final equations

$$\frac{\partial}{\partial r}\frac{1}{2}\sqrt{2}\,\pi(I_r - J_r) + \frac{1}{4}\sqrt{2}\,\pi\left(\frac{I_r - J_r}{r}\right) = -K\pi(I_r + J_r) + 2ak\sigma T^4 \qquad (22)$$

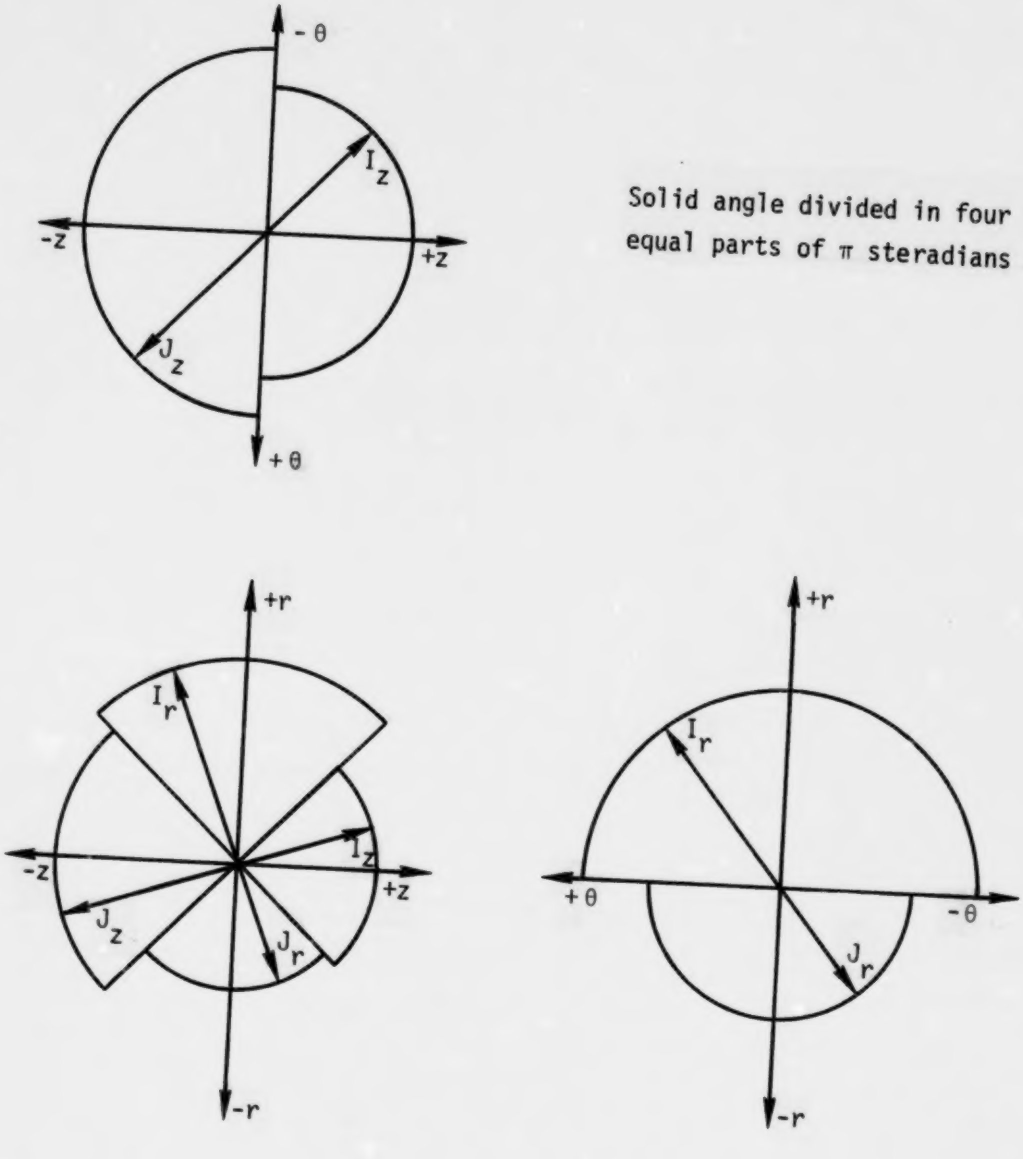
$-\theta$
I_z
$-z$
$+z$
J_z
$+\theta$
$+r$
I_r
I_z
$-z$
$+z$
J_z
J_r
$-r$
$+r$
I_r
$+\theta$
$-\theta$
J_r
$-r$

Solid angle divided in four equal parts of π steradians

Figure 3.8. Intensity Distribution for Four-Flux Model in Axisymmetric Systems

$$\frac{\partial}{\partial r}\frac{1}{2}\sqrt{2}\,\pi(I_r + J_r) + \frac{1}{4}\sqrt{2}\,\pi\left(\frac{I_r + J_r - I_z - J_z}{r}\right) = K\pi(I_r - J_r) \tag{23}$$

$$\frac{\partial}{\partial r}\frac{1}{2}\sqrt{2}\,\pi(I_z - J_z) + \frac{1}{4}\sqrt{2}\,\pi\left(\frac{I_r - J_r}{r}\right) = -K\pi(I_z + J_z) + 2aK\sigma T^4 \tag{24}$$

$$\frac{\partial}{\partial r}\frac{1}{2}\sqrt{2}\,\pi(I_z + J_z) = -K\pi(I_z - J_z) \tag{25}$$

For a series of gray gases the net radial flux is equal to

$$q_r = \sum_{n=1}^{m}\frac{1}{2}\sqrt{2}\,\pi(I_{r,n} - J_{r,n}) \tag{26}$$

The boundary condition at the axis is

$$\pi I_{r,n} = \pi J_{r,n} \tag{27}$$

The incoming flux at the wall $(r = R)$ is equal to

$$q_{in,w} = \sum_{n=1}^{n=m}\frac{1}{2}\sqrt{2}\; I_{r,n} + \frac{1 - \frac{1}{2}\sqrt{2}}{2}\pi(I_{z,n} + J_{z,n}) \tag{28}$$

and the outgoing flux at the wall $(r = R)$ is equal to

$$q_{out,w} = \sum_{n=1}^{m}\frac{1}{2}\sqrt{2}\,\pi J_{r,n} + \frac{1 - \frac{1}{2}\sqrt{2}}{2}\pi(I_{z,n} + J_{z,n}) \tag{29}$$

The wall boundary condition, which can be written separately for each gray gas takes the following form

$$q_{out,w} = (1 - \varepsilon_w)q_{in,w} + \varepsilon_w\sigma T_w^{\ 4} \tag{30}$$

The solution procedure requires that the partial differential equations be transformed to finite difference equations. An iterative procedure is necessary due to the coupled nature of the equations. Assuming a knowledge of $\pi(I_z-J_z)$ and $\pi(I_z+J_z)$ the first two equations are solved simultaneously and it is necessary to travel in steps from the sidewall to the axis and back. $\pi(I_r-J_r)$ and $\pi(I_r+J_r)$ are obtained in each point of the finite difference grid. This procedure uses the multiplication of 3 x 3 matrices in a way similar to the method used by Gibson and Monahan(26). With the derived values for $\pi(I_r-J_r)$ and $\pi(I_r+J_r)$ the calculation of $\pi(I_z-J_z)$ and $\pi(I_z+J_z)$ can continue and the solution procedure is executed for each gray gas.

The computer program requires as inputs wall boundary conditions, the temperature field and the concentration field in terms of partial pressures of radiating gases and concentrations of radiating solids. The same inputs are necessary for the two-flux program.

3.3.3 A Six-Flux Discrete Coordinate Model in Cartesian Coordinates

Cartesian coordinate flux models can be derived in a similar manner to flux models for the axisymmetric system. The intensity at a point is now a function of the spherical coordinates ϕ and γ and the Cartesian coordinates x, y and z. The assumed intensity distribution is similar to that used in the four-flux model and is illustrated in Figure 3.9. The intensity is assumed to be constant over a given solid angle $(2/3\pi)$ in the positive and negative coordinate directions giving I_x, J_x, I_y, J_y, I_z and J_z.

Equation 11 must be rewritten in Cartesian coordinates giving

$$\begin{aligned}(\hat{n}.\nabla)I &= \cos\phi\,\frac{\partial I}{\partial x} + \sin\phi\,\cos\gamma\,\frac{\partial I}{\partial y} + \sin\phi\,\sin\gamma\,\frac{\partial I}{\partial z} \\ &= -\,KI + Ka\,\frac{\sigma T^4}{\pi}\end{aligned} \tag{31}$$

Six partial differential equations are obtained if equation 31 is integrated over 2/3 steradians taking account the different beam directions.

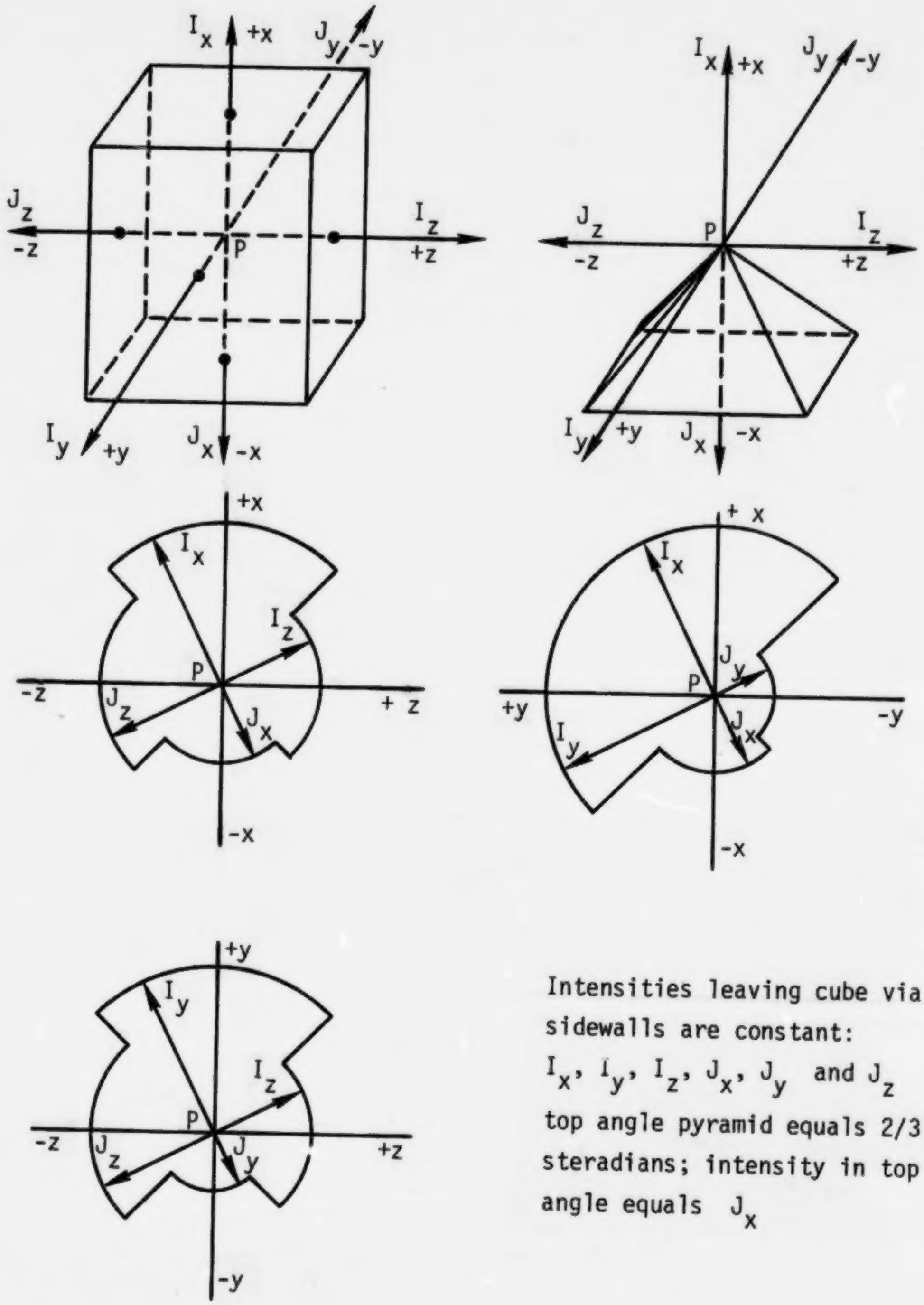
I x
+x
J y
-y
J z
-z
P
I z
+z
I y
+y
J x
-x
-y
-z
+z
P
I x
I z
J z
J x
+ x
+y
J y
J x
I y
-x
I y
J y

Intensities leaving cube via sidewalls are constant: I_x, I_y, I_z, J_x, J_y and J_z top angle pyramid equals 2/3 π steradians; intensity in top angle equals J_x

Figure 3.9. Intensity Distribution for Six-Flux Model in Cartesian Coordinates.

Solution of these equations yields net fluxes equal to

$$q_x = q_{+x} - q_{-x} = 0.55416\pi(I_x - J_x)$$

$$q_y = q_{+y} - q_{-y} = 0.55416\pi(I_y - J_y)$$

$$q_z = q_{+z} - q_{-z} = 0.55416\pi(I_z - J_z)$$

The boundary conditions are defined by

$$q_{out,w} = (1-\varepsilon_w)q_{in,w} + \varepsilon_w \sigma T_w^4$$

There are two possibilities for $q_{out,w}$

- $$q_{out,w} = \pi I_{out,w} \qquad (32)$$

  In this case the intensity distribution at the wall differs from the assumed intensity distribution in the gas.

- $$q_{out,w} = 0.55416\pi I_x + 0.11146\pi I_y + 0.11146\pi J_y + 0.11146\pi I_z + 0.11146\pi J_z \qquad (33)$$

  In this case the leaving flux from the wall has the same intensity distribution as the flux in the gas volume.

3.3.4 Evaluation of Flux Models

Two methods were used in order to evaluate the effectiveness of the flux models which were developed:

- Comparisons were made between measured and predicted incident heat flux for the IJmuiden furnace.

- Uncertainties in measurements prevented an adequate evaluation of the models by this method; consequently a series of theoretical test cases were conducted.

Measurements were made during the M-2 Trial Series(28) of incident radiant flux at the furnace walls for several flames of distinctly different character. Also, measurements were made throughout the furnace of species concentration, temperature and velocity distribution to facilitate the development of predictive procedures for furnace performance. Johnson(27), working on the results of the M-1 Trial Series, developed a direct and total exchange area program for the IFRF furnace. The furnace is divided into 3 radial and 17 axial zones and the program can be used with a clear gray gas formulation to predict radiative heat transfer to the furnace walls from a knowledge of flow, heat release and radiating species concentration. This program was modified(29) to accept zone temperatures as input; thus, allowing a direct comparison between a coarse zone method and flux methods. The zone method should have errors less than five percent for KBs less than 0.4(30).

Figures 3.10 and 3.11 compare radiative heat flux to the furnace sidewall for the zone method and a four-flux model against measurements made for a long nonswirling flame (Flame 29, see later). In Figure 3.10

- curve a is the measured flux;
- curve b is the calculated flux using the one clear/two gray formulation of Johnson (see Section 3.5);
- curves c and d are calculations assuming a gray medium with K=0.1 and 0.2 respectively.

K=0.2 represents the mean attenuation coefficient for a furnace 2.22 m diameter and 6.29 m length containing combusted products (5 percent excess air) at a uniform temperature of 1500K. K=0.1 is considered as the practical lower limit since in practice temperatures greater than 1500K occur and the furnace is not filled completely with combusted products.

The same emission/attenuation formulations were used in the four-flux model calculations shown in Figure 3.11. The measured temperature and

3-26

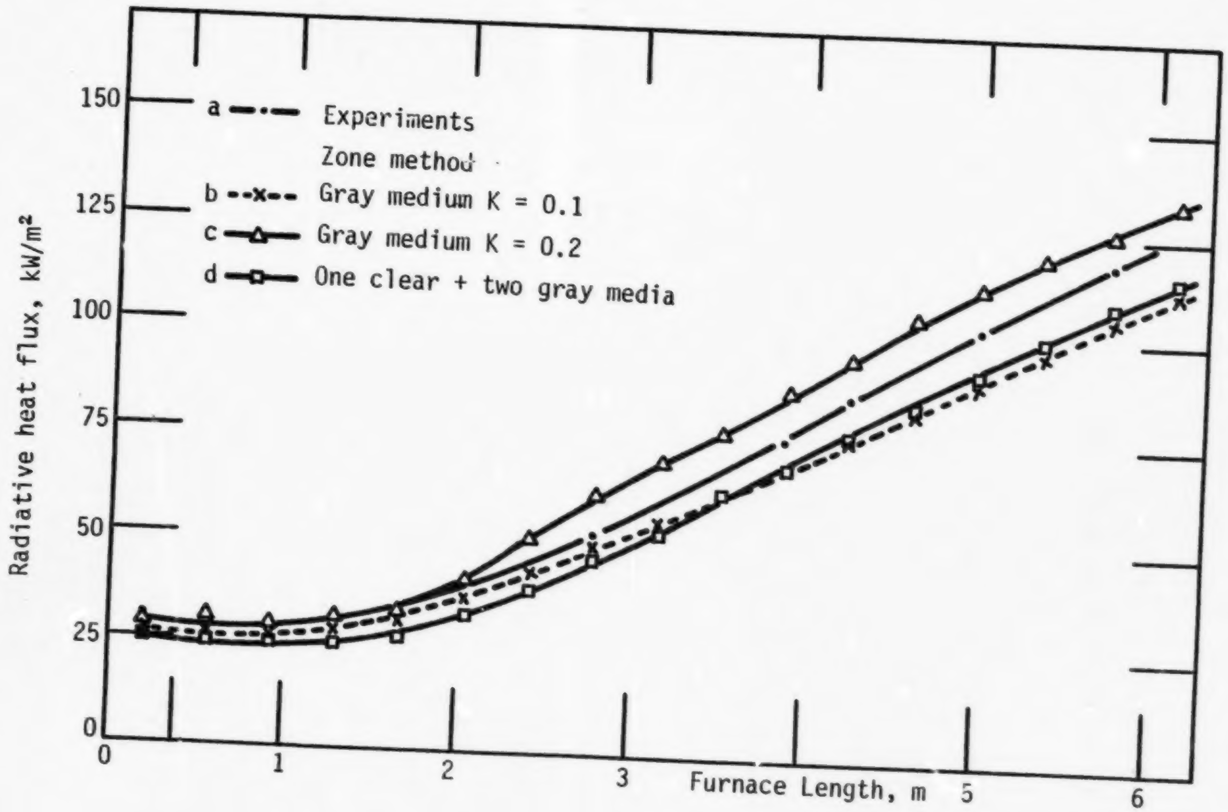

Figure 3.10. Predictions of Incident Radiant Wall Heat Flux Distributions Using the Zone Method with Different Attenuation Coefficient Formulations

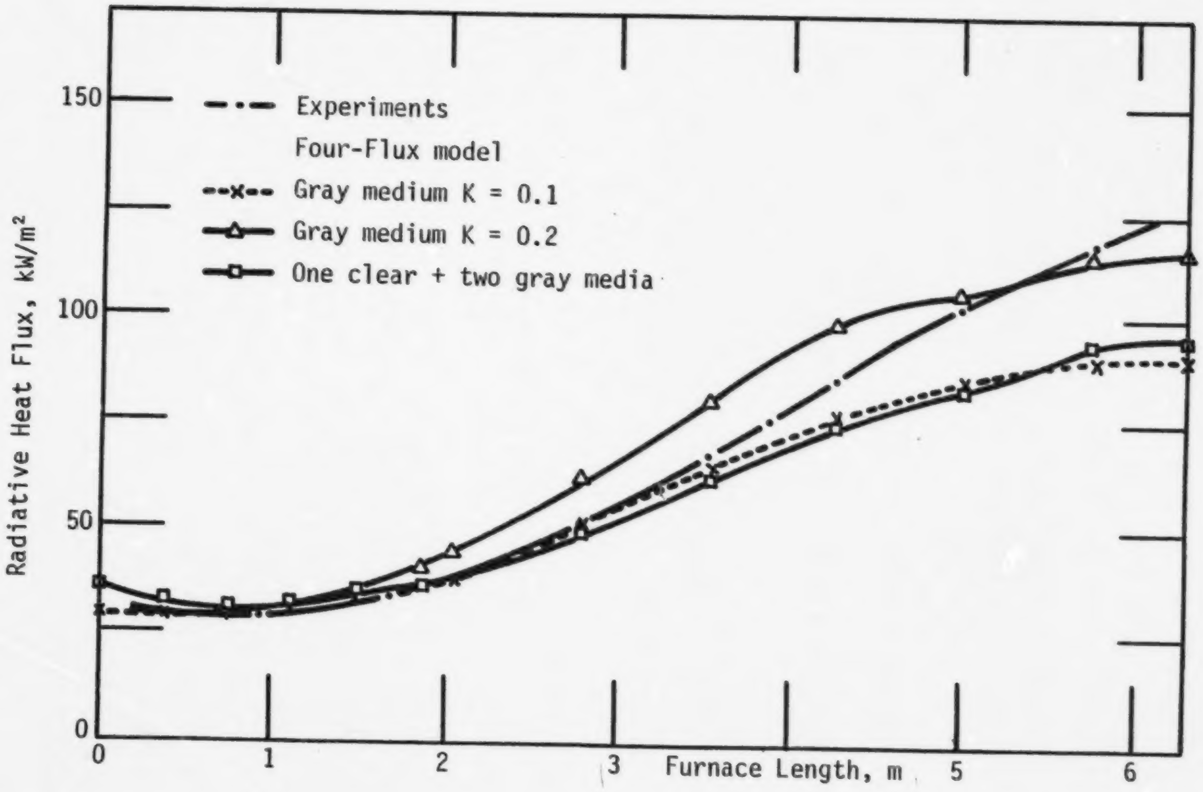

Figure 3.11. Predictions of Incident Radiant Wall Heat Flux Distributions Using the Four-Flux Model With Different Attenuation Coefficient Formulations

concentration fields were used as point values on the grid used for the four-flux model which has 19 radial and 13 axial grid lines. The radial grid is nonuniform to accommodate regions of strong gradients. Zone method predictions are generally superior to those of the flux model, particularly in the region where the radiant fluxes are high at the rear of the furnace.

Figure 3.12 compares predictions obtained with the four-flux model and the zone method for a one clear/two gray formulation with measured incident flux for a high swirling natural gas flame (Flame 11). Close to the firing wall, in the region of maximum heat release, both models appear to be equally inaccurate.

The comparisons provided by Figures 3.10, 3.11 and 3.12 do not give a clear indication of the potential of flux models to calculate radiant exchange. Certainly the four-flux model does not appear to predict the measured values as accurately as the results calculated with the zone method. The differences between measurement and prediction can be attributed to several factors:

- radiant transfer is evaluated based upon measured gas temperatures and concentrations which will have an error associated with them. An error of one percent in measured temperature will give an error of approximately 4 percent in σTg^4. Also, smoothed profiles were used in the calculations which may not adequately represent the real flame. This is particularly true for the Zone method where an average is taken over a coarse zone;
- the predictions may differ from the measurements because of errors in the representation of the emission attenuation characteristics of the furnace gases or in the boundary conditions;
- errors in the flux model prediction may be associated with interaction between axial and radial radiation.

The uncertainties associated with the comparisons discussed above made it necessary to formulate theoretical test cases which would not only identify deficiencies in the flux models, but also make it easier to

3-29

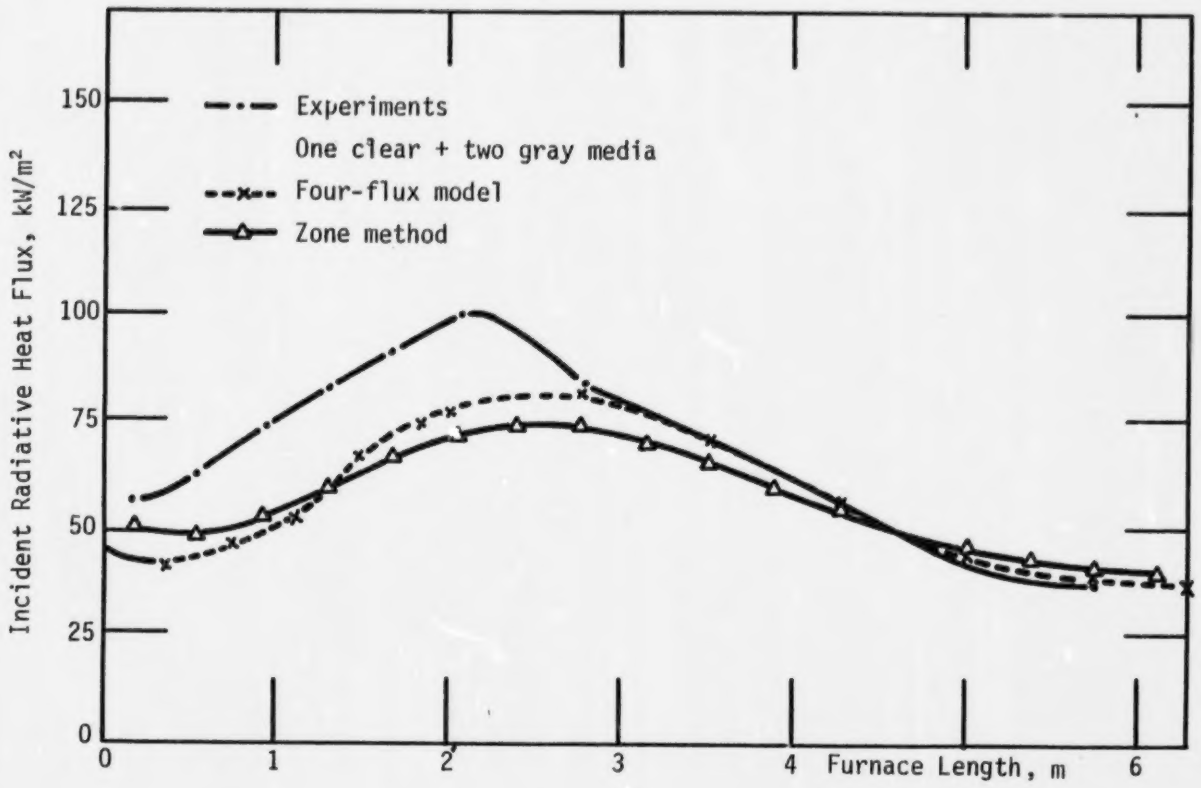

Figure 3.12. Comparison of Predictions by Zone Method and Four-Flux Model With Experimental Results

suggest ways to overcome these deficiencies. The theoretical test cases were devised to allow the zone method to accurately calculate the radiant fluxes. Thus the emission/attenuation coefficients were specified and all temperature gradients coincided with zone boundaries. In this way the effectiveness of both two and four-flux models could be determined.

In order to minimize programming effort, the zone size was that used previously and the separate cases were chosen to provide information on the following topics:

I Ability of flux models to predict radiative transfer to the boundaries in well-stirred situations (i.e., no gradients exist within the enclosure).

II Ability of flux models to predict radiative transfer to the boundaries when radial gas temperature gradients exist.

III Ability of flux models to predict radiative transfer to the boundaries when there are axial temperature gradients in both the furnace wall and the furnace gases.

In the majority of the test cases the gray gas assumption was invoked with a range of emission/attenuation characteristics corresponding to natural gas, fuel oil and pulverized coal.

Case I - Well-Stirred Tank

Figure 3-13 gives the conditions and calculations associated with two well-stirred tanks. In case I-1 the furnace wall has a constant temperature 1000K greater than case I-2. It can be seen that for the range of gray gas attenuation coefficients the maximum difference between the incident radiative flux for the Zone method and the various flux models is less than 10 percent. In general, the two-flux models give a higher flux than the Zone method while the four-flux model gives lower fluxes for the lower K values. For the one clear/two gray formulation the flux model results are all higher than the Zone model results.

The different Ks used in the one clear/two gray formulation were 0, 0.5 and 0.9. The discrepancies shown in Figure 3.13 cannot be attributed to the clear gas nor the gray gas with K=0.5. Comparison with exact

Case I

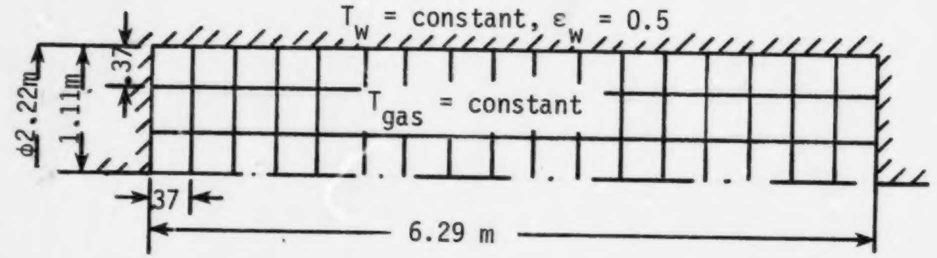

I-1 T_G = 1500 K
T_W = 1300 K

I-2 T_G = 1500 K
T_W = 300 K

Maximum incident radiative heat flux densities at sidewall, kW/m²								
emission/ absorption formulation	zone method		Schuster - Schwarzschild two-flux model		Milne - Eddington two-flux model		four-flux model	
	I-1	I-2	I-1	I-2	I-1	I-2	I-1	I-2
one clear - two gray gases	184.5	77.7	191.9	85.9	192.8	88.3	191.7	85.3
K = 0.1	200.8	89.5	203.4	95.5	204.5	98.0	197.8	82.8
K = 0.2	224.4	143.5	227.6	150.9	229.2	154.5	222.3	138.7
K = 0.5	258.5	221.1	260.6	226.6	263.0	232.0	259.4	223.9
K = 0.8	271.5	251.3	272.5	253.8	275.5	260.7	273.5	256.1
K = 1.2	278.8	268.6	278.6	268.0	282.4	276.3	280.6	272.3
one clear - one gray gas					117.7	116.8		
K = f (temp, comp)					270.0	248.6		
K = f (Tw, Tg)					239.5	58.1		

Figure 3.13. Comparison of Zone Method and Flux Models

solutions for simple geometric shapes(30) revealed that the Zone method would give less accurate values than the flux models for the one clear/two gray formulation due to Johnson's(32) extrapolation of KB (where B is the zone dimension). Consequently, Zone method calculations with this one clear/two gray formulation will tend to be low.

Case II - Cold Wall Variable Gas Temperature

The second series of test cases which were used had a non-uniform gas temperature distribution. The middle gas zone was at a higher temperature than the other two radial gas zones (see Figure 3.14). Differences in the calculated incident radiative heat flux are similar to those obtained on Case I. Comparison between the results presented in Figures 3.13 and 3.14 indicates that:

- the Schuster-Schwarzschild approximation is capable of predicting radial heat flux for a range of attenuation coefficients and temperatures;
- the two-flux Schuster-Schwarzschild model gives more accurate results than the two-flux Milne-Eddington model;
- for the case of constant wall temperature there is very little difference between two- and four-flux models.

Case III - Axial Temperature Gradients

The third theoretical test series was devised to assess flux models under conditions which included axial gradients in both gas and wall temperature. The idealized situations used for these tests are presented in Figures 3.15 and 3.16. Cases III-1-1 and III-1-2 are representative of combustion conditions with high rates of heat release in the initial regions (Figure 3.15) and Cases III-2-1 through III-2-5 represent conditions more typical of slower fuel/air mixing rates. The effect of wall temperature and attenuation coefficient variations on the magnitude and accuracy of the predictions has been assessed in both instances.

Figures 3-17 and 3-18 compare predicted incident and net radiation flux for two attenuation coefficients calculated by the Zone method, a

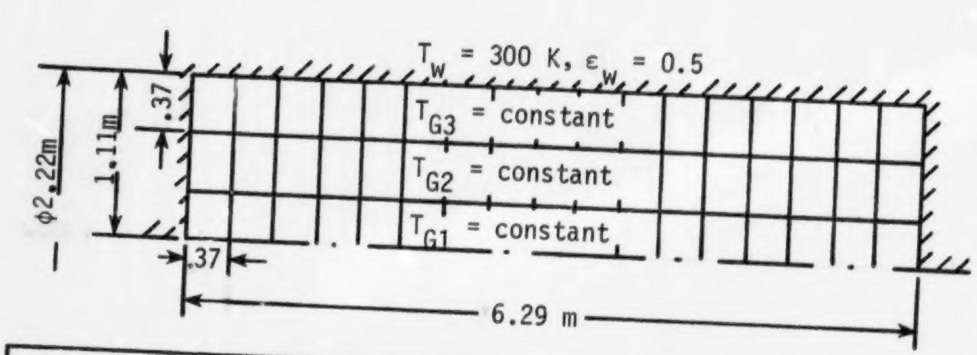

Case II

II - 1 T_{G1} = 1300 K
$T_{G2} = T_{G3}$ = 1200 K
II - 2 T_{G1} = 1500 K
$T_{G2} = T_{G3}$ = 1200 K
II - 3 T_{G1} = 1500 K
$T_{G2} = T_{G3}$ = 1300 K

Maximum incident radiative heat flux densities at sidewall, kW/m²												
emission/ absorption formulation	zone method			Schuster - Schwarzschild two-flux model			Milne - Eddington two-flux model			four-flux model		
	II-1	II-2	II-3	II-1	II-2	II-3	II-1	II-2	II-3	II-1	II-2	II-3
one clear - two gray gases	39.7	41.7	52.3	44.1	46.2	58.0	45.3	47.3	59.5	43.9	46.0	57.7
K = 0.1	38.3	42.5	54.8	40.9	45.4	58.5	41.9	46.3	59.9	35.7	40.0	51.2
K = 0.2	61.2	67.7	87.5	64.5	71.5	92.3	65.9	72.7	94.1	59.4	66.1	85.1
K = 0.5	93.8	102.8	133.8	96.2	105.6	137.3	98.3	107.4	140.0	95.2	104.7	135.9
K = 0.8	106.1	115.1	150.7	107.0	115.7	151.9	109.7	117.8	155.2	108.3	118.0	161.7
K = 1.2	112.7	120.4	159.3	112.0	118.4	157.6	115.2	120.7	161.4	114.4	122.5	161.7
one clear - one gray gas							62.3	63.2	79.0			
K = f (temp, comp)							110.1	118.3	154.1			
K = f (Tw, Tg)							29.8	29.8	37.9			

Figure 3.14. Comparison of Zone Method and Flux Models

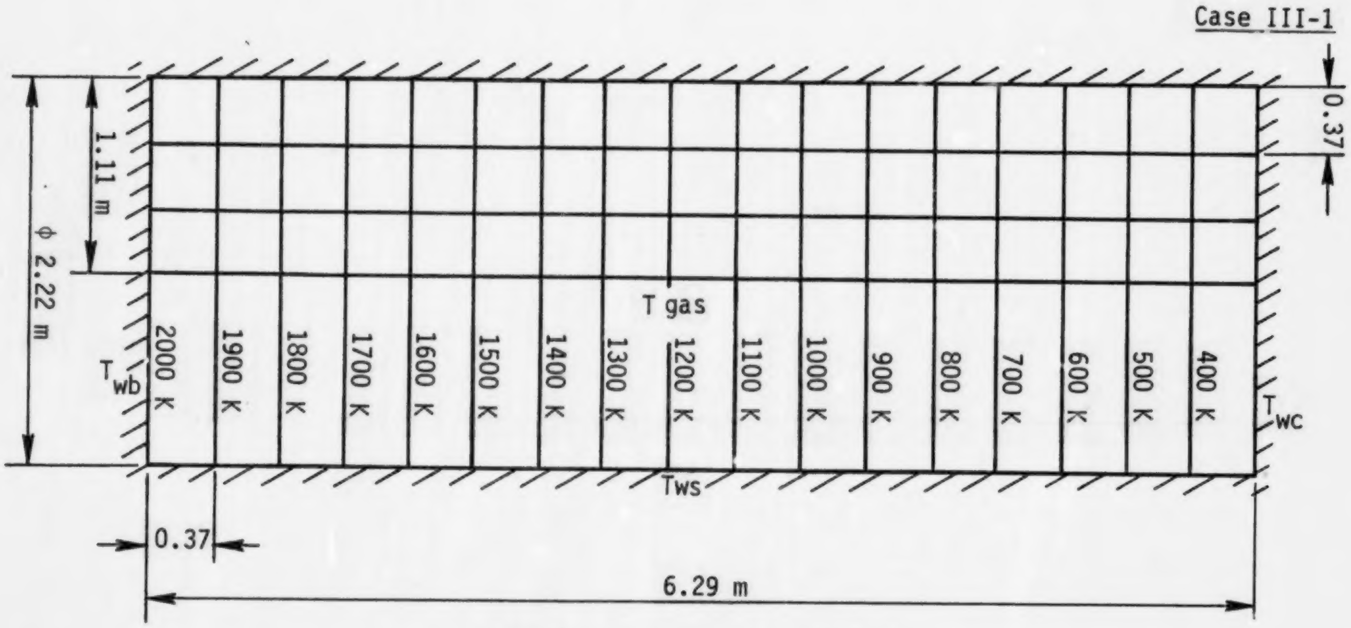
Case III-1
0.37
T_{wc}
400 K
500 K
600 K
700 K
800 K
900 K
1000 K
1100 K
1200 K
1300 K
1400 K
1500 K
1600 K
1700 K
1800 K
1900 K
2000 K
T gas
Tws
T_{wb}
1.11 m
ϕ 2.22 m
0.37
6.29 m

III-1-1 $T_{wb} = T_{ws} = T_{wc} = 300$ K

III-1-2 $T_{wb} = 1300$ K

$T_{ws} = T_{wc} = 300$ K

Figure 3.15. Comparison of Zone Method and Four-Flux Model

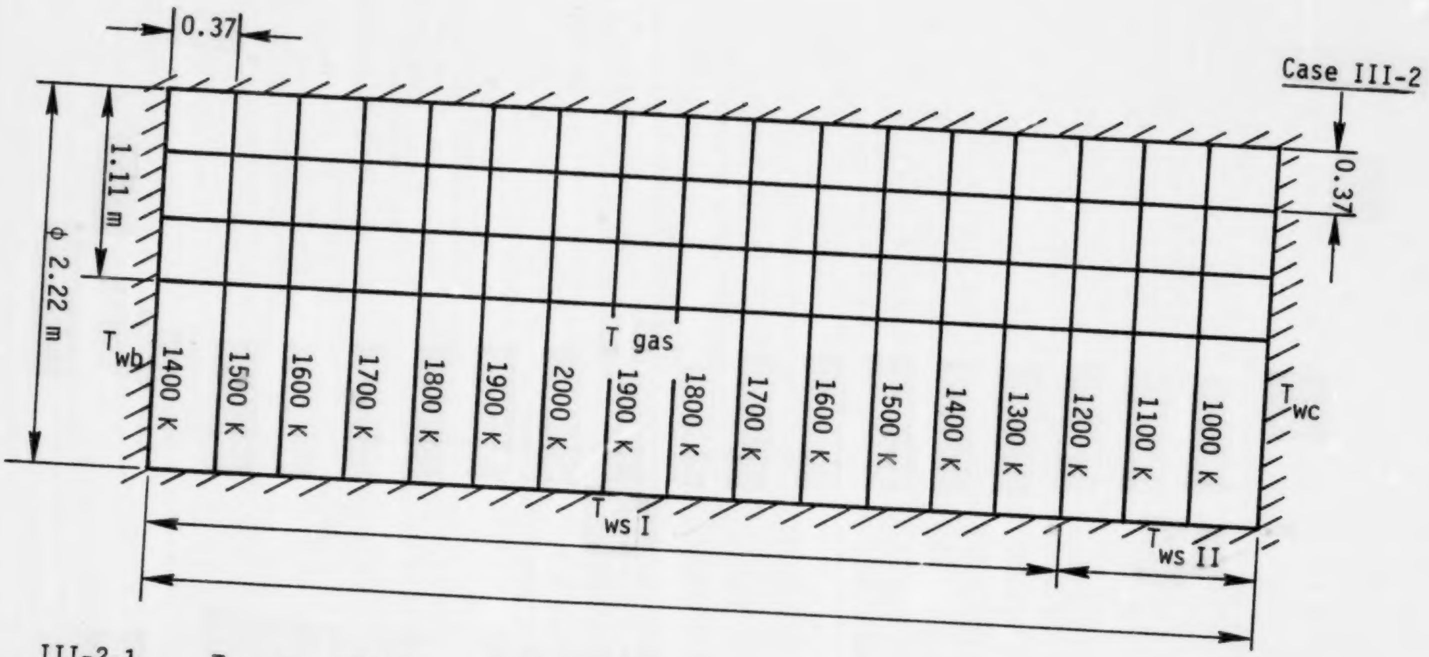
Case III-2
0.37
0.37
1.11 m
ϕ 2.22 m
T gas
T_{wb}
T_{wc}
$T_{ws\,I}$
$T_{ws\,II}$
1400 K
1500 K
1600 K
1700 K
1800 K
1900 K
2000 K
1900 K
1800 K
1700 K
1600 K
1500 K
1400 K
1300 K
1200 K
1100 K
1000 K

III-2-1	T_{wb} = 300 K	$T_{ws\,I}$ = 300 K	$T_{ws\,II}$ = 300 K	T_{wc} = 300 K
III-2-2	T_{wb} = 1300 K	$T_{ws\,I}$ = 300 K	$T_{ws\,II}$ = 300 K	T_{wc} = 300 K
III-2-3	T_{wb} = 1300 K	$T_{ws\,I}$ = 300 K	$T_{ws\,II}$ = 300 K	T_{wc} = 1000 K
III-2-4	T_{wb} = 300 K	$T_{ws\,I}$ 1300 K	$T_{ws\,II}$ = 1000 K	T_{wc} = 300 K
III-2-5	T_{wb} = 1300 K	$T_{ws\,I}$ = 1300 K	$T_{ws\,II}$ = 1000 K	T_{wc} = 1000 K

Figure 3.16. Comparison of Zone Method and Four-Flux Model

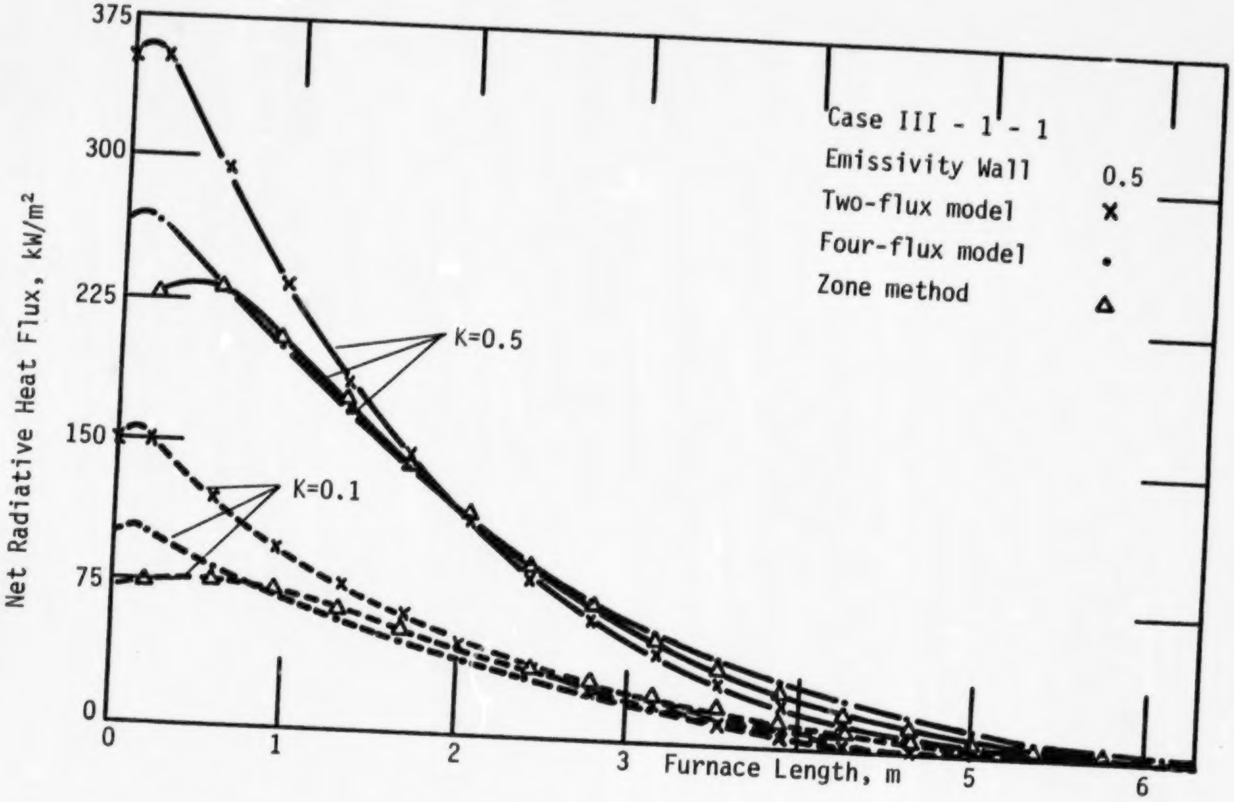

Figure 3.17. Comparison of Radiative Heat Flux Predictions by the Two-Flux Schuster-Schwarzschild Model, the Four-Flux Model and the Zone Method

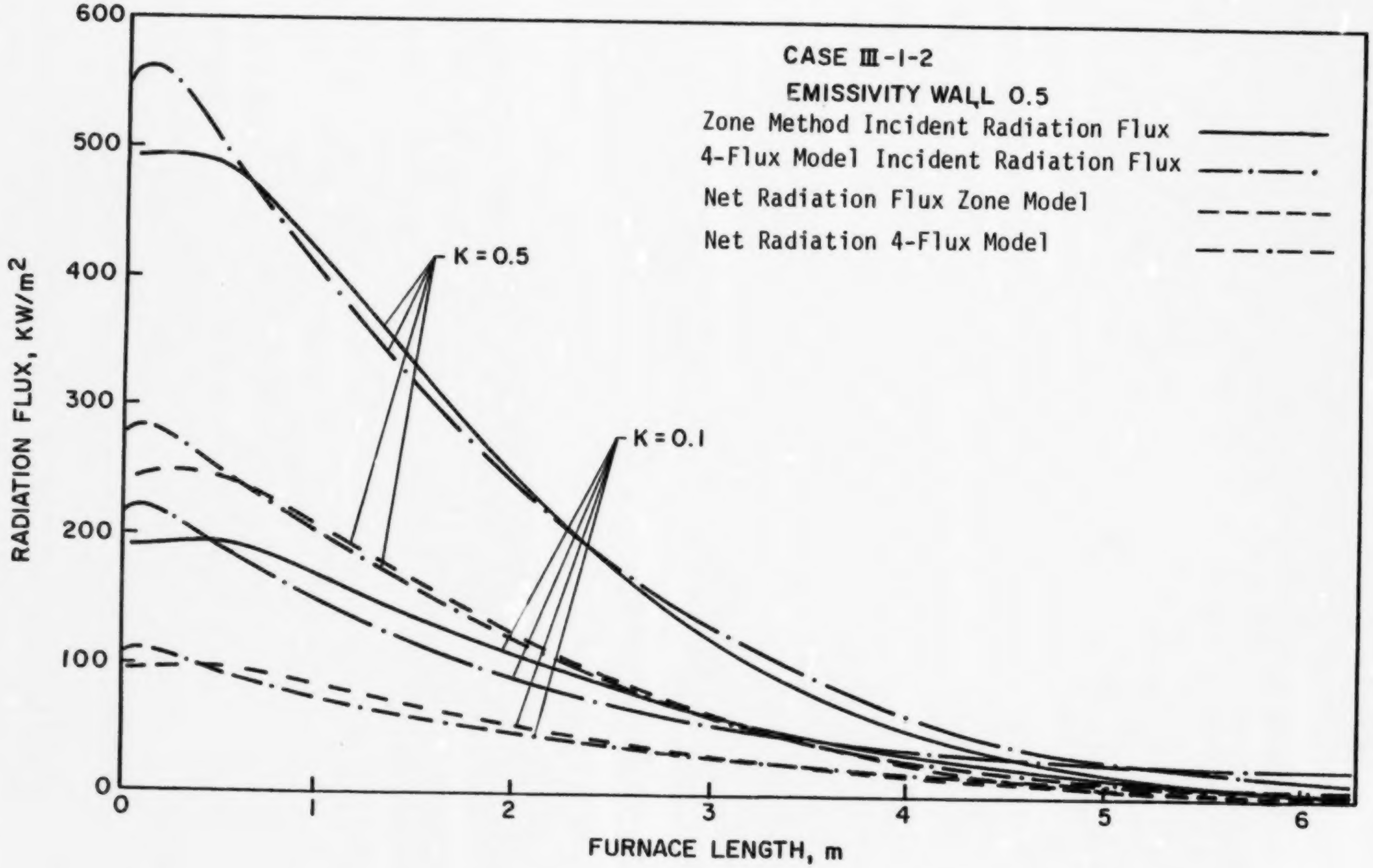

Figure 3.18. Prediction of Incident and Net Radiation Flux at Sidewall for Different Attenuation Coefficients Using the Zone Method

two-flux model and a four-flux model. The calculated axial profiles obtained with the four-flux and the Zone model are similar. Major errors occur close to the firing wall with the four-flux model and maximum errors for both Cases III-1-1 and III-1-2 lie between 15 and 20 percent. Larger errors are evident with the two-flux model since there is no account taken of axial exchange.

In order to adequately test the four-flux model it is necessary to examine situations which include both gas and wall temperature gradients. Selected comparisons for these test cases are presented in Figures 3.19 and 3.20 showing that:

- the two-flux model appears to be inadequate. In Figure 3.19 it can be seen that the net radiative flux predicted by the two-flux model has a much higher value than that predicted by either of the other two methods. This is because the two-flux model cannot accommodate axial exchange.
- compared to the Zone method, the four-flux model always overpredicts the peak heat flux;
- larger errors occur near hot end walls than those near to cold walls; and
- when there is a step change in wall temperature (Figure 3.20, Case III-2-4) there is no effect on the incident radiation calculated by the Zone method. However, there is an influence in the incident flux predicted by the four-flux model for lower Ks.

Differences in the calculated peak heat flux between the Zone method and the four-flux model can be attributed to the fact that the I_r and J_r fluxes are mainly characterized by the zone with the maximum temperature and do not adequately take account of adjacent cooler zones. As the errors on either side of the peak are minor, it appears that the flux model can accommodate changes in gas temperature except when the gradient changes from positive to negative. The errors introduced by the end wall suggest that the coupling between the axial and radial fluxes in the four-flux

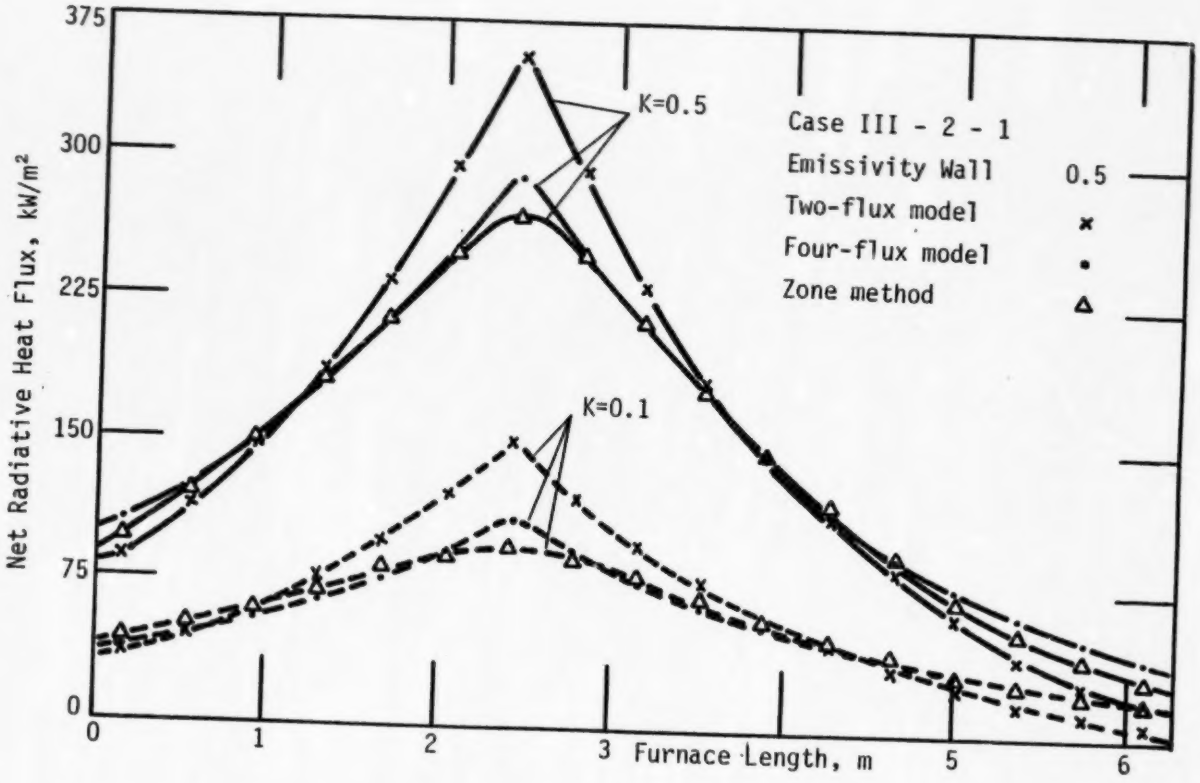

Figure 3.19. Comparison of Radiative Heat Flux Predictions by the Two-Flux Schuster-Schwarzschild Model, the Four-Flux Model and the Zone Method

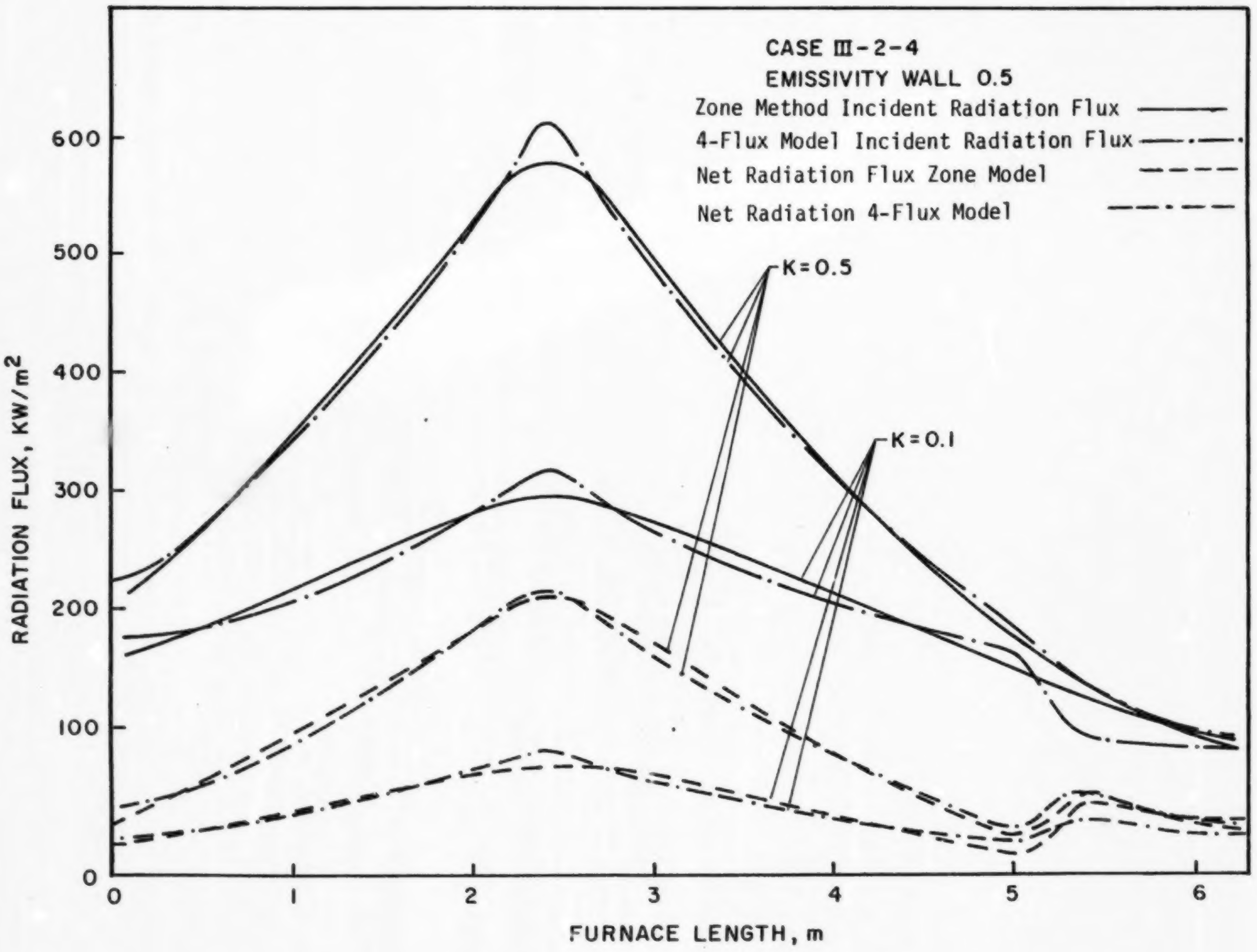

Figure 3.20. Prediction of Incident and Net Radiation Flux at Sidewall for Different Attenuation Coefficients Using the Zone Method

model do not adequately represent the end wall effect under all circumstances.

3.4 The Development of a Radiative Heat Transfer Model Utilizing a Continuous Intensity Distribution with Six Parameters

In the previous section it was demonstrated that a four-flux discrete coordinate model was capable of predicting heat flux distributions with a reasonable accuracy under situations considered typical of furnace applications. However, errors greater than 10 percent can be expected in certain instances. An alternative approach has been developed which describes the intensity distribution around a point as a continuous function for those instances requiring a higher degree of accuracy. The assumed intensity distribution around a point should approach physical reality. When this is not possible an alternative formulation must be established which is closer to physical reality and yet leads to the same type of equations described in the previous section. Situations where this might exist are furnaces with hot refractory walls partially covered with water-cooled pipes.

The intensity distribution in a simple case is illustrated in Figures 3.21, 3.22 and 3.23. The furnace is assumed to have a radius of 1.0 m and a length of 6.29 m. A gray gas attenuation coefficient of 0.5 is used and the wall temperature is equal to absolute zero and the wall emissivity is equal to 1.; therefore, there is no reflection. Shown in the figures are the intensities as fractions of the maximum attainable intensity. It can be seen from this simple example how difficult it is to obtain the correct intensity distribution at a point. The intensity is a function of position and space angle, therefore the distributions illustrated in these figures only indicate the intensity distribution in other parts of the furnace with different space angles.

From the above it is clear that the approximation of the intensity in terms of simple functions is necessary. In Figures 3.6 and 3.8 the assumed intensity distribution for the two-and-four-flux models was presented. The

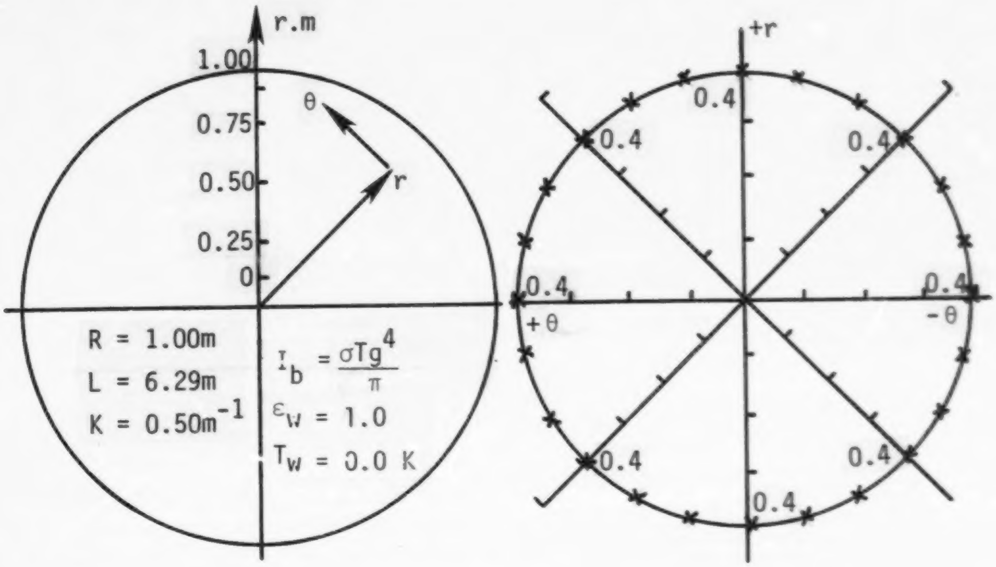

$\boxed{\frac{I}{Ib} = 1-e^{-kl}}$

furnace

distribution of I/Ib for r=0.00m

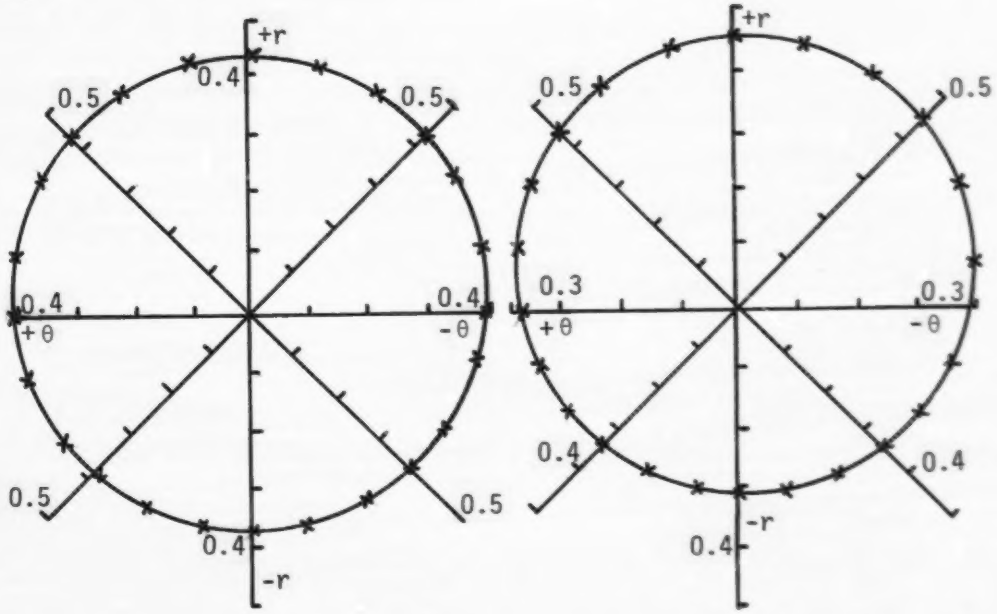

distribution of I/Ib for r=0.10m

distribution of I/Ib for r=0.25m

Figure 3.21. Intensity Distributions in a Cross Section of a Cylindrical Furnace.

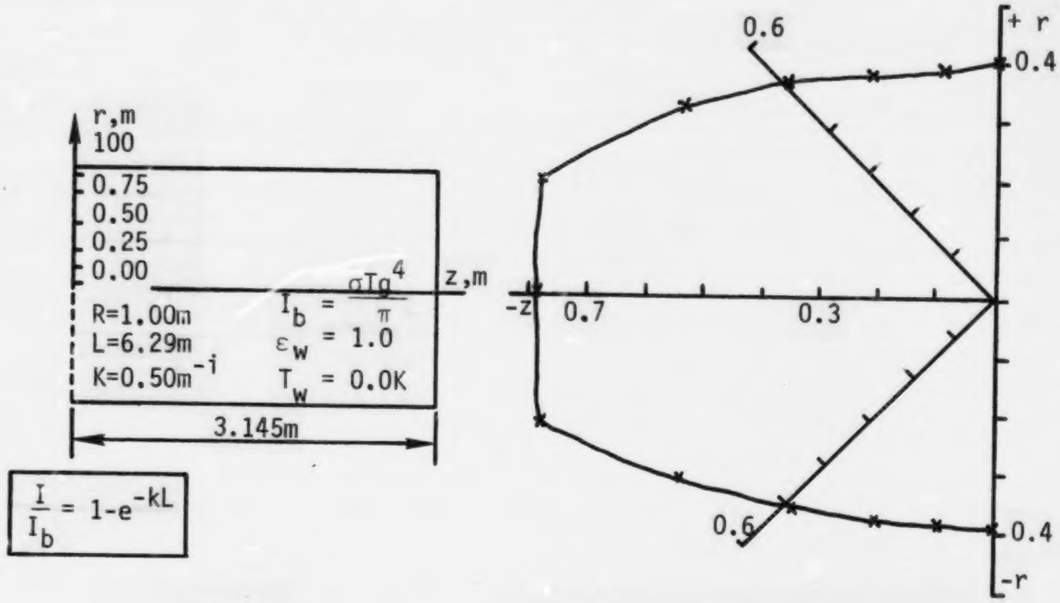

Furnace

Distribution of I/I_b for r=0.00 m

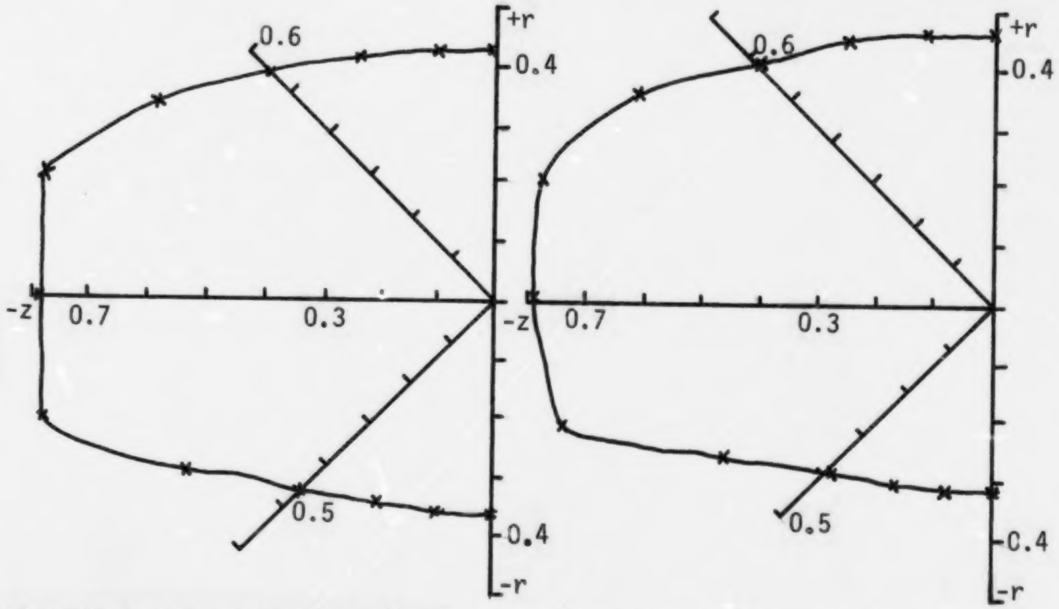

Distribution of I/I_b for r=0.10

Distribution of I/I_b for r=0.25 m

Figure 3.22. Intensity Distributions on a Longitudinal Section of a Cylindrical Furnace

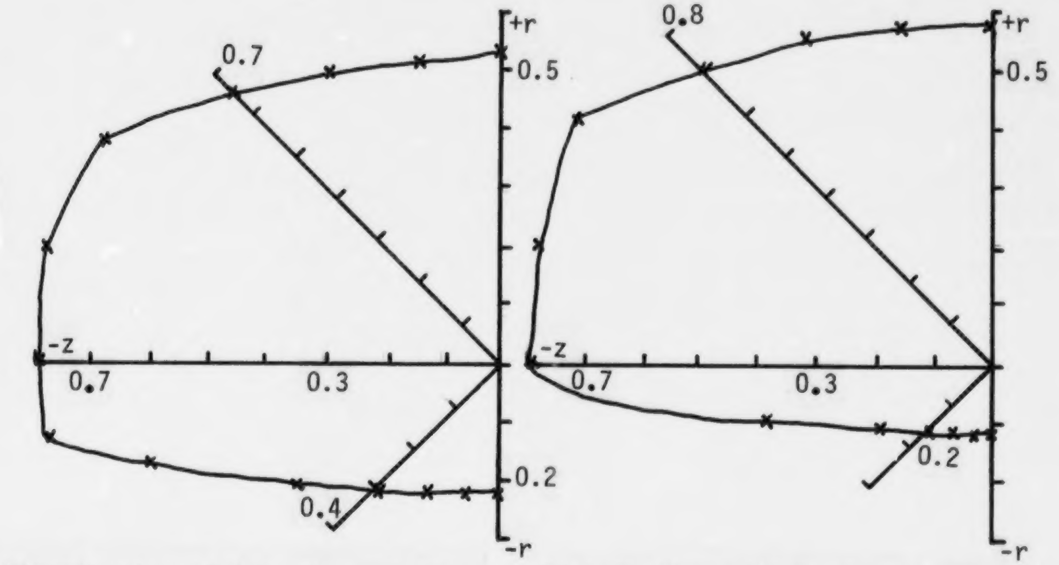

Distribution of I/I_b for r=0.50 m   Distribution of I/I_b for r=0.75 m

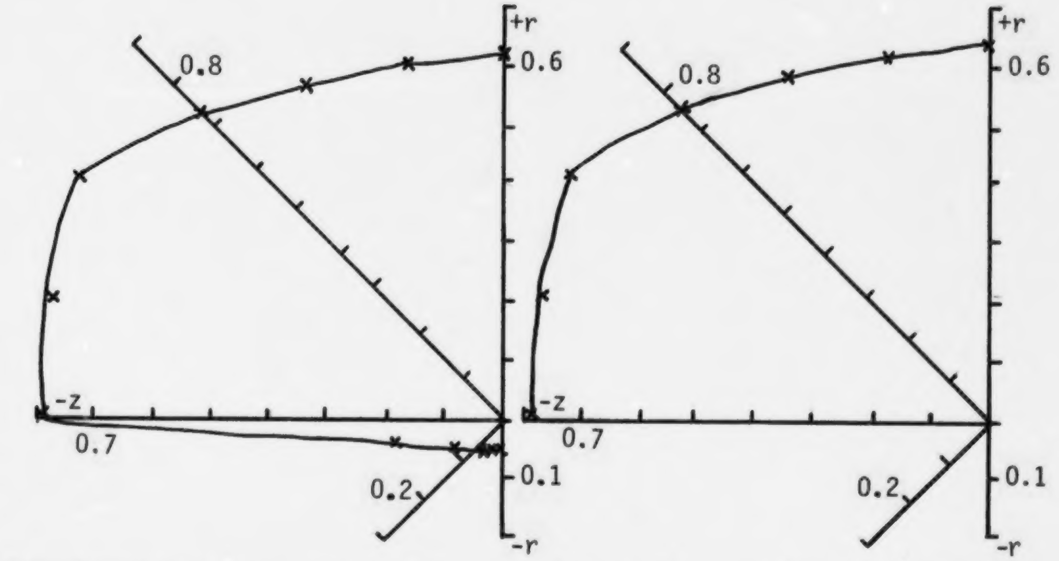

Distribution of I/I_b for r=0.90 m   Distribution of I/I_b for r=1.00 m

Figure 3.23. Intensity Distributions in a Longitudinal Section of a Cylindrical Furnace

intensity distribution for the four-flux model approaches more closely to the real intensity distribution than the two-flux model can ever do, and this explains why four-flux calculations give more accurate results than two-flux calculations.

In axisymmetrical systems the complicating fact arises that beams which initially travel radially inwards giving a contribution to the inward flux, change direction. During their path of travel they change from radial inwards to radial outwards, thus contributing to the radially outward flux. In fact, this happens to all the beams at different radial positions if the beams that change from the inward to the outward direction at r-0 are included. This means that the intensity distribution has to be formulated more accurately in axisymmetrical systems as the derivatives of the intensity

direction

$$(\frac{\partial I}{\partial \phi}, \frac{\partial I}{\partial \gamma}, \phi \text{ and } \gamma \text{ space angles})$$

give rise to radius terms with 1/r, which can play important roles for small values of r.

In Figure 3.22 the intensity distribution is discontinous at the wall and because of the cylindrical geometry, this only occurs in the r-z plane. One can expect discontinuities in intensity at the end of a cylindrical furnace at end walls in the plane of the walls and at side walls in the plane of the wall only into the axial direction. Within the furnace volume the discrete radiation beams almost form a continuous pattern as a function of the spherical angles. Discontinuities in the distribution of intensity such as those assumed in the four-flux model do not exist in practical situations. To improve the accuracy of the radiative heat transfer calculation in a furnace it is necessary to use a better approximation of the actual intensity distribution around a point in the furnace.

The assumed continuous distribution must satisfy the following:

- If the furnace volume and walls are at the same temperature, the intensity has to be constant giving zero net fluxes;

- Parameters are needed to define the intensity distribution. The formulation of intensity has to be such that intensity and the parameter do not conflict when they coincide.

A continuous intensity distribution that satisfies these rules is:

$$I = I_r \cos^2 \phi + I_z \sin^2 \phi \sin^2 \gamma + I_\theta \sin^2 \phi \cos^2 \gamma \qquad (34)$$

with ϕ and γ as spherical coordinates (Figure 3.5). Because there are six coordinate directions there are six equations of this type with I_r, J_r, I_z, J_z, I_θ and J_θ as parameters. Axisymmetry requires that J_θ equals I_θ, thus reducing the number of parameters to five. This distribution is illustrated in Figure 3.24. This model has been programmed (31) for an axisymmetric system to determine whether this formulation is superior to the flux methods discussed earlier.

Figure 3.25 compares predictions obtained with the CID-5 model (this was an axisymmetric system) and the measured furnace values discussed earlier. Results were presented in Figure 3.11 comparing the four-flux predictions with the same furnace results and it is not possible to judge which of the models is better. In an attempt to quantitatively determine the improvement in calculation of radiant heat transfer associated with the CID-5 model comparisons have been made with the ideal test cases (see Figures 3.15 and 3.16) and a coarse grid zone model.

In Figure 3.26 comparisons are presented for calculations made with a Zone model, a two-flux, and four-flux and a CID-5 model and different gray gas attenuation coefficients (test Case III.1.1, Figure 3.15). The Zone method predictions in the figures are drawn in the form of bars, and more clearly demonstrate the fact that the predicted incident heat flux is calculated per zone. The Zone method results are considered to be very accurate predictions for these test cases, and it can be concluded from these tests that accurate predictions can also be obtained with the CID-5 model. Similar comparisons are presented in Figures 3.27 and 3.28 for

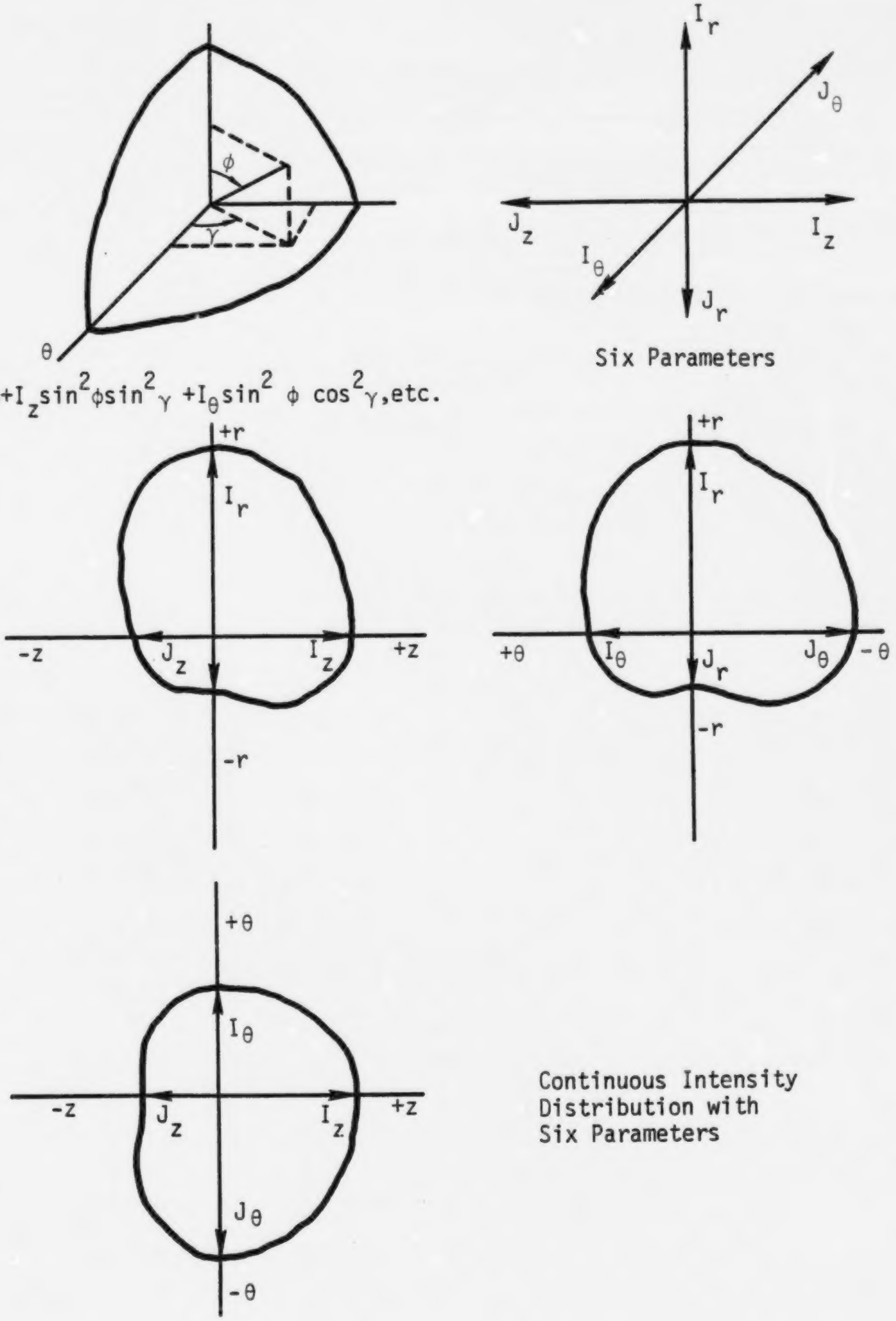
θ
φ
γ
I_r
J_θ
J_z
I_z
I_θ
J_r
+r
I_r
-z
J_z
I_z
+z
-r
+r
I_r
+θ
I_θ
J_r
J_θ
-θ
-r
+θ
I_θ
-z
J_z
I_z
+z
J_θ
-θ

$I = I_r \cos^2 \phi + I_z \sin^2 \phi \sin^2 \gamma + I_\theta \sin^2 \phi \cos^2 \gamma$, etc.

Six Parameters

Continuous Intensity Distribution with Six Parameters

Figure 3.24. Intensity Distribution for CID-6 Model.

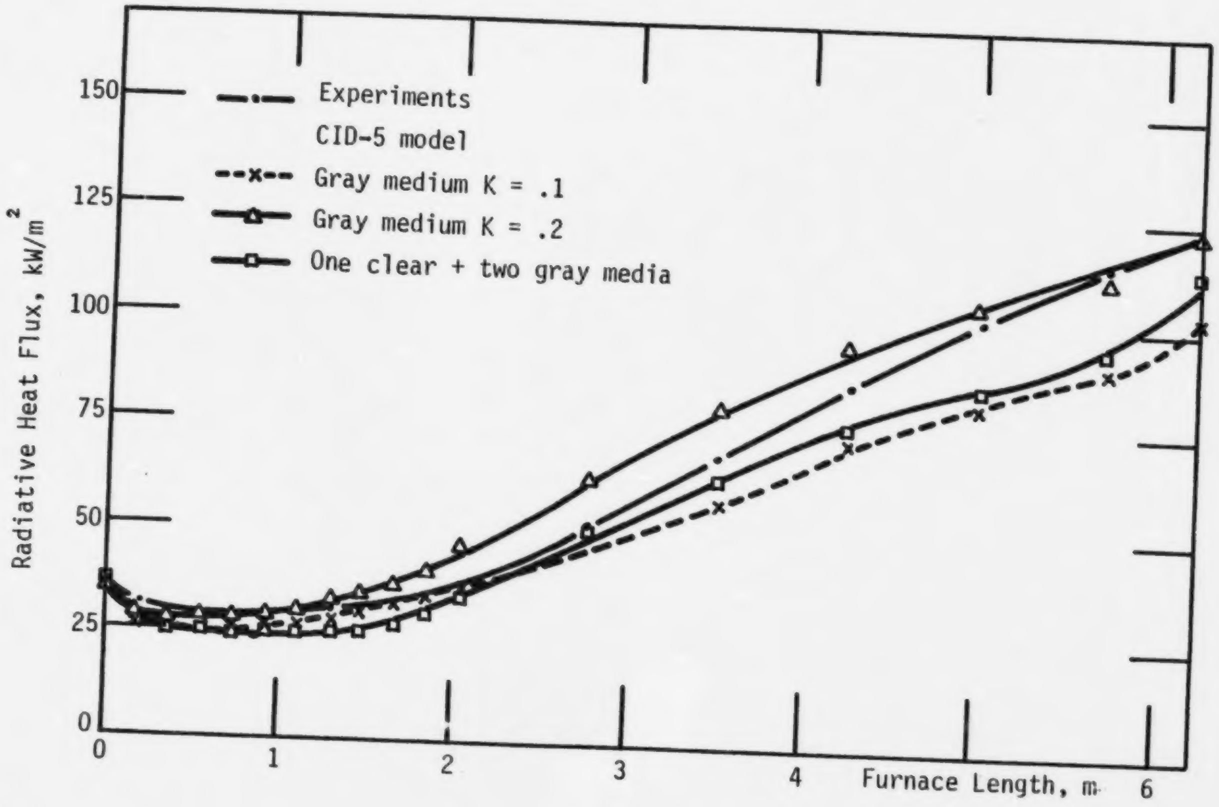

Figure 3.25. Comparison of Predictions by the CID-5 Model With Experimental Results

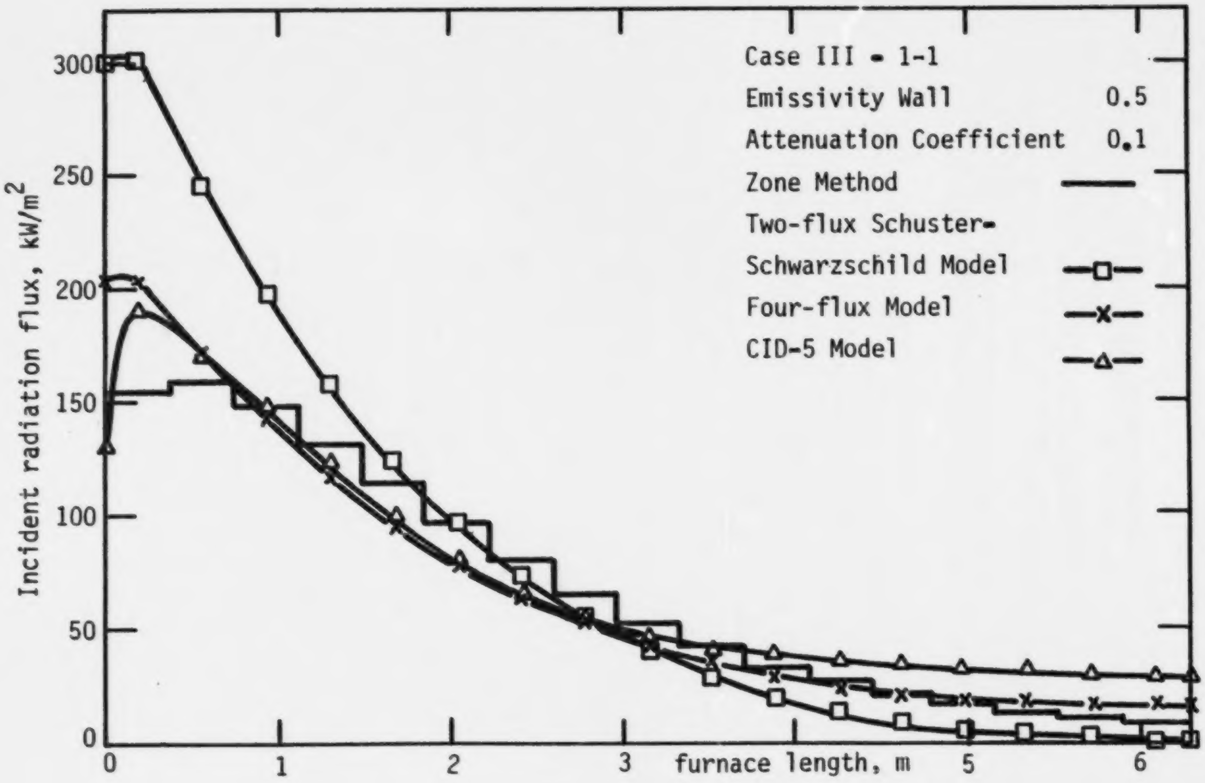

Figure 3.26. Comparison of Two-Flux Model, Four-Flux Model and CID-5 Model Predictions With a Zone Method Prediction

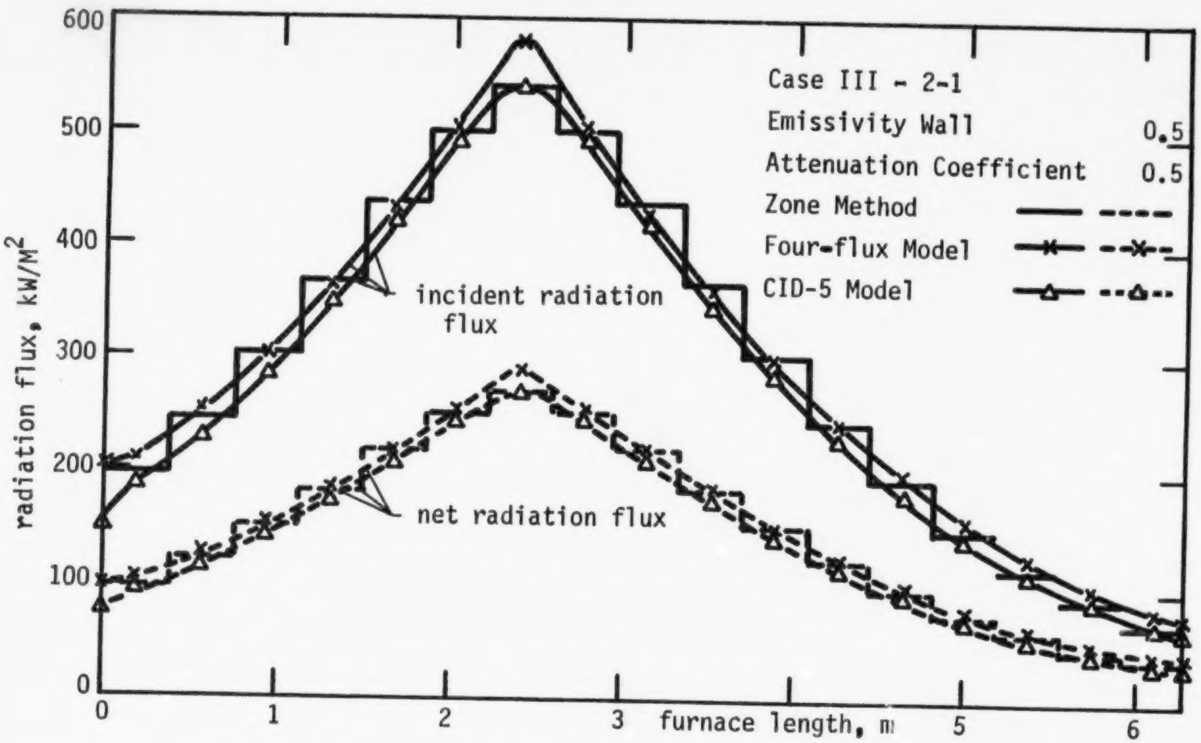

Figure 3.27. Comparison of Four-Flux Model and CID-5 Model Predictions With a Zone Method Prediction

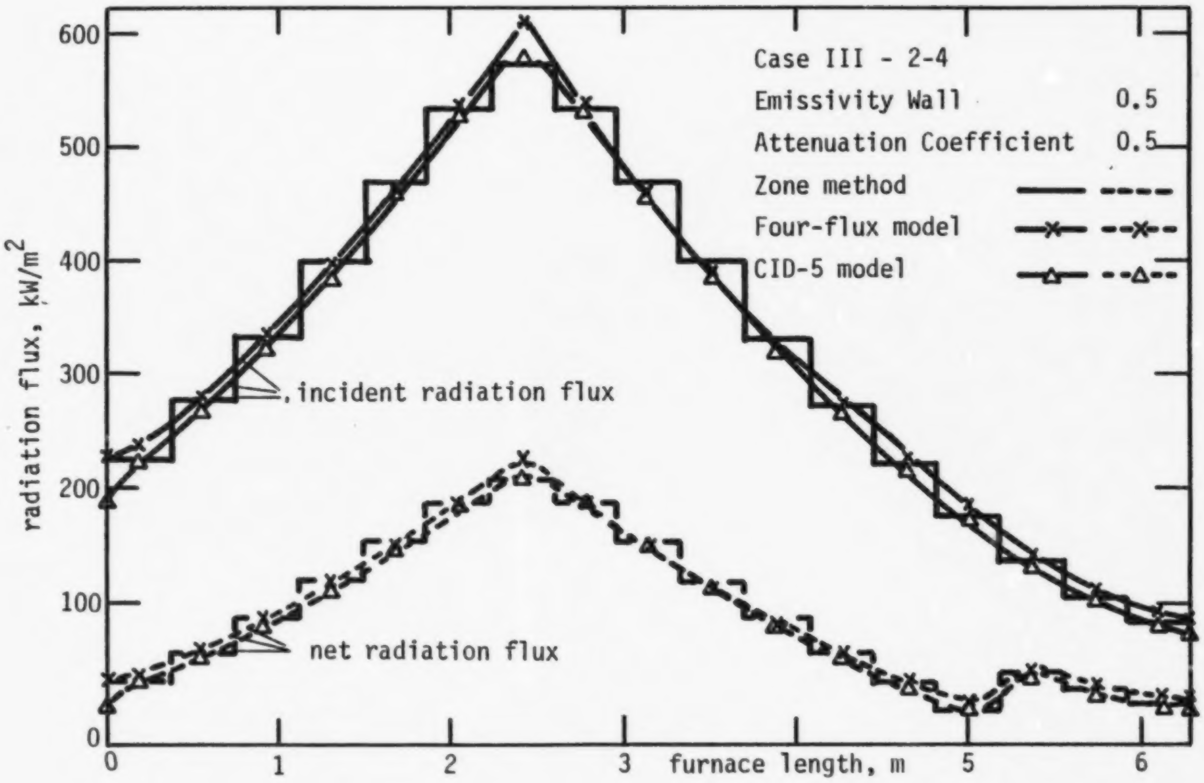

Figure 3.28. Comparison of Four-Flux Model and CID-5 Model Predictions with a Zone Method Prediction

different test cases which also demonstrates the acceptability of the CID-5 model for typical furnace situations.

The incident heat flux in the zone with the maximum heat flux calculated by the CID-5 model for these test cases appears to deviate from the Zone model predictions by 3 percent on average with a maximum of 13 percent, compared to 13 percent on average with a maximum of 30 percent for the four-flux model predictions. Thus it appears that a model has been developed which describes the intensity distribution at a point as a continuous function which is more complex but also more accurate than the four flux model described earlier. It would be used for the cases in which a higher accuracy was required and the other components of the analytical prediction were at least as accurate.

3.5 The Representation of the Radiative Properties of Furnace Gases

The previous sections have discussed the development and evaluation of various models to calculate radiant transfer in combustors. In order to use these models it is necessary to be able to adequately describe the radiative properties of the furnace gases. In this section the present state of knowledge concerning the emission attenuation characteristics of particle-free furnace gases will be reviewed briefly and the remainder of this section addresses the question of how best to use this information to calculate emission and absorption in natural gas flames when there are steep temperature and concentration gradients.

3.5.1 Radiative Properties of Flames and Combustion Products

Radiation from conventional gaseous fuels is mainly due to the triatomic molecules H_2O and CO_2. The absorption and emission of thermal radiation is associated with transitions between energy levels. At the temperatures of interest vibration-rotation transitions in the infrared make the most significant contribution to the radiant energy flux. The intensity of emission of a particular frequency due to an excitation level transition is proportional to the number of molecules occupying the vibrational-rotational level corresponding to the frequency and the probability that transition will take place. The monochromatic intensity from a column of gas of partial pressure p and length l equals:

$$I_\omega \; + \; I_{b,\omega} \, (1 - e^{-k_\omega pl}) \qquad (35)$$

where

$I_{b,\omega}$ is the black body intensity at the considered wave number

K_ω is the spectral (specific) attenuation coefficient

I_ω is the monochromatic intensity.

Both $I_{b,\omega}$ and k_ω are dependent upon the gas temperature. The manner in which K_ω varies over the spectrum determines the total gas emissivity and absorptivity.

The transition from one energy level to a lower level ideally occurs at a single frequency, but in practice the emission line is broadened and spreads over a range of frequencies about the transition frequency. In most gases of practical interest, the emission lines do not occur in isolation, but are spaced so closely together that the broadened lines overlap to a large extent. When a number of lines overlap the specific absorption coefficients are additive. The contribution to the intensity of radiation from the entire band can be found by integration between the frequency limits of the band.

$$I \; = \; \int_{\omega_1}^{\omega_2} I_{b,\omega} \, (1 - e^{-k_\omega pl}) \, d\omega \qquad (36)$$

The total emissivity of a gas at temperature T_g is equal to the ratio of the emission by a gas layer of length L to the black body emission at temperature T_g.

$$\varepsilon_g = \frac{\int_0^\infty I_{b,\omega}(T_g)\left[1 - e^{-k_\omega(T_g)pL}\right] d\omega}{\int_0^\infty I_{b,\omega}(T_g)d\omega} = f\,(T_g,pL) \qquad (37)$$

In a similar way the total gas absorptivity can be evaluated, but in this case the distribution of energy in the spectrum is related to the temperature at which the intensity, absorbed in a certain gas layer, is emitted.

$$\alpha_g = \frac{\int_0^\infty I_{b,\omega}(T_s)\left[1 - e^{-k_\omega(T_g)pL}\right] d_\omega}{\int_0^\infty I_{b,\omega}(T_s)\,d\omega} = f\,(T_g,T_s,pL) \qquad (38.a)$$

where $I_{b,\omega}(T_s)$ is emitted at a source temperature T_s and the spectral intensity is dependent on this source, and assumes the emitter to be a black body. However, the radiation source can be a gas layer of a given temperature and composition distribution. In this case the absorptivity is given by:

$$\alpha_g = \frac{\int_0^\infty I_\omega(T_s)\left[1 - e^{-k_\omega(T_g)pL}\right] d_\omega}{\int_0^\infty I_\omega(T_s)d\omega} = f\,(T_g,T_s,pL) \qquad (38.b)$$

The source temperature need not be constant and the distribution of spectral intensity can be extremely complex. Although a number of models have been proposed to avoid the problem of formulating the attenuation coefficient as a complex function of wave number it is normally easier to rely on measured total emissivity data in order to avoid problems associated with handling the spectral properties of gas mixtures.

Total water vapor emissivity and carbon dioxide emissivity charts are presented by Hottel and Sarofim(30) and the information has been drawn from several sources. Johnson(27) discusses these charts and cites recent work indicating inaccuracies in these charts. Hadvig's(32) charts for total emissivities of water vapor/carbon dioxide mixtures are based on the charts of Hottel and Sarofim(30). Hottel and Sarofim(30) present a chart on the total emissivity of carbon monoxide based on the measurements of Ullrich(33).

Furnace gases are normally composed of two or more radiating components. For a mixture of two gases the total emissivity equals:

$$\varepsilon_{1+2} = \frac{\int_0^\infty I_{b,\omega}\left[1 - e^{-(k_{\omega,1}p_1 + k_{\omega,2}p_2)L}\right]d\omega}{\int_0^\infty I_{b,\omega}\,d\omega}$$

$$= \frac{\int_0^\infty I_{b,\omega}\left[(1 - e^{-k_{\omega,1}p_1L}) + (1 - e^{-k_{\omega,2}p_2L})\right]d\omega}{\int_0^\infty I_{b,\omega}\,d\omega} - \frac{\int_0^\infty I_{b,\omega}\left[(1 - e^{-k_{\omega,1}p_1L})(1 - e^{-k_{\omega,2}p_2L})\right]d\omega}{\int_0^\infty I_{b,\omega}\,d\omega}$$

$$= \varepsilon_1 + \varepsilon_2 - \Delta\varepsilon_{1+2} \qquad (39)$$

The emissivity of a mixture of two gases is equal to the sum of the emissivities of the two gases minus a correction for spectral overlap. If there is no spectral overlap the correction factor equals zero.

The absorptivity α_g of any component of a gaseous mixture depends upon the temperature of the (black body) source of the absorbed radiation T_b, in addition to the gas temperature. Hottel and Sarofim(30) suggest that the absorptivity of CO_2 and H_2O should be found from the corresponding emissivity data by taking

$$\alpha_g(T_g,\ T_b,\ pL) = \left(\frac{T_g}{T_b}\right)^{\beta}\ \varepsilon_g\left(T_b,\ pL\ \frac{T_b}{T_g}\right) \tag{40}$$

where $\beta = 0.65$ for CO_2 and 0.45 for H_2O.

Hadvig(32) has shown that for $T_g/T_b > 1.1$ satisfactory results can be obtained by using the simplified form:

$$\alpha_g(T_g,\ T_b,\ pL) = \varepsilon_g(T_b, pL) \tag{41}$$

and that it is only necessary to use the more complicated procedure for $1.1 > T_g/T_b > 1.0$.

When emissivity data taken from charts is used in detailed calculations of radiative transfer, it is more convenient if the emission is expressed in an algebraic form. The simplest, most commonly used expression, and one which is consistent with equation (5), for flame emissivity is called the gray gas approximation:

$$\varepsilon_g = 1 - e^{-K_g L} = 1 - e^{-k_g pL} \tag{42}$$

It gives the correct emissivity for only one optical depth L at a specified temperature.

For a longer range of optical depths, another representation(30) giving more accurate results is required. This approximation is called the clear/gray gas approximation. For a CO_2/H_2O mixture it can be written as

$$\varepsilon_g = \sum_{n=1}^{n=m} a_{g,n}(1 - e^{-K_{g,n}L}) = \sum_{n=1}^{n=m} a_{g,n}(1 - e^{-k_{g,n}(p_c + p_w)L}) \tag{43}$$

where $a_{g,n}$ is a polynomial in T, e.g., $a_{g,n} = b_{1n} + b_{2n}\, T$ with $T = T_g$ for ε_g.

The same equations can be used for absorption but with $T = T_b$ for α_g(32).

3.5.2 The Prediction of Unidirectional Radiation Intensity in a Particle-Free Absorbing Emitting Medium

One method of evaluating the various models, which are available to describe the emission attenuation characteristics of combustion products and flame gases is to attempt to predict the change in unidirectional radiation through a flame given the incident radiation and the distribution of gas temperature and concentration along the radiation path. The intensity at any point x + Δx along this path is composed of the fraction of incident radiation I_x transmitted through the layer of thickness Δx and the radiation emitted by that layer:

$$I_{x+\Delta x} = (1 - \alpha_g) I_x\,(T_s) + \varepsilon_g\, I_b\,(T_g) \tag{44}$$

The contribution provided by emission in that layer is given by

$$\varepsilon_g \int_o^\infty I_{b,\omega}(T_g)\, d\omega = \varepsilon_g \frac{\sigma T_g^{\,4}}{\pi} \tag{45}$$

The emissivity, ε_g, can be determined from charts for the appropriate partial pressure path length and temperature. For mixtures containing water vapor and carbon dioxide an approximate evaluation of the absorptivity α_g can be obtained using the relations given by Hottel and Sarofim(30).

$$\alpha_{CO_2}\,(T_g, T_s, pL) = \left(\frac{T_g}{T_s}\right)^{0.65} \varepsilon_{CO_2}\left(T_s, pL\,\frac{T_s}{T_g}\right) \tag{46}$$

3-58

$$\alpha_{H_2O}(T_g, T_s, pL) = \left(\frac{T_g}{T_s}\right)^{0.45} \varepsilon_{H_2O}\left(T_s,\ pL\,\frac{T_s}{T_g}\right) \qquad (47)$$

$$\alpha_g = \alpha_{CO_2} + \alpha_{H_2O} - \Delta\alpha_{(H_2O+CO_2)} \qquad (48)$$

where $\Delta\alpha_{(H_2O+CO_2)}$ is a correction factor to account for spectral overlap. The absorptivity given by equation (48) is applicable if the radiation intensity is composed mainly of black body radiation emitted from a surface at T_s. In furnaces and combustors with cool or cold walls the emission is largely attributable to the furnace gases.

Measurements had been made during a series of furnace trials(28) which were used to assess the errors associated with the representation of the furnace gases as a gray medium or as the sum of several gray gases. This assessment was made by comparing calculated and measured unidirectional radiation intensity through natural gas flames. Radial distributions of gas species concentration and gas temperature were made at various axial distances from the firing wall and intensity traverses were made across the flame at the same axial positions using a narrow angle radiometer. This instrument, which was constructed as described by Chedaile and Braud(34), measures total (integrated over the spectrum) radiation intensity in kW/m^2/steradian. Measurements were made with the radiometer aimed at both a hot and cold target.

uni-direc-tional

Equation (44) combined with equations (37) and (39) provides the basis for the stepwise calculation of radiation intensity as follows:

$$\begin{aligned} I_{x+\Delta x} &= \int_0^\infty I_{x+\Delta x;\omega}\, d\omega \\ &= \int_0^\infty I_{x,\omega}(T_s)\, e^{-k_\omega(T_g)p\Delta x}\, d\omega + \int_0^\infty I_{b,\omega}(T_g)\left[1 - e^{-k_\omega(T_g)p\Delta x}\right] d\omega \end{aligned} \qquad (49)$$

Representation of Real Gases by a Gray Medium

If the variation of K, the absorption coefficient with respect to spectral position, partial pressure and temperature is neglected and a mean value is used, then equation 49 becomes:

$$I_{x+\Delta x} = I_x e^{-K\Delta x} + \frac{\sigma T_g^4}{\pi} (1\ e^{-K\Delta x}) \tag{50}$$

i.e., emissivity and absorptivity are equal

$$\varepsilon_g = \alpha_g = 1 - e^{-K\Delta x} = 1 - e^{-kp\Delta x} \tag{51}$$

As discussed earlier, values of K = 0.1 and 0.2 gave acceptable predictions of incident radiant flux at the furnace wall using either the zone model or a four-flux model. These values, together with K = 0.3, were used in an attempt to predict the narrow angle traverses. Reasonable results were obtained with K = 0.2 at large distances from the firing wall which may account for the acceptable predictions of total flux using a mean absorption coefficient; however, in general, the comparisons between measured and predicted radiation intensity were poor (compare Figures 3.29 and 3.30). The difference in the agreement obtained with calculated and measured total incident flux and those calculated for unidirectional intensity distributions can be attributed to the fact that the whole furnace volume contributes to the incident flux. However, only the gas layers along the line of sight of the narrow angle radiometer contribute to measured intensities. Thus, the representation of the emissivity and the absorptivity of the gases is much more critical.

The Weighted Sum of Gray Gases

An improved representation of real gas emissivity assumes that the emissivity is given by the weighted number of gray gases, i.e.,

$$\varepsilon_g = \sum_n a_{g,n} \left(T_g\right) (1 - e^{-k_n pL}) \tag{52}$$

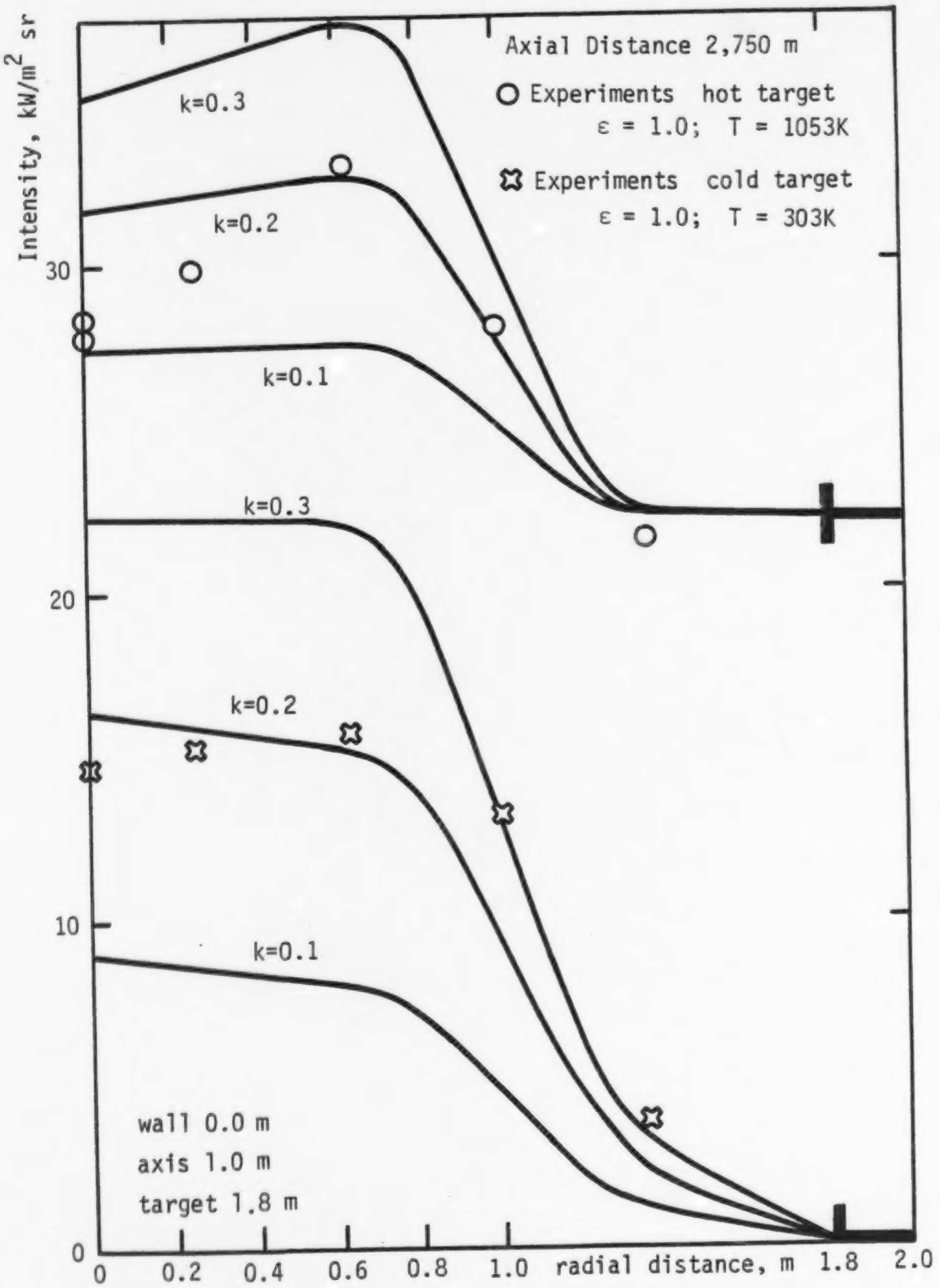

Figure 3.29. Prediction of Narrow Angle Traverses Through a Natural Gas Flare Using Different Gray Gas Attenuation Coefficients

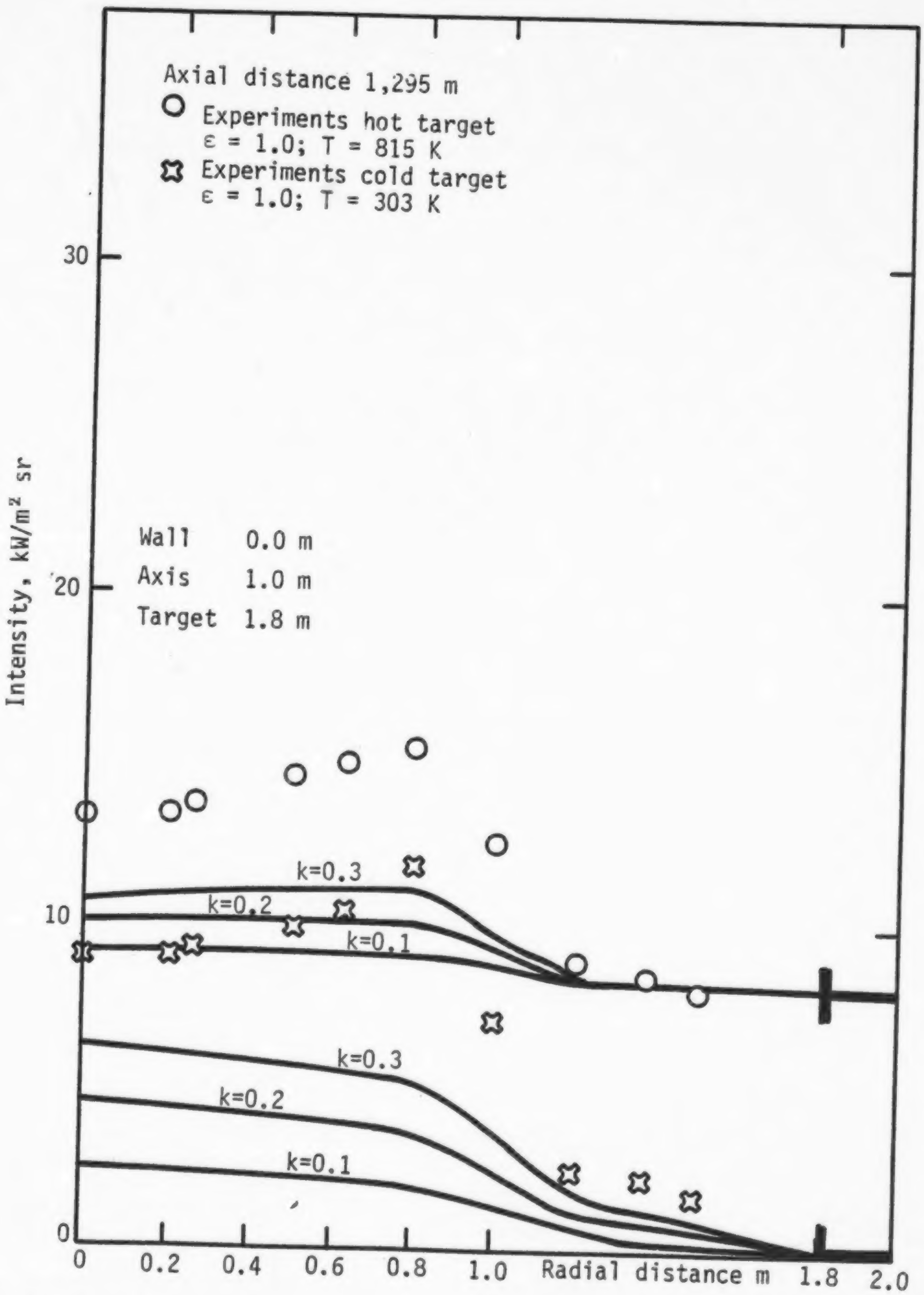

Figure 3.30. Prediction of Narrow Angle Traverses Through A Natural Gas Flare Using Different Gray Gas Attenuation Coefficients

In this instance the emissivity approaches one as the path length approaches infinity. Hottel and Sarofim$^{(30)}$ describe a graphical method for fitting equation (52) to the measured total emissivity curves. Equation (52) is an approximation of equation (37) which describes the total emissivity in the spectral form where the spectral absorption coefficient is assumed to be independent of temperature and constant over certain wavelength regions. Thus, for a gray gas

$$ {}_{g,n} = \frac{\int_{\omega_1}^{\omega_2} I_{b,\omega}(T_g)\, d\omega + \int_{\omega_3}^{\omega_4} I_{b,\omega}(T_g)\, d\omega}{\int_0^{\infty} I_{b,\omega}(T_g)\, d\omega} (1 - e^{-k_n pL}) \qquad (53) $$

$$ = a_{g,n} (1 - e^{-k_n pL}) $$

where ω_1, ω_2, ω_3 and ω_4 represent the wave numbers between which the absorption coefficient is assumed to be constant. Thus the weighting factors $a_{g,n}$ (equation 52) are the fractions of the total black body emissive power emitted in the wave number regions where $k_\omega = k_n$. In those non-absorbing parts of the spectrum k_ω is small and these "windows" are referred to as clear gas components. The radiation intensity can now be expressed by

$$ I_{x+\Delta x} = \sum_n I_{x+\Delta x,n} = \sum_n \left[I_{x,n}\, e^{-k_n p\Delta x} + a_{g,n}(1 - e^{-k_n p\Delta x}) \frac{\sigma T_g^{\,4}}{\pi} \right] \qquad (54) $$

Johnson$^{(27)}$ fitted a clear/2-gray formulation to the emission characteristics of soot, CH_4, CO, CO_2 and H_2O suitable for the partial pressure path length (pL's) of 0.02 to 1.5 m atm. The fit is satisfactory over intermediate pL's but less satisfactory at the end of the range. The constants suggested by Johnson for inclusion in equation 52 are listed in Table 3-2.

Table 3-2. Constants for the Clear/2-Gray Formulation $a_{g,n} = b_{1n} + b_{2n} T_g$ After Johnson(27)

n	b_{1n}	$b_{2n} \cdot 10^3$	k_n
1	+.255	+.260	0.00
2	+.500	-.157	1.83
3	+2.45	-.103	32.30

Unidirectional radiation intensities were calculated using the constants listed in Table 3-2. The calculations were made with step lengths of 0.1 m and the gas temperature and concentration was evaluated by linear interpolation of the measured curves. The results of these calculations can be summarized by:

- the 1-clear/2-gray formulation appears to give satisfactory predictions for both hot and cold backgrounds when the line of sight does not pass through regions of strong gradients (i.e., flame regions).
- discrepancies of up to 40 percent occur when the line of sight includes steep temperature and concentration gradients. Predicted values deviate most from the measurements where the temperature decreases with increasing distance (axis is 1.0 m) from the target i.e., between 1.0 m and 0.8 m (see Figure 3.32).

The comparison between measured and predicted values of unidirectional radiation intensity presented in Figures 3.31 and 3.32 are typical of many different calculations(31) and several explanations can be proposed to account for the differences between the measured and predicted intensities including:

- Interpolation and Averaging Errors. Several of the calculations were repeated with step lengths of 0.1 m and 0.02 m; however, no appreciable effect on the predicted curve was observed.

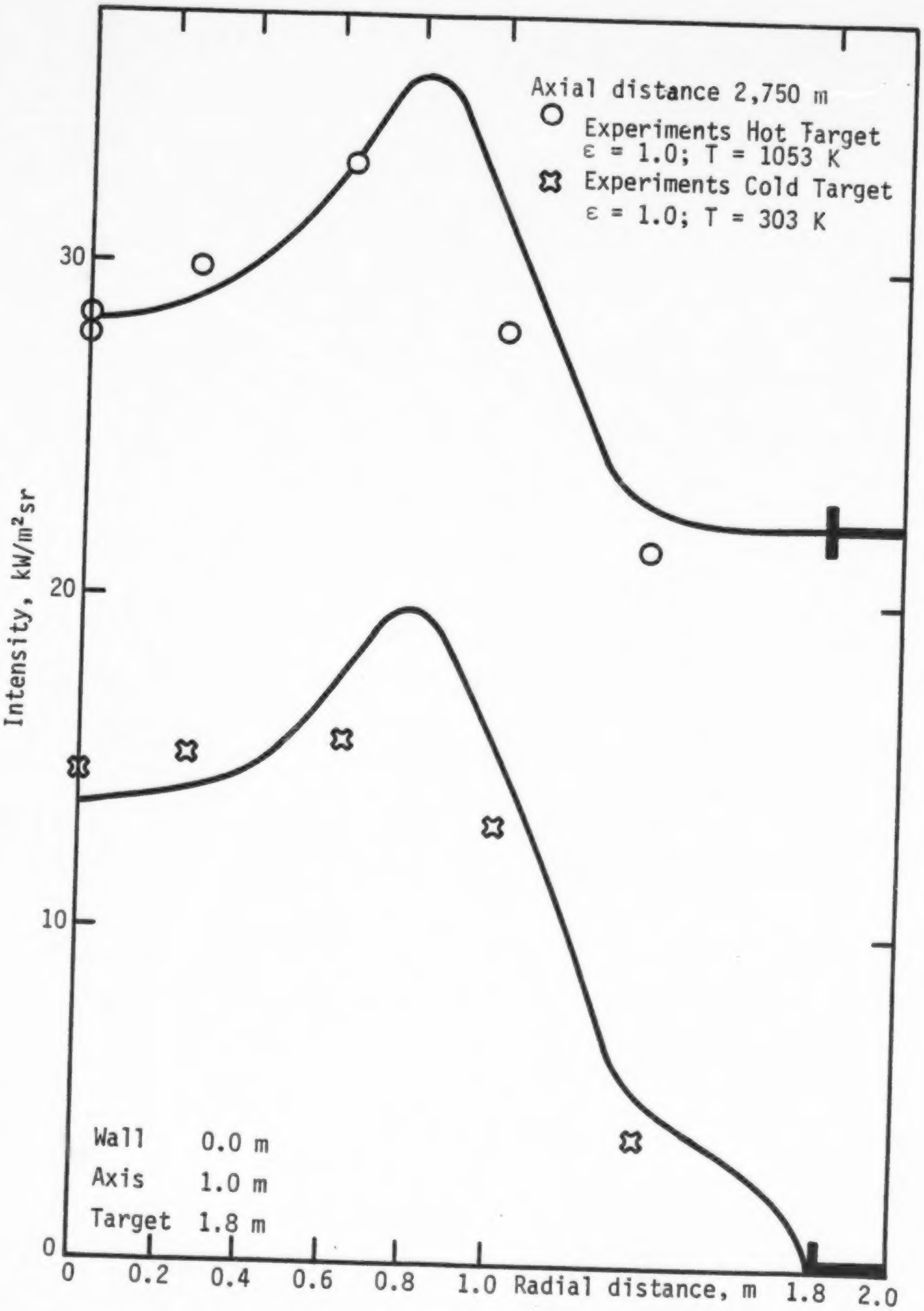

Figure 3.31. Prediction of Narrow Angle Traverses Using a 1 Clear/2 Gray Gas Attenuation Formulation

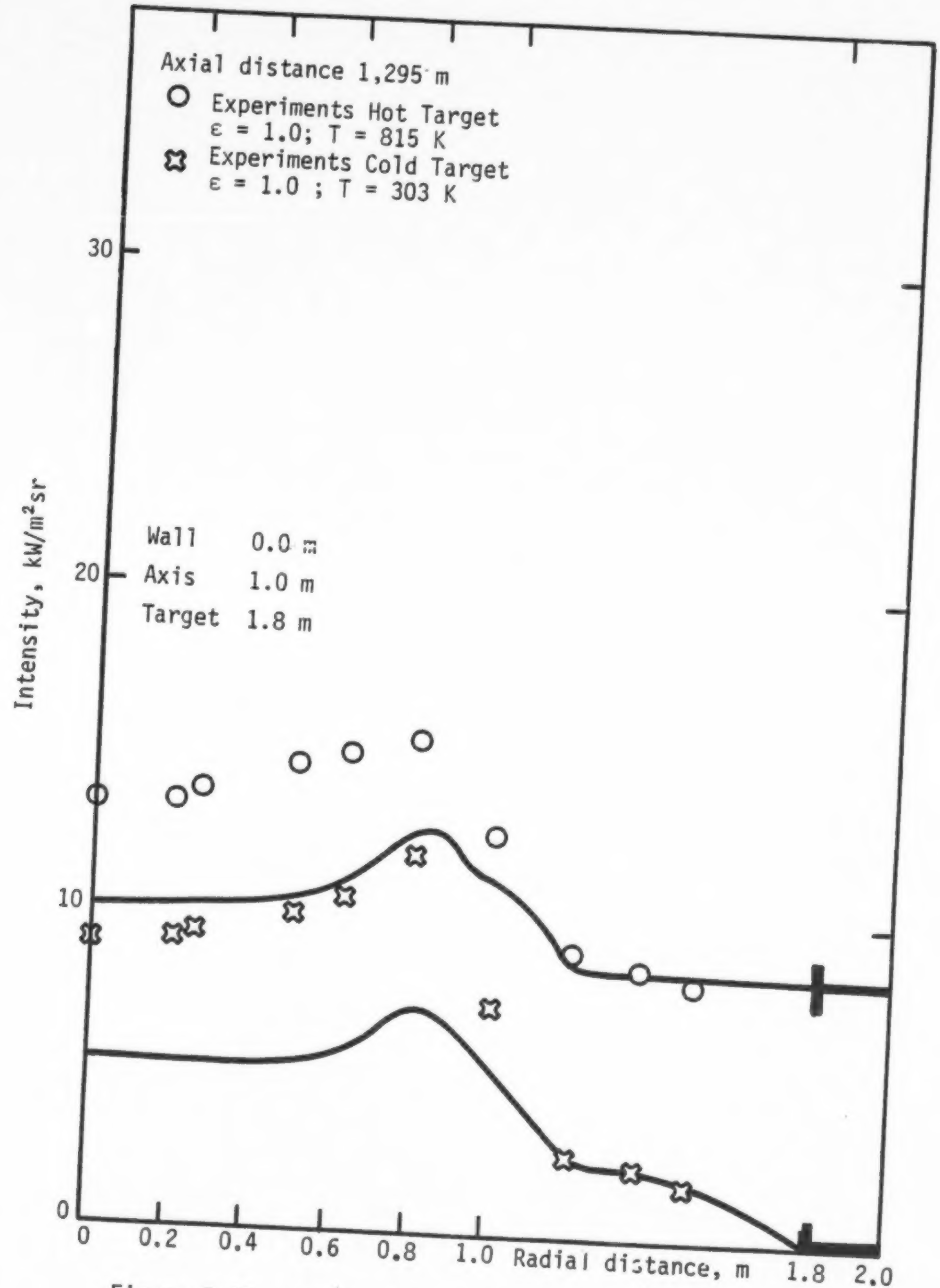

Figure 3.32. Prediction of Narrow Angle Traverses Using a 1 Clear/2 Gray Gas Attenuation Formulation

- Inadequacy of the One-Clear/Two-Gray Formulation. A four gray gas formulation was fitted to the nonluminous emissivity data (to be discussed later). However the results were similar for both formulations suggesting that other explanations were necessary.

- Inadequacy of the Clear/Gray Formulation. The clear/gray formulation contains two deviations from physical reality which were apparent from an examination of spectral data(35,36). Evidence exists showing that the emitted wavelength ranges and monochromatic emission/attenuation coefficients vary with gas temperature. Consequently some radiation emitted at high temperatures cannot be attenuated by gas at a lower temperature. Also the change in monochromatic emission/attenuation coefficient with temperature means that a gray gas assumption cannot be valid over a range of temperatures.

- Measurement Errors. Although measurement errors are difficult to assess, it is considered that they are unlikely to be the principal cause of the discrepancy between measurement and prediction. If measurement errors were the major cause of the discrepancies it is reasonable to expect that errors would occur on both sides of the axis of symetry and not as shown in Figure 3.32. Possible measurement errors include:
    - alignment problems. Errors due to misalignment could occur if the measured temperature, concentration and radiation traverses were carried out off the flame axis.
    - target characteristics. The targets were considered to be black bodies of uniform temperature which could introduce some errors. However, these are considered to be small because predictions in the vicinity of both targets are generally good.

period

- The Effect of Temporal Fluctuations in Temperature and Concentration.

  Temperature and concentration fluctuation effects are difficult to assess as the magnitude of the fluctuations and their periodicity are unknown. Both the temperature and the concentration (or partial pressure) affect emission ($\varepsilon\sigma T^4$), but as the effect of temperature and concentration on ε is small compared to the effect of temperature on T^4, fluctuations in temperature will probably have the most important influence for the emission characteristics. After examining the possible influence of temperature variations it was concluded that the magnitude of the influence was too small to explain the differences between measurement and prediction.

- Characteristics of the Narrow Angle Radiometer. The radiometer receives radiation from the emitting source via a long tube of small diameter. Consequently, each point on the receiver sees the source under a different small finite angle. This causes a small reduction in signal as the radiometer is withdrawn from a black body oven. During measurement the viewing tube of the radiometer is purged with air to prevent the entry of flame gases. This will cause some dilution and cooling of the gases close to the probe. Neither of these errors will cause the differences between measurement and prediction.

- Flame Phenomena. Radiation from soot and radicals have been neglected. Soot concentrations were below the lower limit of detection(28).

From the above it is most likely that the discrepancy between measurement and prediction is associated with the clear/gray concept, and alternative methods of representing the emission attenuation characteristics of combustion gases were investigated.

3.5.3 Emissivity Represented by a Four-Gray Gas Formulation

The number of gray gases was increased to provide a more accurate approximation of total emissivity data over a larger partial pressure path length range. Emissivity is given by

$$\varepsilon_g = \sum_{n=1}^{4} a_n(T)\,(1 - e^{-k_n pL}) \tag{55}$$

where

$$a_n(T) = b_{1n} + b_{2n}T + b_{3n}T^2 + b_{4n}T^3 \tag{56}$$

The constants K_n, b_{1n}, b_{2n}, b_{3n} and b_{4n} were determined by a trial and error procedure combined with a least squares method and are listed in Table 3-3. The fit was made over the temperature range 1000-2000 K and a partial pressure path length of 0.003-1.2 m atm.

Table 3-3. Constants Used in the Four-Gray Gas Formulation

n	b_{1n}	$b_{2n}\cdot 10^3$	$b_{3n}\cdot 10^6$	$b_{4n}\cdot 10^9$	k_n
1	+0.218331	+0.282735	+0.065471	-0.0256803	0.106165
2	+0.534365	-0.240326	+0.008598	+0.0016552	1.652680
3	+0.131198	+0.089167	-0.127374	+0.0318849	21.212000
4	+0.116106	-0.131576	+0.053305	-0.0078598	146.308000

Calculation of intensities using the four-gray formulation gave similar results to those obtained with the one-clear/two-gray formulation. A maximum variation of 6 percent was found between the two calculations.

The lack of difference is attributed to a cancellation of errors when the one-clear/two-gray formulation is used.

3.6 Conclusions and Summary

The optimum design of a burner combustor combination for efficient utilization of fossil fuels without the production of excessive amounts of pollutants requires the development of analytical tools to aid designers and engineers. A method of assessing radiative heat transfer within combustors will be an integral part of any successful tool and the various methods of calculating radiation heat transfer models have been developed for the first step in the development of a complete analytical capability. As part of this program radiate heat transfer models have been developed for both cylindrical and Cartesian coordinate systems. Comparisons have been made both against experimental results and against test cases for which the zone method can be considered to give an exact solution. The specific models investigated include:

- 2-Flux Models based upon both the spherical harmonics method and the discrete coordinate method. Provided steep gradients do not exist, errors of less than 9% were obtained. However, the inability of the models to accept axial gradients restricts their usefulness.
- 4-Flux Models based upon the discrete coordinate method which gave a maximum discrepancy of less than 10% for the majority of the cases tested. These test cases included situations with axial gradients. Major errors occurred in the region close to end walls although these errors had a minor influence upon the overall heat transfer.
- 6-Flux Models based upon the discrete coordinate method.
- A continuous intensity distribution (CID) model in which the intensity at a point is described as a continuous function thus overcoming the lack of physical reality associated with flux

3-70

models with non-continuous intensity distributions. The intensity distribution was represented by 5 parameters (thus CID-5) and the model gave more accurate predictions than those obtained with the four-flux model. An average deviation of 3 percent in peak heat flux was found between the zone method results and those obtained with the CID-5 model.

All of the above models were suitable for coupling either with physical models or other analytical models which were capable of calculating mass transfer and heat release profiles to enable gas temperatures to be calculated.

An accurate description of the radiative properties of furnace gases is a necessary input for any radiation model. Several different emission/ absorption models have been evaluated for gas flames. The models can be classified into three different groups depending upon whether the real gas is represented as a single gray gas, a combination of gray gases or a combination of a clear and several gray gases. The single gray gas model appears to be most inaccurate, whereas neither of the other formulations appears to have an advantage of the other in flame regions (i.e., where there are significant specie and temperature gradients).

The development of low polluting combustion devices would be helped by the availability of predictive models which could be used as design tools. Although a heat transfer model is an essential feature of a predictive model, it is not the pacing item in the development of the total tool. The lack of understanding of turbulent transport in two-phase turbulent flames is a more serious drawback to the development of predictive models. Heat transfer models available currently can be used effectively in two areas:

- To estimate the effect of changes in heat release pattern produced to provide low NO_x emissions on heat flux distribution in the radiant section of utility boilers.
- To estimate bulk gas temperatures in combustors which can be modeled empirically as a combination of ideal reactors.

3-71

The attainment of low levels of nitrogen oxide may well be controlled by the relaxation of nitrogenous species in a rich zone toward a low equilibrium level. This relaxation process is kinetically controlled, and therefore, temperature is important. This type of system can be analyzed by the techniques discussed in this report where it is very important to design a section of the combustor to give a precise time/temperature profile for the rich combustion gases.

4.0 REFERENCES AND NOMENCLATURE

1. Heap, M.P., et al Burner Criteria for NO_x Control, vol. 1, Influence of Burner Variables on NO_x in Pulverized Coal Flames. EPA 600 2-76-061a, March 1976.

2. Pershing, D.W., Martin, G.B. and Berkau, E.E., "Influence of Design Variables on the Production of Thermal and Fuel NO_x from Residual Oil and Coal Combustion." Paper presented at the AIChE 66th Annual Meeting, Philadelphia, 1973.

3. Fenimore, C.P., Thirteenth Symposium (International) on Combustion, p. 373, The Combustion Institute, 1971.

4. De Soete, G., Revue de I'Institut Francias du Petrole, 28, 95 (1973)

5. Bartok, W., Engleman, V.S. and del Valle, E.G., "Laboratory Studies and Mathematical Modeling of NO_x Formation in Combustion Processes," Esso Research and Development Co., EPA report APTD 1168 (NTIS No. PB 211-480), 1972.

6. Sarofim, A.F., Williams, G.C., Modell, M. and Slater, S.M. "Conversion of Fuel Nitrogen to Nitric Oxide in Premixed and Diffusion Flames," Paper presented at the AIChE 66th Annual Meeting, Philadelphia, 1973.

7. Armento, W.J., Effects of Design and Operating Variables on NO_x From Coal Fired Furnaces, EPA 650/2-74 002 b, February 1975.

8. Leuckel, W., Swirl Intensities, Swirl Types and Energy Losses of Different Swivel Generating Devices, Doc. G02/a/16 IFRF IJmuiden, Holland.

9. Pershing, D.W., Brown, J.W. and Berkau, E.E., Proceedings, Coal Combustion Seminar, June 19-20, 1973, p. 87, EPA 650/2-73-021, September 1973.

10. Axworthy, A.E., et al, "Chemistry Reactions in the Conversion of Fuel Nitrogen to NO_x Proceedings of the Stationary Source Combustion Symposium," vol. 1, EPA 660/2-76-152a, June 1976.

11. Beer, J.M., Private Communication.

12. Viskanta, R., Radiative transfer and interaction of convection with radiation heat transfer, Advances in Heat Transfer (eds. Irvine, T.F. and Hartnett, J.P.), 3, 175-252, Academic Press, New York, 1966.

13. Howell, J.R., Application of Monte Carlo to heat transfer problems, Advances in Heat Transfer, 5, 1-54, Academic Press, New York, 1968.

14. Steward, F.R., and Cannon, R., The calculation of radiative heat flux in a cylindrical furnace using the Monte Carlo method, Int. J. Heat and Mass Transfer, 14, 245-262, 1971.

15. Hottell, H.C., and Cohen, E.S., "Radiant heat exchange in a gas-filled enclosure: allowance for non-uniformity of gas temperature," AIChE. Journal, 4,3-14, 1958.

16. Hottel, H.C., and Sarofim, A.F., Theory and Fundamental Research in Heat Transfer (ed. J.A. Clark), 139-160, Pergamon Press, New York 1963.

17. Oppenheim, A.K., Trans. A.S.M.E., 78, 7250735, 1956.

18. Schuster, A., Astrophys, J., 21, 1-22, 1905.

19. Schwarzschild, K., Nachr. Akad. Wiss. Gottingen, Math. - Physik. Kl. 1,41, 1906; Sitzber. Preuss. Akad. Wiss., Physik. - Math Kl. 1183, 1914.

20. Hamaker, H.C., "Radiation and heat conduction in light scattering material," Philips Res. Rep. 2, 55, 103, 112 and 420, Eindhoven, The Netherlands, 1947.

21. Milne, E.A., in Handbuch der Astrophysik, G. Eberhard et al., eds, 3, part 1, 65-255, Springer, Berlin, 1930.

22. Eddington, A.S., The Internal Constitution of Stars, Dover Publ., New York, 1959.

23. Stott, J.B., and Garrod, C.W., "A Method of applying electrical analogues to calculation of radiative heat transfer," Proceedings of Chemeca 70, Australian Academy of Science, Melbourne, 1970.

24. Gibson, M.M., and Monahan, J.A., "A simple model of radiation heat transfer from a cloud of burning particles in a confined gas stream," Int. J. Heat Mass Transfer, 14, 141-147, 1971.

25. Siddall, R.G., "Flux methods for the analysis of radiant heat transfer," Fourth Symposium on Flames and Industry, British Flame Research Committee I.F.R.F. and Inst. of Fuel, London, 1972.

26. Gosman, A.D., and Lockwood, F.C., "Incorporation of a flux model for radiation into a finite-difference procedure for furnace calculations," Imperial College, CCK/TN/A/9, London, 1972.

27. Johnson, T.R., "Application of the zone method of analysis to the calculation of heat transfer from flames," Ph.D. thesis, Sheffield University, 1971.

28. Michelfelder, S., and Lowes, T.M., Report on the M2-trials, Doc. no. F36/a/4. I.F.R.F., IJmiuden, 1974.

29. Computer programme for the zone method of analysis with 3 radial and 17 axial zones, no. 422044, I.F.R.F., IJmuiden, 1973.

30. Hottel, H.C., and Sarofim, A.F., Radiative Transfer, McGraw-Hill, New York, 1967.

31. Bartelds, H., Summary of I.F.R.F. Radiation Modeling Study, Contract 68-02-0202.

32. Hadvig, S., "Gas emissivity and absorptivity: A thermodynamic study," J. Inst. Fuel, 43, 129-135, 1970.

33. Ullrich, W., Sc. D. thesis in Chemical Engineering, M.I.T., Cambridge, Mass., 1953.

34. Chedaille, J., and Braud, Y., "Measurements in Flames, Volume I," International Flame Research Foundation, Edward Arnold, London, 1972.

35. Sparrow, E.M., and Cess, R.D., Radiation Heat Transfer, Brooks/Cole, Belmont, USA, 1970.

36. Lee, R.H.C., and Happel, J., "Thermal radiation of methane gas," Ind. and Eng. Chem. Fundamentals, vol. 3, no. 2, 167-176, 1964.

NOMENCLATURE

A	effeciency factor for abosrption	-
a	factor in two-flux equations	-
a	weighting factor or energy fraction in black body spectral region	-
a_g	ibid., subscript refers to gas radiation	-
a_{gs}	ibid., subscripts refer to gas/soot radiation	-
$a_{g,n}$	ibid., subscripts refer to gas radiation and to term number n in series	-
a_n	ibid., subscript refers to term number n in series	-
B	zone dimension in Zone Method of Analysis	m
b	factor in two-flux equations	-
$b_{g,n}$	weighting factor for absorption, subscripts refer to gas radiation and to term number n in series	-
D	diameter furnace	m
E	efficiency factor for emission	-
E_b	black body emissive power	$W.m^{-2}$
E_b	hemispherical black body emissive power of gas	$W.m^{-2}$
E_n	efficiency factor for emission at wavelength λ for particles in nth size range	-
E_λ	efficiency factor for emission at wavelength λ	-
f_ν	photon density	$m^{-3}.sec^{-1}$
G	total intensity of incident radiation	$W.m^{-2}$
I	intensity of radiation integrated with respect to wavelength	$W.m^{-2}$
$I_{b\lambda}$	intensity of black body radiation at wavelength λ	$W.m^{-3}$
$I_{b\lambda p}$	intensity of particle black body radiation at wavelength λ	$W.m^{-3}$
$I_{b,n}$	intensity of black body radiation, subscript n refers to term number n in series	$W.m^{-2}$
$I_{b,\omega}$	intensity of black body radiation at wavenumber ω	$W.m^{-1}$
$I_{s+\Delta s}$	intensity at point s +Δs along path of travel of radiation beam	$W.m^{-2}$
I_x	intensity at point x in positive x - direction	$W.m^{-2}$

$I_{x+\Delta x,\omega}$	intensity at point $x+\Delta x$ in positive x - direction at wavenumber ω	$W.m^{-1}$
I_z	intensity in positive z - direction	$W.m^{-2}$
I_θ	intensity in positive θ - direction	$W.m^{-2}$
I_λ	intensity of radiation at wavelength λ	$W.m^{-3}$
I_ν	intensity of radiation at frequency ν	$W.m^{-2}.sec^{-1}$
I_ω	intensity of radiation at wavenumber ω	$W.m^{-1}$
I_o	intensity leaving wall at $r = o$ or $z = o$	$W.m^{-2}$
K	emission/absorption/attenuation coefficient	m^{-1}
K_a	gray gas/mean attenuation coefficient	m^{-1}
K_e	gray gas/mean emission coefficient	m^{-1}
K_e	Planck mean absorption coefficient	m^{-1}
K_e	gray gas/mean absorption coefficient at point east of point P	m^{-1}
K_{gs}	gray gas/mean absorption coefficient for gas/soot radiation	m^{-1}
$K_{g,n}$	gray gas/mean absorption coefficient for gas radiation, subscript n refers to term number n in series	m^{-1}
K_{ma}	mean absorption coefficient	m^{-1}
K_{me}	mean emission coefficient	m^{-1}
K_n	gray gas/mean absorption coefficient, subscript n refers to term number n in series	m^{-1}
$K_{\lambda a}$	monochromatic absorption coefficient	m^{-1}
$K_{\lambda ag}$	monochromatic absorption coefficient for gas radiation	m^{-1}
k	specific absorption coefficient	$m^{-1}.atm^{-1}$
$k_{g,n}$	gray gas/mean specific absorption coefficient for gas radiation, subscript n refers to term number n in series	$m^{-1}.atm^{-1}$
k_λ	specific monochromatic absorption coefficient	$m^{-1}.atm^{-1}$
k_ω	specific absorption coefficient at wavenumber ω	$m^{-1}.atm^{-1}$
L	length of furnace, cylinder	m
L	optical beam length, path length	m
L_m	mean beam length	m
p_g	total partial pressure of radiating components in gas mixture	atm
q	net heat flux density	$W.m^{-2}$

$q_{in,w}$	flux density arriving at wall	$W.m^{-2}$
$q_{out,w}$	flux density leaving wall	$W.m^{-2}$
q_r	net heat flux density	$W.m^{-2}$
$q_{in,w}$	flux density arriving at wall	$W.m^{-2}$
$q_{out,w}$	flux density leaving wall	$W.m^{-2}$
q_r	net flux density in radial direction	$W.m^{-2}$
q_x	net flux density in x-direction	$W.m^{-2}$
q_y	net flux density in y-direction	$W.m^{-2}$
q_z	net flux density in z-direction	$W.m^{-2}$
q_θ	flux density in θ-direction	$W.m^{-2}$
R	radial or Cartesian coordinate at wall	m
r	radius	m
T_b	black body temperature	K
T_g	gas temperature	K
T_s	temperature of radiation source	K
T_w	wall temperature	K
$T(x,y,z)$	temperature at coordinate position (x,y,z)	K
α_g	absorptivity of gas (mixture)	-
α_w	absorptivity of wall	-
γ	angle in spherical coordinate system	-
ΔI	change of intensity over finite step	$W.m^{-2}$
ε	emissivity	-
ε_g	emissivity of gas	-
$\varepsilon_{g,n}$	emissivity of gas, subscript n refers to term number n in series	-
ε_w	emissivity furnace wall	-
λ	wavelength	m
ν	frequency of radiation	sec^{-1}
ϕ	coordinate angle in spherical coordinate system	-
ω	solid angle	-
R_s	Relative Swirl	